A SPATIO-TEMPORAL ANALYSIS OF TRENDS IN NORTHERN HEMISPHERE SEASONAL SNOW-COVER, 1971-2017

by

Michael Ian Allchin

B.Sc. (Hons), University of Bristol, 1986
M.Sc., University of Southampton, 2013

DISSERTATION SUBMITTED IN PARTIAL FULFILLMENT OF
THE REQUIREMENTS FOR THE DEGREE OF
DOCTOR OF PHILOSOPHY
IN
NATURAL RESOURCES AND ENVIRONMENTAL STUDIES

UNIVERSITY OF NORTHERN BRITISH COLUMBIA

April 2020

© Michael Allchin, 2020

Abstract

Seasonal snow-cover (SSC) substantially alters surface physical properties over the Northern Hemisphere (NH). It modulates processes within the energy and water cycles, thereby influencing climatology, hydrology, geomorphology and ecology. In spring and summer, snowmelt provides an essential resource for humankind. The identification, quantification and explanation of changing spatial and temporal distributions of SSC helps to predict future impacts on natural and human environments, and informs development of mitigation and adaptation strategies. Because SSC is spatially and temporally heterogeneous, meaningful estimation of trends in its distribution and duration is dependent on long records of remotely-sensed imagery. The Rutgers University Global Snow Laboratory and the United States' National Oceanic and Atmospheric Administration provide the longest such archive (NOAA-Rutgers Snow Archive, NRSA), dating from 1966. However, several studies have raised questions about the credibility of the signs and magnitudes of trends derived from the NRSA, suggesting that they may be artifacts of technological improvements introduced in 1999.

This dissertation improves the spatial resolution at which NH SSC extent and duration trends during the NRSA's longest continuous section (since 1971) are reported, building on previous hemispheric and continental studies. It demonstrates that the magnitudes of area-related trends are sensitive to assumptions adopted when estimating SSC extent from the NRSA, and that these sensitivities vary spatially. The study assesses whether temporal trajectories of SSC-onset trends imply abrupt changes in 1999, particularly over more complex terrain, and finds no evidence of this. It also explores the broader climatological contexts of these trends, together with estimated departures from mean conditions. Evidence is presented at monthly intervals for causative chains linking advection of mid-tropospheric warming from lower to higher latitudes,

consequent inception of climatologically novel airflows, and the incidence of significant SSC-onset trends of both signs. Earlier onset of snow-dominated conditions is found to be driven by augmented moisture advected from lower latitudes (in eastern Eurasia) or zonally from oceanic sources (in North America) over regional monthly mean 0°C isotherms. Delayed onset is associated with drier or warmer airflows. These findings support the interpretation that the NRSA-based trends are plausible within their spatial and temporal contexts.

Table of Contents

List of Tables

List of Figures

List of Appendices

Glossary

20CR	20th Century Reanalysis
AFC	Actual Fractional Cover
AT2m	2m Air Temperature
CRU	University of East Anglia Climatic Research Unit
CUSUM	Cumulative Summation of Anomalies
DGP	Dataset Grid-Point
DoSY	Day of Snow-Year
GLOBE	Global Land One-km Base Elevation Project
HKH	Hindu Kush - Himalaya Mountains
IMS	Interactive Multisensor Snow and Ice Mapping System
MODIS	Moderate Resolution Imaging Spectro-Radiometer
NASA	National Aeronautics and Space Administration (United States of America)
NH	Northern Hemisphere
NOAA	National Oceanic and Atmospheric Administration (United States of America)
NRSA	NOAA-Rutgers Snow Archive
On1	Date of first onset of snow-cover persisting for at least one week
On4	Date of first onset of snow-cover persisting for at least four weeks
PoI	Period of Interest
PoR	Period of Record
SAF	Snow-Albedo Feedback
SCA	Snow-Covered Area
SCD	Snow-Covered Duration
SDA	Snow-Dominated Area
SDD	Snow-Dominated Duration
SLP	Sea-Level Pressure
SSC	Seasonal Snow-Cover
TP	Thiessen Polygon
TPW	Total Precipitable Water
U_{500}	Zonal Wind-Speed at 500 hPa
U_{850}	Zonal Wind-Speed at 850 hPa
V_{500}	Meridional Wind-Speed at 500 hPa
V_{850}	Meridional Wind-Speed at 850 hPa
Z_{500}	Geopotential Height at 500 hPa

Acknowledgements

I am very thankful for the opportunity provided by Dr Stephen Déry to pursue this research, for his advice and support, and for the various tranches of funding he has made available (primarily from a Discovery Grant provided by the Natural Sciences and Engineering Research Council of Canada). I recognize that my life-stage and personal characteristics may have presented special challenges during this studentship, and appreciate his patience and tolerance. I am additionally grateful for the interest, advice and support provided by members of the advisory committee, Dr Richard Kelly, Dr Dezene Huber, Dr Brian Menounos, and Dr Roger Wheate, and also to Dr Dorothy Hall, and to colleagues in the Northern Hydrometeorology Group.

I thank the University of Northern British Columbia for a range of financial support, including a Graduate Entry Scholarship and Research Award, assistance with the costs of presenting at several major conferences, and a Doctoral Dissertation Completion Award. I am also grateful for funding provided by the Canadian Sea-Ice and Snow Evolution Network (principal investigator Dr Paul Kushner, University of Toronto), sourced originally from the Natural Sciences and Engineering Research Council of Canada as part of the Climate Change and Atmospheric Research initiative.

I particularly appreciate the provision of, and helpful technical assistance and other advice relating to, the Northern Hemisphere snow-cover Climate Data Record, by Dr David Robinson and Mr Thomas Estilow of Rutgers University. I also thank the Climatic Research Unit at the University of East Anglia, the Department of Geography at the University of Delaware, the National Oceanic and Atmospheric Administration Physical Sciences Division and the Cooperative Institute for Research in Environmental Sciences at the University of Colorado, for

making various climate datasets publicly available, and the GLOBE team for publishing their global digital elevation model.

Heartfelt thanks are due to my wife and family for their patient endurance of the many constrictions associated with this extended experience, relating to short supplies of spare time, prolonged financial penury, and sparse personal lucidity.

1. Introduction

1.1. The Importance of Seasonal Snow

Seasonal snow-cover substantially influences physical conditions at and near the land-surface, thereby modulating a wide range of natural and human-related processes. These influences primarily affect the terrestrial mid-latitudes and circumpolar areas of the Northern Hemisphere (NH), which hosts 98% of the global incidence of seasonal snow (Armstrong and Brodzik, 2001; NSIDC web). The high albedo and insulating effects of snow transform landscape characteristics, strongly influencing energy exchanges, in turn cooling the atmospheric boundary layer, and thereby reinforcing winter conditions (Stieglitz et al., 2003; Zhang, 2005; Qu and Hall, 2007; Vavrus, 2007; Cohen et al., 2014). Because snow occurs over large areas even at relatively low extra-tropical latitudes across the NH (e.g. in mountainous areas of the south-west United States of America, Iran, and south-central Eurasia), it accounts for a greater fraction of cryospheric cooling in the NH than polar sea-ice from January to April (Flanner et al., 2011). In ecosystems where snow is the dominant phase of precipitation during the cooler months, many forms of biota have adapted specifically to the challenges and opportunities introduced by these conditions (Jones, 1999). Mankin et al. (2015) estimated that the runoff released by NH snowmelt provides the principal water resource through spring and / or summer for approximately two billion people.

Any substantial disruption in the extent and duration of seasonal snow-cover will alter the distribution, timing and magnitude of transfers within the water and energy cycles, thereby imposing widespread impacts on climatological, hydrological, ecological and anthropological processes. Widely accepted syntheses of anthropogenic climate-change trajectories foresee a

high risk of such outcomes (Kirtman et al., 2013; Vaughan et al., 2013), so there is clear benefit in improving understanding of shifts away from historical snow-cover patterns, by inference from observations made during recent decades. The principal motivation of this research was therefore to contribute new information to this field of study, by generating more detailed descriptions of, and explanations for, spatio-temporal distributions of snow-cover trends.

1.2. Prior Research

Recognition of these key influences of seasonal snow, and of the potential for shifts from historical distributions as a consequence of anthropogenic climate-change, has prompted a series of investigations into inter-annual trends in snow-covered area and duration. Snowpack is inherently spatially heterogeneous, primarily as a result of influences of topography and vegetation on patterns of accumulation, redistribution and ablation (e.g. Pomeroy et al., 1998; Sturm and Benson, 2004; Déry et al., 2004), so it is generally unreliable to use fixed-point measurements to represent conditions over wider areas (Neumann et al., 2006). An additional consideration is that where a station is installed for a specific purpose, perhaps at a site chosen to meet requirements for ready access and security, its setting may be unrepresentative of the wider locale. For example, observations at an airport's meteorological station would not usefully represent conditions in a surrounding extensive forest. More generally, terrestrial observation stations are distributed unevenly, and are particularly sparse in remote or rugged terrain (Peng et al., 2013; WMO web). Moreover, many automated weather stations are unable reliably to distinguish between liquid and frozen precipitation (Mekis et al., 2018). Most investigations have therefore depended largely or entirely on − and been limited in temporal scope by − the availability of remotely-sensed imagery.

The most comprehensive archive of NH snow-cover is provided by the Climate Data Record of weekly visible NH Snow-covered Area (SCA), compiled and curated by the Rutgers University Snow Laboratory, and published by the U.S. National Oceanic and Atmospheric Administration (NOAA) (Rutgers Snow Lab. web; Robinson et al., 1993; Robinson et al., 2012; Estilow, 2013 − hereafter the 'NOAA-Rutgers Snow Archive', NRSA). Spanning the period from October 1966 to the present day, this forms the longest continuous satellite-derived record of any environmental variable (Estilow et al., 2015), and it has been used repeatedly to describe changing patterns of seasonal snow-cover since the mid-1990s. Although data accumulated by microwave sensors have also been used to infer snow conditions at continental to hemispheric scales since the late 1970s (e.g. Biancamaria et al., 2011), reliable interpretation of these datasets depends on detailed knowledge of spatially heterogeneous properties such as snow density and grain-size, snowpack stratigraphy, water-content and vegetation, which may not be available at adequate extents and resolutions (Nolin, 2010; Frei et al., 2012; Pampaloni, 2015). The spatial and temporal frameworks adopted by prior investigations vary widely, and they report disparate metrics, so direct comparisons are seldom possible. However, several principal messages recur among their findings.

Firstly, there has been consistently strong consensus that seasonal snow has been melting earlier in the NH spring, and that these losses have intensified during recent decades (Groisman et al., 1994; Brown, 2000; Dye, 2002; Rikiishi et al., 2004; Déry and Brown, 2007; Choi et al., 2010; Brown and Robinson, 2011; Vaughan et al., 2013; Hernández-Henríquez et al., 2015; Chen et al., 2016). The periods of interest (PoI) on which these studies have been based have ranged from approximately one century (using 'hybrid' datasets reconstructed from ground and spaceborne observations – e.g. Brown, 2000; Brown and Robinson, 2011) to a few decades.

Many of these studies have relied at least in part on the NRSA. While most have explored trends at hemispheric or continental scales, several have also depicted regional variations. For example, Groisman et al. (1994) identified distinct regions of high SCA variability in each season, reflecting fluctuations and systematic changes between 1972 and 1992. They described these Snow Transient Regions as the 'centres of action' of changing SCA patterns, and recommended that they should be monitored through time as key indicators of changing climatic conditions. A key mechanism invoked by this study to explain the observed acceleration of spring ablation was the Snow-Albedo Feedback (SAF), in which less reflective surfaces exposed by snow-melt convert more short-wave insolation into outgoing radiation at longer wavelengths, leading in turn to further melting through heat advection. Thus, as snow-free area increases and snow-patch size decreases, the sensible heat flux to remaining snow patches increases substantially (Marsh et al., 1999). Such effects would be expected to reach their peak in spring, when snow still lies over large areas of the NH and insolation potential rises with increasing day-length (Déry and Brown, 2007; Flanner et al. 2011; Qu and Hall, 2007; Thackeray et al., 2016).

Several investigations have explored regional variability in Snow-cover Duration (SCD) rather than SCA (Dye, 2002; Rikiishi et al., 2004; Choi et al., 2010). SCD anomalies correspond linearly to SCA anomalies (Dye, 2002), so these also provide information about changing spatial patterns. Both Dye (2002) and Rikiishi et al. (2004) found that the date of spring snow melt-out had occurred progressively earlier from the early 1970s to the late 1990s, at rates of between five and three days per decade, with stronger trends at higher latitudes. Choi et al. (2010) showed subtler regional patterns among changes in both the core and full snow seasons, based on simple differencing between two 16-year periods spanning 1972 to 2004. The areas most affected (by either reductions or increases in the season) corresponded broadly to the centres of action

identified by Groisman et al. (1994). While these studies mapped the distribution of shortening or lengthening snow seasons across the NH, they did not provide detailed information about how such trends translated to intra-annual spatial shifts in SCA.

The consistent datasets, spatio-temporal frameworks and analytical methods used by Déry and Brown (2007) and Hernández-Henríquez et al. (2015) to explore trends in NH SCA at weekly intervals (between 1972-2006 and 1971-2014, respectively) provide the most detailed NRSA-derived representations of changes in global SCA trends during the past 15 years. Both studies identified statistically-significant spring declines in SCA: these increased in magnitude from early March to late June, and were broadly coherent between North America and Eurasia. The later paper identified a shift in the week of peak depletion from early- to mid-June; an intensification in the magnitudes of associated trends from ~1.32×10^6 km^2 $decade^{-1}$ (4.63×10^6 km^2 over 35 years) to ~1.50×10^6 km^2 $decade^{-1}$ (6.46×10^6 km^2 over 43 years) over the intervening seven years; and a greater fractional increase in SCA losses in Eurasia (~34%) than North America (~21%). However, as both studies reported results only at continental and hemispheric scales, there would be substantial benefit in building on their findings by exploring distributions of trends at finer spatial resolutions.

Secondly, while overall trends in SCA at continental scales are negative, some regions of the NH have seen augmented SCA during the transition from late summer to winter (Frei et al., 1999; Brown, 2000; Rikiishi et al., 2004; Choi et al., 2010; Cohen et al., 2012). Indeed, Brown (2000) identified overall positive tendencies through a 1915-1997 SCA record reconstructed from both ground and spaceborne observations in every month from November to April, with significant ($p < 0.05$) trends from November to January. This study concurred with the suggestion of Frei et al. (1999) that the North American snow season may be shifting, with an

earlier start and finish. Rikiishi et al. (2004) identified trends of nearly two weeks per decade in earlier onset of snow-cover throughout the mountain ranges of eastern Europe, central Asia, the eastern Tibetan Plateau and Rocky Mountains between 1972 and 2000. Regional increases in both the full and core seasons were also shown by Choi et al. (2010), particularly in the U.S. prairies, from central-eastern Europe to the Caucasus, over the eastern Tibetan Plateau and in central China, with smaller pockets in the eastern U.S.A., southern Scandinavia, Siberia, and Japan. Both Déry and Brown (2007) and Hernández-Henríquez et al. (2015) identified substantial positive trends in weekly SCA within North America, Eurasia and the entire NH from October to February, although few individual values achieved statistical significance. Cohen et al. (2012) also described highly significant SCA trends over Eurasia in October from the NRSA.

However, several studies have cast doubt on the veracity of positive early-season SCA trends generated from the NRSA (Wang et al., 2005; Brown et al., 2007; Brown and Derksen, 2013; Mudryk et al., 2017; Hori et al., 2017). These authors found no comparable evidence for increases in snow-covered area during autumn and early winter in several other representations of NH SCA, both modelled and observed. They also asserted that negative trends yielded by the NRSA through spring and summer are considerably stronger than those from other sources. An explanation suggested for these disagreements was that the NRSA's ability to distinguish snow-covered from snow-free ground was improved considerably by the replacement of the original manual interpretation process with the substantially more automated Interactive Multisensor Snow and Ice Mapping System (IMS), together with improvement of the imagery's spatial resolution from ~190 km to 24 km, and temporal resolution from weekly to daily, in 1999 (Ramsay, 1998; Estilow et al., 2015). On the other hand, concerted efforts were made to ensure that these advances did not result in inconsistencies in the detection of snow arising either side of

their introduction (Romanov et al., 2000; Helfrich et al., 2007; Estilow, 2013; Estilow et al., 2015). Furthermore, the studies raising these concerns did not adequately represent several aspects of uncertainty associated with the estimation of SCA trends based on the NRSA's binary classification and spatial framework, so further investigation is warranted.

Thirdly, SCA and SCD trends vary with latitude, elevation and surface vegetation, and their distributions shift through the snow-year. With rates of warming in the Arctic approximately twice those at lower latitudes (Serreze et al. 2009; Screen and Simmonds, 2010), and SCA heavily dependent on surface temperature (Groisman et al., 1994; Mudryk et al., 2017), it is expected that major losses would be identified in terrestrial circumpolar regions. Moreover, as snow persists here well into the summer, when day-length may be up to 24 hours, and SAF intensifies with insolation potential (Qu and Hall, 2007), it follows that larger losses are likely in these settings. This is also the case for high-elevation areas at lower latitudes, where an enhanced climate-change signal was first suggested by Fyfe and Flato (1999), and recently revisited by Wang et al. (2015) and Sharma and Déry (2016). Both Déry and Brown (2007) and Hernández-Henríquez et al. (2015) identified signs of amplification of negative NH SCA trends at higher latitudes and elevations, but did not map their spatial distributions. It would therefore be beneficial to refine understanding of associations between snow-related trends, latitude, altitude and other contextual characteristics.

The fourth recurrent finding is that SCA and SCD are strongly influenced by surface temperature and atmospheric circulation patterns. Both the accumulation and ablation of snow depend on numerous influences, so tracing the drivers of SCA trends is not straightforward, and this has prompted extensive investigation and discussion. Prior research has been guided by the recognition that – within a specified geographic domain – different atmospheric indices may be

associated either with the coincidence of sub-freezing temperatures and adequate humidity to result in snowfall, or with warm and / or dry and / or windy conditions, accelerating snowpack losses. These studies have considered (among others) the El Niño Southern Oscillation (Groisman et al., 1994); North Atlantic / Arctic Oscillation (Clark et al., 1999; Brown and Robinson, 2011; Biancamaria et al., 2011; Cohen et al., 2012; Zhao et al., 2016); Atlantic Multidecadal Oscillation (Biancamaria et al., 2011); Eurasian Type 1 (Clark et al., 1999); Siberian Pattern (Clark et al., 1999; Zhao et al., 2016); Pacific Decadal Oscillation, Pacific North American and North Pacific Index (Mote, 2006; Biancamaria et al., 2011); and the Antarctic Pattern (Zhao et al., 2016). However, each of these indices describes a distinct component of atmospheric activity: interference and resonance between them may drive contrasting responses in different areas. It would therefore be useful to explore whether associations exist between snow-related trends and more comprehensive representations of the overall continuum of atmospheric circulation.

Representations of the behaviour of the Arctic Front and associated polar jet are of particular interest, because of their close relationships with mid-latitude NH weather systems (e.g. Thompson and Wallace, 2001). Several studies have linked Arctic amplification of warming with weaker circumpolar tropospheric and stratospheric winds, leading to an increase (reduction) in meridional (zonal) airflows, and thus the potential for southward (northward) incursions of arctic (tropical) air-masses (Overland et al., 2011; Francis and Skific, 2015; Francis et al., 2017; Kretschmer et al., 2017). Regional variation in the sign and intensity of these effects has also been linked to contrasting maritime / continental contexts (Screen and Simmonds, 2014). These more frequent and / or extensive polar outflows may advect atmospheric water vapour sourced from more ice-free Arctic waters, thereby augmenting snowfall at lower latitudes (Cohen et al.,

2014; Wegmann et al., 2015; Kretschmer et al., 2016; Cohen et al., 2018). While some authors see these developments as extreme events within the range of long-term natural variability rather than clear manifestations of anthropogenic climate-change, particularly over Eurasia (Sun et al., 2016; McCusker et al., 2016), they would nevertheless be expected to have altered the distribution of snow-cover during recent decades. In principle, shifting influences of this nature could translate into longitudinal variations in snow-cover trends, so there is value in exploring the development of such patterns during recent decades.

In summary, prior studies have shown that seasonal snow has been melting earlier in the NH spring, and that these losses have intensified during recent decades. In contrast, the NRSA indicates that SCA has been augmented during the transition from late summer to early winter, particularly over Eurasia. However, questions have been raised about the credibility of these observations. More generally, SCA trends vary in sign and magnitude with spatial and temporal context. Because SCA is strongly influenced by temperature, humidity and wind-speed (and direction), key factors include insolation potential (and thus latitude and time of year), degree of exposure to the free atmosphere (and thus elevation), availability of precipitable water vapour, and the contrast in albedo between snow-covered and snow-free conditions (and thus land-cover). Linked with these considerations, shifting atmospheric circulations, whether driven by anthropogenic warming or long-term natural variability, are also likely to play an important role in determining changing distributions of snow-cover.

1.3. Research Scope, Goals and Dissertation Structure

This review (Section 1.2) suggests that it would be beneficial to augment existing knowledge of the locations, timings and magnitudes of trends in snow-covered area (and their

variation throughout the year) and snow-season duration across the NH during recent decades. Doing so would respond to the recommendation of Groisman et al. (1994) that 'centres of action' of inter-annual SCA variability should continue to be monitored through time as key indicators of changing climatic conditions, and illustrate seasonal variation of associations with context. The principal goals identified for this investigation were therefore to generate more detailed quantitative spatio-temporal descriptions of the variability of SCA and SCD trends across the NH, and to improve understanding of their driving influences.

The NRSA provides a comprehensive and consistent representation of NH snow-cover on which to base this research. However, the questions raised about the NRSA's credibility by several authors (Wang et al., 2005; Brown et al., 2007; Brown and Derksen, 2013; Mudryk et al., 2017; Hori et al., 2017) imply a pressing need to examine critically whether or not it offers a reliable foundation for research of this type. An additional goal identified for this study was therefore to assess the degree to which trends identified from the NRSA may derive wholly or partly from technological improvements associated with the introduction in 1999 of the IMS, against the alternative possibility that they correspond temporally and spatially with external causative factors represented by independent metrics. A further consideration was the influence on trend magnitudes of assumptions adopted when translating the NRSA's binary classification of snow-cover to representations of NH snow-covered area, and its variation through the snow-year.

This dissertation therefore describes the results of research intended to attain the following principal objectives:

1) Generate detailed descriptions of the spatio-temporal variability of trends in the extent and duration of NH seasonal snow-cover between 1971 and 2014 from the NRSA. Quantify associations with latitude and elevation at relevant spatial and temporal scales.

2) Assess the influence on trend magnitudes of assumptions adopted when translating the NRSA binary classification of snow-cover to representations of NH snow-covered area, and its variation through the snow-year, within broad landscape categories.

3) Describe the spatial and temporal distributions of trends in the onset of NH snow-dominated conditions between 1972 and 2017, as identified from the NRSA. Quantify associations with contextual metrics, including latitude, elevation, mean date of onset, and associated monthly mean precipitation and temperature.

4) Describe the temporal trajectories of onset-date anomalies, and compare these with equivalent summaries for temperature and precipitation. Assess the degree to which these patterns imply major changes coinciding with technological improvements to the NRSA in 1999.

5) Describe the spatio-temporal contexts of significant NH snow-onset trends between 1972 and 2017, in relation to means of, and trends in, metrics of relevant tropospheric activity. Assess the degree to which these imply that plausible climatologically-based explanations exist for the observed snow-onset trends.

The methods adopted to make progress towards these goals, and the findings generated, are presented in the following three chapters, each of which comprises a paper published in, or (at the time of writing) in review by, a peer-reviewed journal.

Chapter 2 (published in *Annals of Glaciology* – Allchin and Déry, 2017) describes spatial distributions of trends in the seasonal duration and, at monthly intervals, the area of snow-dominated conditions across the terrestrial NH between 1971 and 2014. It also demonstrates how the sensitivity of estimated trend magnitudes to assumptions made when inferring 'snow-covered' area from the NRSA's binary classification varies with context during the snow-year.

Driven by the perception that changing patterns in the onset of snow-dominated conditions identified from the NRSA are more counter-intuitive than those relating to their melting, and should therefore be prioritized for investigation, Chapter 3 (published in *Journal of Climate* – Allchin and Déry, 2019) explores related trends across the NH between 1972 and 2017. This paper maps their spatial distribution, describes variations in sign and magnitude, and illustrates their associations with a range of contextual metrics. It also describes the temporal trajectories of their anomalies, and compares these with equivalent summaries of changes in temperature and precipitation.

Chapter 4 (in review as of February 2020 for the *Journal of Geophysical Research – Atmospheres*) develops this analysis in greater detail, by establishing the climatological context of incidences of significantly earlier and later snow-onset across the NH between 1972 and 2017, with reference to a range of metrics describing relevant tropospheric dynamics at monthly intervals, and thereby building explanatory syntheses for the observed trends.

The closing chapter summarizes the key findings of these studies, describes their limitations, recommends pathways for related research in the future, and assesses the implications of the results presented.

2. Spatio-Temporal Analysis of Trends in Northern Hemisphere Snow-Dominated Area and Duration, 1971-2014

This chapter was published in *Annals of Glaciology* (distributed under the terms of the Creative Commons Attribution licence, detailed at http://creativecommons.org/licenses/by/4.0/):

Allchin, M.I., and Déry, S.J. (2017). A spatio-temporal analysis of trends in Northern Hemisphere snow-dominated area and duration, 1971-2014 *Annals of Glaciology,* **58**(75): 21–35 DOI: 10.1017/aog.2017.47

2.1. Abstract

Seasonal snow-cover modulates water and energy budgets across large areas of the Northern Hemisphere. Previous research, based on satellite imagery interpreted and curated by the Rutgers University Snow Laboratory, has identified significant negative and positive trends in annual snow-covered duration and area at hemispheric and continental scales between 1971 and 2014. This study uses the same dataset to generate more detailed descriptions of spatial variations in these trends, maps intra-annual variations in sign, statistical significance and strength, and quantifies associations with latitude and elevation. It also considers the limitations and uncertainties associated with a binary classification of this type, and the implications for trend magnitudes of adopting alternatives to the conventional assumption of 100% (0%) actual fractional snow-covered area in 'snow-covered' ('snow-free') spatial units at different stages of the snow-season. This prompts adoption of alternative terminology, referring to 'snow-dominated' area and duration. In response to questions about the dataset's veracity raised by some prior studies, it discusses climatological factors of potential relevance in explaining spatio-

temporal trend patterns, and considers how biases might possibly have been introduced as a result of extraneous influences.

2.2. Introduction

The importance of seasonal snow-cover to climatological, hydrological, ecological and anthropological processes over large areas in the terrestrial mid-to-polar latitudes of the Northern Hemisphere (NH) is difficult to overstate. Mankin et al. (2015) estimated that the runoff released by snowmelt provides the principal water resource through spring and / or summer for approximately two billion people across the NH, which hosts 98% of global seasonal snow-cover (Armstrong and Brodzik, 2001). Snow also substantially transforms landscape physical characteristics, strongly influencing energy budgets through its high reflectivity and insulating effects (Zhang, 2005; Stieglitz et al., 2003). Because it occurs over relatively wide areas even at lower latitudes, it accounts for a greater fraction of cryospheric cooling in the NH than polar sea-ice from January to April (Flanner et al., 2011). In ecosystems associated with climates where snow is the dominant phase of precipitation during the cooler months, many forms of biota have adapted specifically to the challenges and opportunities introduced by these conditions (Jones, 1999).

Recognition of these key influences of seasonal snow, and of the potential for shifts from historical distribution patterns as a consequence of anthropogenic climate-change, has prompted a series of investigations into inter-annual trends in snow-covered area (SCA) and duration (SCD) (Groisman et al., 1994; Frei et al., 1999; Clark et al., 1999; Brown, 2000; Dye, 2002; Rikiishi et al., 2004; Mote, 2006; Déry and Brown, 2007; Choi et al., 2010; Brown and Robinson, 2011; Biancamaria et al., 2011; Cohen et al., 2012; Liu et al., 2012; IPCC, 2013;

Hernández-Henríquez et al., 2015; Zhao et al., 2016; Yeo et al., 2016). Snowpack is inherently spatially heterogeneous (Pomeroy et al., 1998; Sturm and Benson, 2004; Déry et al., 2004), and terrestrial observation stations are distributed unevenly (Peng et al., 2013), so remotely-sensed imagery has provided an invaluable resource from which to infer representations of snow-covered area over large spatial domains. The datasets used, spatial and temporal frameworks adopted, and metrics reported vary widely, so direct comparisons are seldom possible. However, these studies have consistently delivered four key messages.

Firstly, there is strong consensus that seasonal snow has been melting earlier in the NH spring, and that these losses have intensified during recent decades. Secondly, while overall SCA trends at continental scales are negative, some regions have seen augmented SCA in autumn and / or winter. Thirdly, snow-cover trends vary with latitude and elevation. Because snow persists longer in circumpolar and mountainous regions, and insolation potential increases through the spring and summer, it is to be expected that greater attrition would be identified in these contexts under warming atmospheric conditions. Indeed, enhanced climate-change signals have been detected in both the Arctic (Serreze and Barry, 2011) and mountain ranges (Fyfe and Flato, 1999; Wang et al., 2015). However, no study has as yet described in detail the spatial distribution of trends in both snow-covered area and duration at regional scales across the NH throughout the year. Doing so would respond to the recommendation of Groisman et al. (1994) that 'centres of action' of inter-annual SCA variability should continue to be monitored through time as key indicators of changing climatic conditions, and illustrate any seasonal variation of associations with latitudinal and elevational context. Generating a quantitative representation of these patterns was therefore identified as the principal objective of this investigation.

The fourth point of broad agreement is that NH SCA and SCD are strongly influenced by temperature and atmospheric circulation patterns. The accumulation and persistence of snow both depend on a range of influences: for example, sufficiently cold and humid air is required for snowfall to occur, whereas warm and / or dry and / or windy conditions accelerate its loss. It follows that cyclic patterns such as the El Niño Southern Oscillation (Groisman et al., 1994); North Atlantic or Arctic Oscillation (Clark et al., 1999; Brown and Robinson, 2011; Biancamaria et al., 2011; Cohen et al., 2010; Cohen et al., 2012; Liu et al., 2012; Zhao et al., 2016; Yeo et al., 2016); Atlantic Multidecadal Oscillation (Biancamaria et al., 2011); Eurasian Type 1 Pattern (Clark et al., 1999); Siberian Pattern (Clark et al., 1999; Zhao et al., 2016); and the Pacific Decadal Oscillation, North Pacific Index and Pacific North American pattern (Mote, 2006; Biancamaria et al., 2011) play important roles in the distributions of SCA and length of SCD. Tracing the effects of these multiple meteorological drivers is complex, as they may vary monotonically as well as cyclically, and are further complicated by interference, resonance and teleconnection. A detailed consideration of these influences is therefore outside the scope of this study.

The primary aim of this paper is to build on earlier studies of snow-related trends at hemispheric and continental scales (Déry and Brown, 2007; Hernández-Henríquez et al., 2015) by generating a detailed description of spatial and temporal variations of snow-cover trends across the NH. As well as identifying contexts experiencing major shifts in snow climatology, this will help to identify areas in which changing patterns might signify increasing stress on summer water resources, provide a foundation on which to base analyses of attribution, and contribute to the assessment of potential hydroclimatological regime transitions. The resultant description of intra-annual variations in spatial distributions of snow-cover trends will also guide

future validation studies of the dataset on which the analysis is based, thereby assisting with the quantification of associated uncertainties.

2.3. Data

In common with prior related studies (Déry and Brown, 2007; Hernández-Henríquez et al., 2015), this analysis was based on the U.S. National Oceanic and Atmospheric Administration's (NOAA) Climate Data Record of weekly visible NH snow-cover, compiled and curated by the Rutgers University Snow Laboratory (http://climate.rutgers.edu/snow-cover: Robinson et al., 1993; Estilow, 2013 – hereafter the 'NOAA – Rutgers Snow Dataset', NRSA). With a Period of Record (PoR) dating from 1966, this dataset forms the longest satellite-derived record of any environmental variable (Estilow et al., 2015), and it has therefore been used repeatedly to study NH snow trends. It comprises a binary classification of snow-cover associated with dataset grid points (DGPs) at weekly intervals on a Cartesian 89 × 89 grid overlaid on the NH polar stereographic projection (Estilow, 2013). It is important to note that the area associated with each DGP (supplied with the dataset) varies with latitude, from ~10.7×10^3 km² at the lowest latitudes to ~41.8×10^3 km² near the geographic North Pole (Estilow, 2013).

Each temporal granule of the NRSA is generated over a seven-day period, from Tuesday to Monday. For a given week, if (on the latest day of that week on which it is unobscured by cloud on the source imagery) at least 50% of the area associated with an DGP is identified by the interpretative process as being snow-covered, the DGP is classified as such. This analysis used the same masks applied by the prior studies (Déry and Brown, 2007; Hernández-Henríquez et al., 2015) to exclude DGPs in oceanic areas or having perennial cryospheric cover (mainly

Greenland), together with an additional 33 DGPs previously associated with questionable snow-cover records (Déry and Brown, 2007).

While the NRSA PoR begins in October 1966, it includes gaps during nine months between 1968 and 1971, so this study was based (as in Hernández-Henríquez et al., 2015) on the continuous series from October (week 40) 1971 to September (week 39) 2014. The dataset was supplied directly by the Rutgers University Snow Laboratory in November 2014, and was identical to the 'version 1 revision 1' instance archived by NOAA to the same date (Robinson et al., 2012; T. Estilow, personal communication, August 2017).

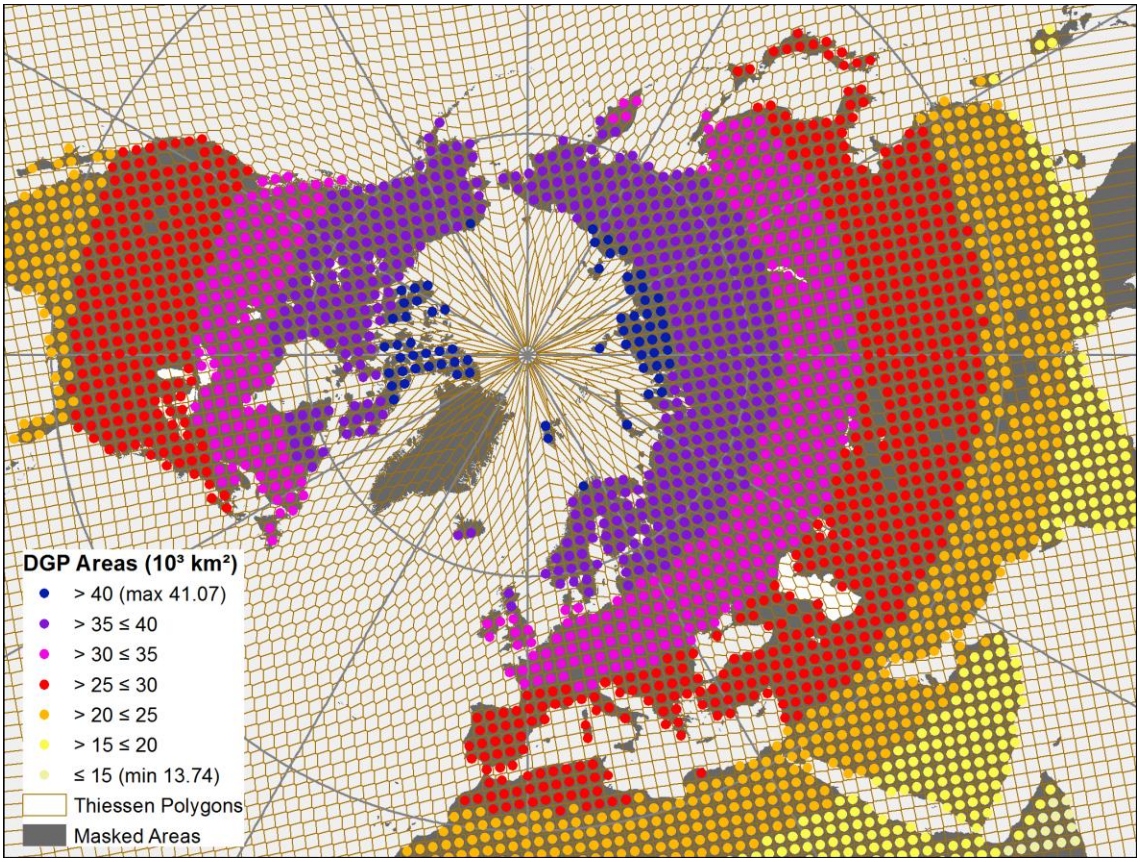

Figure 2.1: NRSA dataset grid points (DGPs), with associated Thiessen Polygons (TPs) and corresponding areas. TPs coloured entirely grey or white are excluded from the analysis.

During its history, major advances in hardware and software capabilities have enabled a series of improvements to the sensors and processing algorithms used to generate the dataset: in

particular, interpretation shifted from a primarily manual process to the more automated Interactive Multisensor Snow and Ice Mapping System in 1999 (Ramsay, 1998). While considerable care has been taken to ensure overall consistency throughout the entire PoR (Romanov et al., 2000; Helfrich et al. 2007; Estilow, 2013; Estilow et al., 2015), several authors have suggested that these developments may have resulted on the one hand in the identification of substantially more snow during the early stages of the annual snow-accumulation season (snow-onset), and less in the latter stages of the ablation season (snow-offset), giving rise to spurious positive and negative trends at these times, respectively (Wang et al., 2005; Brown et al., 2007; Brown and Derksen, 2013; Mudryk et al., 2017; Hori et al., 2017). The PoR and spatio-temporal frameworks adopted by these studies contrast markedly with those described in this paper, so it is not possible to draw direct comparisons. However, it is hoped that new information generated by this analysis will help to guide further investigation of where, when and why the disagreements reported by these authors occur.

2.4. Methods

2.4.1. Improved Estimation of Terrestrial Area for Coastal DGPs

The spatial extent associated with the NRSA DGPs was represented by Thiessen Polygons (TPs) (Figure 2.1), generated using QGIS software (http://qgis.org). Marine areas within TPs were excluded using a regular grid of points at 10' intervals, classified as terrestrial or oceanic by means of a QGIS spatial join with a spatial dataset of global land-masses. A second spatial join between the TPs and the 10' points enabled computation of the terrestrial and oceanic fractions related to each DGP. Scaling the DGPs' nominal areas by the former thus provided improved estimates of their associated terrestrial areas. The marine portions excluded amounted to 5.7% of

the total area associated with the 1666 NRSA DGPs identified by the standard masks as being 'terrestrial' and having mean annual SCD of at least one week (3.1×10^6 km² of 53.8×10^6 km²).

2.4.2. Estimation of Snow-Dominated Area

Snow-covered area is usually estimated from binary snow-cover classifications such as the NRSA by summing, for each temporal granule, the areas associated with spatial units classified as 'snow-covered'. The implicit assumption is that 'snow-covered' ('snow-free') spatial units consistently have actual snow-cover of 100% (0%). However, 'snow-covered' cells in many spatio-temporal contexts often include snow-free areas, and *vice versa*: this leads to over- and under-estimation of snow-covered area at different times of year, potentially exacerbated by specific land-cover types (Rittger et al., 2013). This assumption would be expected to be particularly erroneous early and late in the snow-season, when actual fractional snow-cover may be slightly less than 50% in some years, and slightly more in others. However, this is the conventional approach on which prior studies have been based, and – in the absence of any reliable indication of actual fractional snow-cover throughout the full PoR – it is therefore also adopted here. A discussion of the possible implications of considering alternative assumptions is included in Section 2.5.2.2, but the key message is that the trends reported here relate more strictly not to changes in 'snow-covered' area, but in the area over which there is judged to be more snow-covered than snow-free terrain. Therefore, the term 'snow-dominated' area (SDA) is used hereafter.

2.4.3. Spatial Aggregation and Trend Estimation

Bearing these points in mind, it is not meaningful to estimate areal trends for individual DGPs in a binary dataset. The investigation of spatial variations in SDA across the NH from the

NRSA therefore required aggregation of DGPs within an appropriate spatial framework. This was achieved using a layer of cells drawn at regular 5° intervals of latitude and longitude, and identifying the DGPs falling within each (again using QGIS spatial joins). While this grid does not align with that adopted by the NRSA, the density of DGPs in the latter is sufficiently high compared with the partitioning imposed by the former (except at very high latitudes, where there is little or no terrestrial area) that adequate representation is achieved across the spatial domain. This partitioning scheme seeks a balance between competing considerations. On the one hand, it is fine enough to provide a useful representation of regional variations in trend signs and magnitudes, while reducing the effects of Scale and Zonation (or Aggregation) associated with the Modifiable Areal Unit Problem (e.g. Dark and Bram, 2007). On the other, it is large enough that each spatial unit covers sufficient of the original DGPs that area-related trends could be estimated, whilst also being computationally and graphically manageable.

Total weekly SDA was computed throughout the PoR in each 5° cell as the sum of the terrestrial areas of all constituent snow-dominated gridpoints. The dataset includes details to support inference of the month(s) with which each weekly granule is associated, enabling monthly mean SDA values to be extracted. In this way, a time-series comprising 43 SDA values (spanning 1971 – 2013 for October to December, 1972-2014 for January to September) was generated for each month in every 5° cell.

Because the surface footprint of the 5° cells decreases towards the North Pole, and also because individual cells include considerable oceanic fractions and / or DGPs excluded from the analysis by the various masks described previously, the terrestrial area of each cell represented within the NRSA varies considerably (further detail is provided in Appendix 1, Section A1.1). This constrains the maximum potential SDA in each cell, and therefore also its maximum

possible trend magnitude when expressed in absolute units. In view of these considerations, SDA time-series were also compiled for each cell as fractions of the total terrestrial area associated with the DGPs located within its footprint and included in the analysis (i.e., not excluded by the various masks). Trends generated from the absolute units are useful for providing metrics aggregated at regional to hemispheric scales, particularly for comparison with values from other studies, while those based on the fractional cover improve the spatial consistency of cartographic visualisation, and more directly support the quantification of associations with latitude and elevation.

Monotonic trends were identified from these series by Mann–Kendall Trend Analysis (MKTA: Mann, 1945; Kendall, 1975), and the magnitudes of significant ($p < 0.05$) trends were estimated by least-squares regression. The rationale for using this approach, rather than the Theil–Sen method (Theil, 1950; Sen, 1968), is provided in Appendix 1, Section A1.2.

2.4.4. Snow-Season Duration

As described by Dye (2002), anomalies in the area and seasonal duration of snow-cover share a strong linear relationship. For consistency with the definition of SDA provided above, that used here for Snow-Dominated Duration (SDD) is the count of weeks per snow-year (1 October to 30 September in the following year) in which an DGP is flagged in the NRSA as being 'snow-covered' (i.e., its associated area is at least 50% snow-covered). The sub-set of NH DGPs with appreciable but clearly seasonal snow-cover was identified as those having median 1971-2014 SDD of at least four weeks and no more than 48 weeks. SDD trends were again identified by MKTA, and the magnitudes of significant ($p < 0.05$) trends quantified by least-

squares regression. For this analysis, no distinction was made between the core and full snow seasons (c.f. Choi et al., 2010).

2.5. Results and Discussion

2.5.1. Spatial Distribution of SDD Trends

Over the total area experiencing median seasonal SDD of 4 – 48 weeks (total area 47.3×10^6 km²), significant ($p < 0.05$) negative SDD trends were identified for DGPs representing 23.3% (11.0×10^6 km²), and positive trends were detected over 5.4% (2.5×10^6 km²) of the same spatial domain. These trends are mapped in Figure 2.2, which also depicts associations between their spatial distribution and SDD climatology, latitude and topography (as derived from DGP nominal elevations provided with the dataset).

Of particular note are the highly significant negative trends in south-central Eurasia (where the analysis suggests a reduction of SDD by as much as 23 to 32 weeks over the 43-year PoR), the Alborz and Zagros ranges of north-western Iran, the eastern front ranges of the Himalayas, the Rocky Mountains of western North America, and throughout the circumpolar regions of North America, Scandinavia and Russia.

In contrast, the only larger clusters of DGPs with significant positive SDD trends of appreciable magnitude are found in northern and eastern parts of the Himalayan region, including much of the Tibetan Plateau, and in Japan and near the central Pacific coast of Russia. Other DGPs in which increases in SDD are implied are more spatially sporadic.

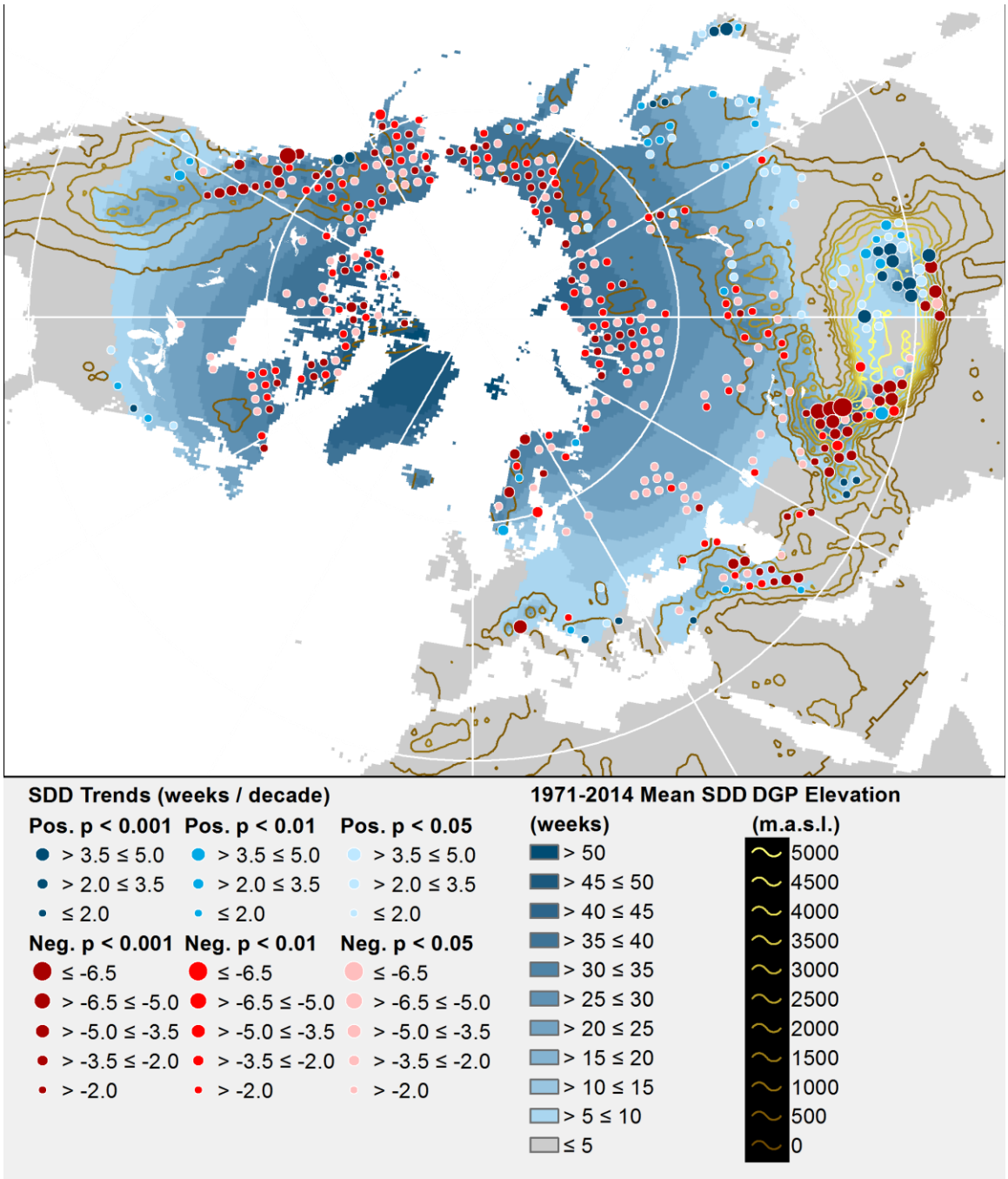

Figure 2.2: Spatial distribution of significant ($p < 0.05$) trends in seasonal duration of DGP snow-dominance, overlaid on 1971-2014 mean annual SDD and coarse topographic contours derived from nominal DGP elevations.

Remembering that the terrestrial area associated with DGPs varies (mainly with latitude), additional information is provided by scaling the magnitude of significant SDD trends (weeks $(43\ a)^{-1}$) by the corresponding DGPs' areas, thereby expressing them in terms of the change in

both time and area over which snow-cover is dominant through the PoR (km^2 weeks $(43\ a)^{-1}$). Binning these metrics across the NH by DGP median annual SDD shows (Figure 2.3) that positive trends occur mainly in areas where snow-cover of at least 50% usually persists for less than approximately four to five months of the year. This relatively short season is most likely to occur in the NH mid-winter (approximately late November to early March), when day-length is short and maximum insolation potential low. This in turn attenuates the potential for disruption of energy budgets by a negative snow-albedo feedback during these times.

It will also be seen that negative shifts only marginally outweigh positive changes, so there is no major overall shift across the NH in areas with these relatively short snow-dominated seasons. In contrast, across areas where snow seasons of 28 to 44 weeks have historically been experienced (so that cover persists well into the spring and summer), negative trends dominate. With maximum insolation potential much higher during these times, particularly at higher latitudes, this will increase the absorption of solar radiation at the land surface, because terrestrial snow-free albedo is much lower than that of snow for virtually all types of land-cover. However, these effects would be expected to vary in strength with land-cover and topography.

The spatial associations apparent in Figure 2.2 suggest links between SDD trends and DGP elevation and latitude, so this was explored in more detail by linear regression (Figure 2.4). The results indicate that the magnitudes of both positive and negative SDD trends strengthen with increasing elevation and at lower latitudes, but that the strongest sensitivity is between negative trend magnitudes and elevation. With both signs of trend thus stronger among the major mountain ranges at lower latitudes (Figure 2.2), longitudinal variations were also explored. This revealed a clear split between the strongest negative (positive) trends on the highest westward (eastward) slopes of the south-Asian mountain ranges (Figure 2.5). There also appears to be a

preponderance of negative trends on the westward (i.e. windward) slopes of the North American Western Cordillera.

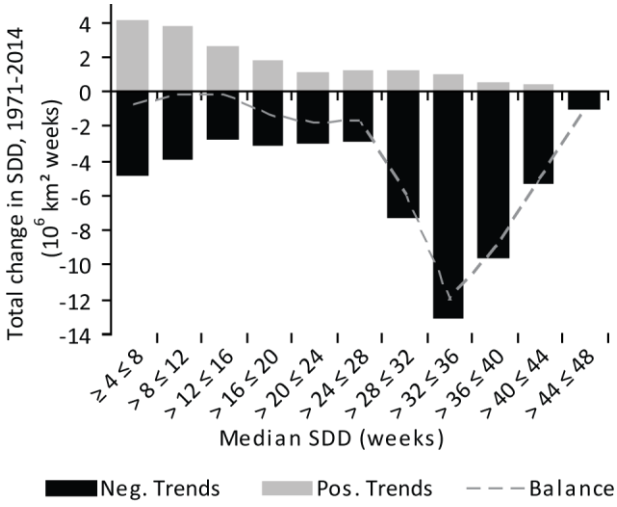

Figure 2.3: Summed significant 1971-2014 changes in NH snow area-duration (km² weeks), in bins of median SDD.

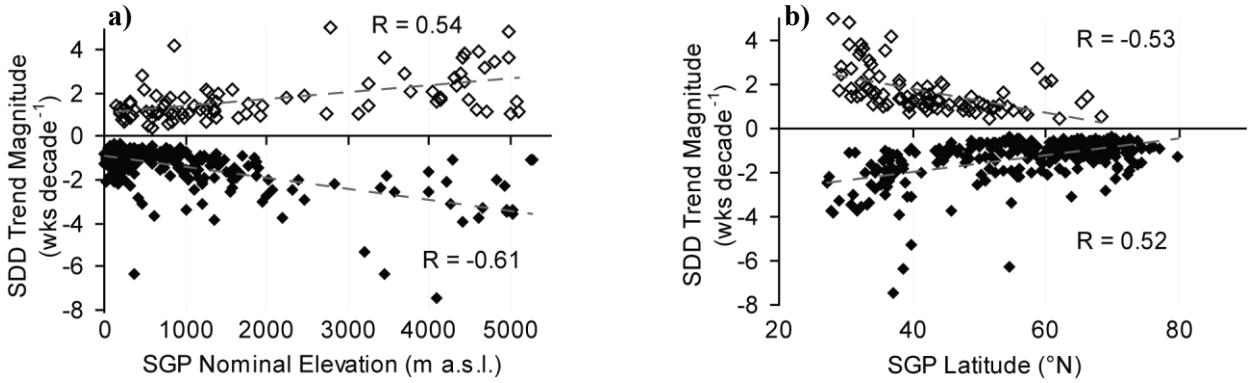

Figure 2.4: Variation in significant ($p < 0.05$) 1971-2014 SDD trend magnitudes with a) elevation and b) latitude for DGPs with median (1971-2014) SDD of 4 to 48 weeks. All correlations are significant with $p < 0.001$.

With the strongest trends of each sign thus identified at similar altitudes and latitudes, but with a clear longitudinal split relating closely to topography, it is difficult to account for them purely as artifacts of improvements in spatial resolution of the source imagery. A possible explanation for positive trends is that higher humidity in the warmer atmosphere, in conjunction

with orographic uplift (and perhaps altered airflows), may have been augmenting snowfall in these contexts. Meanwhile, in upland areas across which losses are identified, exposure to circulations of warmer air in the free atmosphere may have been accelerating ablation, as suggested by Fyfe and Flato (1999). The longitudinal split between high-altitude SDD losses and gains identified here fits neatly with these invocations of contrasting atmospheric influences, particularly in the light of ideas relating to shifts in the frequencies and strengths of zonal and meridional air-flows driven by amplified climate-change in the Arctic (e.g. Francis and Skific, 2015).

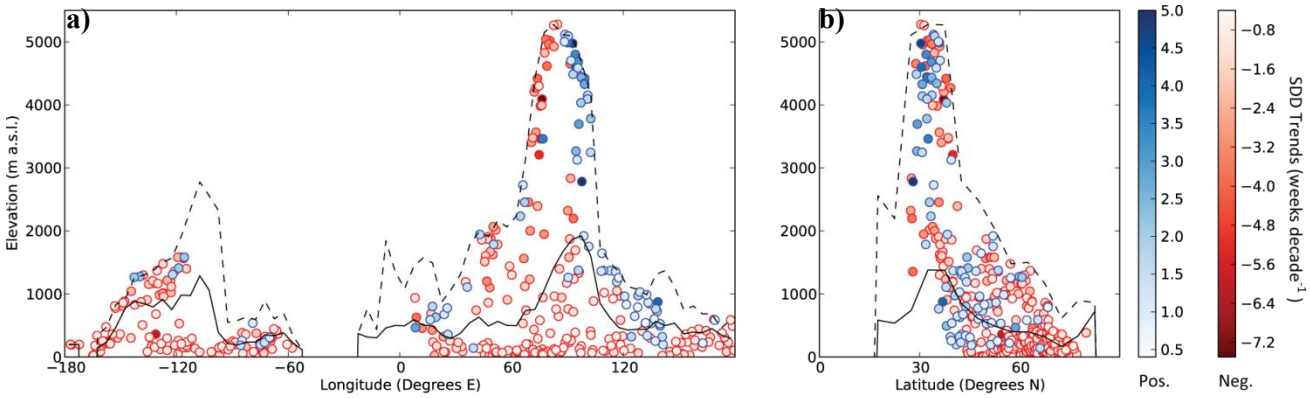

Figure 2.5: Distributions of significant ($p < 0.05$) 1971-2014 SDD trends with elevation, longitude and latitude among DGPs with median (1971-2014) SDD of 4 to 48 weeks. The solid (dashed) lines represent meridional (in a) and zonal (in b) mean (maximum) elevations.

While generally stronger at higher elevations (and thus lower latitudes), significant positive SDD trends are also identified for approximately 37 DGPs with associated nominal elevations below 2000 m and south of latitude 50° N. These are scattered along a latitudinal band around 40° N, from eastern through central Asia, southern Europe, and near both coasts of North America. In general, these areas are associated with positive SDA trends during early winter, for which descriptions and possible causative factors are provided in Section 2.5.2. However, some of these DGPs are close to the southern limit of the zone experiencing at least four weeks of

snow-cover annually, and / or near coastlines: as snow extent will probably be less continuous in such contexts, it is possible that additional areas of this patchy cover have been identified by higher-resolution imagery deployed in the latter part of the PoR. These locales thus present an interesting focus for comparisons between the NRSA and ground observations or other remotely-sensed imagery.

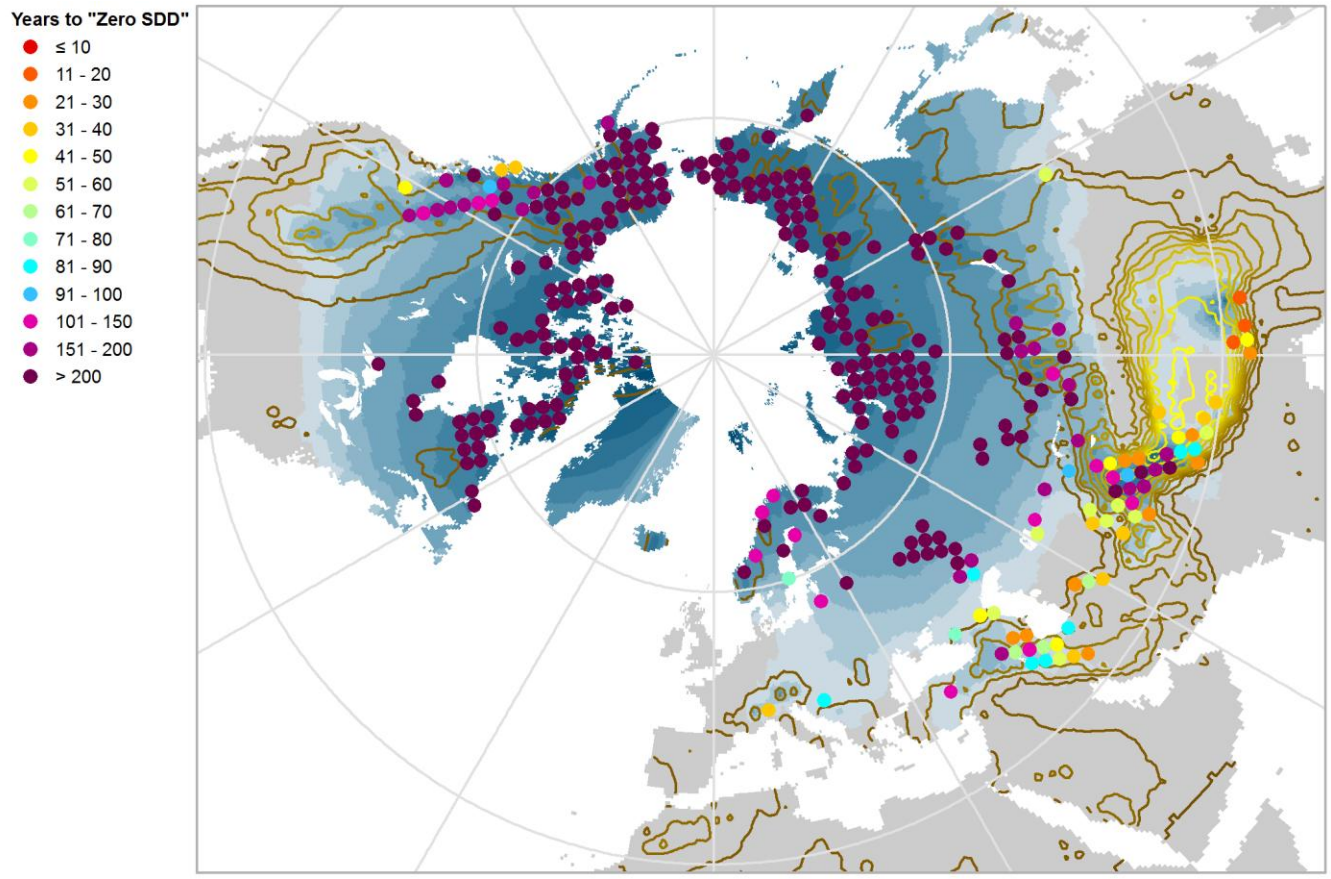

Figure 2.6: DGPs with significant ($p < 0.05$) negative SDD trends, rendered by quotients of 1971-2014 mean snow season length (weeks) and trend magnitude (weeks year^{-1}). This (nominally) represents the number of years remaining, at current rates of change, until the annual count of snow-dominated weeks drops to zero. Shading (1971-2014 mean SDD) and contours (elevation m a.s.l.) as in Figure 2.2.

The relative vulnerabilities of the snow-dominated seasons associated with DGPs experiencing significant negative SDD trends were quantified by dividing their 1971-2014 mean annual SDDs by the corresponding trend magnitudes (Figure 2.6). While these values might in

principle be interpreted as first-order approximations of the years remaining before the number of weeks with at least 50% snow-cover diminishes to zero, assuming a continued linear decline, it would clearly be highly simplistic to do so. Future reductions in SDD will depend heavily on rates of atmospheric warming (IPCC, 2013) and the amplification of SDA losses by the positive snow-albedo feedback (Thackeray and Fletcher, 2016), so it is highly improbable that these trajectories will be linear.

Nevertheless, this approach helps to identify focal points of dramatic shifts in snow climatology within the next few decades. By this measure, the areas likely to be most seriously affected are seen to be concentrated in the uplands south of the Caucasus into north-western Iran, from the Hindu Kush to the southern fringe of the Himalayas, and more sporadically in parts of southern Europe and western North America. It is notable that many of these DGPs are located within areas identified by Mankin et al. (2015) as depending on snowmelt to provide large fractions of otherwise unmet demand during the spring and summer months.

2.5.2. Spatio-Temporal Distribution of SDA Trends

Overall, total NH SDA trends yielded from the NRSA vary in line with the annual solar cycle, with gains identified in autumn and winter, and losses in spring and summer (Figure 2.7). The majority of the significant trends identified are negative, and these dominate from March to September. Summed positive trends outweigh losses from October to February, but their total magnitudes and spatial extent are considerably smaller than the summer losses.

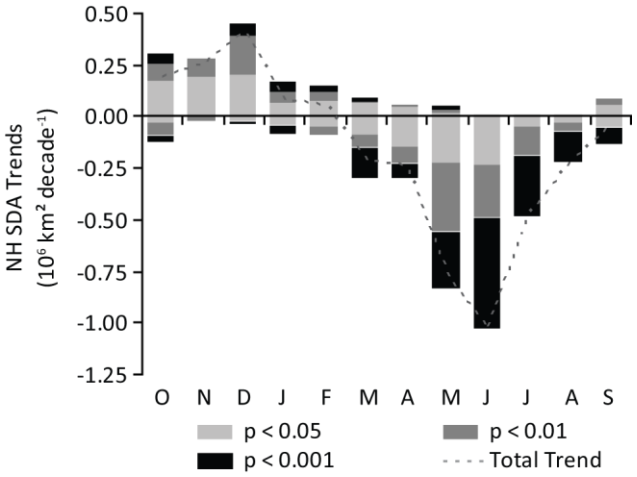

Figure 2.7: Monthly variation in total NH SDA trend magnitudes (1971-2014) by statistical significance level.

The month of peak gains derived by these methods from the 1971-2014 PoR is December, in contrast to that identified from the NRSA using the spatial and temporal frameworks adopted by Mudryk et al. (2017) and Hori et al. (2017), which occurs in October. The maximum aggregate positive monthly trend identified by this analysis (0.415×10^6 km² decade^{-1}) is approximately 40% of that reported in these studies. However, the timing and magnitude of peak losses in June broadly agree with their estimates. It is again important, though, to note that these estimated magnitudes are based on the erroneous – but, for practical purposes, currently unavoidable – conventional assumption that the areas associated with DGPs flagged as being 'snow-covered' ('snow-free') are 100% (0%) snow-covered: more realistic values would be considerably lower (see Section 2.5.2.2).

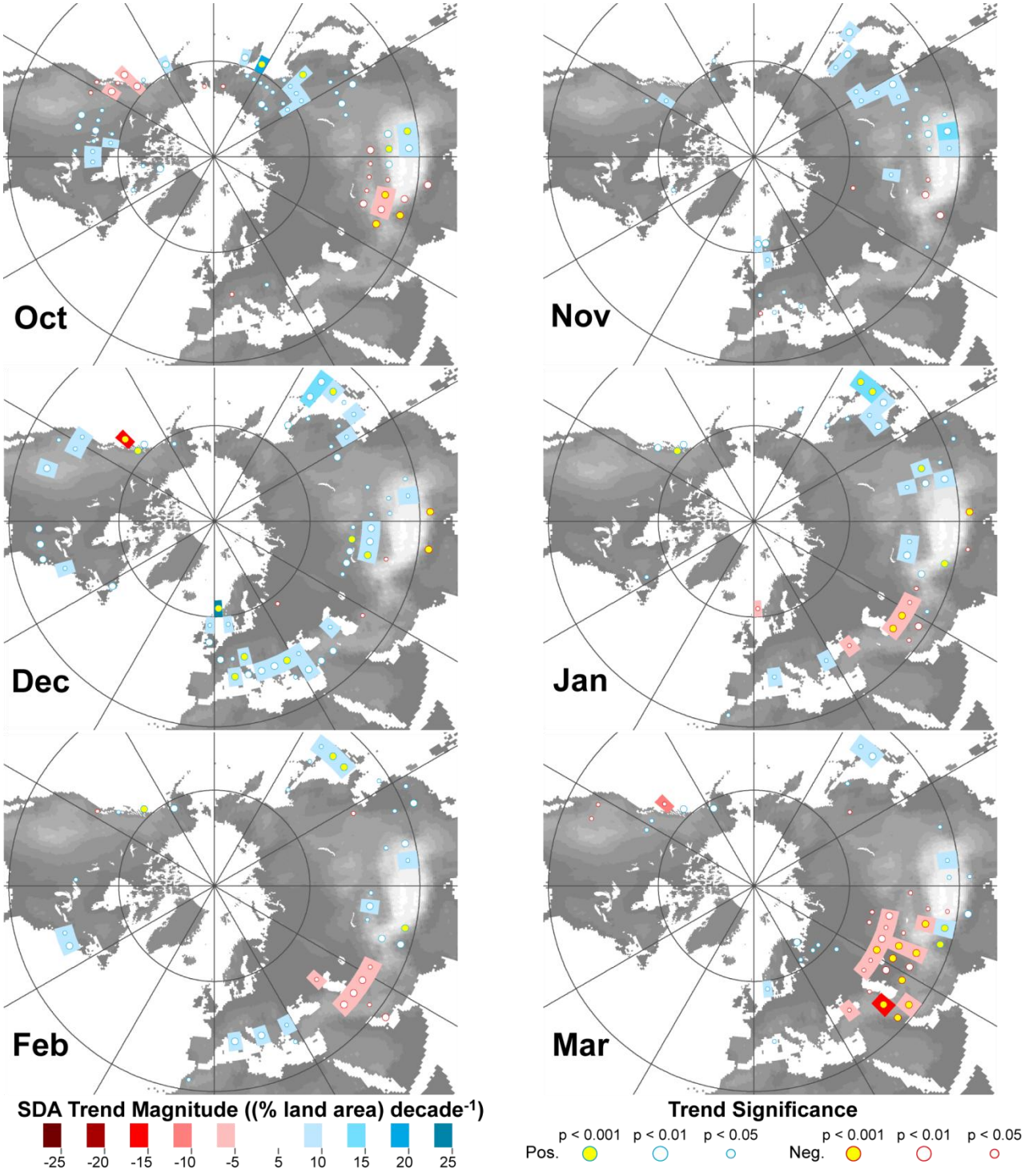

Figure 2.8: Monthly distributions of NH SDA trends (1971-2014) as (% terrestrial area) decade^{-1} (Oct. – Mar.). (Shading represents topographic variation, from lower (darker) to higher (lighter) elevations.)

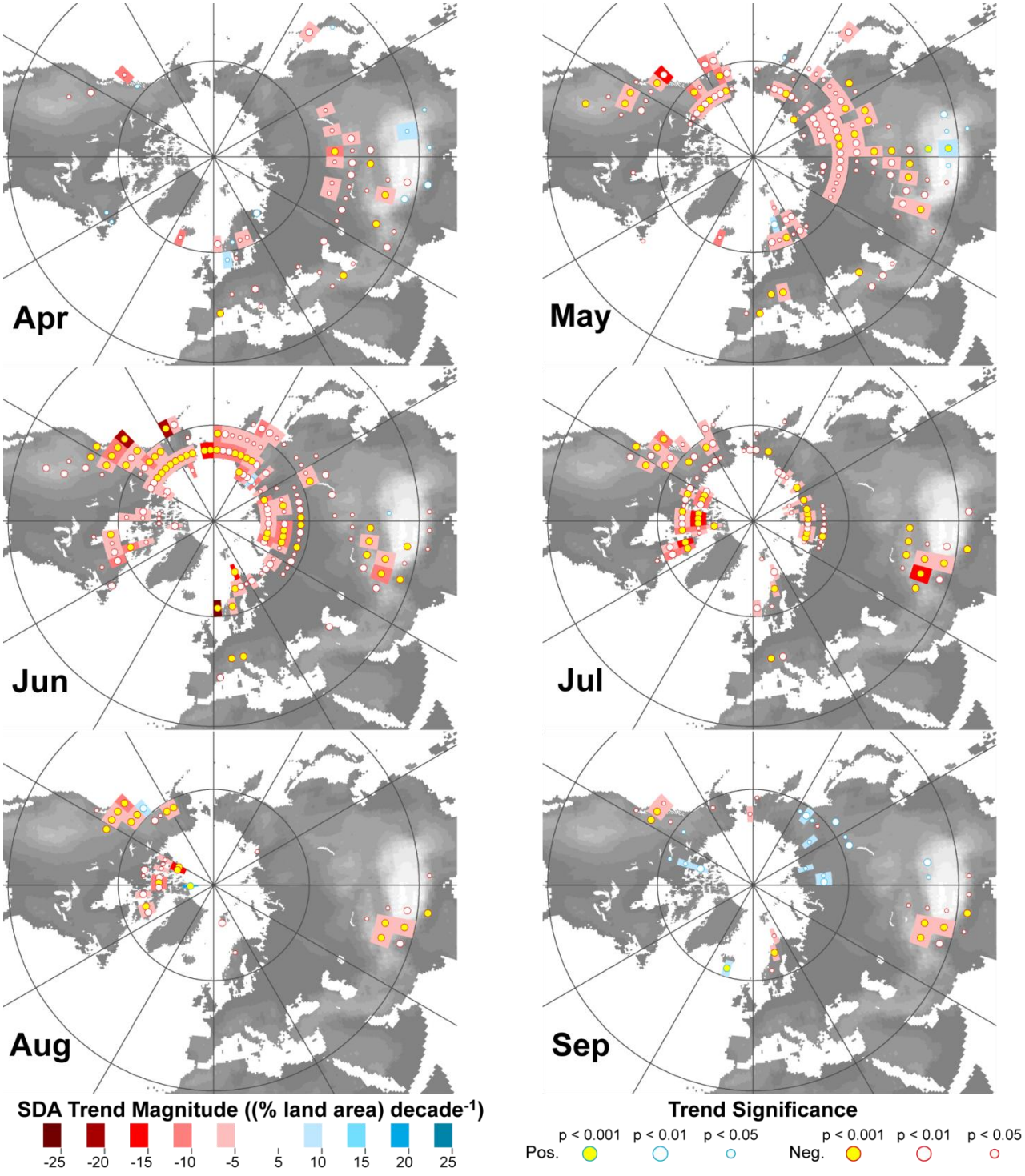

Figure 2.9: Monthly distributions of NH SDA trends (1971-2014) as (% terrestrial area) decade^{-1} (Apr. – Sep.). (Shading represents topographic variation, from lower (darker) to higher (lighter) elevations.)

This provides a spatially consistent illustration of variation in trend magnitude, by avoiding distortion within those 5° cells containing substantial oceanic areas and / or masked NRSA

DGPs. (An equivalent map for trends expressed as absolute areas per unit time is available in Section A1.3 of Appendix 1.) By comparing Figure 2.2 with Figures 2.8 and 2.9, it will be seen that SDD trends coincide spatially with areas experiencing SDA trends, but that the latter vary in location, sign and magnitude through the year. They develop in the form of two extended pulses, one positive and the other negative: because the incidence of snow is controlled largely by latitude and elevation, the migration of these pulses is also guided by these attributes.

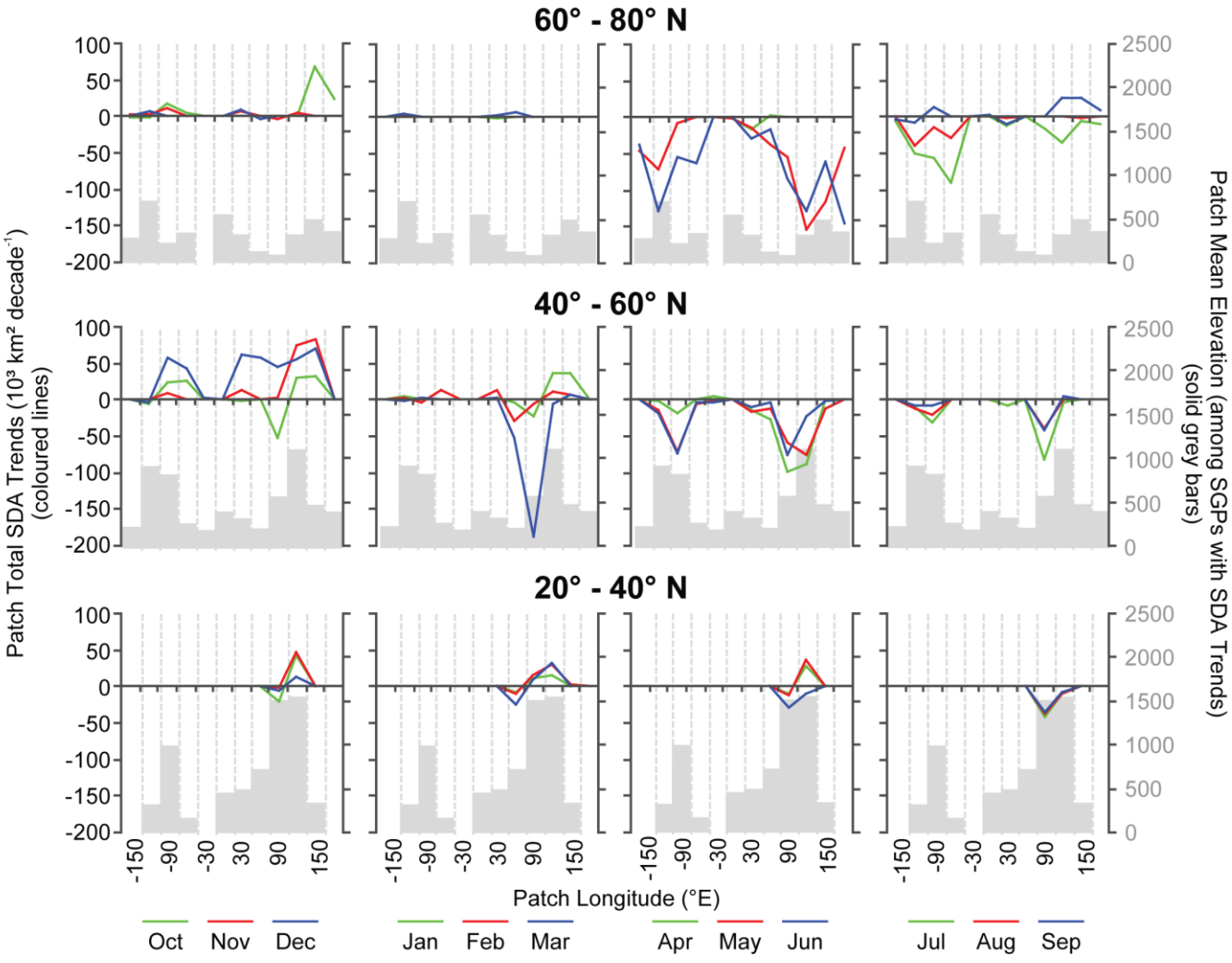

Figure 2.10: Seasonal variations in significant ($p < 0.05$) 1971-2014 monthly SDA trends for 5° cells (as km² decade^{-1}) summed within 20° latitude by 30° longitude patches.

The maps in Figures 2.8 and 2.9 depict the 5° grid rendered by monthly SDA trend magnitudes (significant at $p < 0.05$) derived from time-series of SDA as a percentage of cell terrestrial area.

The positive pulse is moderate in strength, and more widespread and persistent on the Eurasian landmass than in North America. In contrast, negative trends are more widespread, of higher magnitude, and identified at higher levels of statistical significance. Losses are seen initially at lower latitudes of central Eurasia in March and North America in April and May, before migrating rapidly northward, guided along pathways where the influences of latitude, elevation, and continentality have in the past yielded extensive spring and summer SDA. With snow thus limited to the highest latitudes and altitudes by mid-summer, negative trends largely dissipate and retreat, persisting through September only in the mountain ranges of western Canada and from the Himalayas to the Hindu Kush.

To complement this relative depiction, seasonal variations in trends derived from absolute SDA (km^2 $decade^{-1}$) in the 5° cells were aggregated within 20° (latitude) × 30° (longitude) patches (Figure 2.10). These plots, together with representations of corresponding mean elevations, again show that both positive and negative trends may occur in a given month at comparable latitudes and elevations, but in different longitudinal ranges. For example, negative trends occur through most of the year on the western side of the Hindu Kush – Himalayan region, but positive trends are meanwhile seen in the eastern Himalayas and Tibetan Plateau. This corresponds with the identification of stronger negative SDD trends on the upper westward slopes of the south Asian ranges, and positive trends on the upper eastward slopes (Figure 2.5). Indeed, more detailed figures relating SDA trend sign and magnitude to latitude, longitude and elevation (provided in Section A1.4 of Appendix1) suggest that associations exist between

positive trends and eastward slopes, and negative trends with westward slopes, in the mid-latitudes of both Asia and North America. The possibility thus arises again that interactions between atmospheric circulations, associated weather systems and (where appropriate) major topographic features are influencing these patterns, particularly in the light of recent studies relating changes in zonal / meridional airflows to shifting regional meteorological conditions (Screen and Simmonds, 2010; Francis and Skific, 2015; Wegmann et al., 2015; Francis et al., 2017).

2.5.2.1. Associations between SDA Trends, Elevation and Latitude

Figure 2.10 suggests that the NRSA records strong negative impacts on SDA climatologies, predominantly through the NH spring and summer in upland areas and in (the more generally lower-elevation) terrain at higher latitudes. However, the same plots suggest that positive trends coincide mainly with mountainous areas. Therefore, covariant associations were sought between monthly SDA trends of both signs and the latitudes and mean elevations of the 5° cells by linear regression.

The magnitudes of significant ($p < 0.05$) monthly SDA trends used here were again generated from the time-series of SDA expressed as fractional cover of terrestrial areas, to negate the influence of significant associations between latitude, elevation and the area of the 5° cells (see Appendix 1, Section A1.1). To simplify the visualisation of relationships between negative trend strengths and each influence, their absolute values were used. The elevation of each 5° cell was represented by the mean of the elevations of DGPs falling within it (as supplied with the NRSA), with its latitude taken at the cell centroid.

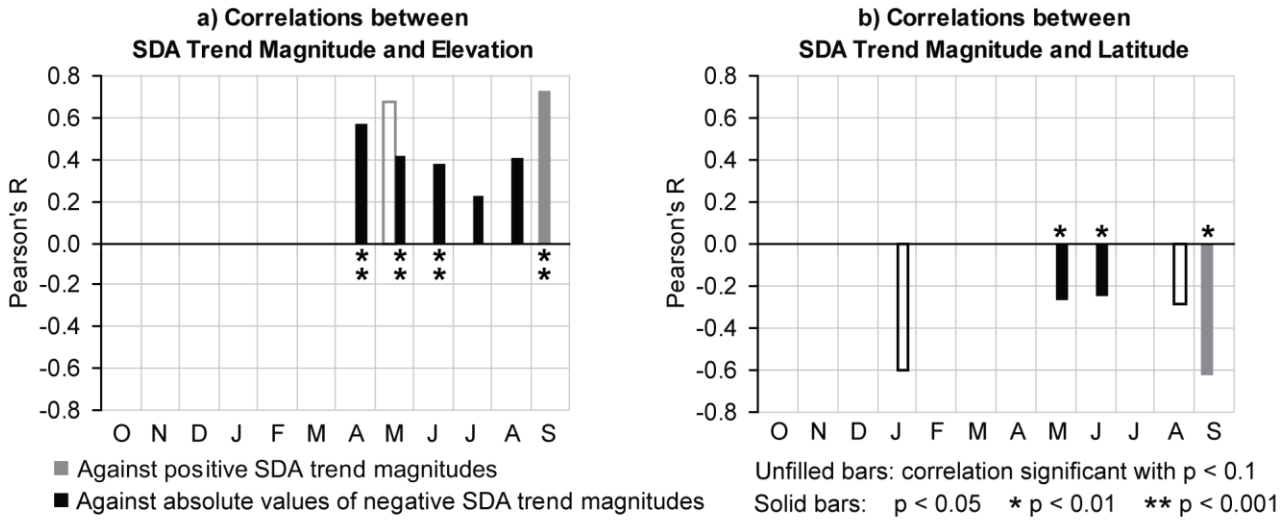

Figure 2.11: Variation in correlation coefficients (Pearson's R) between monthly SDA trend magnitudes generated in 5° cells from % terrestrial snow-covered area (1971-2014) and a) cell mean DGP elevation, b) cell centroid latitude. Note that absolute values of negative trend magnitudes were used in the correlations, to simplify representation of how their strengths relate to each potential influence.

This analysis yielded significant correlations primarily in the NH summer (Figure 2.11), with negative trends strengthening from April to August at higher latitudes, and in May and June at lower elevations. Significant correlations for positive trends are identified only in September, when they are found to strengthen at higher latitudes and lower elevations (noting again that a significant negative correlation exists between elevation and latitude, as detailed in Appendix 1, Section A1.1).

2.5.2.2. Implications of Alternative Assumptions Relating to the Binary SDA Classification.

As described in Section 2.4.2, the estimates of trend magnitude presented here were derived using the conventional assumption that the actual area of snow-cover associated with an DGP flagged as being 'snow-covered' ('snow-free') is 100% (0%) of its associated terrestrial footprint. However, as demonstrated by Rittger et al. (2013), this is seldom the case. Early and late in the snow-season, when the area covered by snow within each spatial unit passes through

the 50% threshold, the contrast in actual fractional cover (AFC) between the two states may only be of the order of a few percentage points. In summer, while 0% AFC is generally much more feasible, 100% AFC is improbable even in the areas associated with highly snow-prone DGPs (remembering that this analysis seeks to exclude those with perennial cryospheric cover). Similarly, in winter (and given the NRSA's range of spatial resolutions) many 'snow-free' DGPs would reasonably be expected to have some appreciable amount of snow-cover. While the terminology employed here of 'snow-dominated' – rather than 'snow-covered' – duration and area aims to acknowledge and emphasize this point, it is useful to consider the results of making alternative assumptions about AFC in the two states. While these values would be expected to vary throughout the PoR for any given DGP and week, additional insights are provided by quantifying the effects of making different assumptions of the contrast between them as if they were fixed, and re-computing the trend magnitudes.

This was explored (using the same 1971-2014 PoR) for the months in which significant trends were identified within spatial units comparable to those adopted by Mudryk et al. (2017), as follows: a) pan-NH ('NH'); b) areas higher than 1500 m above mean sea-level (as indicated by the nominal elevation associated with DGPs within the NRSA: note that Mudryk et al. (2017) distinguished their equivalent sub-unit as areas with standard deviation of elevation greater than 200 m) ('Alpine'); c) lower-elevation areas poleward of latitude 60° N ('Arctic'); and d) lower-elevation areas south of latitude 60° N ('Mid-Latitude'). In each scenario, a different percentage value was used to represent the AFC in the areas associated with 'snow-covered' and 'snow-free' DGPs (Table 2.1): the implicit monthly snow-covered areas of each were then aggregated within these spatial units, and trends computed. (Additional detail of this process is provided in Appendix 1, Section A1.5.)

Table 2.1: Scenario values of fractional snow-cover used to generate alternative time-series of snow-covered area

% snow-cover assumed when 'snow-covered'	% snow-cover assumed when 'snow-free'	contrast (%)
100	0	100
90	15	75
100	45	55
55	0	55
60	35	25
55	45	10

The resultant magnitudes vary linearly with the contrast in AFC between the two snow-cover states (as listed in the 'contrast' column in Table 2.1), while the slope of this association varies with the month and sub-unit (Figure 2.12). In every month, the Arctic sub-unit shows the highest sensitivity, driven by the larger surface area associated with DGPs at higher latitudes (Figure 2.1). The sensitivity of the Alpine sub-unit is much lower, as most mountains are at lower latitudes, and the corresponding DGPs are therefore associated with smaller land-areas. It seems possible that Mid-Latitude sensitivities in July and August drop below those of the Alpine sub-unit because the only DGPs having any appreciable snow-cover in these months will be those associated with footprints including some mountains (though not over sufficiently large an area to raise the spatial mean elevation over 1500 m). These are again more likely to be found at lower latitudes, and are thus associated with smaller areas. Note that the sums of the sub-units' sensitivities match those for the NH in May to August and December, but not in April or November, when only the Mid-Latitude and Alpine sub-units (respectively) exhibit significant snow-area trends. This implies that the pan-NH associations in these months (during which snow-cover would be expected to be transitional over large areas) may be exaggerated, as the

overall snow-area trend depends on the aggregated areas within the sub-units for which significant trends are not individually identified.

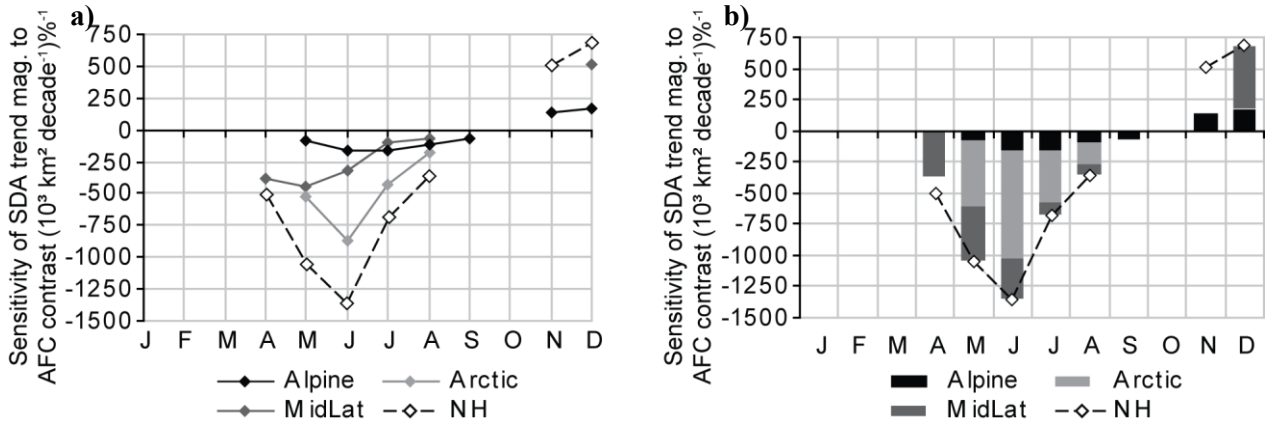

Figure 2.12: Sensitivities of SDA trend magnitudes to the contrast in actual fractional cover assumed when spatial units are classified as 'snow-covered' and 'snow-free' a) individually and b) aggregated.

More generally, these findings present important implications for trend magnitudes computed from the NRSA. For example, the AFC in the area associated with a snow-prone DGP in a given week at the beginning and end of the snow-season would reasonably be expected to vary by a few percentage points either side of the 50% threshold from year to year. If the AFC during these times is of the order of 45% when flagged as 'snow-free' and 55% when 'snow-covered', this represents a contrast of only 10% between the two states, and the magnitude of a trend computed using this difference would in turn be only 10% of that generated using the conventional assumption of 100% contrast. Similarly, in summer (remembering again that this analysis sought to exclude areas with perennial cryospheric cover), the AFC in 'snow-covered' areas might be of the order of 55%, whereas that in 'snow free' areas would probably be close to zero, with a corresponding contrast of around 55%. The reverse actual coverages in snow-prone regions are more likely in winter, but the contrast would remain the same. In both cases, the resultant trend magnitudes would be around half those estimated based on the conventional

assumption. (Note that these percentages are purely speculative, to illustrate the effects of different contrasts between the two states.)

A further complication is that individual DGPs will be at different stages of their snow-season in a given week or month, depending on their physiographic and climatological characteristics. For example, DGPs with short SDD will generally experience later initial accumulation and earlier ablation of seasonal snow, so these transitions (in which lower AFC contrasts would be expected) will coincide with mid-season conditions (and contrasts) in areas with longer SDD. In this way, overall aggregated snow-area trends for a given month will emerge from a range of disparate AFC contrasts. It follows that trend magnitudes generated purely from the conventional assumption of 100% snow-cover contrast in AFCs between the two states should be considered as the outer bounds of an uncertainty range (i.e., maxima for positive trends, minima for negative trends), with the actual magnitude for a given DGP being considerably smaller during transitions to and from the snow-season than mid-way through its snowier and less-snowy seasons.

Information about the intra-annual variation in the AFCs associated with DGPs, even if only as monthly climatologies, would thus help to reduce these uncertainties. In principle, it might be possible to estimate these through some – possibly most – of the NRSA PoR, for example by developing a form of data-assimilation or -fusion process, perhaps drawing on imagery from the successive Landsat platforms (which date from the early 1970s).

2.5.2.3. Notes on the Credibility of the Identified SDA Trends

As noted previously, doubt has been cast by several authors on the credibility of the positive balance of SDA trends across the NH observed from October to December, and the strength of

negative trends through the summer months (Wang et al., 2005; Brown et al., 2007; Brown and Derksen, 2013; Mudryk et al., 2017; Hori et al., 2017). While this study adopts markedly different temporal and spatial frameworks, so direct comparisons are not possible, some observations on this topic are offered here. While some of the reported disagreements may have been driven by analytical assumptions or possible interpretive biases, it seems possible that others (particularly with modelled datasets) may relate to emergent climatological phenomena.

2.5.2.3.a. 'Snow-covered' versus 'snow-dominated'

The key point is that discussed previously, on the distinction between estimates of 'snow-covered' and 'snow-dominated' areas. When framed in the latter terms, the values reported here are more reasonable than if the former label is applied. Improved estimates of the magnitudes of trends in snow-covered area, *per se*, will depend on identifying more representative ranges of actual fractional area in spatial units when flagged in the two binary states, and of their intra-annual variations. This will attenuate these estimates substantially, particularly early and late in the snow-season, but it would not change their signs. It is therefore also worth considering the possibility that the trends identified may, at least in part, be artifacts arising from extraneous influences.

2.5.2.3.b. Potential for bias in newly-deforested areas

Initial comparison with land-cover datasets suggests that many of the 5° cells in which positive SDA trends identified from the NRSA in October to December include large areas of coniferous forest. It is important to consider precisely what is meant by 'snow-covered' in such areas. Snow may lie on both the canopy and ground, or on the ground only. When classifying snow-cover, NRSA analysts seek to identify areas in which snow is expected to be on the ground, taking cues from visible patches in clearings – but this need not mean that it exists on the

canopy (D. Robinson, personal communication, January 2016). Unfortunately, many published studies do not distinguish explicitly between these states, and this may confound comparisons.

Nevertheless, if spatio-temporal instances of positive SDA trends coincide with areas in which widespread deforestation has occurred during recent decades, and where natural (and intact) stand characteristics and climatology do not favour retention of canopy-intercepted snow – thereby providing few clues for the existence of snow on the ground – it is possible that the newly-cleared patches may have revealed previously masked areas of snow. Both logging and increased wildfire activity have resulted in clearances over large areas of Russia (Achard et al., 2006; Smirnov et al., 2013): meanwhile, widespread salvage logging in response to major pest infestations (Bentz et al., 2010; Carroll et al., 2003), and deforestation for hydrocarbon extraction (Pickell et al., 2016) continue in western North America. Such effects may have been further compounded by more of such clearings becoming apparent in imagery of finer spatial resolutions. In principle, this might result in a progressive positive bias through the PoR. However, the possibility also exists that substantial areas of newly-unmasked snow may be driving a negative snow-albedo feedback, potentially contributing to wider and / or more persistent snow-cover. This presents an intriguing area of further investigation.

2.5.2.3.c. Ground observations and atmospheric circulations

Some support for positive trends is provided by observations of increasing snow depth, reported during the NH autumn and winter from ground stations across large areas stretching from eastern Europe to south-eastern Asia (Zhong et al., 2018). A mechanism has been suggested to link increasing early-season snow-cover in mid-latitudes, particularly in Eurasia, with the delivery of additional humidity from more ice-free Arctic waters by stronger meridional winds, driven by amplified waves in the Polar Jet (Cohen et al., 2014; Francis et al., 2017). It is

therefore noteworthy that the results reported here identify a significant positive correlation between positive SDA trend-strength and latitude in September, when Arctic sea-ice area is at its annual minimum (Figure 2.11). In an analysis of changes in the seasonal frequencies of high-amplitude waves, Francis and Skific (2015) found that such activity over Asia more than doubled during October to December between 1979 – 1994 and 2000 – 2013, the highest of any of the spatio-temporal units they considered by a considerable margin. This presents a particularly promising line of enquiry when seeking an explanation for the clear split between negative and positive SDA and (particularly) SDD trends on the highest westward and eastward slopes, respectively, of the major south-Asian mountain ranges (Figure 2.5, and Appendix 1, Section A1.4). While several comparable studies have relied on the NRSA for snow-cover data, similar results have also been generated from observations recorded at an extensive network of Russian ground stations (Wegmann et al., 2015).

One of the postulated drivers for these patterns is that widespread additional early-season Eurasian snow-cover has resulted in higher albedo and cooling of the lower boundary layer, thereby reinforcing the probability of such conditions persisting (Cohen et al., 2012). The results presented here do not offer substantial support for this hypothesis, as significant SDA gains during October and November are identified over only a relatively small area of the eastern Asian mid-latitudes, implying additional snow-dominance of the order of 5% to 10% of terrestrial area per decade (over the 1971-2014 PoR). However, the area in which positive SDA trends are identified increases longitudinally and spreads further south during mid-winter, moving in a broadly clockwise sweep around the eastern side of the area associated with the Siberian High. As maximum insolation potential at these lower latitudes is higher, perhaps a negative snow-albedo feedback is playing a role in such areas, depending in part on land-cover

and topography. Associations between atmospheric circulation patterns, topography and additional atmospheric humidity thus offer a key avenue of continuing investigation to improve understanding of early-season positive SDA trends.

2.5.2.3.d. Spring and summer trends in circumpolar lands

Another area of contention has been the strength of negative SDA trends during the summer months, particularly in circumpolar regions (Wang et al., 2005; Brown et al., 2007; Mudryk et al., 2017). As described in Section 2.5.2.2, the larger surface footprint associated with DGPs at high latitudes, in combination with the over-estimation of SDA trend magnitudes using the conventional assumption of a 100% contrast in the actual snow-covered fractional area associated with 'snow-covered' and 'snow-free' DGPs, is thought likely to account for much of the identified discrepancy. It would thus again be useful to obtain insights about fractional snow-cover climatologies, perhaps through some form of data-assimilation or -fusion process, potentially based on imagery from the Landsat or MODIS platforms.

However, inverting earlier discussion of the potential for land-cover influences on positive trends, there is also the possibility that increases in shrub vegetation over circumpolar lands may be obscuring patchy late-season snow (Mao et al., 2016). On the other hand, as more prominent foliage develops, it is more likely to emerge through the depleting snowpack earlier in the season, thereby enhancing the snow-albedo feedback and hastening ablation (Ménard et al., 2014).

2.5.2.3.e. Potential influence of the Modifiable Areal Unit Problem

A final consideration is that the spatial framework adopted also limits the reliability of trend estimates. The pitfalls of using an arbitrary partitioning scheme to describe and explain

geographical phenomena are well-established, and known in general as the Modifiable Areal Unit Problem (e.g. Dark and Bram, 2007). Detailed consideration of this issue (and similar factors relating to the temporal framework used) is beyond the scope of this paper, but while the finer grid applied in this analysis helps to reduce the Scale Effect compared to those conducted at hemispheric or continental scales, the still-considerable size of each cell implies that they will often be heterogeneous in terms of their physiographic and climatological characteristics, so there are likely to be persisting problems relating to the Zonation (or Aggregation) Effect. Such influences may help to explain why some trends are spatially and / or temporally isolated, and this in turn could help to exclude artifacts. The authors are currently addressing this challenge in a related project, by adopting a more snow-aware segmentation at finer temporal scales. Nevertheless, the main positive and negative 'centres of action' presented here evolve with both spatial and temporal coherence, supporting the interpretation that they are driven primarily by interactions between climatological and physiographic influences, rather than being artifacts of improvements in sensor and / or processing technologies.

2.5.3. Potential Implications for the Water and Energy Cycles

This improved description of spatio-temporal distributions of long-term trends in seasonal cryospheric cover will help to identify key locales in which to investigate a range of linkages with the water and energy cycles. However, scope for the assessment of potential impacts on the former is limited, without additional information describing associated variations in the depth and density of snowpack. New methods for inferring these details more accurately, particularly in complex or forested terrain – as sought by programmes such as NASA's SnowEx initiative (https://snow.nasa.gov/snowex) – are therefore essential. In conjunction with the spatial trends described here, they will inform assessments of shifts in the timing and intensity of freshet (melt-

derived) flows, altered patterns of flood behaviour (Blöschl et al., 2017) and / or reductions in streamflow and soil moisture (Berghuijs et al., 2014; Blankinship et al., 2014). These in turn will help to quantify evolving pressures on water resources for human use, primarily where mountain 'water towers' have historically supplied large areas at lower latitudes through the warmer months (e.g. Barnett et al. 2005; Viviroli et al., 2007; Immerzeel et al., 2010; Callaghan et al., 2012; Mankin et al., 2015). There are also indirect effects to consider: for example, positive SDA trends identified over the Tibetan Plateau may presage diminished summer rainfall in south and south-east Asia (Wu and Qian, 2003; Turner and Slingo, 2011); earlier inception of drier conditions could disrupt phenological cycles for vegetation (including crops) and migrations of anadromous fish species; and larger soil-moisture deficits in forests are thought likely to lead to more widespread wildfire activity (Westerling, 2016; O'Leary et al., 2016).

Given that snow makes a greater contribution to atmospheric cooling than polar sea-ice from January to April (Flanner et al., 2011), the development and expansion of negative SDA trends over large areas of central Asia in the spring months also has major implications. Their subsequent rapid expansion over sub-polar lands across Eurasia and North America through the summer adds to concerns over the likelihood of widespread thawing of permafrost, and consequent release of large volumes of 'old carbon', previously sequestered for thousands of years (Schuur et al., 2009). However, the quantification of impacts will rely on improved estimates of snow-covered areas and the rates at which they are changing, and of albedo variations in different landscape contexts.

2.6. Conclusions

The principal aim of this analysis was to describe spatial and temporal variations among significant trends in snow-dominated duration and area throughout the NH, as represented within the NRSA from 1971 to 2014. It responds to the recommendation of Groisman et al. (1994) that areas experiencing significant monotonic shifts in SDA should continue to be monitored closely within the context of a warming global climate. A purely graphical comparison reveals that the seasonal 'centres of action' of global variability in inter-annual snow climatology identified by this seminal study (which dates from well before the shift from mainly-manual to more automated interpretation using the Interactive Multisensor Snow and Ice Mapping System in 1999) largely coincide with the principal areas identified here as having experienced significant shifts in SDD and / or SDA.

It is again emphasized that these findings, being based on the conventional assumption of 100% (0%) snow-cover in 'snow-covered' ('snow-free') cells, represent the outer limits of uncertainty ranges for total SDA trend magnitudes: actual values, based on improved estimates of fractional snow-cover, are likely to be considerably smaller, particularly during onset of the snow-season and the ablation period, and at higher latitudes in summer. It is worth noting, however, that the mountainous areas in which many trends are identified show relatively low sensitivity to this parameter.

Nevertheless, this analysis resolves the spatial distributions, signs and (maximum) magnitudes of monthly trends in snow-dominated area, describes their associations with elevation, latitude and longitude, and explores relationships with shifts in snow-season duration. As well as considering potential causative factors driven by climatological and physiographic

influences, it presents possible alternative (or contributary) explanations for disagreements identified in prior studies between these metrics and other datasets, and suggests topics for future research aimed at reconciling these contrasting perceptions. These findings are therefore offered as a resource to guide and inform future hydrological, climatological, ecological and socio-economic studies relating to the changing seasonal cryosphere.

3. Shifting Spatial and Temporal Patterns in the Onset of Seasonally Snow-Dominated Conditions in the Northern Hemisphere, 1972-2017

This chapter was published in *Journal of Climate* (© American Meteorological Society. Used with permission.):

Allchin, M.I., and Déry, S.J. (2019). Shifting spatial and temporal patterns in the onset of seasonally snow-dominated conditions in the Northern Hemisphere, 1972-2017 *Journal of Climate,* **32**: 4981–5001 DOI: 10.1175/JCLI-D-18-0686.1

3.1. Abstract

The potential for anthropogenic climate-change to impact patterns of seasonal snow-cover has motivated numerous studies seeking trends in its extent and duration. Many have been based on the NOAA-Rutgers record of Northern Hemisphere snow-cover. Several studies have found augmented early-season snow identified from this archive to be anomalous, and related it to the introduction of higher-resolution imagery and a more automated interpretation process in 1999. This study contributes to the discussion by describing in greater detail the spatial and temporal distributions of trends in the onset of seasonally snow-dominated conditions between 1972 and 2017, and relationships to their physiographic and climatological contexts. It also identifies change-points between negative and positive onset-date anomalies, and relates these to corresponding meteorological patterns. Most trends identified indicated earlier onset, and were associated with mid-latitudes, low to moderate elevations, and colder, drier climates. These were situated largely north-east of major topographic chains, south-west of increasingly ice-free Arctic waters, and to the east of areas associated with blocking systems. Onset-date anomalies switched from positive to negative in approximately 70% of the affected points before 1997. These

change-points generally occurred earlier at higher elevations to the south and west, and later at lower elevations to the north and east. Overall temporal trajectories correspond broadly to shifts in temperature and precipitation over the same areas. In contrast, positive (later) onset trends were found over much smaller areas, associated with warmer, wetter climates, and higher elevations, particularly on west-facing slopes: temporal variations in anomalies of their onset-dates and associated meteorological conditions were distinct from those having negative trends.

3.2. Introduction

The annual transformation of terrestrial physical properties and conditions by seasonal snow-cover (SSC) modulates a wide range of climatological, hydrological, ecological and geomorphological processes, and controls both the provision of water resources and the risk of flood or drought for large human populations (Mankin et al. 2015). These influences are particularly important over the Northern Hemisphere (NH), which hosts approximately 98% of the total global area of SSC (Armstrong and Brodzik 2001). The extensive area of NH SSC even at relatively low latitudes means that snow contributes a greater negative top-of-atmosphere radiative forcing than sea-ice in every month outside May to August (Flanner et al. 2011 – based on analysis from 1979 to 2008). Investigations of the potential for disruption of hitherto reliable distributions of NH SSC by atmospheric warming and / or changing precipitation patterns are therefore highly relevant to research into trajectories of anthropogenic climate-change.

The description and quantification of snow-related trends has been a key topic of interest among these studies, supported by a range of lengthening observational series. Remotely-sensed imagery has proven particularly useful for monitoring the spatial extent of SSC, as it supports the frequent inference of conditions over wide areas – including remote and complex terrain – and

long time-periods. Among such resources, the United States National Oceanic and Atmospheric Administration's climate data record of NH snow-cover, compiled and curated by the Rutgers University Snow Laboratory (hereafter the 'NOAA-Rutgers Snow Archive', NRSA), offers the longest period of record of all remotely-sensed environmental datasets (Robinson et al. 2012; Estilow et al. 2015). It has therefore formed the foundation for a series of SSC-related investigations since the mid-1990s (Robinson et al. 1993; Groisman et al. 1994; Frei et al. 1999; Dye 2002; Rikiishi et al. 2004; Déry and Brown 2007; Choi et al. 2010; Brown and Robinson 2011; Cohen et al. 2012; Liu et al. 2012; Hernández-Henríquez et al. 2015; Allchin and Déry 2017).

However, the credibility of the NRSA has been debated in recent years. One point of discussion has centred on significant positive trends in snow-covered area identified from its records during the seasonal transition to boreal winter. These were first reported by Frei et al. (1999) and Brown (2000), based on annual series ending no later than 2000. Rikiishi et al. (2004), using the same timespan, suggested that changing atmospheric circulations might have caused the widespread negative trends in SSC-onset they described across the NH mid-latitudes. Having extended the period of interest (PoI) to 2008, Choi et al. (2010) also noted signs of earlier onset, and observed that warming need not preclude additional snowfall while temperatures remain below freezing. Déry and Brown (2007), Hernández-Henríquez et al. (2015) and Allchin and Déry (2017) all reported increases in NH snow-dominated area between October and December. However, several studies have found these early-season gains to be anomalous when compared to metrics derived from a variety of other modelled and observed datasets (Brown and Derksen 2013; Mudryk et al. 2017; Hori et al. 2017). The explanation most frequently suggested has been that they may be artifacts relating to the introduction of imagery at

higher temporal and spatial resolutions, in conjunction with a more automated interpretation process, in 1999 (as described by Ramsay 1998). A further complication arises from recognition that calculating snow-covered area based on the conventional assumptions of 100% (0%) actual fractional snow-cover within the NRSA's spatial sub-units when classified in the binary state of 'snow-covered' ('snow-free') is likely to exaggerate estimates of trend magnitudes, and that this may be particularly problematic during transitions to and from the snow-dominated season (Allchin and Déry 2017).

Nevertheless, others have incorporated these representations of more widespread early-season snow within conceptualizations of feedbacks between rapid rates of warming and more ice-free waters in the Arctic, leading to perturbations in atmospheric circulations (relating particularly to the boreal polar jet). These in turn have been identified as potential drivers of extreme weather in the mid-latitudes, with some areas experiencing colder winter conditions as a consequence of meridional outflows from higher to lower latitudes, while others have been anomalously warm due to heat advection in the opposite direction (Overland et al. 2011; Cohen et al. 2014; Francis and Skific 2015; Wegmann et al. 2015; Francis et al. 2017; Kretschmer et al. 2017; Cohen et al. 2018).

This study was therefore conceived with the goal of generating more detailed information relating to the NH snow-onset season, without depending on estimates of SSC extent. Its principal aim was to describe the spatial distributions of areas which, according to the representation of snow-cover provided by the NRSA, have experienced significant negative (earlier) or positive (later) trends in the onset-date of SSC during recent decades, their associated physiographic and climatological characteristics, and the times of year in which these shifts occurred. A secondary goal was to determine the timings of any clear transitions during the

period of record from one sign of snow-onset date anomaly to the other, and if so, to compare these with equivalent trajectories in metrics of meteorological activity.

3.3. Data

As well as enabling contribution to the discussion surrounding the veracity of early-season SSC trends identified from the NRSA, use of this archive also provided the benefit of a long period of record, and opportunity for comparison of results with prior research relating to shifting patterns of SSC over the NH. The dataset's spatial framework comprises a grid of 89 rows and columns in the NH stereographic polar projection, so that the areas associated with each dataset grid-point (DGP) vary with latitude, from ~10,700 km² at the lowest latitudes to ~41,800 km² near the geographic North Pole (Estilow 2013). DGPs associated with primarily oceanic areas, or terrestrial areas of (hitherto) perennial cryospheric cover, together with an additional 33 previously associated with questionable snow-cover records (Déry and Brown 2007), were excluded using masks supplied with the archive or developed in previous studies (Déry and Brown 2007; Hernández-Henríquez et al. 2015; Allchin and Déry 2017). The remaining spatial domain includes 1980 DGPs, associated with a total area of 5.9×10^7 km².

Each weekly NRSA granule comprises a series of binary values, one per DGP, signifying whether or not at least 50% snow-cover existed over the associated terrestrial area on the last unobscured day of the prior seven (Tuesday to Monday). While the archive's first observations date from October 1966, gaps totalling 37 weeks between July 1968 and September 1971 have guided selection of October 1971 as a start-date for the period adopted in previous analyses (Déry and Brown 2007; Hernández-Henríquez et al. 2015; Allchin and Déry 2017). In this case, for reasons clarified below, week 32 (7 to 13 August) of 1972 was chosen as the start-date. In the

version of the archive kindly supplied by the Rutgers Snow Laboratory, records were available to week 31 (31 July to 6 August) of 2018.

Through the long history of the NRSA, advances in hardware and software capabilities have driven a series of improvements to the sensors and processing algorithms used in its production. The greatest such shift occurred in 1999, when the original – mainly human-dependent – interpretation process was replaced by the more automated Interactive Multisensor Snow and Ice Mapping System (IMS). At the same time, the imagery's spatial resolution improved from ~190 km to 24 km, and its temporal resolution changed from weekly to daily (Ramsay 1998; Estilow et al. 2015). While considerable care has been taken to ensure overall consistency throughout the entire period of record (Romanov et al. 2000; Helfrich et al. 2007; Estilow 2013; Estilow et al. 2015), this upgrade has nevertheless been identified by several authors as a potential causative factor behind disagreements with snow-related metrics derived from other datasets (Brown and Derksen 2013; Mudryk et al. 2017; Hori et al. 2017), including the early-season trends of interest here.

The long-term climatological contexts of DGPs were derived from the 1961-1990 mean temperature and precipitation datasets published by the University of East Anglia's Climatic Research Unit (CRU) (version 2.0, released in 2002: http://crudata.uea.ac.uk/cru/data/hrg/tmc). The constituent values, supplied at a spatial resolution of 10 arc-minutes, were averaged within polygons representing the DGP surface footprints. The usual caveats relating to the uncertainties associated with interpolating ground-observations over wide separations between stations (particularly in remote and / or complex terrain) are noted.

Meteorological activity during the PoI was represented by monthly mean terrestrial temperature and precipitation datasets published (on a 0.5° grid) by Willmott and Matsuura of the University of Delaware (version 5.01, released August 2018: http://climate.geog.udel.edu/~climate), processed in the same manner.

3.4. Methods

3.4.1. Derivation of Metrics of Seasonal Snow-Onset

To distinguish between the initial (often ephemeral) onset of snow-cover during the transition from autumn to winter, and its greater persistence through the subsequent colder months, two metrics were tracked for every DGP. The first date in the latter part of each calendar year on which snow-cover switched from < 50% to ≥ 50% was named On1, and the beginning of the first period of uninterrupted snow-dominated conditions continuing for at least four weeks was termed On4. Mean On4 dates were found to correlate strongly with mean start-dates of the longest continuous runs of snow-dominated conditions ($R = 0.99$, $p < 0.0001$, slope = 0.9), so it is reasonable to equate them with the beginning of the main winter season. On4 occurs within one week of On1 in ~50% of DGPs in which both dates were identifiable in at least 30 years: this fraction rises to 80% within two weeks, and 93% within three weeks.

For consistency with prior studies, this analysis adopted a snow-year beginning on 1 October. However, initial exploration of the dataset revealed that – of the 1980 DGPs considered – mean On1 dates from 1971 to 2017 were earlier than this for 185 (associated with a total area of 6.2×10^6 km², comprising 10.5% of the spatial domain). Over the same period, mean On4 occurred before 1 October in 134 DGPs (total area 4.4×10^6 km², 7.5% of the spatial domain). The earliest mean value of either metric was 30 August. To capture these transitions as

comprehensively as possible, they were therefore sought in granules captured in or after week 32 of each year, as this begins between 2 and 9 August (depending on the year). Onset dates before 1 October in any year were therefore represented by negative values. This in turn dictated that the first year in which to seek onset dates would be 1972 (rather than 1971, as a data-gap exists to September of that year), and the last 2017, a total of 46 years. (Note that all statistics quoted hereafter pertain to this 1972-2017 PoI, unless explicitly stated otherwise.)

3.4.2. Identification and Estimation of Trends

The principal goal of this study was to identify DGPs associated with snow-onset time-series manifesting significant monotonic trends. A common confounding factor in trend analysis is the existence of temporal autocorrelation within the series of interest (e.g. Weatherhead et al. 1998). Where this takes the form of a lag-1 autoregressive structure, it is possible to mitigate its effects by 'pre-whitening' (Yue et al. 2002). Evidence of this phenomenon was therefore sought among the time-series of snow-onset dates, using the full and partial autocorrelation functions described by Anderson (1977). However, no such patterns were identified.

Trends were identified from the On1 and On4 series using Mann-Kendall Trend Analysis (Mann 1945; Kendall 1975). With the goal of reporting conservative results, the series for each DGP was considered only if it comprised a full set of 46 annual values. The magnitudes of trends identified as significant at the 5% level were estimated using the Theil – Sen method (Theil 1950; Sen 1968).

3.4.3. Spatial, Temporal and Climatological Distribution of Trends

Having identified DGPs associated with significant snow-onset trends, descriptions were generated of their spatial and temporal distributions. The latter is a key point, as mean snow-

onset dates vary with contextual attributes such as latitude, elevation and proximity to an upwind coastline (Figure 3.1), so the drivers of any trend identified for a given DGP must be active at (and / or potentially before) the corresponding time of year.

The principal physical characteristics of the spatial sub-domains associated with each type and sign of trend were compared in cumulative spatial frequency curves, generated by ranking the corresponding sub-sets of DGPs by metrics representing their latitude, elevation, and mean day of snow-year (where 0 = 1 October) of On1 and / or On4.

To support the derivation of additional spatial statistics, the terrestrial area associated with each DGP was estimated by superimposing a layer of points drawn at 10 km intervals (identified previously as being located over land) over another containing polygonal features representing the surface footprints associated with the DGPs. Each of the raw DGP surface footprint areas (as supplied with the dataset) was then scaled by the corresponding fractional coverage of terrestrial points. This enabled illustrations integrating the spatial incidence and strength of trends to be generated, using the product of DGP terrestrial area (km^2) and trend magnitude (days $decade^{-1}$), termed 'area-magnitude' plots (km^2 days $decade^{-1}$).

An additional aspect of interest was the range of climatological settings in which On1 and On4 trends were identified. To explore this, the CRU 1961-1990 mean monthly precipitation and temperature within the spatial footprint associated with each DGP was retrieved for the month(s) containing that DGP's 1972-2017 mean dates of On1 and On4. This permitted the preparation of cumulative spatial frequency curves describing the distribution of climatological characteristics among DGPs associated with each type and sign of trend.

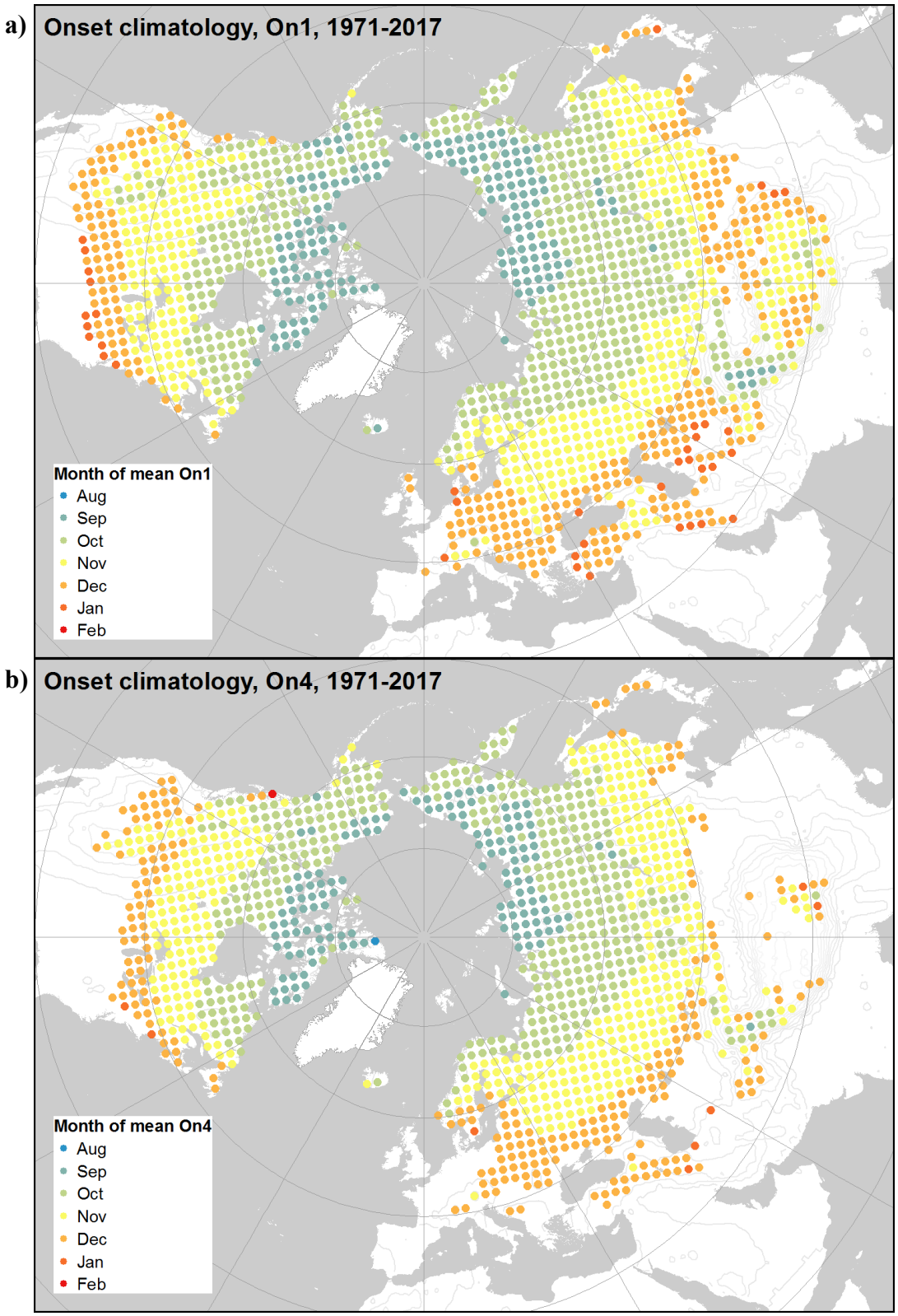

Figure 3.1: Spatial distributions of months containing mean (1972-2017) date of a) On1, b) On4. (Meridional interval of graticule is 15°, zonal interval 30°.)

Table 3.1: Incidence of significant On1 and On4 trends

	On1				On4			
	n	**%**	**10^6 km²**	**%**	**n**	**%**	**10^6 km²**	**%**
Domain*	1228	100	39.8	100	944	100	31.6	100
Sig. neg. trends	307	25.0	9.9	24.9	236	25.0	7.9	25.0
Sig. pos. trends	57	4.6	1.7	4.3	25	2.6	0.8	2.4

**The domain is the sub-set of NRSA grid-points (DGPs) for which On1 / On4 dates were identified in all 46 years from 1972 to 2017*

3.4.4. Assessment of the Temporal Evolution of Trends

The temporal evolution of shifting snow-onset dates giving rise to significant trends was explored using a simple form of change-point analysis. While a range of relatively complex techniques has been developed for this purpose (e.g. Ducré-Robitaille et al. 2003; Reeves et al. 2007; Aminikhanghahi and Cook 2017), the large number of series to be considered here dictated that a more straightforward approach was required, and that described by Pettitt (1980) was selected. This method generates a cumulative summation (CUSUM) series (S_i) from a time-series of values (X_i) by adding successive anomalies relative to the series mean, thus: $S_i = S_{i-1} + X_i - \overline{X}$, where $S_0 = 0$, and $\overline{X}$ is the series arithmetic mean. In the resultant series, sub-sections with generally positive (negative) gradients correspond to periods during which the same sign of anomaly prevails, while approximately constant sections imply conditions close to the average: it follows that maxima and minima indicate change-points from one sign of anomaly to the other, while inflections mark shifts in rates of change.

CUSUM series were generated for the time-series of On1 and On4 dates associated with DGPs for which significant trends were identified, and for the series of monthly mean temperatures and precipitation depths (University of Delaware data) in the month containing the mean date of On1 / On4. The month of mean onset was used because tracking values in the

month of actual onset each year risks – for the example of temperature – jumping from a warmer (colder) month to a colder (warmer) one where a positive (negative) trend is identified. Series were also constructed from 3-year and 5-year running means of the CUSUM values. The overall form of these series, and the years in which their extreme values occurred, were used to identify pattern-changes in snow-onset dates and the associated meteorological data.

3.5. Results

3.5.1. Snow-Onset Trends

A On1 (On4) date was registered in each of the 46 years from 1972 to 2017 for 1228 (944) DGPs. Significant trends were identified for 364 (261) of the points in each of these sub-domains, associated with approximately 29% (27%) of their respective areas (Table 3.1). The two signs of trend were found to occur within broadly distinct and contiguous regions: the overall spatial patterns were similar for both metrics, with relatively few exceptions and additions (Figure 3.2). Variations of trend magnitude with longitude, latitude and elevation are depicted in Figures 3.3 to 3.6. Their cumulative spatial frequency distributions in relation to latitude, elevation, mean onset-date, mean monthly temperature and precipitation (in the month containing the mean onset-date), and magnitude are illustrated in Figure 3.7. Associations between magnitude and latitude, longitude, elevation and mean onset-date are shown in Figure 3.8, with regression metrics in Table 3.2. Distributions of the product of area and trend magnitude with latitude, longitude, elevation and mean onset-date are provided in Figure 3.9. The following sections summarize the distributions of positive and negative On1 and On4 trends in relation to these key contextual characteristics.

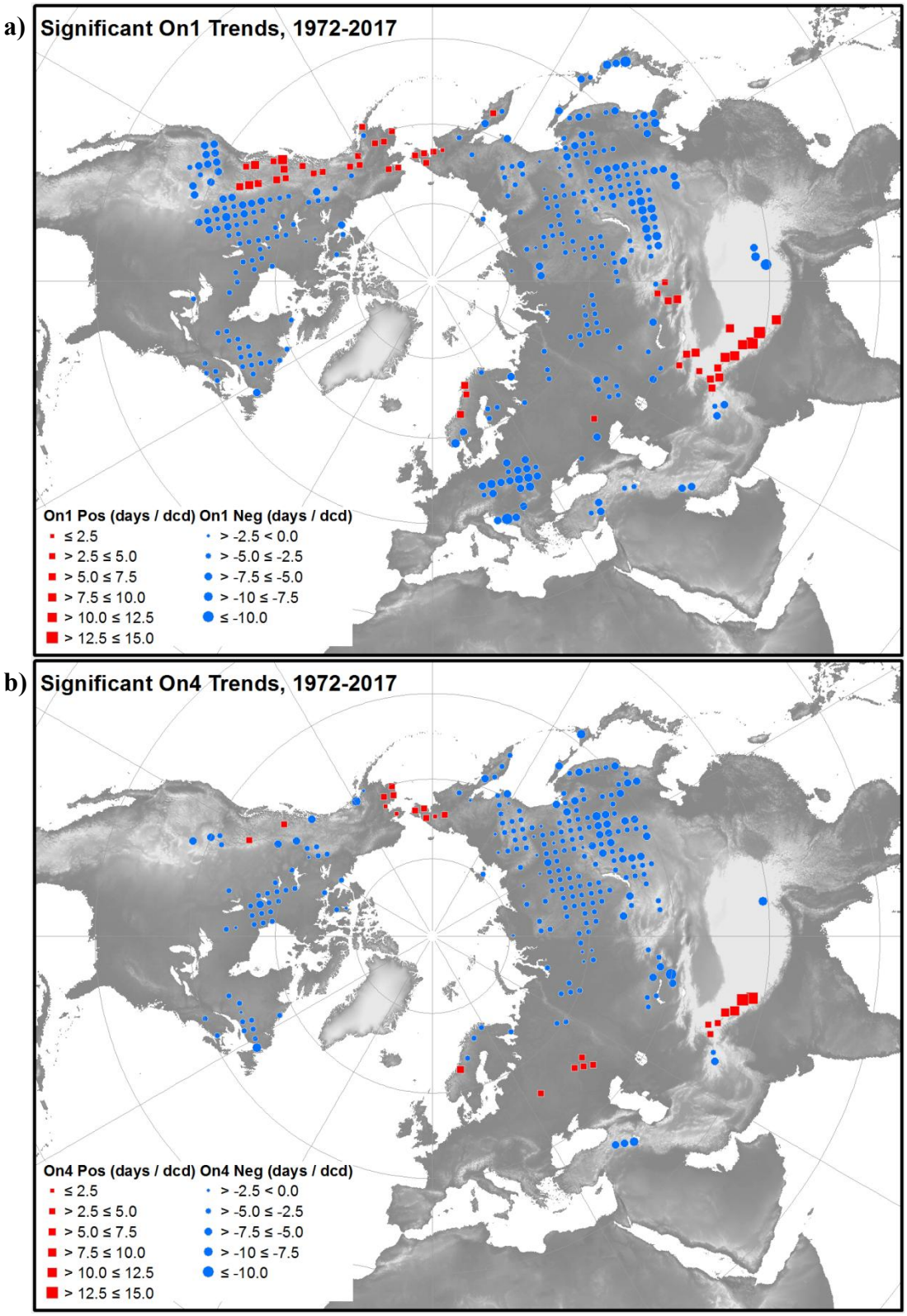

Figure 3.2: Spatial distributions of significant ($p < 0.05$) a) On1 and b) On4 trends (1971-2017). (Meridional interval of graticule is 15°, zonal interval 30°.)

3.5.1.1. Significant On1 Trends

On1 trends represent significant shifts in the date of the first transition from < 50% to ≥ 50% snow-cover, during the onset of cooler conditions in the latter stages of the calendar year. The summary spatial metrics shown in Table 3.1 indicate that significant negative trends (and thus progressively earlier snow-onset) out-number significant positive trends (later onset) by a ratio exceeding 5:1. When expressed in terms of their associated areas, this ratio rises to 6:1 (driven by more widespread occurrence of negative trends at higher latitudes, where the areas associated with individual DGPs are larger than at lower latitudes.)

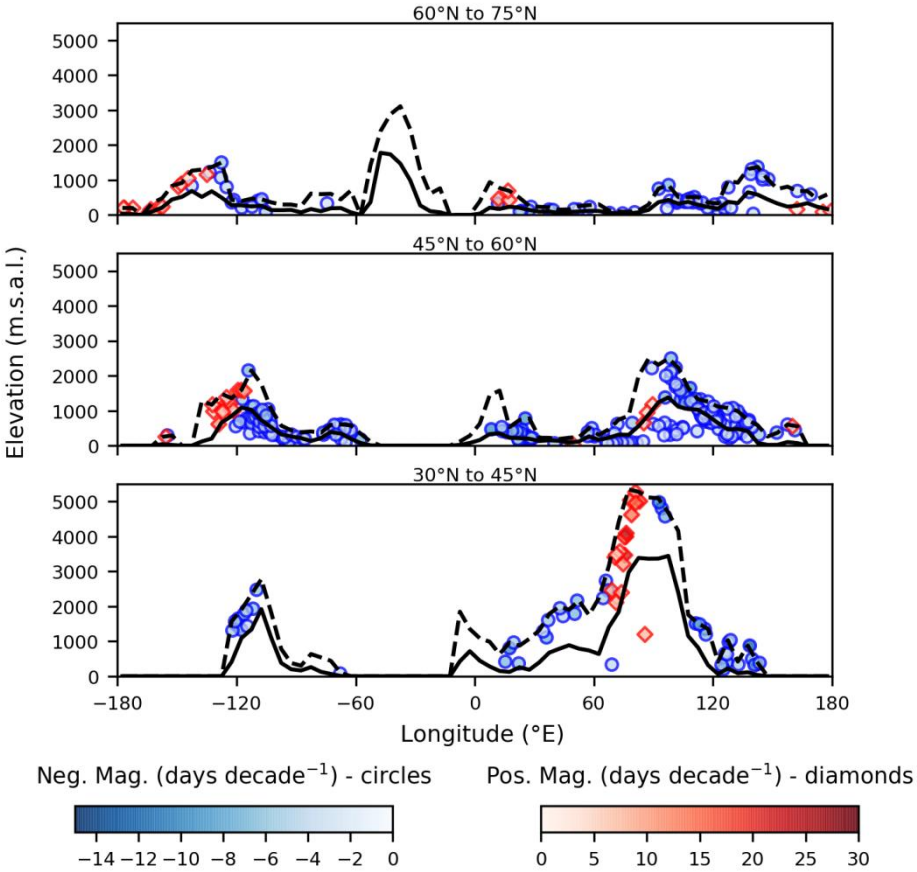

Figure 3.3: Variation of On1 trend magnitude longitude and elevation within latitudinal bands of 15° meridional width. Solid (dotted) lines represent variation of meridional mean (maximum) elevation within 5° bands.

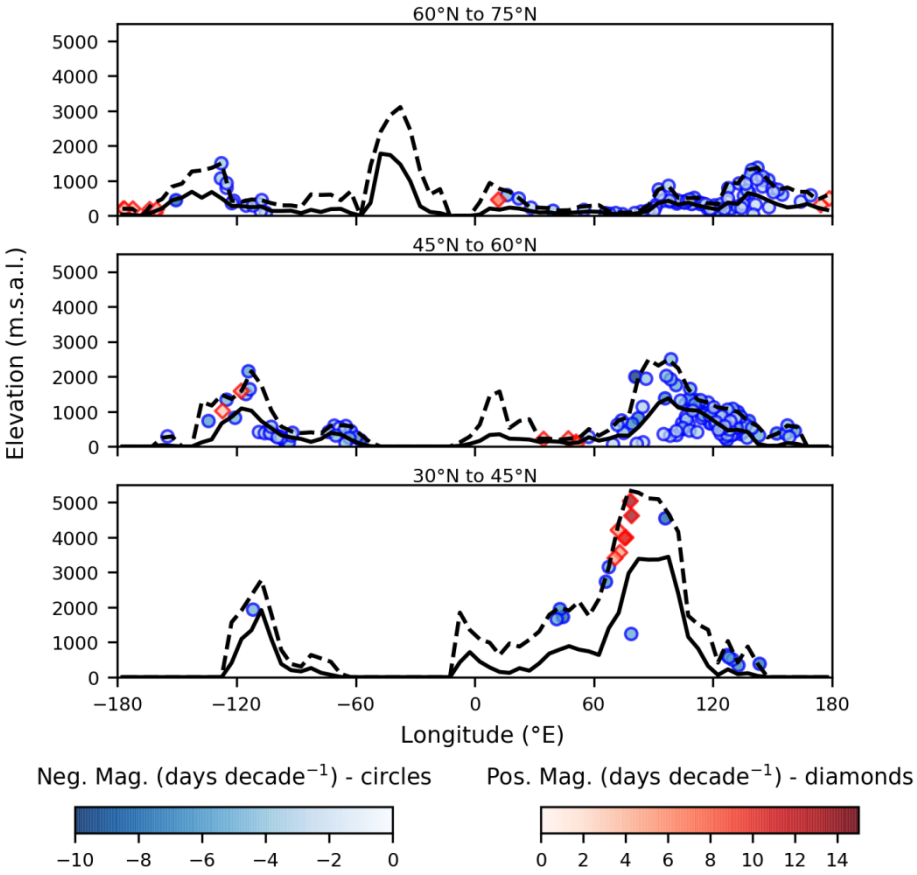

Figure 3.4: Variation of On4 trend magnitude longitude and elevation within latitudinal bands of 15° meridional width. Solid (dotted) lines represent variation of meridional mean (maximum) elevation within 5° bands.

The four main clusters of positive trends are located principally on the south-western slopes of the Himalayan Massif north-westward to the Pamir, between the Tien Shan and Altai mountains, in central to northern Norway, and along the Western Cordillera of North America, extending north and west to both sides of the Bering Strait (Figure 3.2a). While they are distributed approximately evenly through NH latitudes (Figure 3.7a), they are longitudinally much more limited, being associated primarily with the upper and western (and, at these latitudes, therefore windward) slopes of the Himalayas, central to northern parts of the Western Cordillera, and Norwegian mountains (Figure 3.3). 55% (33%) are found above elevations of

1000 m (1500 m) (Figures 3.7b, 3.8e, 3.9c). Most of the lower-altitude DGPs experiencing positive trends are distributed either side of the Bering Strait.

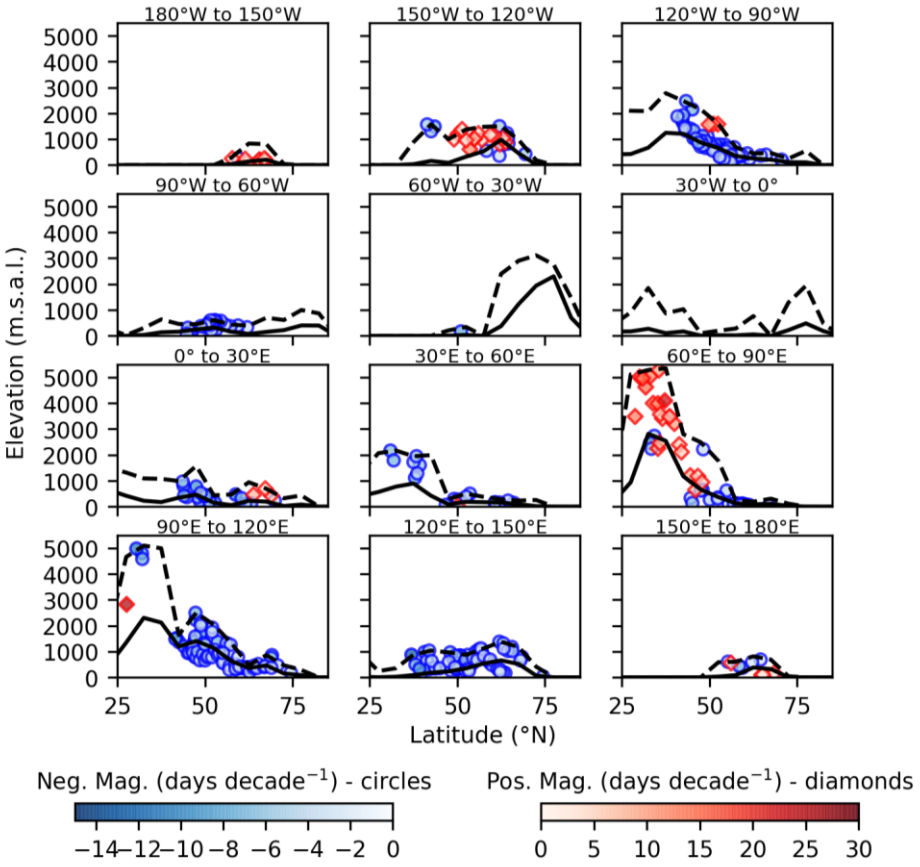

Figure 3.5: Variation of On1 trend magnitude with latitude and elevation within longitudinal bands of 30° zonal width. Solid (dotted) lines represent variation of zonal mean (maximum) elevation within 5° bands.

Negative trends are found over extensive swaths of north-eastern and central Eurasia, central-eastern Europe, north-eastern Canada, and western North America. The three largest spatially-coherent clusters are found to the north and east of the Himalayas, European Alps, and Western Cordillera of North America, and occupy areas roughly proportional to the uplands' lateral extents (Figures 3.2a, 3.3, 3.5). Smaller patches are seen in the eastern Himalayas, the Hindu Kush, and through Iran and Anatolia to the Balkans. There is a particularly clear association with the eastern slopes of major mountain ranges, except at relatively low latitudes in

western North America, where they occur on the Pacific-facing upper western slopes of the coastal ranges (Figure 3.3). They are more strongly associated with mid-latitudes (40° – 60°N) than those further to the north or south (Figures 3.7a, 3.9a). 79% (92%) of the associated area is found below 1000 m (1500 m) (Figures 3.7b, 3.8e, 3.9c).

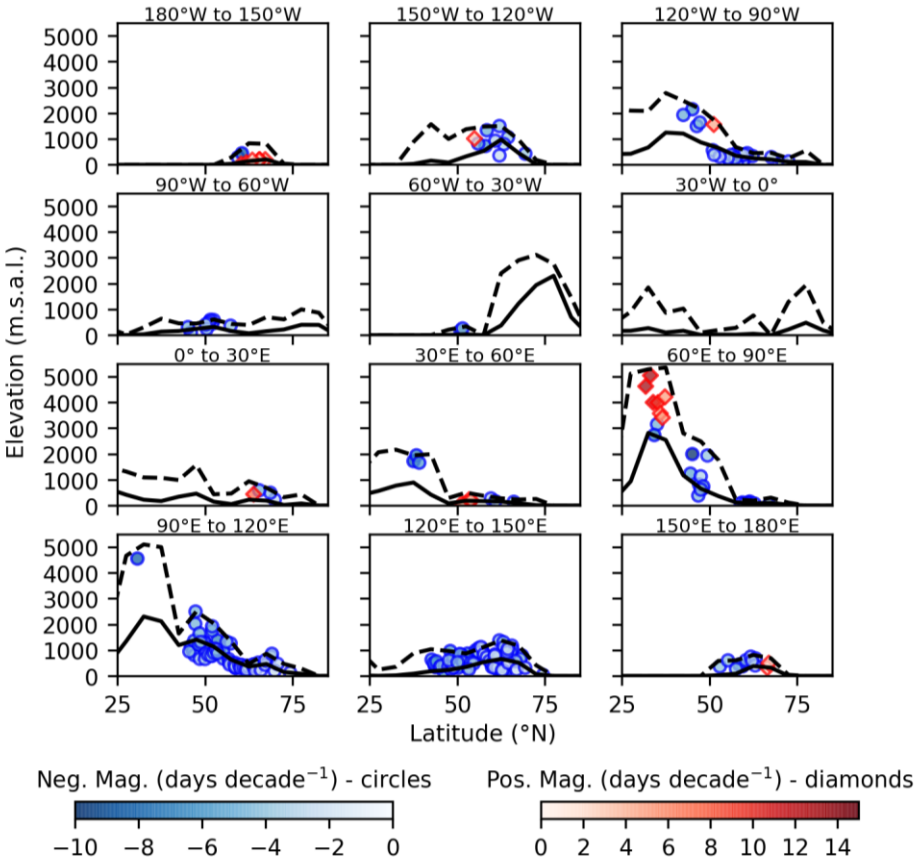

Figure 3.6: Variation of On4 trend magnitude with latitude and elevation within longitudinal bands of 30° zonal width. Solid (dotted) lines represent variation of zonal mean (maximum) elevation within 5° bands.

Snow-onset in the areas affected by positive trends has historically occurred early in the seasonal transition, mainly within the first two weeks of October. In contrast, those experiencing negative trends have not generally seen their first major snowfall until sometime between mid-October and late-November (Figure 3.7e). In the month containing the mean date of initial snow-onset, areas experiencing positive trends are warmer by ~5°C than those experiencing negative

trends (Figure 3.7c). Temperatures are below freezing over only ~53% of the area associated with positive trends, with 29% below -5°C and 5% below -10°C. In comparison, 86% of the area seeing negative trends is below freezing, with > 60% below -5°C, and > 24% below -10°C. Approximately 50% of the area affected by positive trends receives appreciably greater precipitation during the month of mean onset than those experiencing negative trends (Figure 3.7d).

Table 3.2: Metrics of correlation between On1 / On4 trend magnitudes and latitude, elevation, mean onset date

		On1			On4		
		R	**p**	**slope**	**R**	**p**	**slope**
Trend mag. vs latitude [(1)]	Sig. neg.	0.56	<0.0001	0.11	0.57	<0.0001	0.10
	Sig. pos.	**-0.70**	<0.0001	-0.29	**-0.75**	<0.0001	-0.19
Trend mag. vs elevation [(2)]	Sig. neg.	-0.44	<0.0001	-1.09	-0.44	<0.0001	-1.11
	Sig. pos.	**0.70**	<0.0001	2.30	**0.80**	<0.0001	1.46
Trend mag. vs mean onset [(3)]	Sig. neg.	-0.55	<0.0001	-0.29	-0.56	<0.0001	-0.28
	Sig. pos.	0.36	<0.01	0.85	0.29	non-sig.	0.35
Elevation vs latitude [(4)]	Sig. neg.	-0.52	<0.0001	-41.7	-0.52	<0.0001	-37.4
	Sig. pos.	**-0.88**	<0.0001	-109.2	**-0.91**	<0.0001	-129.7
Mean onset vs latitude [(5)]	Sig. neg.	**-0.80**	<0.0001	-2.18	**-0.88**	<0.0001	-2.23
	Sig. pos.	-0.43	<0.001	-0.52	-0.37	non-sig.	-0.57
Mean onset vs elevation [(6)]	Sig. neg.	0.08	non-sig.	2.82	0.23	<0.001	7.91
	Sig. pos.	0.13	non-sig.	1.22	0.09	non-sig.	0.96

Units of slope:

[(1)] trend magnitude vs latitude: (days decade^{-1}) (° latitude)$^{-1}$

[(2)] trend magnitude vs elevation: (days decade^{-1}) (1000 m)$^{-1}$

[(3)] trend magnitude vs mean onset date: (days decade^{-1}) (7 days)$^{-1}$

[(4)] elevation vs latitude: m (° latitude)$^{-1}$

[(5)] mean onset date vs latitude: days (° latitude)$^{-1}$

[(6)] mean onset date vs elevation: days (1000 m)$^{-1}$

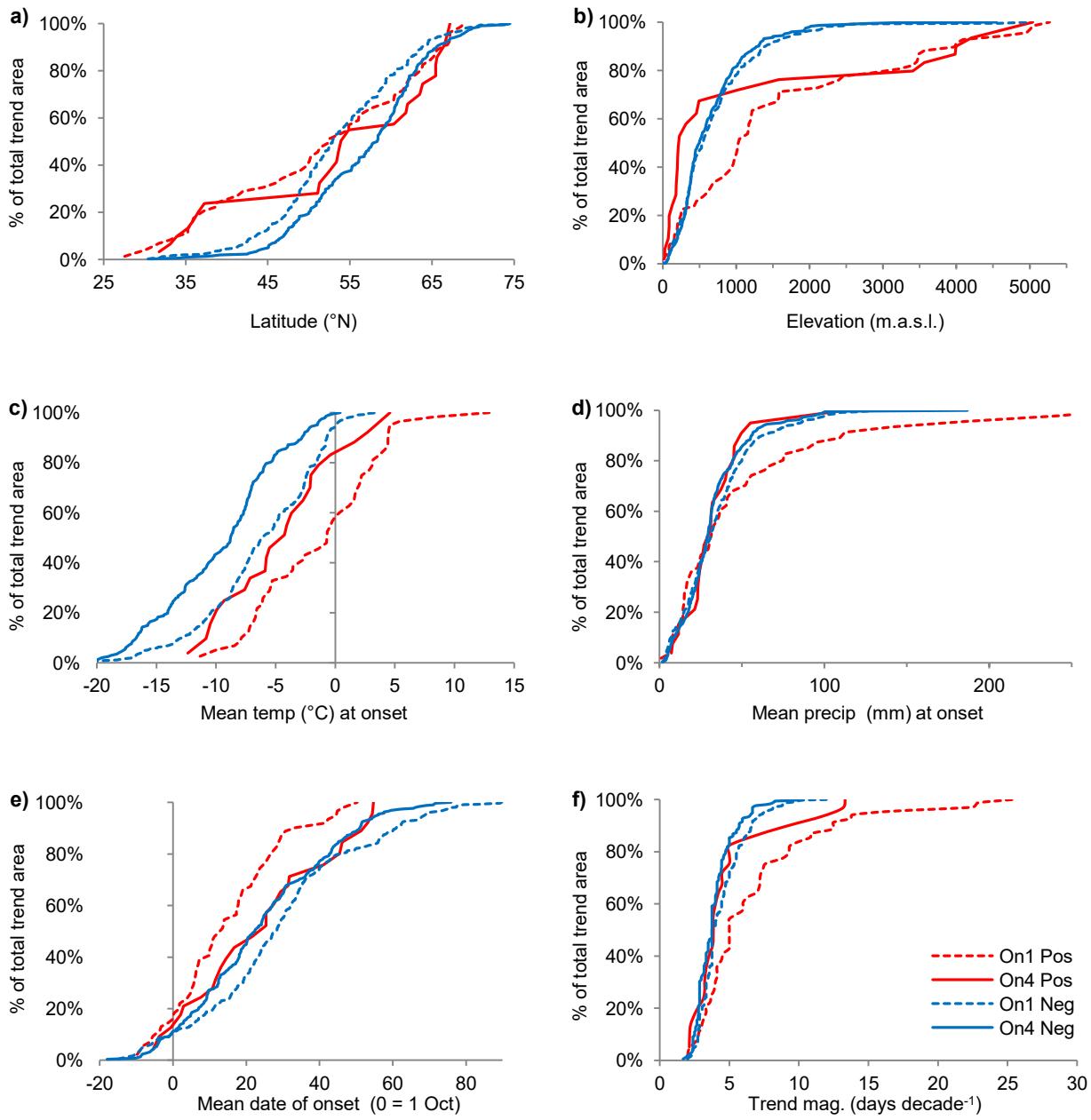

Figure 3.7: Distributions of areas affected by significant On1 and On4 trends, ranked by a) latitude, b) elevation, c) monthly mean (1961-1990) temperature in the mean (1972-2017) month of onset, d) precipitation in the mean (1972-2017) month of onset, e) mean (1972-2017) date of onset, and f) trend magnitude (note – absolute values for negative trends). Dotted (solid) lines represent On1 (On4): red (blue) lines represent positive (negative) trends

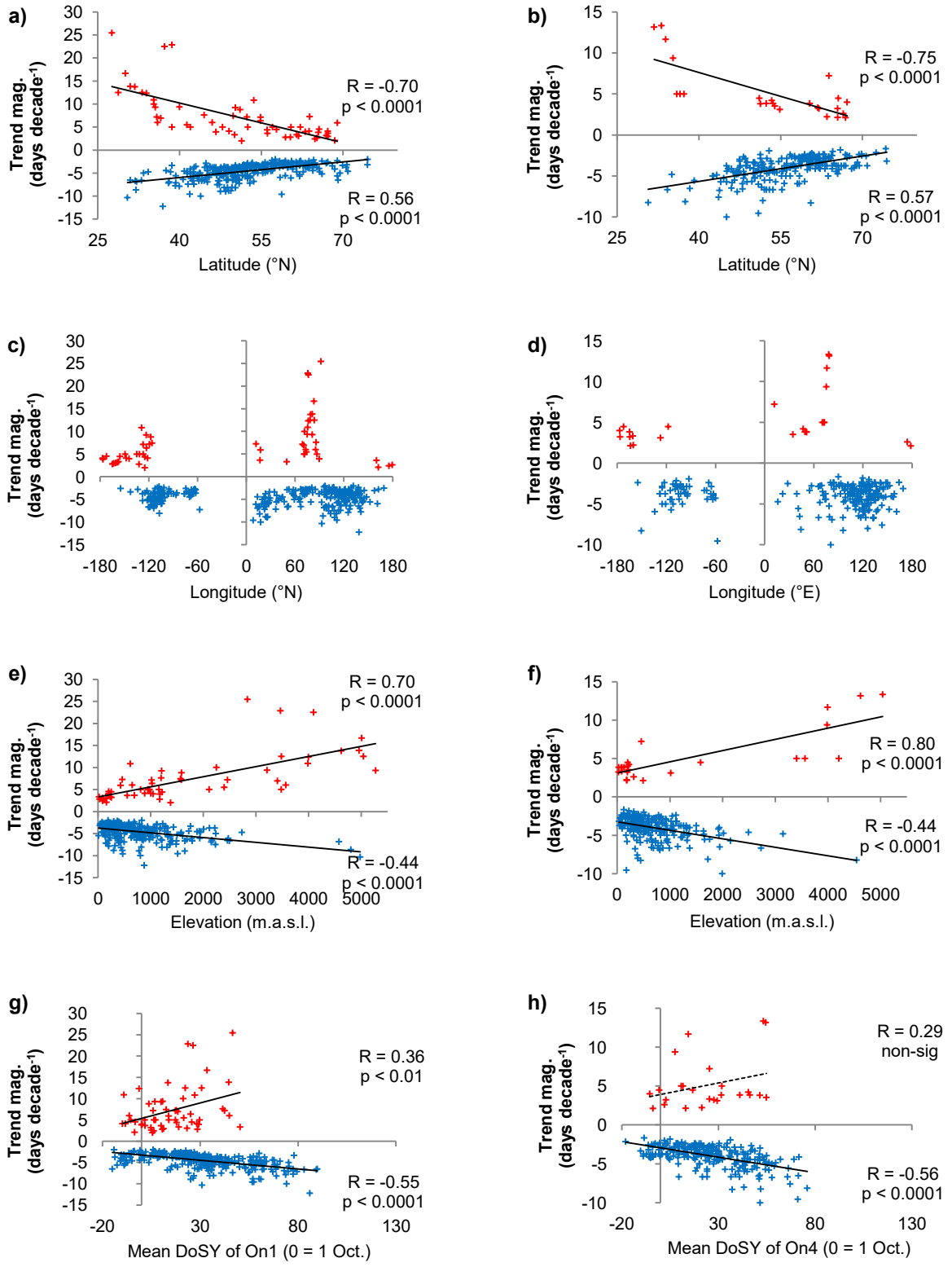

Figure 3.8: Variation of trend magnitude with(a, b) latitude, (c, d) longitude, (e, f) elevation, (g, h) mean onset date. On1 trends are depicted in a, c, e, g, with On4 trends in b, d, f, h. (DoSY = Day of Snow Year)

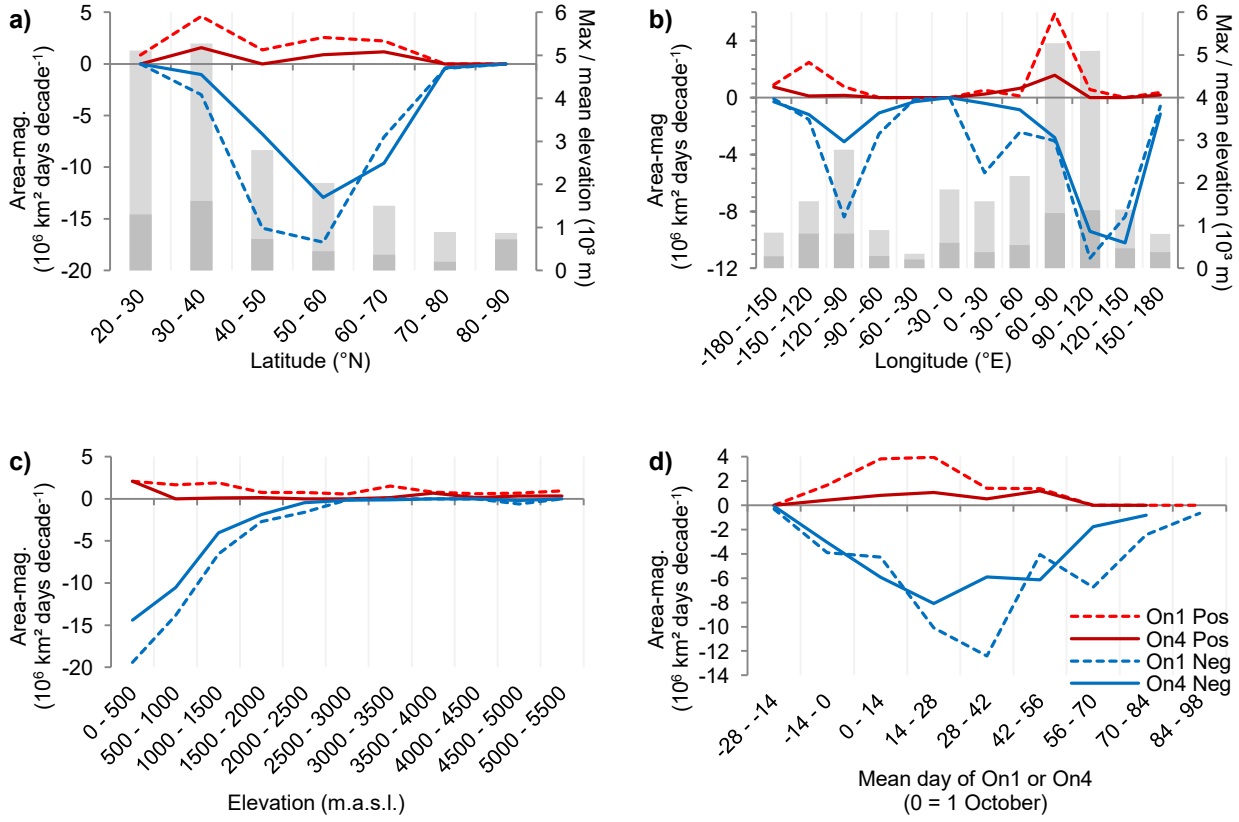

Figure 3.9: Area-magnitudes by a) latitude,b) longitude, c) elevation and d) mean date of snow onset. Dotted (solid) lines represent On1 (On4): red lines represent positive trends (later onset), blue lines negative (earlier onset): pale (dark) grey bars are zonal (in a) / meridional (in b) maximum (mean) elevations.

Positive trends have considerably larger absolute magnitudes than negative trends (Figure 3.7f). Nearly 60% of the area associated with positive trends have been experiencing progressive delay of onset-dates at rates greater than 5 days decade^{-1}. Over 15% of the total affected area, the rate is in excess of 10 days decade^{-1}, and over 3% it is greater than 20 days decade^{-1}. Negative trends are more moderate, with 73% of the associated area seeing rates of change no greater than 5 days decade^{-1}, and fewer than 1% above 10 days decade^{-1}.

While the magnitudes of both signs of trend increase at higher elevations and lower latitudes, positive trends correlate more strongly with, and are more sensitive to, both apparent influences (Table 3.2). These associations persist within the meridional strips shown in Figure

3.5, where sufficient DGPs with negative or positive trends exist (see also Appendix 2, Table A2.1). Much weaker relationships exist between climatologically cooler temperatures in the historical mean onset-month and stronger negative trends ($R = -0.15$, $p < 0.05$, slope = -0.05 (days decade^{-1}) (°C)$^{-1}$)), and climatologically wetter conditions in the historical mean onset-month and stronger positive trends ($R = -0.30$, $p < 0.05$, slope = -0.03 (days decade^{-1}) mm^{-1}: additional detail is provided in Appendix 2, Figure A2.1).

3.5.1.2. Significant On4 Trends

On4 trends represent significant shifts in the date of the first transition from < 50% to ≥ 50% snow-cover, when this subsequently persists for at least four weeks. As established above, this approximates the onset of the longest continuous period of snow-cover each winter. As evident from Table 3.1, the ratio of negative to positive trends is considerably higher than the equivalent for On1 trends, at 9:1 by the number of DGPs in each group, and 10:1 by area (again driven by more widespread occurrence of negative trends at higher latitudes, where the areas associated with individual DGPs are larger than at lower latitudes).

The overall spatial distribution of positive and negative On4 trends shadows that of the On1 trends, with several exceptions and one addition (Figure 3.2b). There are considerably fewer instances of positive trends, with clusters involving more than a single DGP occurring only at higher elevations of the Himalayan Massif's south-western extremities, either side of the Bering Strait, and in a relatively small patch of central-western Russia, north of the Caspian Sea. Negative trends are also diminished in several regions, particularly in central-eastern Europe, north-eastern Canada, and most of the more southerly parts of central-western North America affected by On1 trends. A possible anomaly exists in the Tien Shan (where mainly positive On1 trends were identified), in the form of a small group of negative On4 trends: together, these

imply later initial snow-onset, but earlier persistent onset, among DGPs in reasonable proximity to one another (although not coincident: no DGP yields trends of both types with opposite signs).

As positive On4 trends occur only within a few small patches, their latitudinal distribution appears as a series of discrete 'steps' (Figures 3.7a, 3.8b). That for the negative trends is more continuous. A considerably larger fraction of the area associated with positive On4 trends occurs at lower elevations, compared to that for On1: this corresponds to the persisting incidence of positive trends either side of the Bering Strait. The distribution of elevations among negative On4 trends is identical to that for negative On1 trends. Thus, positive On4 trends are again more commonly associated with lower latitudes and higher elevations, while negative trends are found mostly at lower elevations in the mid-latitudes. This is made additionally clear by the combination of area and magnitude in Figures 3.9a, 3.9c.

It is noteworthy that the distributions of mean On4 onset date associated with the DGPs for which positive and negative trends were identified are essentially identical (Figure 3.7e). This implies that – when considered over the entire domain – the influences driving both earlier and later arrival of more persistent snow-cover are occurring at the same time of year in different areas.

The distributions of climatological mean precipitation expected during the mean onset-month are also identical for the DGPs associated with both signs of trend (Figure 3.7d). Profiles of mean temperature at onset remain separated, with the areas seeing negative trends approximately 5°C to 7°C cooler than those with positive trends (Figure 3.7c). Thus, among areas seeing positive trends, 86% have monthly mean temperatures in the mean month of the onset of persistent snow-cover at or below freezing , 48% below -5°C, and 16% below -10°C,

while for those with negative trends, the corresponding values are 100% at or below freezing, 83% below -5°C, and 44% below -10°C. No significant correlations exist between either climatological metric and the magnitudes of either sign of On4 trend (see Appendix 2, Figure A2.1).

The cumulative spatial frequency profiles of (absolute) trend magnitude are again similar, over the 80% of their respective associated areas with relatively weak values (~2 to 4 days decade^{-1}) (Figure 7f). However, the remaining 20% by area of positive trends are stronger than their negative equivalents, with ~13% greater than 7 days decade^{-1}, and 10% above 9 days decade^{-1}, the maximum being ~13 days decade^{-1}. These extremes are all located at altitudes above 3500 m and latitudes south of 35°N.

3.5.1.3. Summary: Contextual Comparison of On1 and On4 Trends

Overall spatial patterns of the incidence of On1 and On4 trends are broadly similar, with positive trends associated with the upper western slopes of major mountain ranges, and negative trends found at more moderate elevations, almost always to the north and east of upland areas. Positive trends are more commonly associated with lower latitudes and higher elevations than negative trends, except in extreme eastern Siberia and western Alaska. Latitudinal distributions of both signs of On4 trend indicate slight northward shifts of a few degrees of latitude relative to those of On1 trends. During the month containing their respective mean onset-dates, On4 trends of both signs are associated with generally cooler conditions (by ~5°C) than those seeing On1 trends, and somewhat (for negative trends) to considerably (for positive trends) drier conditions. The magnitudes of positive On1 trends are stronger than (the absolute values of) all other categories. Overall, magnitudes of both signs of trend strengthen at higher elevations, lower latitudes, and with later mean onset-dates. These correlations are essentially identical for On1

and On4 trends of the same sign (Figure 3.8, Table 3.2). The metrics plotted in Figure 3.9, illustrating variation in both the rate of change in onset-date and the area affected, further emphasize the distinctions between the two trend-signs.

It is interesting to note that mean On1 dates among the DGPs experiencing progressively later onset of initial snow-cover (positive On1 trends) are all earlier than those experiencing later onset of more persistent snow-cover (positive On4 trends). However, the reverse is true among negative trends (i.e., mean onset dates of DGPs with negative On1 trends are later than those associated with DGPs having negative On4 trends). The patchy spatial distribution of positive trends severely limits the potential for inferences to be drawn about these from this observation. However, the more widespread incidence of negative trends is more useful, supported further by the strong metrics of correlation between latitude and onset-date in the same sub-set of DGPs (Table 3.2). Thus, while there may be some possible sign of a link between progressively later onset (at high altitudes) each year in more southerly areas and later onset further to the north, there is much stronger evidence that earlier onset at higher latitudes is followed by earlier onset at lower latitudes.

3.5.2. Are Change-Points Discernible in Temporal Trajectories of Snow-Onset and Meteorological Conditions?

Where significant trends exist, it is useful to explore the timings of shifts from anomalies of one sign to the other within the associated series of snow-onset dates, and to compare these with patterns in meteorological data relating to the same areas. This was achieved using cumulative anomaly summation (CUSUM) series generated from the records of On1 and On4 onset-dates, and also from series of mean temperature and precipitation (based on the datasets made available

by Willmott and Matsuura of the University of Delaware) in each year during the month containing the mean onset-date for the corresponding DGPs. In principle, any distinct extreme values within the CUSUM series mark change-points in the overall trajectory of the metrics to which they relate, and thus provide information about the corresponding trends' temporal development. (Note that meteorological records were not available for 10% (8%) of the DGPs for which negative On1 (On4) trends were identified, nor for 9% (12%) of those with the respective positive trends.) Given the number of points involved, the comparison offered here is necessarily generalized, and it is not possible to consider the nuances of relationships between sub-sets of patterns among the various series. Nevertheless, it provides a foundation for subsequent more detailed analysis.

3.5.2.1. Snow-Onset Change-Points

Among the CUSUM profiles generated from snow-onset dates associated with significant negative On1 and On4 trends, the extreme values are all clear maxima, indicating a distinct temporal change-point from positive to negative anomalies. These suggest that snow generally arrived later than the series mean until the mid-1990s, and earlier after that point (Figures 3.10 a-b, 3.11 a-b). The modal years for the annual counts of peak 1-year, 3-year mean and 5-year mean CUSUM values for both On1 and On4 lie predominantly between 1994 and 1997: maxima occur before 1997 over approximately 70% (66%) of the total area in which negative On1 (On4) trends were identified (Appendix 2, Figure A2.4). Mapping the peak years, and plotting them against latitude, longitude and elevation (details of which are provided in Appendix 2, Figures A2.7 to A2.10), reveals that the earlier On1 trends located inland from the northern Pacific coast of North America, in central-eastern Europe, and isolated pockets of the Middle East and eastern Eurasia correspond to areas where the switch from positive to negative anomalies occurred in the

1980s. The comparatively small clusters of negative On1 trends situated on higher, west-facing slopes are members of this sub-set. Transitions from later to earlier onset-date anomalies throughout most of eastern Eurasia occurred during the 1990s, while in central and eastern North America they generally took place somewhat later, until the mid-2000s.

Overall, highly significant ($p < 0.001$) but weak (absolute values of R ~0.25 to 0.30) positive (negative) correlations exist between the year of the extreme 3-year mean value of each CUSUM series and latitude (elevation) among DGPs with significant negative On1 trends, and with elevation only for those with negative On4 trends. However, stronger positive associations exist on each continental landmass between the year of peak 3-year mean On1 CUSUM and longitude, with $R = 0.52$ in the Western Hemisphere and $R = 0.36$ in the Eastern ($p < 0.0001$ for both). These findings imply that – in highly simplistic terms – transitions to earlier onset developed initially at higher elevations and lower latitudes, and 'migrated' downward and poleward in a generally north-easterly direction.

The extreme CUSUM values associated with DGPs manifesting significant positive trends are all (with the exception of a single On1 instance) minima, indicating clear shifts from earlier- to later-than-average onset. However, the timings of these transitions are generally less distinct and coherent than the equivalents for negative trends. The annual mean and 95th percentile curves show clear minima in 1998 for both On1 and On4 (Figures 3.10b, 3.11b), and the modal frequencies of extreme CUSUM values in the 1-year, 3-year mean and 5-year mean series coincide with these (see also Appendix 2, Figure A2.4). However, between 1985 and the early 2000s the curve representing the median of annual On1 CUSUM values is more or less flat (indicating that onset-dates during this interval were near the series mean), suggesting that outliers during this period may be exaggerating the means.

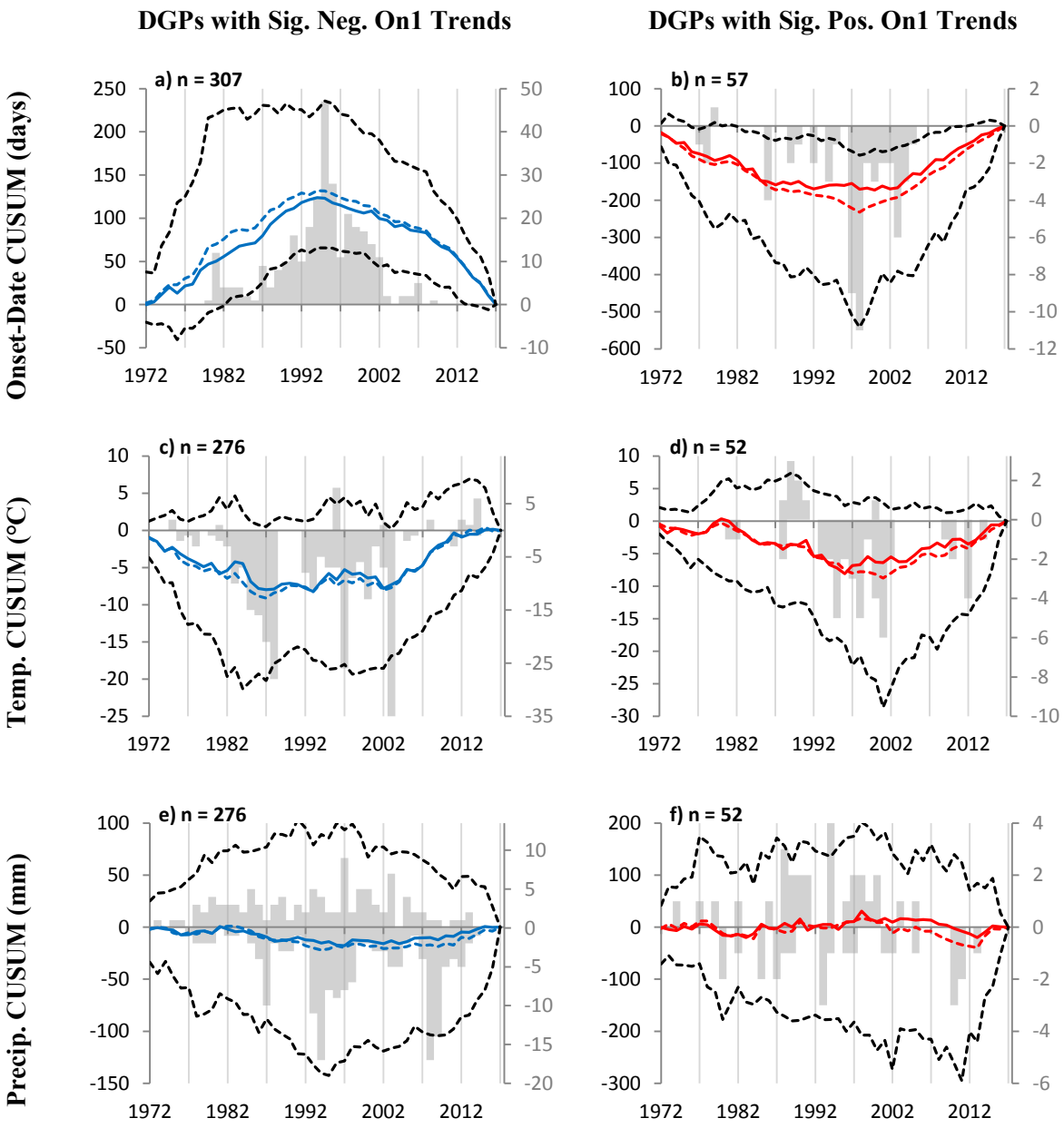

Figure 3.10: Summaries of variation among CUSUM series and change-point years of (a, b) On1 snow-onset dates, (c, d) monthly mean temperature and (e, f) monthly mean precipitation in mean onset-months, for DGPs with significant On1 trends. Blue / red solid (dotted) lines are medians (means) of annual CUSUM values, outer dark dotted lines are 5th and 95th %iles (left axes). Grey bars (right axes) show the annual frequencies of corresponding extreme values in 3-year running means. Where the extreme value for a series is a maximum (minimum), it is counted as a positive (negative) frequency. More detailed plots of the annual means and medians only are provided in Appendix 2, Figure A2.2.

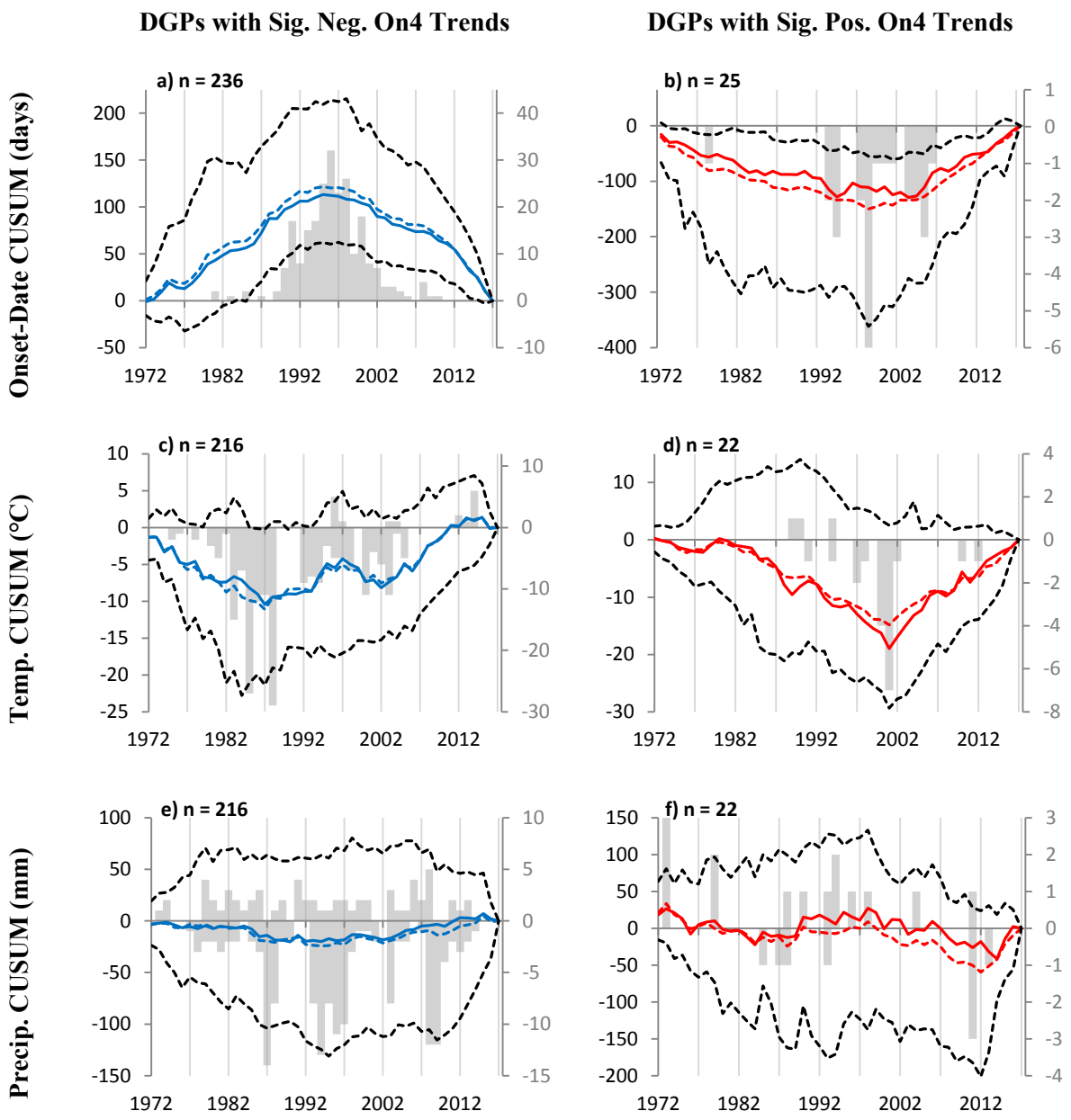

Figure 3.11: Summaries of variation among CUSUM series and change-point years of (a, b) On4 snow-onset dates, (c, d) monthly mean temperature and (e, f) monthly mean precipitation in mean onset-months, for DGPs with significant On4 trends. Blue / red solid (dotted) lines are means (medians) of annual CUSUM values, outer dark dotted lines are 5th and 95th %iles (left axes). Grey bars (right axes) show the annual frequencies of corresponding extreme values in 3-year running means. Where the extreme value for a series is a maximum (minimum), it is counted as a positive (negative) frequency. More detailed plots of the annual means and medians only are provided in Appendix 2, Figure A2.3.

Given that nearly half of the 1-year, 3-year mean and 5-year mean CUSUM change-points fall between 1997 and 2001 (see Appendix 2, Figure A2.4), and the temporal proximity of these

years to the introduction of major technological improvements to the NRSA with implementation of the IMS in 1999, this in particular demanded investigation of associated patterns of temperature and precipitation.

3.5.2.2. Temperature Change-Points

Trajectories of temperature during the period of interest in the areas associated with DGPs yielding significant On1 / On4 onset-date trends were explored using CUSUM series based on mean temperatures in the months containing the corresponding mean onset dates. (Note again that this approach was preferred over using the month of actual onset in each year, as there are considerable differences in monthly means, so using these would have exaggerated the results.)

The extreme values of these CUSUM series were found to be minima for ~93% of those associated with both On1 and On4 negative (i.e. earlier) snow-onset trends, and ~85% of those having positive (later) On1 / On4 trends. This suggests that the great majority of areas seeing all four categories of trend have experienced distinct shifts from negative to positive temperature anomalies, and thus overall warming, during the period of interest (Figures 3.10 c-d, 3.11 c-d). While it is perhaps somewhat counter-intuitive that this applies to points for which negative, as well as positive, snow-onset trends were identified, there are distinct contrasts between their detailed trajectories.

Among those experiencing negative trends, extreme minima occurred principally in three main temporal clusters, in the latter 1980s (more dominant for points having On4 than On1 trends), latter 1990s, and early 2000s (Appendix 2, Figure A2.5). Over approximately 40% (55%) of the total area experiencing negative On1 (On4) trends, temperature anomalies switched from negative to positive before 1990. Warming progressed at a relatively slow rate from 1987 to

2003, although it was faster (apparently with a brief hiatus in the late 1990s) for areas seeing On4 than On1 trends. Since the early 2000s, warming has accelerated considerably in these areas. When compared with the corresponding snow-onset CUSUM series (Figures 3.10a, 3.11a), the peak of the latter may be seen to occur approximately 5 – 10 years after the first major shift from negative to slightly positive temperature anomalies.

Among DGPs for which positive trends were identified, a tighter grouping of change-points from negative to positive temperature anomalies is evident through the latter 1990s (slightly earlier for On4) to early 2000s, with a sharp minimum in 2001. This follows the clear minimum in the snow-onset CUSUM series (Figures 3.10b, 3.11b) by 3 – 5 years. Mean overall cumulative cooling until ~2000 in areas associated with positive On4 trends was approximately twice that for DGPs having negative On4 trends (Figures 3.11c, d). These profiles demonstrate that areas seeing later onset, although generally warmer than those with negative trends, experienced a longer initial period of negative temperature anomalies, followed by a sharper transition to the rapid rates of warming observed since ~2000.

3.5.2.3. Precipitation Change-Points

The CUSUM series generated from records of mean monthly precipitation in the mean onset-month within each category of trend display considerably greater spreads of annual values between 1972 and 2017, and comprise more sub-decadal variability in the implied anomalies, than those seen in the equivalent series for snow-onset and temperature (Figures 3.10e, f; 3.11e, f). This translates into less temporal consensus in the incidence of change-points, which often involve a mixture of minima and maxima of appreciable magnitudes in individual series (see Appendix 2, Figure A2.6). (As is so often the case, information is unfortunately not available to describe the precipitation phase.)

However, among DGPs experiencing negative trends and thus progressively earlier On1 (On4) dates, the extreme values of their precipitation CUSUM series are minima for 62% (68%) of the total number of each type of trend, suggesting an overall shift from mainly negative to positive anomalies, and thus a general increase in precipitation during the period of interest. Where positive trends were identified, the extreme values for 52% (64%) of the series associated with On1 (On4) trends are maxima, implying the opposite (see Appendix 2, Figure A2.6).

Generally, areas associated with DGPs for which negative On1 and On4 trends were identified exhibit mainly negative precipitation anomalies until the early 1980s, followed by 15 – 20 years of comparatively low positive anomalies (greater, but more variable, for On4 than On1), before more rapid increases during the 2000s. Three principal clusters of minima are evident, in the latter 1980s, mid 1990s, and latter 2000s (see plots in Appendix 2, Figure A2.6). These correspond reasonably closely (but not precisely) with the years in which minima occur in the temperature CUSUM series associated with DGPs having negative snow-onset trends (see Appendix 2, Figure A2.5). The first two clusters occur during the period of positive snow-onset anomalies, and the third aligns with a small cluster of maxima in the latter 2000s (Appendix 2, Figure A2.4).

The relationship between trajectories of precipitation and positive snow-onset trends is the least distinct of all combinations considered. Nevertheless, the excess of maximum extreme values over minima suggests an overall switch from positive to negative anomalies, and thus a slight overall drying tendency. The plots of mean and median CUSUM values (Figures 3.10 f, 3.11 f; see also Appendix 2, Figures A2.2f, A2.3f) imply a transition from moderate negative anomalies in the early 1970s to increases until the late 1990s, followed by a steep drop to 2013. The local maximum around 1998 corresponds closely with the clear minimum in the snow-onset

CUSUM series (and is also near the switch from negative to positive temperature anomalies) associated with DGPs having positive trends. Although only relatively few DGPs are involved in these sub-sets, it would be useful – given the complexity of the underlying fine detail – to explore these patterns further.

3.6. Discussion and Conclusions

This analysis explored monotonic trends in the onset-date of seasonal snow-cover across the NH between 1972 and 2017. The first major snowfall of the season was termed On1, and the first persisting subsequently for at least four weeks On4. Widespread statistically-significant negative trends, indicating shifts towards progressively earlier onset-dates, were identified, while positive trends (shifts to later onset) were fewer in number and more localized. Negative On1 (On4) trends were found to occur over areas larger than those associated with positive trends by a factor of five (nine). Trends of each sign were associated with clearly distinct contexts, in terms of their physiography, latitude, longitude and climatology.

Perhaps the most striking spatial pattern is the clear longitudinal alternation between areas affected by negative and positive trends (Figures 3.3; 3.8c, d; 3.9b). Those experiencing a delay in snow-onset are almost all located to the west (often south-west) of appreciable uplands, in north-western North America, Scandinavia, to the immediate south-west of the Urals, and in south-western parts of the Himalayan Massif. Meanwhile, earlier onset is associated largely with areas of low-to-moderate elevation to the north and east of major uplands between 40°N and 60°N. The three principal examples of the latter (in decreasing order of extent) extend from the Tien Shan, through the Altai, Sayan, Yablonoi and Stanovoy chain to north-eastern Siberia; from the Rocky Mountains through central-western to central-northern North America; and from the

Alps through central-eastern Europe. The north-eastward continuation of each of these alignments leads to a circumpolar marine area in which autumn sea-ice extent has been receding particularly rapidly, namely the Chukchi Sea (Serreze and Stroeve 2015), Hudson Bay (Andrews et al. 2018), and the Barents / Kara Sea (Wegman et al. 2015; Onarheim and Årthun 2017), respectively. Indeed, the largest increases in ocean-to-atmosphere surface turbulent heat fluxes in the entire Arctic have occurred in the first and last of these (Cohen et al. 2018).

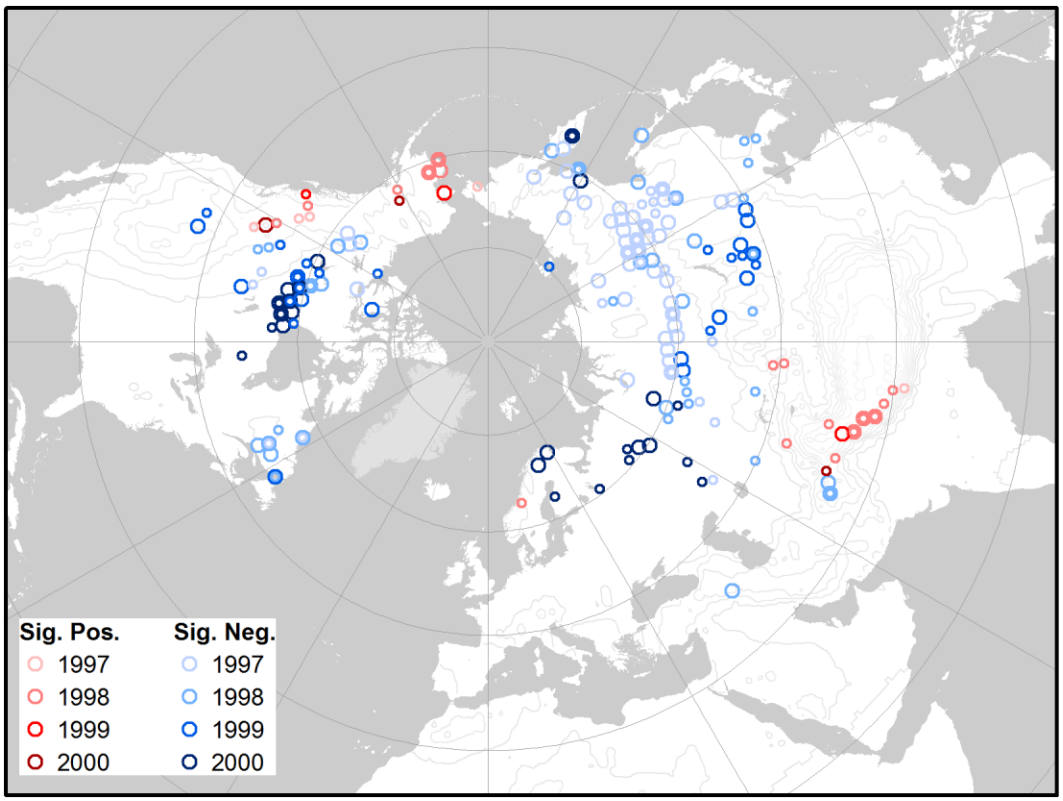

Figure 3.12: Spatial distribution of DGPs with significant On1 (smaller symbols) and On4 (larger symbols) trends, where the change-point years of the corresponding snow-onset dates are between 1996 and 2001. (Meridional interval of graticule is 15°, zonal interval 30°.)

Together with latitude, elevation, aspect, and proximity to an Arctic coastline, the other key modulating influence on trend development is the spatio-temporal evolution of atmospheric circulations, and their interactions with surface relief and other characteristics. While detailed consideration of these factors lay outside the scope of this study, it is noteworthy that the

longitudinal positions of positive trends identified here coincide closely with those in which persistent blocking systems have been found to occur relatively frequently from September to November, while negative trends align with areas immediately to the east of these meridional bands (Barriopedro et al. 2006; Tyrlis and Hoskins 2008; Cheung et al. 2013). The pattern described here over eastern Eurasia conforms closely with current consensus on the most robust mechanism by which amplification of climate-change in the Arctic is affecting extreme meteorological events at mid-latitudes – namely, that ice-loss in the Barents and Kara Seas is contributing to the intensification of the Siberian High and consequent troughing to its east, resulting in additional humidity released from increasingly ice-free areas of the Arctic Ocean falling as snow further to the south (Cohen et al. 2018). Given the juxtaposition of climatologically frequent anti-cyclonic conditions and more open Arctic waters 'upstream' of the two other largest regions affected by earlier snow-onset (to the north of Canada and central Europe), it is reasonable to speculate that comparable processes may also explain these trends. Together with the generally cool climatological settings in which they occur, and the potential for some degree of orographic enhancement of precipitation by uplands further to the south and / or south-west in each instance, these factors help to explain how snow could have been arriving earlier in the year over these areas. Meanwhile, the positive trends could relate to a reduction in the availability of precipitable water, as systems are prevented from travelling eastward by the blocking systems themselves, and / or the northward advection of warmth from areas further to the south. It would thus be useful to explore in more detail how these circulations have evolved within the areas affected by both signs of trend over the same period, particularly in relation to any changes in the spatial patterns of dominant pressure systems.

A key finding pertinent to the wider discussion relating to the credibility of the NRSA is that approximately 70% (66%) of DGPs associated with significant negative On1 (On4) trends had shifted from positive to negative snow-onset anomalies by 1997, two years before introduction of the IMS and imagery of higher spatial and temporal resolutions. These technical improvements would have resulted in the more distinct resolution of snow-covered from snow-free land than the prior system, particularly over areas with greater spatial and / or temporal frequency of variation in snow-cover, such as in complex mountainous terrain or at the fringes of snow-prone areas. It might therefore be expected that snow-onset change-points around 1999 would cluster preferentially over such settings. However, those DGPs for which change-points between 1997 and 2000 were identified are distributed predominantly over the interior shield regions of North America and Eurasia (Figure 3.12). Of the relatively few exceptions, most – particularly in the south-west Himalayan ranges and central Rocky Mountains – are positive trends. While these are less contentious in the context of widespread warming, it would be informative to explore their associations with shifting patterns of precipitation, temperature and meteorological systems in more detail.

While the temporal trajectories of snow-onset anomalies in each sub-set of trends have been shown to correspond generally to shifts in temperature and precipitation anomalies, this analysis does not claim to offer a conclusive explanation for each individual DGP's negative or positive onset trend. The association between negative onset trends and switches from mainly negative to positive temperature anomalies is also counter-intuitive, particularly given current understanding of the sensitivity of snow-cover to temperature (e.g. Mudryk et al. 2017). However, these results offer the basis for a possible explanation, by demonstrating that the areas affected are found in relatively cool climatological settings, immediately to the east of regions in which blocking

systems develop frequently (and which are therefore prone to troughing), and are set between patches of the southern Arctic Ocean in which freeze-up has been delayed to the north-east, and uplands of appreciable height and extent to the south and / or south-west. Together, these influences appear to have resulted in a moderate increase in precipitation falling as snow earlier in the transition from late summer to winter. It seems probable, though – given the accelerated rate of warming observed since the early 2000s – that this augmented early snowfall will change to rain in the near to medium term. In contrast, some combination of a later but sharper shift to warming, together (in some areas) with a downward swing in precipitation, led to snowfall arriving later in the year over DGPs associated with positive onset trends, largely within regions prone to frequent and / or persistent anti-cyclonic conditions at the same time of year.

It is again emphasized, though, that the extreme inter-annual variability of the precipitation patterns severely limits the reliability of the conclusions drawn here. A useful approach for more detailed analysis might be to identify clusters of DGPs with broadly similar CUSUM profiles generated from onset-dates, temperature and precipitation on the basis of curve-shape, using an appropriate multi-dimensional classification method. This would in turn support examination of relationships between the various change-points within sub-sets having comparable trajectories (and thus, notwithstanding equifinality, exogenous influences), and potentially also in more localized spatial contexts. It would also be useful to identify and quantify temperature and precipitation trends within the same spatial framework as that on which the onset trends were based, and to compare temporal patterns of Arctic sea-ice (particularly in the areas of key interest) in the months corresponding and prior to mean snow-onset with those of the onset-dates.

While these results seek to augment understanding of trends in the onset of NH snow-cover derived from the NRSA by identifying their temporal trajectories and relating them to meteorological activity, other explanations must yet be considered. For example, widespread clearances over large areas of the Russian and North American boreal forests during recent decades – caused by fires, major pest outbreaks and the resource-extraction industries (such as those described since 2000 by Hansen et al. 2013) – will have resulted in a proliferation of more open areas. It seems possible that snow may previously have existed at a given time of year in such areas, but was previously hidden by the dense needleleaf forest (once it had been shed from the canopy). The new clearings may have provided more visual cues for the IMS, potentially resulting in the identification of such pre-existing snow-cover as 'new'. Therefore, if – within the footprint associated with a given DGP for which a negative snow-onset trend was identified – the year in which substantial clearance occurred is found to correspond closely with a shift in its onset-date anomalies, this would warrant further investigation. On the other hand, it is at this stage by no means clear that the spatial dimensions of these clearances would be sufficiently large for any newly-revealed snow to be detectable within the imagery from which the NRSA is derived.

This study thus provides a range of new information relating to snow-onset trends across the NH, and relates these details to the physiographic and climatological characteristics of the affected areas. Although no claims are made that these findings represent conclusive explanations for either sign or type of the onset-date trends derived from the NRSA, these new perspectives on their spatial and temporal incidence and evolution offer a useful contribution to the continuing exploration and discussion of this topic.

4. The Climatological Context of Trends in the Onset of Northern Hemisphere Seasonal Snow-Cover, 1972-2017

This chapter was submitted to *Journal of Geophysical Research – Atmospheres* on 31st December 2019

4.1. Abstract

Recognition of the key role played by seasonal snow in modulating water and energy budgets across the Northern Hemisphere has prompted prior research to determine how spatial and temporal patterns of its incidence are changing. Several studies based on the longest remotely-sensed record of snow-cover, generated and curated by Rutgers University, have yielded the counter-intuitive finding that its extent has increased over large areas of Eurasia and North America during the transition from summer to winter. It has been suggested that these early-season increases are artifacts of technological improvements in the dataset's production. Alternatively, if these trends reflect actual changes in the timing and location of snow-onset, associations should exist with altered spatio-temporal patterns of atmospheric activity likely to result in or delay snowfall. This study relates significant NH snow-onset trends between 1972 and 2017 to their climatological contexts, as represented by means of, and trends in, a range of relevant metrics of mid-to-lower tropospheric activity, derived from reanalysis data. The results identify clear explanatory links between earlier / later onset and patterns of trends in 500 hPa geopotential heights and sea-level pressure, airflows at 500 hPa and 850 hPa, atmospheric humidity, and near-surface temperature. These findings suggest that most incidences of progressively earlier Eurasian snow-cover result from northward advection of moisture by stronger southerly winds, driven by altered zonal gradients in geopotential height north of the

Himalayan ranges. Over North America, moisture has been supplied primarily from maritime sources along zonal airflows induced by meridional gradients.

4.2. Introduction

Seasonal snow-cover imposes a widespread transformation of physical conditions over much of the Northern Hemisphere's surface through the cooler months, thereby substantially modulating energy and water budgets. For example, its associated high albedo accounts for a greater fraction of atmospheric negative radiative forcing than sea-ice for nine months of the year (Flanner et al., 2011), and it interrupts the transformation of precipitation to runoff while ambient temperatures remain sufficiently cool. When this frozen reservoir melts during spring and summer, it provides the principal source of water for at least two billion people (Mankin et al., 2015). Identification of the key roles played by snow within the Earth System – influencing thermodynamic, hydrological, geomorphological and ecological processes – has prompted a series of studies to determine whether or not spatial and temporal aspects of its incidence have changed in response to secular trends in atmospheric and oceanic conditions during recent decades. Images captured from satellite-mounted sensors have proven invaluable for inferring conditions across the Northern Hemisphere (NH) at suitable temporal frequency, thus providing the foundation for much of this research (e.g. Robinson et al., 1993; Groisman et al., 1994; Frei et al., 1999; Dye, 2002; Rikiishi et al., 2004; Déry and Brown, 2007; Choi et al., 2010; Brown and Robinson, 2011; Cohen et al., 2012; Liu et al., 2012; Hernández-Henríquez et al., 2015; Allchin and Déry, 2017).

The longest archive provided by any such dataset is the climate data record of weekly NH snow-cover, produced and curated since 1966 by the Global Snow Laboratory at Rutgers

University (https://climate.rutgers.edu/snowcover), and published by the United States' National Oceanic and Atmospheric Administration (NOAA) (hereafter the NOAA-Rutgers Snow Archive, NRSA: Robinson and Estilow, 2012; Estilow et al., 2015). As well as demonstrating the degree to which snow has been melting earlier in spring, the NRSA has repeatedly yielded the finding that snow-covered area has been increasing during the boreal autumn over much of the NH (Frei et al., 1999; Brown, 2000; Rikiishi et al., 2004; Choi et al., 2010; Déry and Brown, 2007; Hernández-Henríquez et al., 2015; Allchin and Déry, 2017). The timings and magnitudes of these – somewhat counter-intuitive – trends have prompted several subsequent studies to raise doubts about their veracity, based on comparisons with those derived from other datasets. It has been suggested that these results may be artifacts related to the introduction in 1999 of more automated processing of imagery at higher spatial and temporal resolutions (Brown and Derksen, 2013; Mudryk et al., 2017; Hori et al., 2017).

However, these disagreements may also derive – at least in part – from assumptions made when estimating snow-covered area from the NRSA. Its binary classification records only whether each grid-cell has at least 50% snow-cover, or less than this amount, in each weekly granule: while these categories have generally been interpreted as implying 'snow-covered' (i.e. 100% snow) and 'snow-free' (0%), it is logical to expect that a given spatial unit will often have a value somewhere between either extreme and the 50% threshold, particularly during the onset and melt seasons. As shown by Allchin and Déry (2017), estimates of trend-magnitude vary in linear proportion to the contrast in percentage snow-cover associated with each category of the classification. It should therefore be recognized that – in the absence of a credible quantification of actual percentage cover in each spatial sub-unit through the period of interest – estimates of

trends in snow-covered area derived using the conventional assumption will be exaggerated, and that this effect will be magnified in autumn and spring.

Nevertheless, useful insights into changing patterns of seasonal snow may be inferred without depending on estimates of changes in its area. For example, Allchin and Déry (2019) considered spatial and temporal patterns of trends in the date at which snow-cover first passes through the 50% threshold during autumn and early winter between 1971 and 2017. The analysis revealed significant amplification of both negative (progressively earlier) and positive (later) snow-onset trend magnitudes at lower latitudes, higher elevations, and in areas where snow usually arrives later in the cold season. It also identified a marked longitudinal alternation between negative and positive trends, with an apparent alignment either side of major mountain ranges. Most of the instances of negative trends in onset-date were found to have switched from positive to negative anomalies (relative to the 1972-2017 mean) well before the NRSA adopted improved imagery and processing methods. While relatively simplistic associations were established between the temporal development of these trends and those in corresponding representations of temperature and precipitation, and speculation offered that they could relate to changing circulation patterns, it was suggested that substantial potential remains for further investigation of links between snow-onset trends and indicators of atmospheric activity.

This study was therefore conceived with the principal goals of describing at monthly intervals how the spatial distribution of snow-onset trends evolves during the transition from summer to winter, and determining the degree to which these could be associated with relevant metrics of climatological change. As well as reinforcing the credibility of the NRSA itself, the identification of such links would underpin the large volume of research based on its representation of NH snow-cover. In addition, a more detailed description of linkages between

seasonal snow-cover and atmospheric dynamics – of which understanding is currently limited (Shepherd, 2016; Francis, 2017; Francis et al., 2017; Overland, 2017; Cohen et al., 2018) – would inform debate relating to the possible influences of amplified circumpolar warming on mid-latitude meteorological activity.

4.3. Data and Methods

If the snow-onset trends identified from the NRSA relate primarily to climatological influences, rather than being essentially observational artifacts, it follows that their incidence should be spatially and temporally associable with patterns of changes in relevant metrics of atmospheric activity, relative to average conditions through the PoI. This section provides details of the datasets and analytical techniques employed to determine whether or not such links exist.

4.3.1. Metrics of Seasonal Snow-cover

The NRSA's binary classification of snow-cover is organized as a regular grid of 89 rows and 89 columns in a polar stereographic projection. This results in greater separation between dataset grid-points (DGPs) at higher latitudes, so the area associated with each increases poleward. Between latitudes 30°N and 75°N, 90% of orthogonal inter-DGP separations lie between 3.9° and 1.5° (median 1.9°): within the same meridional band, 90% of DGP footprint areas (as supplied with the dataset) range from ~39,000 km² to ~24,000 km² (median 31,370 km²). A unit value stored for a DGP in a given weekly granule of the archive signifies that at least 50% of its associated area was snow-covered, as judged from the image depicting the last day of the previous seven (Tuesday to Monday) on which it was visible (Estilow, 2013). The NRSA's first records date from October 1966: its only omissions span a total of 37 weeks, between July 1968 and September 1971.

The principal concerns raised about the plausibility of trends derived from the archive relate to the replacement of the original manual interpretation process with the substantially more automated Interactive Multisensor Snow and Ice Mapping System (IMS), together with improvement of the imagery's spatial resolution from ~190 km to 24 km, and temporal resolution from weekly to daily, in 1999 (Ramsay, 1998; Estilow et al., 2015). Although concerted efforts were made to ensure that these changes did not result in inconsistencies in the detection of snow arising either side of their introduction (Romanov et al., 2000; Helfrich et al., 2007; Estilow, 2013; Estilow et al., 2015), it has been suggested that they may explain disagreements between trends estimated from the NRSA and those derived from other datasets, particularly during the onset and melt seasons (Brown and Derksen, 2013; Mudryk et al., 2017; Hori et al., 2017).

This study contributes to the discussion by investigating whether or not spatial distributions of trends in the onset of seasonal snow-cover correspond to changing climatological influences. In common with Allchin and Déry (2019), trends were identified among two categories of snow-onset, based on the NRSA time-series for each DGP between mid-August and the end of December, from 1972 to 2017. The first, termed On1, tracks the date of the first transition from 'snow-free' (i.e., less than 50% snow-cover) to 'snow-covered' (at least 50% snow-cover), regardless of its subsequent persistence. The second, termed On4, is based on the first such event in each snow-year which is followed by at least four consecutive weeks of dominant snow-cover. On4 dates have previously been found to equate closely to the start of the longest period of unbroken snow-cover within each DGP's associated footprint through each winter (Allchin and Déry, 2019).

In this analysis, masks supplied with the NRSA or developed in previous studies (principally Déry and Brown, 2007) were applied to exclude oceanic areas, land with perennial cryospheric cover, and an additional 33 points associated with snow-cover records identified as questionable. Trends significant with $p < 0.05$ were identified by Mann-Kendall analysis (Mann, 1945; Kendall, 1975), and magnitudes estimated using the Theil-Sen method (Theil, 1950; Sen, 1968). While the NRSA's weekly granularity may amplify these magnitudes to some degree, this effect is likely to have been mitigated by week-to-week variability (due primarily to obscuration by clouds) of the last day within each set of seven daily images on which any given DGP is visible. DGPs were grouped (separately for On1 and On4) by the month containing their 1972–2017 mean onset-date, and by the sign and significance of trend.

4.3.2. Climatological Metrics

The accumulation of snow-cover depends on the coincidence of adequate concentrations of atmospheric water vapour with suitably low combinations of temperature and pressure to allow for snowfall, and – if it is to persist on the ground – continuing low surface temperatures, in the absence of scouring winds. The 20th Century Reanalysis (20CR), published by the NOAA Earth System Research Laboratory's Physical Sciences Division and the Cooperative Institute for Research in Environmental Sciences (NOAA and University of Colorado Boulder) (Compo et al., 2011), was selected to provide data describing these conditions. This choice was guided primarily by its comprehensive suite of metrics, 93% temporal overlap with the prior study's 1972-2017 PoI (only the last three years of the latter are not covered), and its reasonably fine – yet computationally manageable, at pan-NH scales – spatial resolution of 2°.

Developments in mid-tropospheric dynamics were inferred from 500 hPa geopotential heights (Z_{500}), together with meridional and zonal wind-speeds at the same level (V_{500} and U_{500}, respectively). Geopotential heights at 250 hPa were also considered, and found to correlate strongly with Z_{500} ($R > 0.9$, $p < 0.001$, both series detrended) at every grid-point within the spatial domain in each month of interest. The spatial distributions, signs, significances and relative magnitudes of trends in all three metrics were almost identical at both levels, suggesting that the 500 hPa values provide useful proxies for activity higher in the troposphere. Patterns of meteorological activity were represented by sea-level pressure (SLP), total precipitable water (TPW), 2m air temperature (AT2m), and 850 hPa meridional (V_{850}) and zonal (U_{850}) wind-speeds. Baseline conditions at every grid-point, in each month from September to December (inclusive), were provided for these metrics by averaging their monthly means between 1972 and 2014. Significant linear trends over the same PoI were identified, and associated magnitudes estimated, using the Mann-Kendall and Theil-Sen methods, respectively.

While the grids adopted for the NRSA and 20CR are broadly comparable in spatial resolution, they are drawn in different projections, and do not align with each other. Values of monthly atmospheric metrics at each NRSA point were therefore estimated by inverse-distance weighting among a maximum of nine neighbouring 20CR points within a range of 500 km, and 1972–2017 means and trends generated from the time-series so derived.

The means and trends of each metric for each point on the 20CR grid were mapped, and plotted as meridional and zonal transects within discrete bands of longitude and latitude, respectively. The corresponding values associated with the NRSA DGPs at which significant onset trends were identified were also plotted. Variations in mean and maximum elevation at 5° intervals were included, to illustrate associations with major topographic features. These profiles

were generated from the Global Land One-km Base Elevation Project (GLOBE) digital elevation model (Hasting et al., 1999), supplied as a regular grid with spatial resolution of 30 arc-seconds (equating to ~1 km meridionally, and zonally at the Equator).

4.4. Results

4.4.1. Snow-Onset Climatology

Spatial distributions of NRSA points at which On1 / On4 dates were identified in every year from 1972 to 2017, grouped by the month containing the mean date of onset, and rendered by the week containing that date (Figure 4.1). The 1972-2014 monthly mean 5°C, 0°C and -5°C isotherms were also derived and plotted. Over 90% of all September mean On1 / On4 dates occur in the second half of the month: this explains why the majority of points are located south of the September mean 0°C isotherm (as this line would run further to the south in the latter part of the month). Similarly, the majority of December onset occurs in the first two weeks of that month, so most points are found poleward of the monthly mean 0°C isotherm. Those in October and November are more evenly distributed, but with some bias towards the later / earlier half of each month, respectively (see Appendix 3, Figure A3.1).

4.4.2. Onset Trend Spatial Distributions and Magnitudes

Mapping the distribution of snow-onset trends associated with each month reveals a strong degree of spatial coherence in sign and level of statistical significance (Figure 4.2). This also shows that the majority of significant negative onset trends align closely with the monthly mean 0°C isotherm, and are grouped mainly within longitudinal sectors in which this line has historically tracked furthest to the south over each major landmass (excluding major uplands). In

contrast, most positive trends occur in areas where the 0°C isotherm is found at higher latitudes, particularly along or near to coastal margins.

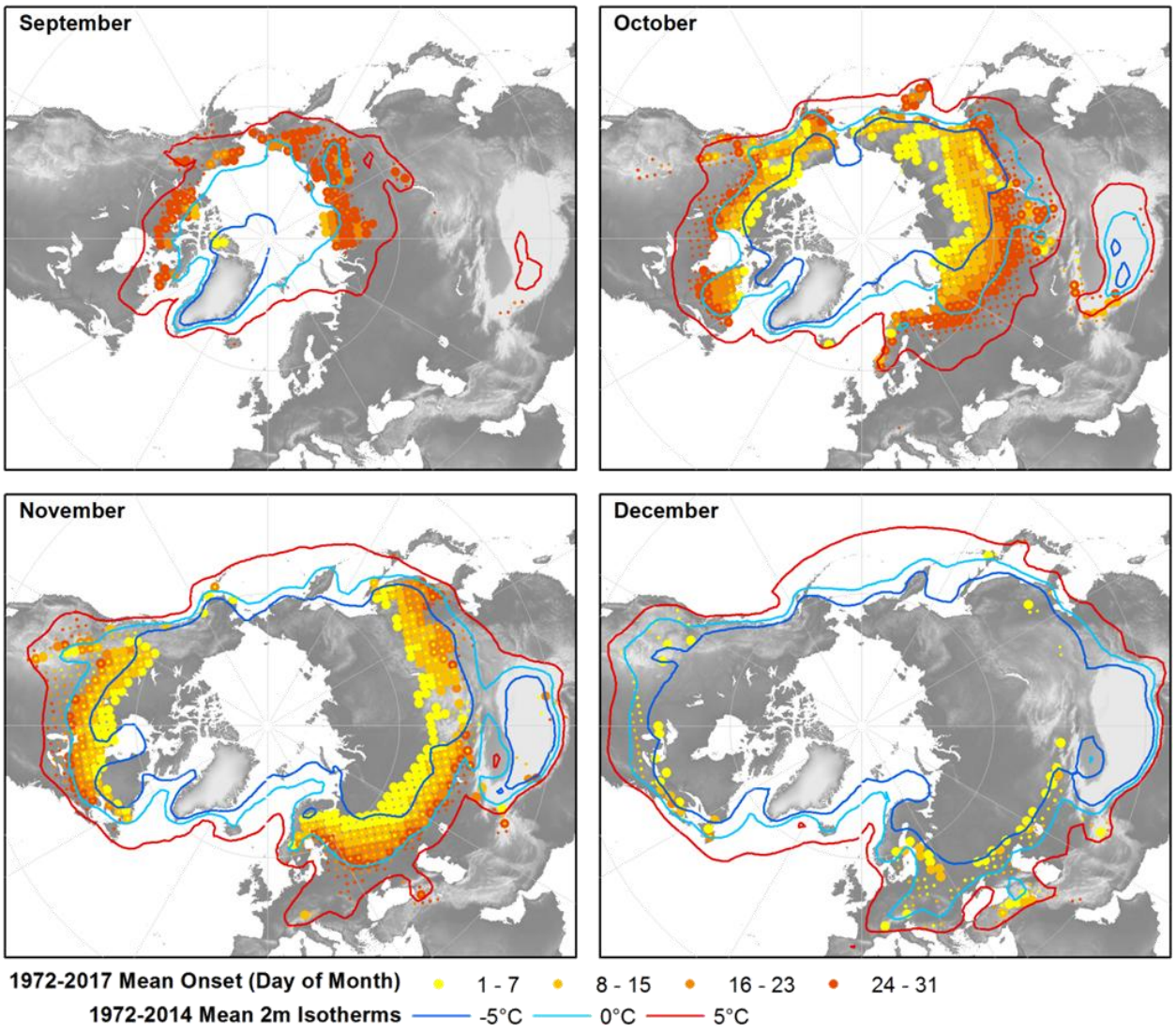

Figure 4.1: Snow-onset climatologies, by month containing 1972-2017 mean date of onset, also showing key 1972-2014 mean monthly isotherms. Larger (smaller) symbols represent On4 (On1) onset dates. (On1 is the date of the first transition in each snow-year from 'snow-free' to 'snow-covered', regardless of persistence: On4 is the date of the first such transition followed by at least four consecutive weeks of snow-cover.) Elevation baselayer from GLOBE digital elevation model.

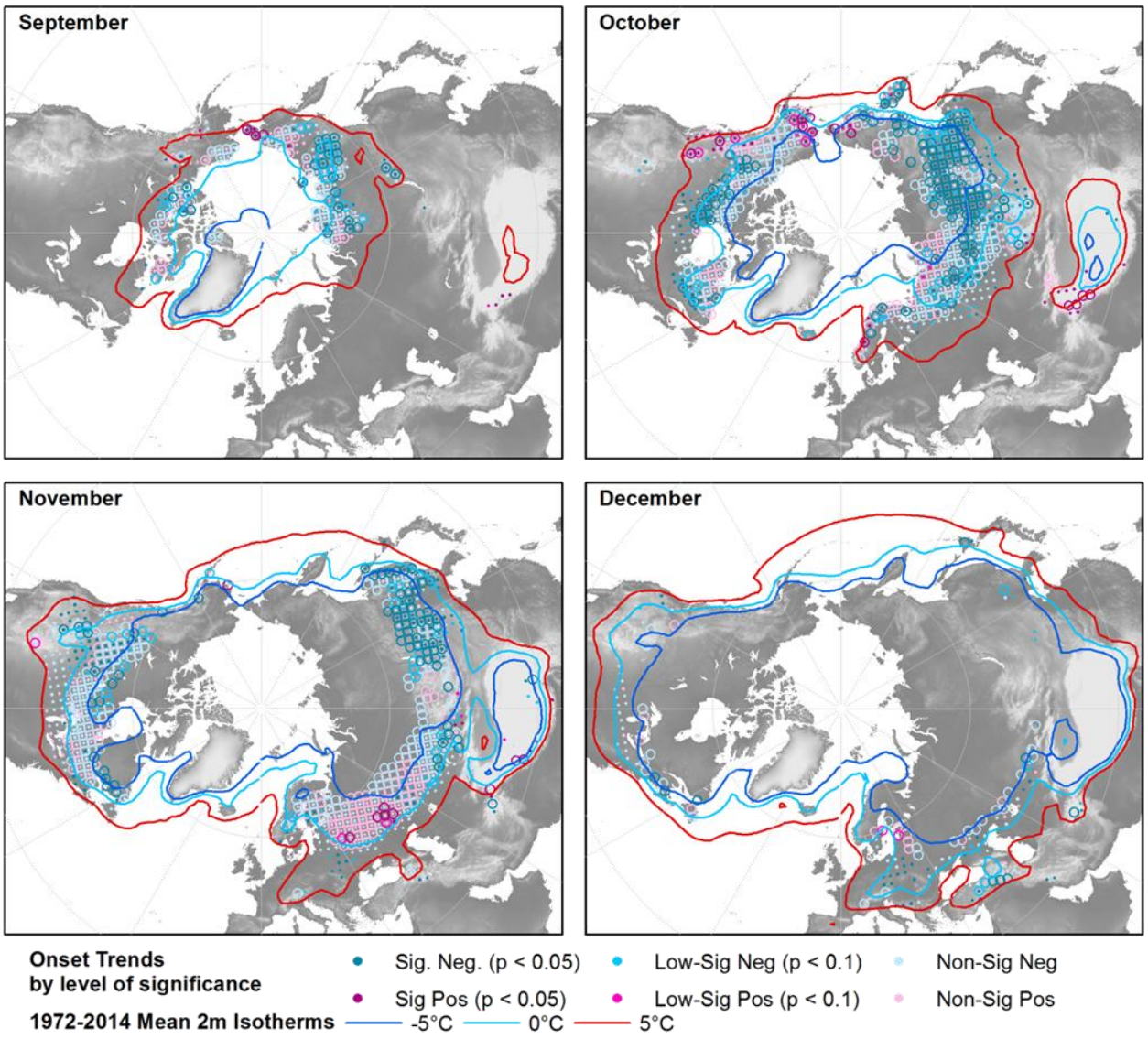

Figure 4.2: Distributions of onset trends by month containing 1972-2017 mean date of onset and level of statistical significance. Larger, unfilled (smaller, filled) symbols represent On4 (On1) onset dates.

These results focus principally on the locations and timings of significant onset trends, in comparison with those associated with relevant climatological metrics. They do not venture to describe relationships between the spatial variation of trend magnitudes and those of possible causative influences. Nevertheless, useful supporting information is provided by overviews of longitudinal and latitudinal variations in the magnitudes of statistically-significant trends, grouped by the month containing their mean onset-dates (Figures 4.3, 4.4). Together, these visualizations demonstrate that the great majority of trends are coherent not only in terms of their spatio-temporal distributions, but also in their magnitudes. A summary of key statistics is shown graphically in Figure 4.5, and tabulated in Appendix 3, Table A3.1. Given that the higher spatial resolution of imagery introduced with the IMS in 1999 would have improved the ability to distinguish snow-free from snow-covered ground over complex terrain, it is noteworthy that the largest magnitudes are seen among positive trends in western parts of the Hindu Kush – Himalaya (HKH) Mountains. However, these high values are not distributed throughout the HKH, but seen only in its extreme west, where they align primarily with the south-western foreslopes. Broadly comparable arrangements, with positive trends to the west and negative trends to the east of the main topographic features, are noted in October in the Western Cordillera of North America and the Scandinavian uplands. The same relative arrangement of trend-signs, but at smaller magnitudes, is also apparent to the north of both the HKH and the Western Cordillera. These observations may suggest that the spatial distribution of these trends is influenced by interactions between major topographic features and patterns of atmospheric circulation.

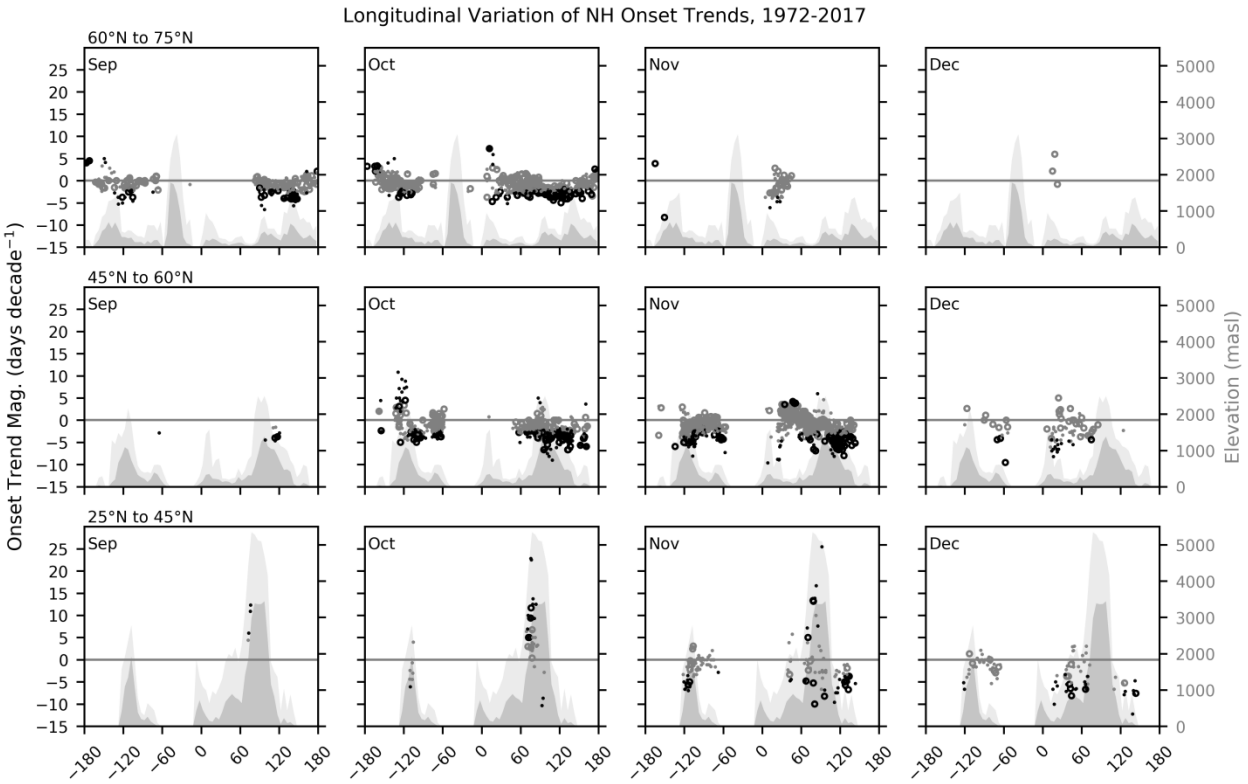

Figure 4.3: Longitudinal distributions of 1972-2017 snow-onset trend magnitudes within three latitudinal bands. Darker (lighter) symbols represent trends significant (non-significant) at the 5% level. Larger, open (smaller, filled) symbols signify On4 (On1) trends. Darker (lighter) shaded areas represent meridional mean (maximum) elevations at zonal intervals of 5°.

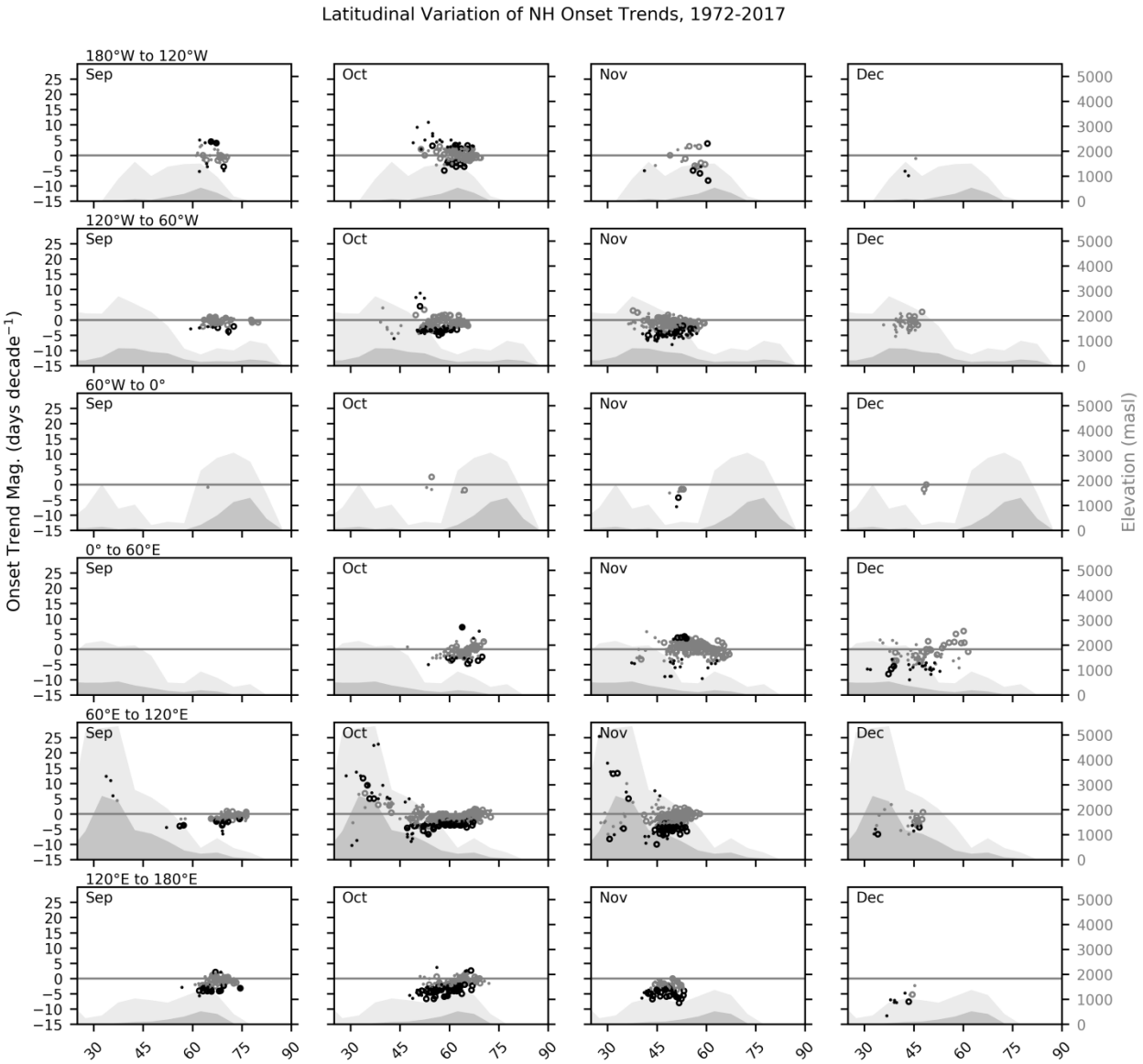

Figure 4.4: As in Figure 4.3, but illustrating latitudinal distributions of 1972-2017 snow-onset trend magnitudes within six longitudinal bands. Darker (lighter) shaded areas represent zonal mean (maximum) elevations at meridional intervals of 5°.

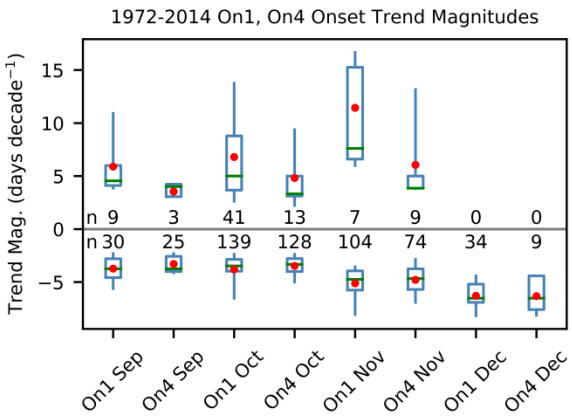

Figure 4.5: Summary statistics of 1972-2017 On1 and On4 trend magnitudes, grouped by the month containing the mean date of onset during the same period. Medians shown as green bars, means as red dots; boxes span 25th to 75th percentiles; whiskers span 5th to 95th percentiles. 'n' is the number of data grid-points manifesting each type and sign of trend in each month. The key statistics represented here are tabulated in Appendix 3, Table A3.1.

4.4.3. Climatological Influences on Onset Trends

4.4.3.1. Mid / Upper Troposphere Geopotential Heights and Winds

Mapping trends in September mean Z_{500} through the PoI reveals a distinct circum-global spiral of significant increases in mid-tropospheric geopotential height (Figures 4.6a, Appendix 3, Figure A3.3). This amplified ridging forms an unbroken chain from the Persian Gulf (and with only a short break, from at least as far as the tropical western Atlantic), eastward over China and Japan, the western U.S.A. and north-eastern Canada to northern Scandinavia and extreme north-western Russia. The pattern is not interpreted as a continuous line of contemporaneous ridging throughout the month, but as the route along which parcels of relatively warm air have travelled from lower to higher altitudes, presumably within Rossby-type wavetrains.

Between the bands of positive Z_{500} trends forming this helical 'conveyor' of enhanced ridging, tendencies range from neutral to moderately negative, but do not attain statistical significance. Nevertheless, the steeper geopotential gradients generated along the northern

margin of these increases drive significant positive trends in (i.e., more westerly) U_{500} wind-speeds, thus delivering warmer air to a terminus over the Barents Sea. Meanwhile, differentials along their southern flank induce significant negative trends in U_{500}, representing at least a substantial decline in westerly wind-speeds, and potentially a reversal to easterly flows. The pattern reverses again to stronger westerlies at lower latitudes, as the spiral continues (Figures 4.6c, Appendix 3, Figure A3.7). The arrangement of these trends, when compared with that of PoI-mean U_{500} wind-speeds (Appendix 3, Figure A3.6), indicates an overall poleward shift of the NH late-summer atmospheric circulation. Undulations along this line of enhanced ridging also give rise to alternating – but relatively localized – patches of positive and negative trends in V_{500} wind-speeds, of which stronger southerlies more often attain statistical significance (Figure 4.6b; Appendix 3, Figure A3.5). The overall pattern thus channels the dominant westerly flows inexorably northward: these encroach into circumpolar areas over north-central Canada, between Greenland and Scandinavia, and – with northward deflection over northern China – eastern Eurasia.

This spiral circulation persists through October and November into December, but becomes increasingly disrupted as continuity along the line of ridging trends decays. As this progresses, three main patches of significantly enhanced Z_{500} develop, initially over north-eastern Canada, northern Scandinavia, and north-eastern Eurasia, each moving to the east in subsequent months. Although Z_{500} trends between these centres are generally not strongly negative (with a few exceptions – Figures 4.7, 4.8), the relative contrasts between maxima and minima form a distinct alternation between augmented ridging and relative troughing: these patterns are strikingly persistent with latitude, particularly over continental areas. This translates into the emergence of a radial pattern – most distinct in October and November – of significant increases in V_{500} wind-

speeds, alternating longitudinally between stronger positive (more southerly) and negative (more northerly) trends (Figures 4.6b; Appendix 3, Figure A3.5). A concomitant latitudinally-alternating pattern of trends in U_{500} wind-speeds is also clearly apparent where regional circulations develop (Figures 4.6c; Appendix 3, Figure A3.7).

While the majority of significant snow-onset trends coincide spatially with the centres of relative Z_{500} troughing tendencies, their arrangement in relation to regional gradients varies. For example, the negative trends over inland eastern Eurasia (~90°E – 120°E) in October correspond closely with relative meridional troughing north of the Himalayas, whereas those in north-eastern North America appear to derive from a north-south dipole. A more detailed understanding of these relationships was sought by examining metrics of atmospheric activity more directly associated with meteorological drivers of the onset and persistence of snow-cover.

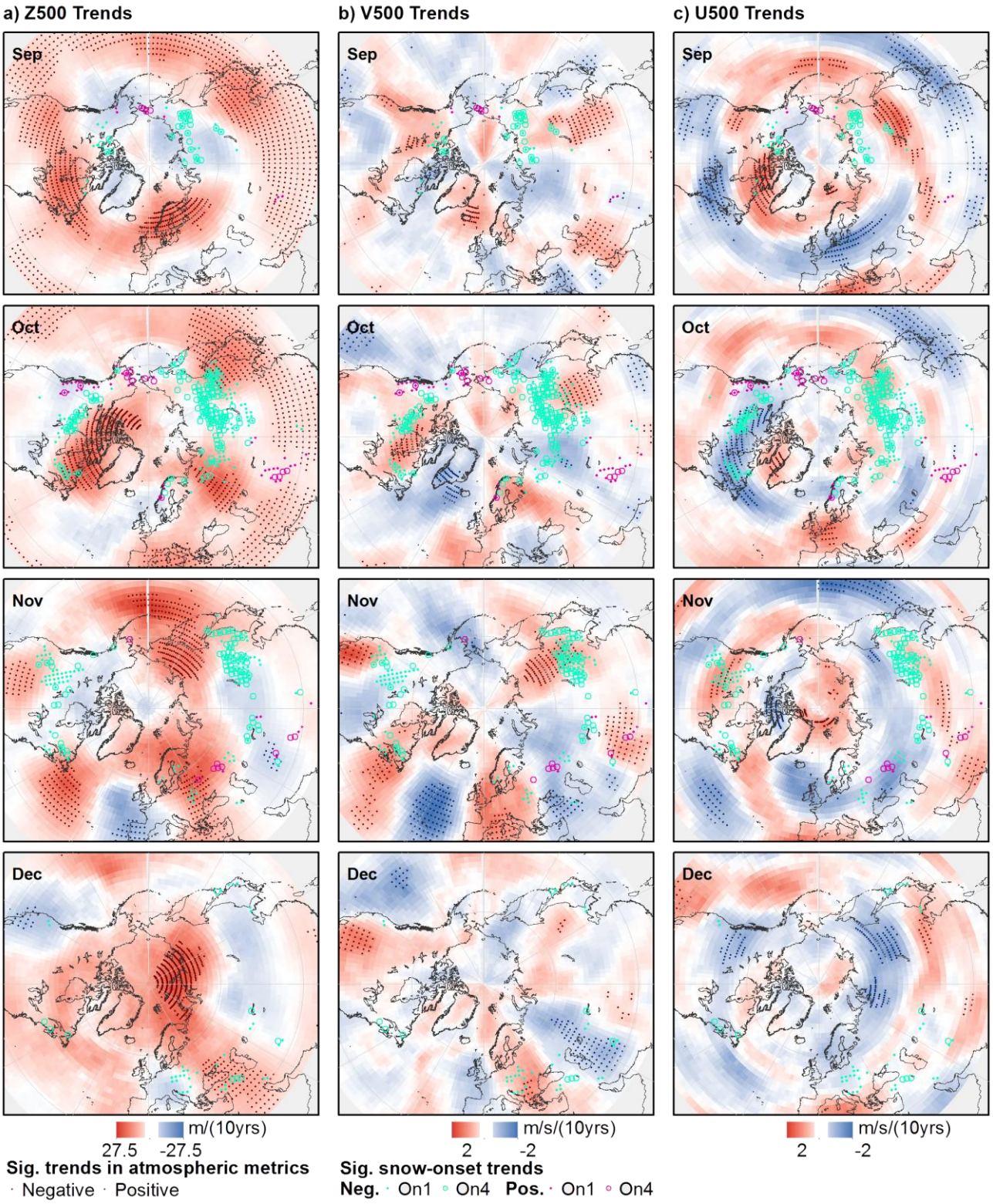

Figure 4.6: Spatial distributions of 1972-2017 snow-onset trends in relation to 1972-2104 trends in 500 hPa mean monthly a) geopotential height, b) meridional wind-speeds and c) zonal wind-speeds.

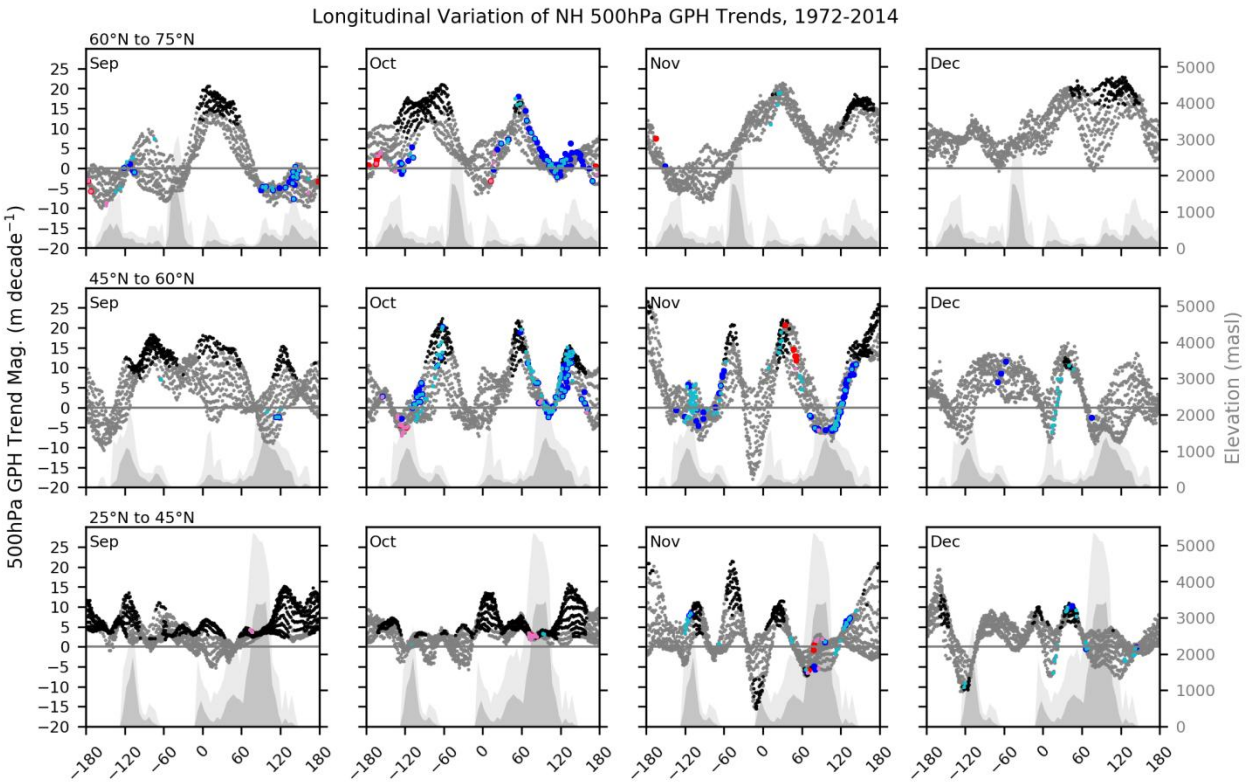

Figure 4.7: Longitudinal distributions of 1972-2014 trends in 500 hPa geopotential height within three latitudinal bands. Darker (lighter) symbols represent trends significant (non-significant) at the 5% level. Dark (light) blue (red) symbols denote values associated with points for which significant negative (positive) On4 (On1) trends were identified. Darker (lighter) shaded areas represent meridional mean (maximum) elevations at zonal intervals of 5°

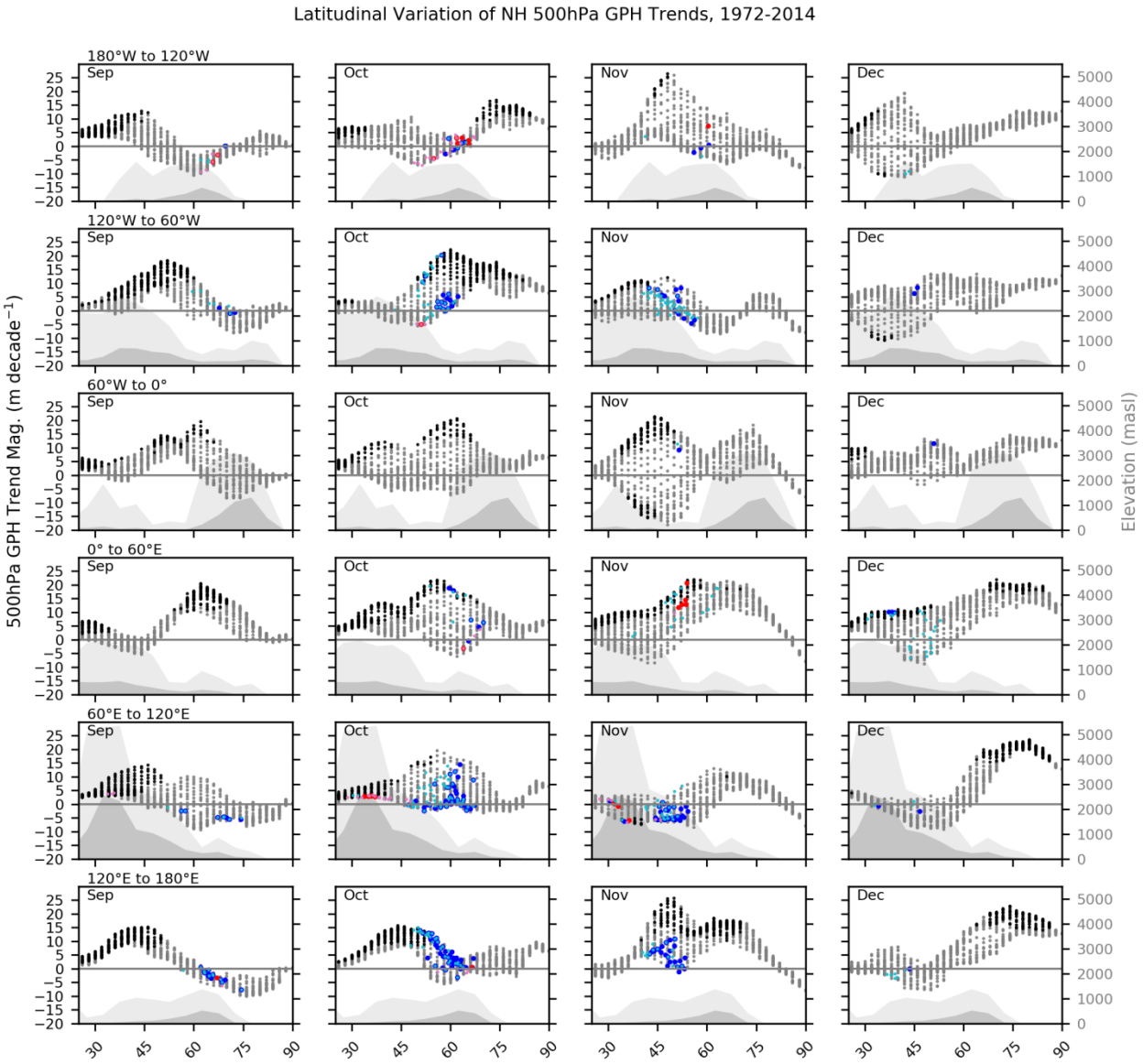

Figure 4.8: As in Figure 4.7, but illustrating latitudinal distributions of 1972-2014 trends in 500 hPa geopotential height magnitudes within six longitudinal bands. Darker (lighter) shaded areas represent zonal mean (maximum) elevations at meridional intervals of 5°.

4.4.3.2. Climatological Change in the Lower Troposphere

Earlier onset of seasonal snow-cover may result either from the augmentation of humidity over a relatively dry area where sub-freezing temperatures have historically been expected, or through the occurrence of cooler temperatures in a climatologically humid area. In contrast, positive onset trends should in principle be associated with progressively warmer and / or drier

conditions. Potential influences on snow-onset trends were therefore explored by examining the spatio-temporal distributions of means and trends in key atmospheric metrics during the 1972-2014 PoI. These results are presented in the main text as maps of the mean values, overlaid with symbols indicating significant positive and negative trends (Figures 4.9, 4.10). Separate maps of means and trends at larger scales, together with meridional and zonal cross-sections, are provided for all metrics in Appendix 3.

4.4.3.2.a. Negative Onset Trends in Eurasia

In September, the positive Z_{500} trends over northern Scandinavia and north-western Russia overlie similarly prominent significant positive SLP trends, centred mid-way along the Ural Mountains (~latitude 60° N, longitude 60° E). This tendency persists with approximately the same peak magnitude (although statistical significance wanes) and location throughout the transition from summer to early winter (Figure 4.9a; also Appendix 3, Figure A3.9). Meanwhile, on the eastern margin of the Eurasian landmass, an initially subordinate patch of enhanced SLP develops over north-eastern China at latitude ~45° N, before subsequently building and spreading first to the north-east over northern Japan and the north-west Pacific Ocean in October, then northward towards the Bering Strait in November, before tracking westward along the Arctic coast of Russia in December, and linking with the Ural-Scandinavia High.

During the PoI, the dominant influence in central Eurasia (east of the Urals and north of the HKH) through the transition from summer to winter has been imposed by the developing Siberian High (Appendix 3, Figure A3.8). In this region, associated mean SLP is climatologically higher, and mean near-surface temperatures (Appendix 3, Figure A3.17) and atmospheric humidity (Appendix 3, Figure A3.16) lower, than in any other longitudinal sector of the NH. Prevailing V_{850} has been northerly in the east and southerly to the west (Appendix 3,

Figure A3.10), with peak speeds at ~70° E and 120° E, close to the western and eastern margins of the HKH, respectively. However, this analysis suggests that these conditions have altered substantially during the PoI, thereby driving changes in spatio-temporal patterns of snow-onset.

The altered airflows are spatially associated with a marked decline in SLP over central-eastern Eurasia, orientated meridionally in approximate alignment with longitude 100° E, and thus bracketed zonally between the two main regional centres of increasing pressure over the Urals and China (Appendix 3, Figure A3.9). Negative SLP trends are strongest between ~45° N and 75° N in September, then subsequently migrate southward. While the spatial extent of these trends contracts substantially after November, a focus of declining SLP persists over the HKH in December. Distinct and statistically-significant positive (i.e., stronger southerly) 850 hPa wind-speed trends are evident along the eastern margins of this area, with negative (more northerly) trends on the western flanks, from September through November (Appendix 3, Figure A3.11). AT2m trends within the spatial domain of declining SLP are in general weakly to moderately negative (except in November, when they are neutral to weakly positive), with few instances attaining statistical significance (Appendix 3, Figure A3.17). While significant positive TPW trends are identified at both high (> 60° N) and low (< 45° N) latitudes, the latter are as much as an order of magnitude stronger than the former (e.g., comparing 30° N and ~75° N between 60° E and 120° E, shown in Appendix 3, Figure A3.15).

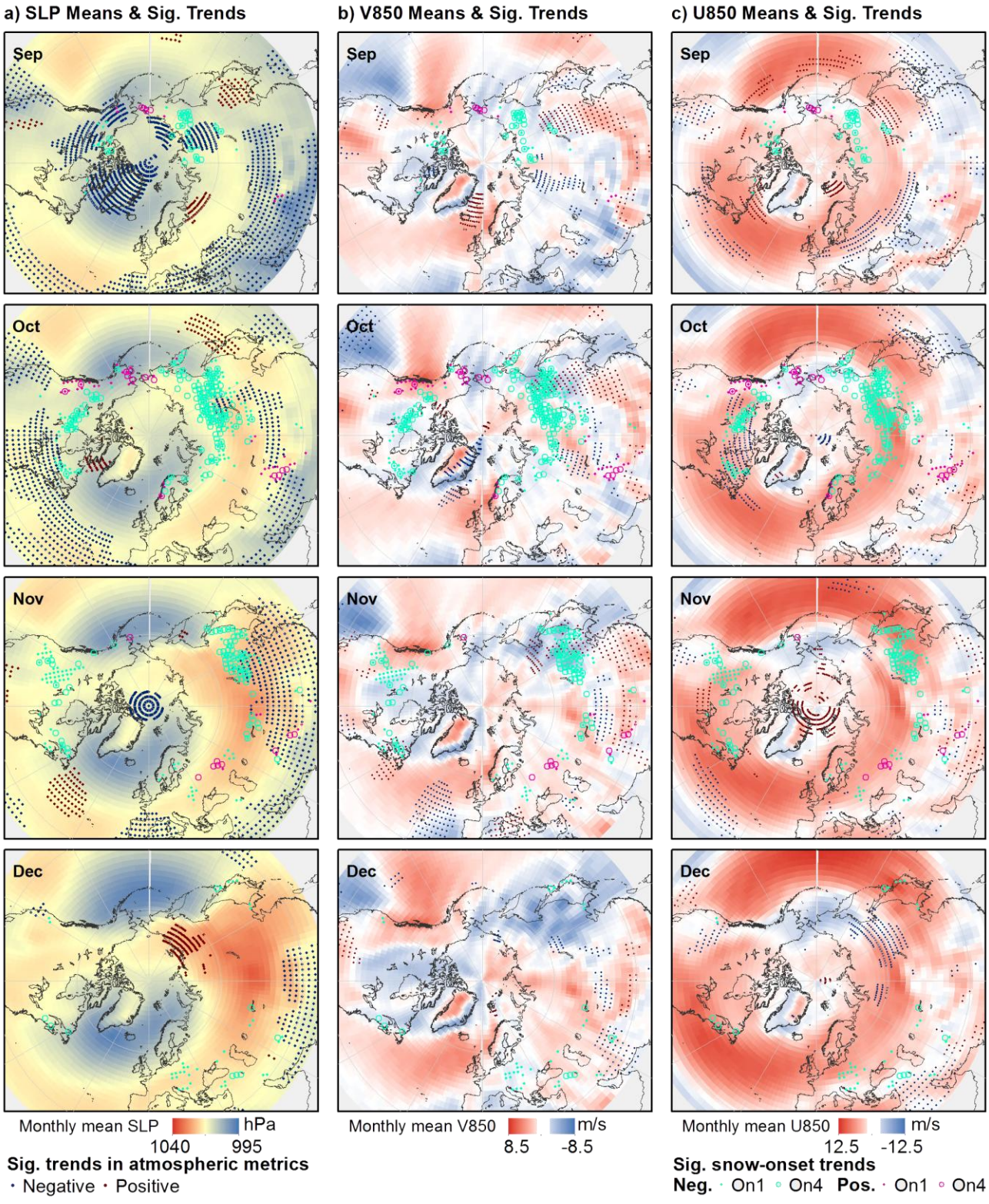

Figure 4.9: Snow-onset trends shown within context of monthly means (raster base-layer), and significant trends (dark blue / red stippling) of a) sea-level pressure, b) 850 hPa meridional wind-speeds and c) 850 hPa zonal wind-speeds.

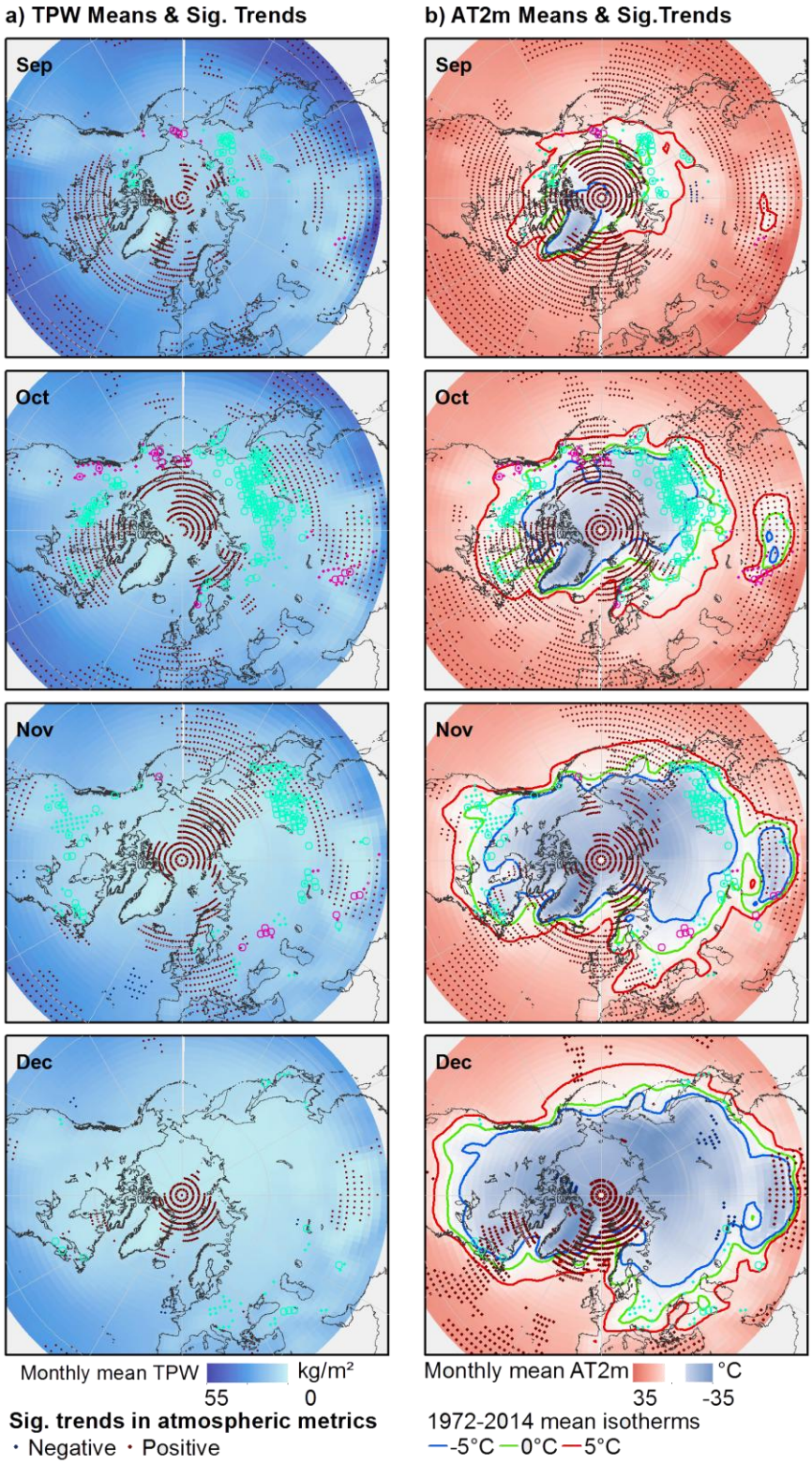

Figure 4.10: Snow-onset trends shown within context of monthly means (raster base-layer) and significant trends (dark blue / red stippling) of a) total precipitable water and b) air-temperature at 2m height. Onset trends are represented using same symbols as in Figure 4.9.

This combination of influences provides the spatio-temporal climatological context for the significant snow-onset trends described over Eurasia in Allchin and Déry (2019). The explanation suggested here identifies the extensive strong positive TPW trends over central-northern China in September – and their northward expansion in subsequent months – as a source of additional tropospheric humidity, advected northward over the mean monthly 0°C isotherm by enhanced southerly flows along the eastern margin of the region of declining SLP. Initially, these developments lead to snowfall only in higher (and therefore cooler) areas – principally the Chersky and Verkohansk ranges in the north-east, the Stanovoy Highlands in the south-east (to the north-east of Lake Baikal), and the Putorana Plateau further to the north-west. While the first two locales lie in the path of a stronger southerly component of V_{850}, the last experiences a shift towards more northerly flows, reinforced by circulation from the north-west around the northern periphery of increasing SLP over the Urals. This in turn raises the possibility of additional humidity being supplied from the (increasingly ice-free – Stroeve and Notz, 2018) Barents, Kara and Laptev seas, as suggested previously by Wegmann et al. (2015). However, while positive TPW trends are evident over these areas, their magnitudes are small, and only statistically significant over the Laptev Sea.

As the season progresses through October and November, both the 0°C isotherm and the focus of strongest negative SLP trends migrate southward, thus moving closer to the persisting expanse of substantially augmented humidity over north-eastern China, and also to the broad swath of significantly declining SLP and increasing TPW spanning southern Eurasia. Note that both means and trends in October V_{850} north of latitude 60° N between longitudes 90° E and 150° E imply prevailing southerlies, so Arctic moisture is unlikely to contribute substantially to the earlier snow-onset further south. Subsequently, as positive Z_{500} trends begin to link along the

Arctic coast of Russia in November, the easterly component of U_{850} wind-speeds strengthens around latitude 60° N. This first subtle shift from the dominant influence of trends in meridional airflows to shifting zonal patterns may help to explain the westward extension of negative snow-onset trends into south-eastern Kazakhstan. By December this transition is complete, with strongly positive SLP trends across northern Eurasia and significant increases in the easterly component of U_{850} winds spanning the continent further to the south.

Explanations for the other more localized patches of negative onset trends in Eurasia – in northern Norway, north-west Russia and on the Kamchatka Peninsula in October, along the southern Pacific coast of Russia in November, and scattered over south-western areas in December – may be found by invoking similar mechanisms. In each case, links are identifiable between changes in regional Z_{500} and SLP gradients, resultant alterations to airflows, a source of augmented atmospheric moisture, and advection over the mean monthly 0°C isotherm.

4.4.3.2.b. Positive Onset Trends in Eurasia

Factors influencing the relatively few instances of more frequent delays in the onset of snow-cover over Eurasia are also identifiable, although these are perhaps less immediately apparent. For example, while positive trends are identified in extreme north-east Siberia and across the Bering Strait into western Alaska in September and October, there is no evidence of major changes in meridional or zonal 850 hPa winds; TPW is neutral or increasing; and while negative SLP trends are identified in the region, these are weak and non-significant. However, near-surface temperature trends immediately to the north are strongly positive in both months, with peak magnitudes of 1°C decade^{-1} in September and in excess of 1.5°C decade^{-1} in October. These are particularly evident over the Chukchi Sea, where turbulent heat fluxes from ocean to atmosphere in late summer (together with those in the Kara Sea) are the highest of any observed

in the Arctic Ocean (Cohen et al., 2018). Presumably linked with this activity, the September 0°C isotherm in this area retreated substantially poleward between 2000 and 2014 (Appendix 3, Figure A3.16d). As mean V_{850} winds through the PoI are northerly (Appendix 3, Figure A3.10), it is reasonable to suggest that this regional warming has contributed to the development of the positive onset trends.

At these spatial and temporal scales, it is more challenging to elicit causes of the strong positive onset trends in October and November near the western extremities of the HKH. Their grouping along the south-western foreslopes suggests that aspect plays a key role, but none of the metrics explored here manifests a distinctive shift in their immediate vicinity. The most plausible explanation is based on their alignment with the western margin of the broad area of declining SLP north of the HKH ranges, and its southward migration: this enhances northerly airflows, placing the area in the lee of the topographic divide, and thereby diminishing precipitation. However, while negative trends in V_{850} are indeed evident to the north of these uplands (Appendix 3, Figure A3.11), positive V_{850} trends also exist to the south, where mean temperatures are considerably higher (Appendix 3, Figure A3.16). This presents the alternative – or complementary – possibility of warm advection from this direction.

The final patch of Eurasian positive onset trends is seen in November over the Pontic Steppe, due north of the Caspian Sea. Relatively weak negative V_{850} and U_{850} trends are identified here, induced by circulation around the centre of increasing SLP further to the north, in conjunction with the developing stronger meridional Z_{500} gradients building at the same time further to the east. However, this implicit shift towards a stronger influence from what might be expected to be colder, drier continental winds has not led to any apparent decline in AT2m and TPW in the immediate vicinity. The possible explanation for later onset suggested here thus

depends on a greater prevalence of anti-cyclonic conditions as SLP rises above the (already relatively high) climatological mean, and consequent lower probability of precipitation.

4.4.3.2.c. Negative Onset Trends in North America

Whereas the majority of negative onset trends in Eurasia are dominated by a persistent pattern of zonal SLP gradients and consequent meridional airflows, the dominant influences over North America more often take a zonal alignment, and change considerably from month to month.

In September, the ribbon of augmented Z_{500} stretching across Canada from south-west to north-east (Figure 4.6a) drives positive trends in zonal airflows along its northern flank (Figure 4.6c). It is logical to infer that moisture-laden Pacific air advected eastward by these winds supplies the augmented TPW observed over most of the landmass east of the Rocky Mountains (Figures 4.10a; Appendix 3, Figure A3.15). Meanwhile, several patches of significant negative SLP trends develop over central-northern North America (Figure 4.9a). The result east of the mountains (between longitudes ~90° W and 120° W) and north of 60° N is positive (more southerly) V_{850} wind-speed trends (Figures 4.9b; Appendix 3, Figure A3.11), in turn supplying additional TPW towards the central Arctic coast. The incidences of earlier snow-onset coincide with areas in which these moist airflows cross the mean 0°C isotherm (Figures 4.2, 4.10b; Appendix 3, Figure A3.16).

The pattern switches completely in October, when positive Z_{500} trends, now detached from their prior linear organization, form an extended region of significant ridging spanning the Beaufort Sea to the north-west Atlantic. The response at lower altitudes is the development of a meridional dipole in SLP, with significant positive trends to the north, and declines across the

continent south of latitude ~50° N. This in turn drives significant negative trends in U_{850}, implying a greater influence of easterly airflows (Figures 4.9c; Appendix 3, Figure A3.13). Meanwhile, the extensive patch of significant positive TPW trends has shrunk from the west, so that it now covers the region between Hudson Bay and the Great Lakes. The earlier snow-onset trends coincide with those areas where the stronger easterly airflows have passed through the augmented TPW and intersect with the October mean 0°C isotherm.

The overall arrangement of influences changes once again in November. The main focus of ridging, together with underlying significant positive SLP trends, has now shifted to the south-east, into the north-west Atlantic. Significant positive V_{850} trends develop along its western margin, feeding moisture from a small coastal remnant of the formerly widespread significant positive TPW trends seen in previous months over much of eastern Canada: significantly earlier onset of snow-cover is again identified where these airflows cross the monthly mean 0°C isotherm. A small number of DGPs in the same region also record negative onset trends in December.

Further west, the influences driving the instances of earlier onset in November scattered across the central interior of the continent – mainly on the north-western slopes of the American Rocky Mountains, and north of ~40° N – are more subtle. The explanation suggested here is based first on detection of a ridging tendency in Z_{500} along the spine of the Western Cordillera (Figures 4.6, 4.7, 4.8), underlain by positive trends in SLP (Figures 4.9a; Appendix 3, Figure A3.9). In the southern part of this sector (south of latitude 45° N, at ~120° W), significant positive trends in V_{850} winds are identified, with significant negative trends to the east (~90° W). These tendencies oppose the climatological pattern within the PoI (Appendix 3, Figure A3.10). Minor trends in U_{850} are also evident, negative (more easterly) to the south and positive to the

north (Figures 9c, S13). The positive V_{850} winds along the topographic grain are accompanied by moderate and significant near-surface warming and significant increases in TPW, whereas the more northerly flows to the east correspond to a (non-significant) cooling trend and significant reduction in TPW (Appendix 3, Figures A3.17, A3.16). Together, these metrics suggest a greater prevalence of anti-cyclonic circulation over south-western North America, immediately east of the Western Cordillera. The earlier onset to the north thus appears to have developed in response to augmented moisture advected from the Pacific around the northern margins of this centre of rising SLP, through the topographic 'col' at latitude ~45° N, assisted by positive trends in U_{500} wind-speeds.

4.4.3.2.d. Positive Onset Trends in North America

With the exception of the delays in onset on the Alaskan side of the Bering Strait already described, the sole incidence of positive trends in North America is observed between the Pacific coast and Western Cordillera, north of latitude ~50° N, in October. These trends are associated with the Coast and Rocky Mountain ranges of British Columbia, extending northward to Alaska. As described above, the dominant atmospheric influence over North America in October is that imposed by strong negative trends in U_{500} and U_{850} wind-speeds. While the widespread negative onset trends over the continental interior appear to have been fed by westward advection of humidity from the positive TPW trends east of Hudson Bay, it seems probable that this augmented moisture would have been spent by the time at which these airflows pass over the major mountain ranges, particularly in view of the dearth of any increase in TPW between longitudes ~90° W and 120° W. Meanwhile, trends in V_{850} and U_{850} over the north-east Pacific are weakly negative, further diminishing the likelihood of any increase in onshore moisture-supply. As AT2m trends in the area of later snow-onset are neutral to slightly negative, warming

is not an important factor. These details suggest that the October delays in onset over western North America are associated with anomalously dry, cool conditions imposed at the downstream end of the trans-continental airflows, themselves induced primarily by Z_{500} ridging between Greenland and the Beaufort Sea.

4.5. Summary and Conclusions

This study describes the spatial and temporal distributions of trends in the onset of NH seasonal snow-cover between 1972 and 2017, placing them within the context of long-term means and trends generated from climatological reanalysis metrics spanning 1972 to 2014. Activity at mid-to-upper levels of the troposphere is represented by geopotential heights and wind-speeds (meridional and zonal) at 500 hPa, and at lower altitudes by near-surface temperature, sea-level pressure, total precipitable water, and meridional and zonal wind-speeds at the 850 hPa level. The analysis offers a cogent explanation for each cluster of onset trends, whether negative or positive, in the form of a clear association with an appropriate combination of historical and evolving phenomena at upper and lower levels of the troposphere. However, the fine details of linkages vary with the location and month of interest.

The fundamental driving influence in the causative chain suggested here is the movement of parcels of significantly higher 500 hPa geopotential height from tropical to circumpolar latitudes, presumably along the northern extremities of Rossby-type wavetrains. In the most general terms possible, every major cluster of statistically-significant snow-onset trends is associated spatially and temporally with an associated significant increase in a zonal or meridional pressure gradient in the mid-to-lower troposphere. These differentials have altered regional airflows, in some instances reversing the climatological prevailing winds. The majority of negative (i.e.,

progressively earlier) onset trends occur where winds have become stronger along a vector linking a region of increasing atmospheric humidity with the path of the regional monthly 0°C isotherm, particularly where such destinations have historically been relatively arid, and the 0°C isotherm has not retreated substantially poleward during the PoI. It is of particular note that the additional moisture is in most instances advected predominantly from the south (as in eastern Eurasia) or zonally (over northern North America), rather than from increasingly ice-free Arctic waters. In contrast, most positive (i.e. delayed) onset trends are found in areas where changing winds are likely to have resulted in the increased incidence of drier air, although some (such as those either side of the Bering Strait) appear to be more probably the result of markedly higher regional air-temperatures.

By situating the onset-trends within their climatological contexts, this analysis offers a range of evidence to support the conclusion that their existence is plausible in terms of atmospheric dynamics, rather than being artifacts of technological improvements to the NRSA furnished by introduction of the IMS. The approach is necessarily inductive: the onset data identify only the week in which percentage snow-cover in each grid-cell passes through the 50% threshold, so – in the absence of any representation of the rate of change in actual percentage cover or snow-water equivalent either side of this event – it is not meaningful to attempt a more deterministic assessment of how they relate to the timings, magnitudes and spatial distributions of trends in metrics of atmospheric activity, and to interactions between these.

Nevertheless, these findings help to establish a conceptual link between understanding of mechanisms by which augmented summer heat moves from lower latitudes to circumpolar regions, and ideas relating tropospheric circulation patterns to impacts on mid-latitude climate systems through the transition to winter. This begins with strong positive trends in mid-to-upper

troposphere geopotential heights across much of the NH at the end of the boreal summer, associated with a poleward shift in circulation patterns (noted previously by Archer and Caldeira, 2008), thereby feeding heat over the peripheral seas of the Arctic Ocean. If atmospheric blocking may be thought of as a "traffic-jam in the atmosphere" (Nakamura and Huang, 2018), the analogous congestion effectively enters a *cul-de-sac* immediately to the south of the Barents Sea. September ice-cover in this region has undergone drastic decline (Onarheim and Arthun, 2017; Stroeve and Notz, 2018), primarily as a result of these anomalous atmospheric circulations (Olonscheck et al., 2019), but also due in part to a poleward shift in the Gulf Stream (Sato et al., 2014). Discussion continues over the degree to which the genesis and persistence of these centres of enhanced ridging have been driven by thermal transfers between more ice-free Arctic waters and the atmosphere (e.g. Nakamura et al., 2015; Kretschmer et al., 2016; Francis et al., 2017; Overland, 2017; Cohen et al., 2018), or are more directly the result of tropical influences (Scaife et al., 2017; Blackport et al., 2019; Matsumura and Kosaka, 2019). Whatever their origins, the steeper pressure-gradients generated around them have driven significant changes in the directions and speeds of both meridional and zonal winds, manifested most clearly in a more meandering path taken by the Polar Jet (Vavrus et al., 2017). In some cases the alignment of this sinuosity has been essentially meridional (such as over eastern Eurasia from September to October), while in others it has been arranged more zonally (e.g. North America during the same months). Negative trends in the date of snow-onset are found where these dynamics have led to the advection in the lower troposphere of more humid air over the regional 0°C isotherm at a date significantly earlier than the long-term mean, particularly where the destination is climatologically dry. In contrast, positive onset-trends are identified where drier and / or warmer

airflows have developed over historically more humid areas, particularly where mean temperatures are higher.

These results thus demonstrate that relationships exist between patterns of ridging and troughing in the NH mid-to-upper troposphere (500 hPa) from September through December; associated changes in the strengths and directions of meridional and zonal winds at these and lower levels; their influences on meteorological activity at lower altitudes; and the spatio-temporal distributions of snow-onset trends. Useful extensions of this work might consider the degree to which individual extreme storm events, rather than a more gradual but persistent increase in snowfall, have contributed to negative onset trends, as the impacts of these categories may differ considerably (O'Gorman, 2014). It would be particularly interesting to explore how the temporal evolution of the trends described here relates to leading atmospheric oscillation indices over the same PoI. Additional information could also be derived by investigating in detail the mechanisms by which major topographic features modulate relationships between patterns of atmospheric circulation and the distribution of snow-onset trends. While the evidence presented here might in strict terms be considered largely circumstantial, it is offered with the goal of providing a framework within which to explore the associated processes of atmospheric physics in greater detail.

5. Dissertation Summary and Conclusions

5.1. Summary of Key Findings

The research described in this dissertation sought to refine and improve understanding of the spatial distributions, timings and magnitudes of trends in a range of metrics associated with Northern Hemisphere seasonal snow-cover between 1971 and 2017, as inferred from the NRSA, the longest of all remotely-sensed environmental archives. This was prompted by recognition of the importance of NH seasonal snow-cover to climatological, hydrological, ecological and geomorphological processes, and as an essential resource for human consumption.

Chapter 2 described the distribution of statistically-significant trends in the annual duration and monthly mean area of snow-cover during the snow-years (1st October to 30th September) from 1971-1972 to 2013-2014. The first section, considering snow-season duration, built on the work of Choi et al. (2010), extending the period considered by six years, and applying Mann-Kendall trend analysis in place of simple differencing between temporal sub-ranges. The magnitudes of both negative and positive trends were found to amplify at higher elevations and lower latitudes, with moderately strong linear correlations at high levels of statistical significance. A metric termed 'area-duration' was used to represent the change in SDD during the PoI at DGPs for which significant trends were identified, in conjunction with the area affected. While gains and losses represented in this way were broadly comparable among DGPs with median SDD of less than approximately six months, losses dominated where the snow-dominated season has (to date) lasted for between 28 and 44 weeks. However, these values are likely to incorporate bias, as many points associated with SDD of this length are in circumpolar regions, and the surface area associated with each is large compared to those at low latitudes. At

DGPs manifesting significant negative trends, a coarse estimate of the number of seasons remaining before snow-dominated conditions may no longer occur was computed as the quotient of 1971-2014 mean SDD and the associated trend magnitude. If current rates of decline persist, such a shift to transient snow-cover is expected within 50 years along southern slopes of the Hindu Kush – Himalaya (HKH) ranges, westward to the Caucasus, and in parts of western Canada. The analysis also identified a marked division between positive (negative) trends on the eastern (western) slopes of the HKH.

The second part of Chapter 2 reported extent-related trends at monthly intervals within cells in a regular 5° grid, thereby augmenting the findings generated previously at hemispheric and continental scales by Hernández-Henríquez et al. (2015), and responding to the recommendation of Groisman et al. (1994) that 'centres of action' of changing snow-cover patterns should continue to be monitored. This revealed more widespread incidence of positive trends over both Eurasia and North America from September to January, but strong dominance of losses, spreading inexorably northward from the southern mountains, through the late winter, spring and summer. A longitudinal alternation in the signs and magnitudes of snow-season duration trends was again identified, and its variation from month to month described. While negative trends in snow-covered area were found to intensify at higher elevations between April and August, positive trends amplified with elevation only in September. Significant correlations between magnitude and latitude were identified only for negative trends in May and June, and for positive trends in September, all indicating amplification progressively further to the south.

While these results offer useful detail and extend prior research, arguably the key point yielded by this study focused on the implications of assumptions made in the interpretation of the NRSA's binary classification. As this distinguishes between conditions on the basis of a 50%

snow-cover threshold, actual cover in a 'snow-free' ('snow-covered') spatial sub-unit may range from 0 – 49% (50 – 100%). It is likely that the mean of this value within a given time-period varies with season, location, and contextual characteristics. This analysis showed firstly that estimated trend magnitudes increase linearly with the difference between the percentage snow-cover assumed to exist in each of the binary states, and secondly that they are magnified further by the size of the spatial sub-unit. It follows that the conventional assumption of 0% (100%) cover in 'snow-free' ('snow-covered') cells exaggerates reported magnitudes substantially over more realistic values, and that this effect is exacerbated at higher latitudes by the progressive increase in NRSA cell-area associated with its cartographic projection.

In the light of these findings, subsequent phases of this research focused on analyses which did not depend primarily on estimates of snow-covered area. They were also guided by the need to address questions raised by several authors about the NRSA's credibility (e.g. Brown & Derksen, 2013; Mudryk et al., 2017; Hori et al., 2017). Additionally, the counter-intuitive nature – given prevailing climatological preoccupations – of more widespread snow identified early in the season over parts of Eurasia and North America demanded priority of attention over consideration of accelerating losses in spring and summer.

Chapter 3 therefore explored trends in the timing of seasonal onset of snow-dominated conditions, marked by the first transition in each year at each data-point from 'snow-free' to 'snow-covered', and thus the first incidence in the snow-year of at least 50% snow-covered area. A distinction was drawn between the first such instance, regardless of duration (termed On1), and that persisting subsequently for at least four weeks (termed On4, and found to correspond closely with the beginning of the longest snow-covered period in each snow-year). On discovering mean On1 (On4) dates earlier than 1st October associated with 10.5% (7.5%) of the

spatial domain, the onset period considered each year was set between early August and the following February. This, together with the availability of a new version of the NRSA, altered the PoI to the snow-years from 1972-1973 to 2017-2018. The results revealed significantly earlier arrival of snow over 25% of the area in which it was recorded in every year of the PoI, predominantly at lower elevations of the NH mid-latitudes (~40° N to 70° N), and where mean onset occurs in October or November. In contrast, On1 (On4) has been delayed over less than 5% (3%) of the same domain, with some spatial bias towards areas at lower latitudes, higher elevations, and with earlier mean onset. A distinctive longitudinal alternation in trend-sign was again identified, with earlier (later) onset associated with the eastern (western) flanks of major upland regions, particularly the Hindu Kush – Himalaya ranges and the Western Cordillera of North America. The magnitudes of trends of both signs were found to amplify linearly at lower latitudes, higher elevations, and where mean onset is later. A simple form of change-point analysis, conducted with the goal of exploring the temporal evolution of these trends, identified that On1 (On4) onset-date anomalies within the PoI had switched from positive to negative before 1997 among ~70% (~66%) of the data-points associated with significantly earlier onset. The timing of the transition from negative to positive anomalies among points experiencing delayed onset was less coherent, being spread through the 1990s and 2000s. While temporal profiles of cumulative anomalies generated from series of monthly mean temperature and precipitation in the vicinity of each NRSA data-point revealed differences in overall patterns, they did not offer a clear explanation for the associated trends in snow-onset.

These results demonstrated the need for a more detailed assessment of the degree to which snow-onset trends may be related to their climatological contexts. Where spatio-temporal associations exist between the incidence of progressively earlier or later onset and likely driving

influences, the probability of their being artifacts of technological improvements diminishes. On the other hand, if no such correspondences are found, this likelihood increases. The study described in Chapter 4 therefore sought to describe the spatial distribution of NH onset trends associated with each month from September to December, and to determine whether or not explanations could be inferred for these patterns from monthly means and trends derived from a range of metrics of relevant atmospheric activity during the PoI. The results of this analysis demonstrated clear links between instances of significant snow-onset trends of both signs, and causative chains incorporating steeper gradients of 500 hPa geopotential height around regions of significantly enhanced ridging, trends in sea-level pressure, consequent airflows (both higher in the troposphere, at the 500 hPa level, and lower, at 850 hPa), the availability of significantly augmented atmospheric humidity, and near-surface temperatures. In the most general terms, positive ridging trends in the mid-troposphere have driven climatologically novel airflows over the areas affected by onset-trends. Where these vectors have travelled over the 0°C isotherm from (warmer) centres of enhanced moisture, particularly where humidity in the destination region has historically been low, earlier onset has occurred. In contrast, onset has been delayed where these altered winds have led to the advection of warmer and / or drier air. Although not considered in detail here, it appears likely that interactions between these changing circulation patterns and major topographic obstacles have influenced the arrangement of onset trends in relation to mountain ranges.

5.2. Limitations

The principal limitations associated with this study relate to the characteristics of the dataset on which it is based. While the NRSA's spatial and temporal resolutions are appropriate for studies at regional to hemispheric scales, and its long period of record supports multi-decadal

analyses, its binary classification of snow-cover imposes major constraints on the nature and accuracy of the inferences which may be drawn from it. This representation also precludes meaningful assessment of serial autocorrelation, which may exist in areas where snowfall is influenced by atmospheric oscillations at decadal scales. By extension, the significance of some trends may be over-estimated. The variation in cell-size with latitude, from ~10.7 × 10^3 km^2 at the lowest latitudes to ~41.8 × 10^3 km^2 near the geographic North Pole (Estilow, 2013) additionally introduces considerable spatial bias into derived metrics. Moreover, this two-dimensional representation of snow-cover provides no information about depth or snow-water equivalent, severely limiting its utility for hydrological studies. These aspects of the dataset preclude its use in detailed deterministic analysis, such as any attempt to relate metrics of atmospheric temperature, humidity and pressure to observed patterns of snow-cover in numerical terms. This study incorporates several critical assessments of the degree to which snow-cover trends may have been driven primarily by technological changes in the NRSA's imagery and post-processing in 1999, and presents a range of evidence to the contrary. In general, this validates the efforts made to ensure overall consistency throughout the archive's entire period of record (Romanov et al., 2000; Helfrich et al. 2007; Estilow, 2013; Estilow et al., 2015). However, it remains possible that some degree of bias may nevertheless have been introduced by these improvements.

Uncertainties are also associated with the climatological datasets utilized in Chapters 3 and 4. In particular, some degree of temporal autocorrelation is likely to exist in each monthly time-series at individual data-points, again driven by multi-annual to multi-decadal atmospheric oscillations. However, at the spatial and temporal scales and resolutions considered in this study, it is challenging to identify where and when autoregressive patterns emerge, and to determine

their structure, so that steps may be taken to address them in an appropriate manner. Moreover, there is a risk that the inappropriate application of commonly-adopted techniques such as pre-whitening (Kulkarni and von Storch, 1995) may distort patterns of variability, resulting in the under-estimation or negation of valid trends (e.g. Bayazit and Önöz, 2007; Razavi and Vogel, 2018). For these reasons, no adjustments were made to the raw data prior to the quantification of trends. It follows that the significance of some trends may again have been over-estimated. However, given the inductive nature of the analysis, and that it considers the spatial organization of variations in both significant and non-significant trends, this is not likely to alter the results presented substantially.

5.3. Recommendations for Future Research

Given the limitations imposed by the NRSA's binary classification, and their influence on estimates of trend-magnitudes, it would be particularly useful to improve estimates of variation in actual percentage snow-cover within the archive's grid-cells through the year. A first step might be to generate monthly or weekly metrics of central tendency and spread in each cell (separately for occasions on which this is less than or at least 50%) from Moderate Resolution Imaging Spectro-radiometer (MODIS) imagery, which has been acquired at daily intervals since 2000. Although it is possible that values derived from this relatively short period may not be reliably representative of conditions between the early 1970s and 2000, they would nevertheless offer more realistic estimates of actual percentage cover in each spatial and temporal sub-unit than the 0% and 100% conventionally assumed from the NRSA's 'snow-free' and 'snow-covered' states. This would permit more meaningful comparisons to be made between the NRSA and other (shorter-duration) datasets, in turn supporting the refinement of modelled representations of snow-cover.

While this research improves the spatial representation of variability in snow-cover trends during the PoI from the hemispheric and continental scales of prior studies (e.g. Déry & Brown, 2007; Hernández-Henríquez et al., 2015), the regular 5° grid adopted is not necessarily the most appropriate framework for doing so. There is merit in considering a form of spatial partitioning based on distinctive associations of climatological, topographic and ecological attributes, thereby grouping related processes relevant to the accumulation, persistence and ablation of snow-cover. For example, the assemblages of vegetative cover associated with different biomes, which have evolved in response to physiographic conditions and climatologies at millennial scales, offer a convenient foundation for such an approach. Alternatively, a classification of NRSA grid-cells might be generated using metrics of topography, land-cover and climatology, or a moving-window approach might be adopted. Initial exploration of these approaches conducted during this project suggests that they offer a promising avenue for further contextualization of snow-cover trends. This in turn would help to refine understanding of associations between the snow-albedo feedback and different landscapes.

These results provide new information relating to trends in the overall length of the snow-dominated season and changing patterns of onset, and describe the distribution of declining snow-cover through the transition from winter to spring and summer. However, within-season changes in the variability of cover was not considered in this study. This could be explored by quantifying trends in the number of week-to-week switches between the NRSA's two binary states at seasonal to monthly intervals, revealing areas in which transient snow-cover is becoming more or less prevalent. It would also be useful to distinguish between areas in which snow has been increasing or decreasing at only the start or finish, or at both ends of the season, and to seek explanations for patterns revealed in this way. If the MODIS-based approach

suggested above improves representation of variability in actual percentage cover, it may also be possible to address questions relating to changes in the frequency of major snow-storms in relation to 'background' snowfall, as different responses to climate-change are expected from each (O'Gorman, 2014).

Inter-annual serial autocorrelation may exist among the climatological metrics used to explain distributions of snow-onset trends, driven by cyclic variation of atmospheric and oceanic conditions such as the Pacific Decadal Oscillation (Mantua et al., 1997) and Atlantic Multi-decadal Oscillation (Schlesinger and Ramankutty, 1994). In principle, different fundamental states in the overall continuum of atmospheric activity may be identified by cluster-analysis of the leading teleconnection indices (Franzke and Feldstein, 2005; Johnson et al., 2008). This may in turn help to distinguish cyclic and secular patterns from the background of substantial internal variability (e.g. Barnes and Screen, 2015; Overland, 2016; Screen et al., 2018). If so, it would be useful to determine whether associations exist between these patterns and higher or lower probabilities of substantial snowfall in particular regions and intra-annual periods, to describe their temporal trajectories since the early 1970s, and so to investigate the degree to which these may have driven snow-related trends.

5.4. Implications

The results generated by this research furnish new information primarily to two areas of interest.

Firstly, they contribute constructively to the discussion relating to the NRSA's credibility. Several authors (e.g. Brown & Derksen, 2013; Mudryk et al., 2017; Hori et al., 2017) have suggested that disagreements between trends identified from the NRSA and those based on other

datasets are primarily artifacts introduced by the adoption of imagery providing greater temporal and spatial detail, together with a more automated interpretation process, in 1999 (Ramsay, 1998; Estilow et al., 2015). In principle, this may have resulted in the improved resolution of snow-free from snow-covered areas, particularly in more complex terrain, thereby enabling the subsequent identification of considerably more or less snow than during the earlier part of the record, and so creating spurious trends. However, the majority of instances of progressively earlier onset are found by this study to be located in areas of low and broadly uniform elevation, and their transition from positive to negative onset-date anomalies occurred well before 1999. Although more of the data-points associated with delayed onset are associated with uplands, these occur only in relatively localized, spatially coherent patches, rather than being evident throughout each major range of mountains. More conclusively, a plausible climatological explanation is identified here for every instance of significant trends of both signs. Together, these findings strongly suggest that the trends identified from the NRSA are not artifacts of the technological improvements introduced in 1999. An alternative (at least partial) explanation for disagreements between NRSA-based trends and those derived from other datasets is that magnitudes are exaggerated primarily by assuming actual percentage snow-cover of 0% (100%) in spatial sub-units recorded in the NRSA as being ‘snow-free’ (‘snow-covered’) during a given week, as these values are likely to be considerably higher (lower), depending on spatial and temporal context (particularly during the transitional seasons). This effect is exacerbated at progressively higher latitudes by the poleward increase in the surface footprint area of NRSA grid-cells. These findings help to reinforce the credibility of the NRSA, thereby underpinning the large volume of prior research based upon it, and supporting the continued use of this unique environmental

archive, with the caveat that assumptions adopted in its interpretation will affect the results generated.

Secondly, these results augment understanding of linkages between the movement of warmer air-masses from the tropics to circumpolar regions, and consequent tropospheric interactions between the polar and mid-latitudes, focusing mainly on the transition from summer to winter. They connect the development of regions of significantly augmented ridging – which appears in this perspective to be driven largely by warming at lower latitudes – with changing patterns of airflows (including, by extension, the Polar Jet), and consequent implications for weather-patterns in the mid-latitudes. While many studies have focused on linkages of this nature primarily in summer or winter (e.g. Overland, 2016; Francis, 2017; Francis et al., 2017, Coumou et al., 2018; Mann et al., 2018; Screen et al., 2018; Cohen et al., 2018), few have explored the associated dynamics through the intervening transition. These findings thus inform discussion of the degree to which more ice-free Arctic waters (particularly in the Barents Sea and Kara Sea) may drive (e.g. Nakamura et al., 2015; Kretschmer et al., 2016; Cohen et al., 2018), reinforce, or merely coincide with (e.g. Scaife et al., 2017; Blackport et al., 2019; Matsumura & Kosaka, 2019) cooling in central Eurasia. In particular, this research offers a cogent explanation for the counter-intuitive response to general atmospheric warming of widespread earlier incidence of snow-dominated conditions over both major NH landmasses. A key point of interest identified here is that the provenance of augmented moisture driving earlier onset of snow-cover over Eurasia relates primarily to advection from a southern source of enhanced total precipitable water, whereas that over North America derives zonally from increases over the Atlantic and Pacific Oceans, depending on region and month. This contradicts hypotheses linking more open Arctic waters directly with substantial increases in atmospheric humidity. Additionally, there is

no evidence for a substantial southward shift among monthly mean near-freezing isotherms during the PoI in the areas affected, suggesting that the observed incidences of earlier snow-onset rely less on colder conditions associated with deeper southward incursions of Arctic air than on the supply of additional moisture over already cold, and hitherto relatively dry, regions. However, it is likely that occasional polar outflows (not discernible at these temporal scales) drive individual storms.

The opening statements of this dissertation referred to the importance of seasonal snow as a key modulating influence on aspects of climatology, hydrology, ecology and geomorphology. Understandably, given concerns related to the implications of anthropogenic climate-change and other emerging pressures in the natural and human systems, research in this field has focused on quantifying the locations, timings and magnitudes of reductions in snow-cover, as these are likely to impose acute stresses on, for example, energy exchanges between the land surface and atmosphere (implying a warming feedback to the lower troposphere, e.g. Thackeray et al., 2019), habitat for vegetation and wildlife (including predator-prey balances – e.g. Barber et al., 2018), the availability of water for human populations through spring and summer (e.g. Mankin et al., 2015), and wildfire risks (e.g. Westerling, 2016). By mapping in greater detail patterns of declining snow-cover as they evolve through the ablation season, and describing spatial variations in coarse estimates of the time to extinction of the snow-dominated season, the results reported here contribute new information to support the development of strategies for mitigation of – and adaptation to – associated future impacts, and help to identify pathways of beneficial further study.

However, it is also important to describe, understand and explain trends associated with the early stages of the snow-dominated season. The direct implications of such changes are primarily

climatological, driven by the fundamental alteration of surface thermal and optical radiative properties by snow-cover, resulting in the reduction of surface radiative heating and relative humidity (Betts et al., 2014). Positive early-season anomalies in snow-covered area, particularly in Eurasia, have repeatedly been associated with subsequent cold winters over North America (Cohen et al., 2014; Francis et al., 2017; Cohen et al., 2018; Tyrrell et al., 2018). However, as these links have often been predicated on trends estimated from the NRSA, questions relating to the plausibility of the latter may diminish the credibility of the former. By establishing a clear connection between overall patterns of NH mid-tropospheric warming towards the end of the boreal summer, and a causative chain leading ultimately to the advection of additional moisture over the regional 0°C isotherm, coinciding spatially and temporally with observations of earlier snowfall, these results help to allay such concerns. This in turn reinforces confidence in the hypothesized mechanisms, thereby permitting their application within models and forecasts. It is nevertheless important to recognize that limits exist on the quality of inferences made from the NRSA, and caveats to this effect are offered here.

More generally, if a paradox is perceived to exist between overall atmospheric warming and observed regional increases in snow-cover, even where the latter are not accompanied by significant cooling trends, this may diminish acceptance of current climate-science paradigms among politicians, industrialists and the wider public. This research offers a range of new evidence to support the assertion that no such dichotomy exists.

References

Achard, F., Mollicone, D., Stibig, H.-J., & Aksenov, D. (2006) Areas of rapid forest-cover change in boreal Eurasia *Forest Ecology and Management,* **237:** 322–334 DOI: 10.1016/j.foreco.2006.09.080

Allchin, M., & Déry, S. (2017) A spatio-temporal analysis of trends in Northern Hemisphere snow-dominated area and duration, 1971–2014 *Annals of Glaciology,* **58** (75): 21–35 DOI: 10.1017/aog.2017.47

Allchin, M., & Déry, S. (2019) Shifting spatial and temporal patterns in the onset of seasonally snow-dominated conditions in the Northern Hemisphere, 1972-2017 *Journal of Climate,* **32:** 4981–5001 DOI: 10.1175/JCLI-D-18-0686.1

Aminikhanghahi, S., & Cook, D. (2017) A survey of methods for time series change point detection *Knowledge and Information Systems,* **51** (2): 339–367 DOI: 10.1007/s10115-016-0987-z

Anderson, O. (1977) The Box-Jenkins approach to time series analysis *RAIRO – Operational Research,* **11** (1): 3–29 DOI: 10.1051/ro/1977110100031

Andrews, J., Babb, D., & Barber, D. (2018) Climate change and sea ice: Shipping in Hudson Bay, Hudson Strait, and Foxe Basin (1980–2016) *Elementa – Science of the Anthropocene,* **6** (1): 19 DOI: 10.1525/elementa.281

Archer, C., & Caldeira, K. (2008) Historical trends in the jet streams *Geophysical Research Letters,* **35:** L08803 DOI: 10.1029/2008GL033614

Armstrong, R., & Brodzik, M.-J. (2001) Recent Northern Hemisphere snow extent: A comparison of data derived from visible and microwave satellite sensors *Geophysical Research Letters,* **28** (19): 3673–3676 DOI: 10.1029/2000GL012556

Barber, Q., Parisien, M.-A., Whitman, E., Stralberg, D., Johnson, C., St-Laurent, M.-H., et al. (2018) Potential impacts of climate change on the habitat of boreal woodland caribou *Ecosphere,* **9** (10): e02472 DOI: 10.1002/ecs2.2472

Barnes, E., & Screen, J. (2015) *WIREs Climate Change,* **6:** 277–286 DOI: 10.1002/wcc.337

Barnett, T., Adam, J., & Lettenmaier, D. (2005) Potential impacts of a warming climate on water availability in snow-dominated regions *Nature,* **438:** 303–309 DOI: 10.1038/nature04141

Barriopedro, D., García-Herrera, R., Lupo, A., & Hernández, E. (2006) A climatology of Northern Hemisphere blocking *Journal of Climate,* **19** (6): 1042–1063 DOI: 10.1175/JCLI3678.1

Bayazit, M., & Önöz, B. (2007) To prewhiten or not to prewhiten in trend analysis? *Hydrological Sciences Journal,* **52** (4): 611–624 DOI: 10.1623/hysj.52.4.611

Bentz, B., Régnière, J., Fettig, C., Hansen, E., Hayes, J., Hicke, J., et al. (2010) Climate change and bark beetles of the Western United States and Canada: direct and indirect effects *BioScience,* **60** (8): 602–613 DOI: 10.1525/bio.2010.60.8.6

Berghuijs, W., Woods, R., & Hrachowitz, M. (2014) A precipitation shift from snow towards rain leads to a decrease in streamflow *Nature Climate Change,* **4:** 583–586 DOI: 10.1038/nclimate2246

Betts, A., Desjardins, R., Worth, D., Wang, S., & Li, J. (2014) Coupling of winter climate transitions to snow and clouds over the Prairies *Journal of Geophysical Research – Atmospheres*, **119**(3): 1118-1139. DOI: 10.1002/2013JD021168

Biancamaria, S., Cazenave, A., Mognard, N., Llovel, W., & Frappart, F. (2011) Satellite-based high latitude snow volume trend, variability and contribution to sea level over 1989/2006 *Global and Planetary Change,* **75:** 99–107 DOI: 10.1016/j.gloplacha.2010.10.011

Blackport, R., Screen, J., van der Wiel, K., & Bintanja, R. (2019) Minimal influence of reduced Arctic sea ice on coincident cold winters in mid-latitudes *Nature Climate Change,* **9:** 697–704 DOI: 10.1038/s41558-019-0551-4

Blankinship, J., Meadows, M., Lucas, R., & Hart, S. (2014) Snowmelt timing alters shallow but not deep soil moisture in the Sierra Nevada *Water Resources Research,* **50:** 1448–1456 DOI: 10.1002/2013WR014541

Blöschl, G., Hall, J., Parajka, J., Perdigão, R., Merz, B., Arheimer, B., et al. (2017) Changing climate shifts timing of European floods *Science,* **357:** 588–590 DOI: 10.1126/science.aan2506

Brown, R. (2000) Northern Hemisphere Snow Cover Variability and Change, 1915-97 *Journal of Climate,* **13:** 2339–2355 DOI: 10.1175/1520-0442(2000)013<2339:NHSCVA>2.0.CO;2

Brown, R., Derksen, C., & Wang, L. (2007) Assessment of spring snow cover duration variability over northern Canada from satellite datasets *Remote Sensing of Environment,* **111** (2–3): 367–381 DOI: 10.1016/j.rse.2006.09.035

Brown, R., & Robinson, D. (2011) Northern Hemisphere spring snow cover variability and change over 1922–2010 including an assessment of uncertainty *The Cryosphere,* **5:** 219–229 DOI: 10.5194/tc-5-219-2011

Brown, R., & Robinson, D. (2011) Northern Hemisphere spring snow cover variability and change over 1922-2010 including an assessment of uncertainty *The Cryosphere,* **5:** 219–229 DOI: 10.5194/tc-5-219-2011

Brown, R., & Derksen, C. (2013) Is Eurasian October snow cover extent increasing? *Environmental Research Letters,* **8:** 24006 DOI: 10.1088/1748-9326/8/2/024006

Callaghan, T., Johansson, M., Brown, R., Groisman, P., Labba, N., Radionov, V., et al. (2012) Multiple effects of changes in Arctic snow cover *Ambio,* **40:** 32–45 DOI: 10.1007/s13280-011-0213-x

Carroll, A., Taylor, S., Regniere, J., & Safranyik, L. (2003) Effect of climate change on range expansion by the mountain pine beetle in British Columbia *The Bark Beetles, Fuels, and Fire Bibliography*: Paper 195 In: *Shore, T. and others (eds) Mountain Pine Beetle Symposium: Challenges and Solutions*, 30-31 Oct. 2003, Kelowna BC. Information Report BC-X-399: 223–232 Natural Resources Canada, Victoria

Chen, X., Liang, S., & Cao, Y. (2016) Satellite observed changes in the Northern Hemisphere snow cover phenology and the associated radiative forcing and feedback between 1982 and 2013 *Environmental Research Letters,* **11:** 84002 DOI: 10.1088/1748-9326/11/8/084002

Cheung, H., Zhou, W., Mok, H., Wu, M., & Shao, Y. (2013) Revisiting the climatology of atmospheric blocking in the Northern Hemisphere *Advances in Atmospheric Sciences,* **30** (2): 397–410 DOI: 10.1007/s00376-012-2006-y

Choi, G., Robinson, D., & Kang, S. (2010) Changing Northern Hemisphere snow seasons *Journal of Climate,* **23:** 5305–5310 DOI: 10.1175/2010JCLI3644.1

Clark, M., Serreze, M., & Robinson, D. (1999) Atmospheric controls on Eurasian snow extent *International Journal of Climatology,* **19:** 27–40 DOI: 10.1002/(SICI)1097-0088(199901)19:1<27::AID-JOC346>3.0.CO;2-N

Cohen, J., Foster, J., Barlow, M., Saito, K., & Jones, J. (2010) Winter 2009-2010: A case study of an extreme Arctic Oscillation event *Geophysical Research Letters,* **37:** L1770 DOI: 10.1029/2010GL044256

Cohen, J., Furtado, J., Barlow, M., Alexeev, V., & Cherry, J. (2012) Arctic warming, increasing snow cover and widespread boreal winter cooling *Environmental Research Letters,* **7:** 14007 DOI: 10.1088/1748-9326/7/1/014007

Cohen, J., Screen, J., Furtado, J., Barlow, M., Whittleston, D., Coumou, D., et al. (2014) Recent Arctic amplification and extreme mid-latitude weather *Nature Geoscience,* **7:** 627–637 DOI: 10.1038/ngeo2234

Cohen, J., Zhang, X., Francis, J., Jung, T., Kwok, R., Overland, J., et al. (2018) Arctic change and possible influence on mid-latitude climate and weather *US CLIVAR Report,* **2018** (1): 41pp DOI: 10.5065/D6TH8KGW

Compo, G., Whitaker, J., Sardeshmukh, P., Matsui, N., Allan, R., Yin, X., et al. (2011) The Twentieth Century Reanalysis Project *Quarterly Journal of the Royal Meteorological Society,* **137** (654): 1–28 DOI: 10.1002/qj.776

Coumou, D., Di Capua, G., Vavrus, S., Wang, L., & Wang, S. (2018) The influence of Arctic amplification on mid-latitude summer circulation *Nature Communications,* **9:** 2959 DOI: 10.1038/s41467-018-05256-8

Dark, S., & Bram, D. (2007) The modifiable areal unit problem (MAUP) in physical geography *Progress in Physical Geography,* **31** (5): 471–479 DOI: 10.1177/0309133307083294

Déry, S., Crow, W., Stieglitz, M., & Wood, E. (2004) Modeling snow-cover heterogeneity over complex Arctic terrain for regional and global climate models *Journal of Hydrometeorology,* **5:** 33–48 DOI: 10.1175/1525-7541(2004)005<0033:MSHOCA>2.0.CO;2

Déry, S., & Brown, R. (2007) Recent Northern Hemisphere snow cover extent trends and implications for the snow-albedo feedback *Geophysical Research Letters,* **34:** L22504 DOI: 10.1029/2007GL031474

Ducré-Robitaille, J.-F., Vincent, L., & Boulet, G. (2003) Comparison of techniques for detection of discontinuities in temperature series *International Journal of Climatology,* **23:** 1087–1101 DOI: 10.1002/joc.924

Dye, D. (2002) Variability and trends in the annual snow-cover cycle in Northern Hemisphere land areas, 1972-2000 *Hydrological Processes,* **16:** 3065–3077 DOI: 10.1002/hyp.1089

Estilow, T. (2013) Northern Hemisphere snow cover extent climate algorithm theoretical basis document *NOAA CDR Program Document* Number: CDRP-ATBD-0156, Rev. 3. National Oceanic and

Atmospheric Administration, United States of America.
https://nsidc.org/sites/nsidc.org/files/files/AlgorithmDescription.pdf
(viewed 23 January 2020)

Estilow, T., Young, A., & Robinson, D. (2015) A long-term Northern Hemisphere snow cover extent data record for climate studies and monitoring *Earth System Science Data,* **7:** 137–142 DOI: 10.5194/essd-7-137-2015

Flanner, M., Shell, K., Barlage, M., Perovich, D., & Tschudi, M. (2011) Radiative forcing and albedo feedback from the Northern Hemisphere cryosphere between 1979 and 2008 *Nature Geoscience,* **4:** 151–155 DOI: 10.1038/ngeo1062

Francis, J., & Skific, N. (2015) Evidence linking rapid Arctic warming to mid-latitude weather patterns *Philosophical Transactions of the Royal Society A,* **373** (2045): 20140170 DOI: 10.1098/rsta.2014.0170

Francis, J. (2017) Why are arctic linkages to extreme weather still up in the air? *Bulletin of the American Meteorological Society,* **98** (12): 2551–2557 DOI: 10.1175/bams-d-17-0006.1

Francis, J., Vavrus, S., & Cohen, J. (2017) Amplified Arctic warming and mid-latitude weather: new perspectives on emerging connections *WIREs Climate Change,* **8** (5): e474 DOI: 10.1002/wcc.474

Franzke, C. & Feldstein, S. (2005) The continuum and dynamics of Northern Hemisphere teleconnection patterns *Journal of Atmospheric Sciences* **62**: 3250–3267 DOI: 10.1175/JAS3536.1

Frei, A., Tedesco, M., Lee, S., Foster, J., Hall, D., Kelly, R., & Robinson, D. (2012) A review of global satellite-derived snow products *Advances in Space Research,* **50:** 1007–1029 DOI: 10.1016/j.asr.2011.12.021

Frei, A., Robinson, D., & Hughes, M. (1999) North American snow extent: 1910–1994 *International Journal of Climatology,* **19:** 1517–1534 DOI: 10.1175/1520-0442(2000)013

Fyfe, J., & Flato, G. (1999) Enhanced climate change and its detection over the Rocky Mountains *Journal of Climate,* **12:** 230–243 DOI: 10.1175/1520-0442-12.1.230

Groisman, P., Karl, T., Knight, R., & Stenchikov, G. (1994) Changes of snow cover, temperature and radiative heat balance over the Northern Hemisphere *Journal of Climate,* **7:** 1633–1656 DOI: 10.1175/1520-0442(1994)007

Hansen, M., Potapov, P., Moore, R., Hancher, M., Turubanova, S., Tyukavina, A., et al. (2013) High-resolution global maps of 21st-Century forest cover change *Science,* **342** (6160): 850–853 DOI: 10.1126/science.1244693

Hastings, D., Dunbar, P., Elphingstone, G., Bootz, M., Murakami, H., Maruyama, H., et al. (1999) The Global Land One-kilometer Base Elevation (GLOBE) Digital Elevation Model, Version 1.0. National Oceanic and Atmospheric Administration, National Geophysical Data Center. http://www.ngdc.noaa.gov/mgg/topo/globe.html
(viewed 23 January 2020)

Helfrich, S., McNamara, D., Ramsay, B., Baldwin, T., & Kasheta, T. (2007) Enhancements to, and forthcoming developments in the Interactive Multisensor Snow and Ice Mapping System (IMS) *Hydrological Processes,* **21:** 1576–1586 DOI: 10.1002/hyp.6720

Hernández-Henríquez, M., Déry, S., & Derksen, C. (2015) Polar amplification and elevation-dependence in trends of Northern Hemisphere snow cover extent, 1971–2014 *Environmental Research Letters,* **10:** 44010 DOI: 10.1088/1748-9326/10/4/044010

Hori, M., Sugiura, K., Kobayashi, K., Aoki, T., Tanikawa, T., Kuchiki, K., & Niwano, M. (2017) A 38-year (1978–2015) Northern Hemisphere daily snow cover extent product derived using consistent objective criteria from satellite-borne optical sensors *Remote Sensing of Environment,* **191:** 402–418 DOI: 10.1016/j.rse.2017.01.023

Immerzeel, W., van Beek\, L., & Bierkens, M. (2010) Climate change will affect the Asian Water Towers *Science,* **328:** 1382–1385 DOI: 10.1126/science.1183188

IPCC (2013) Climate Change 2013: The Physical Science Basis *Contribution of Working Group I to the Fifth Assessment Report of the Intergovernmental Panel on Climate Change* [Stocker, T., et al. (eds.)]. Cambridge University Press, Cambridge and New York
https://www.ipcc.ch/report/ar5/wg1/
(viewed 23 January 2020)

Johnson, N., Feldstein, S. and Tremblay, B. (2008) The continuum of Northern Hemisphere teleconnection patterns and a description of the NAO shift with the use of Self-Organizing Maps *Journal of Climate* **21**: 6354–6371 DOI: 10.1175/2008JCLI2380.1

Jones, H. (1999) The ecology of snow-covered systems: a brief overview of nutrient cycling and life in the cold *Hydrological Processes,* **13:** 2135–2147 DOI: 10.1002/(SICI)1099-1085(199910)13:14/15<2135::AID-HYP862>3.0.CO;2-Y

Jones, P., Lister, D., Osborn, T., Harpham, C., Salmon, M., & Morice, C. (2012) Hemispheric and large-scale land surface air temperature variations: An extensive revision and an update to 2010 *Journal of Geophysical Research,* **117:** D05127 DOI: 10.1029/2011JD017139

Kendall, M. (1975) Rank correlation methods Oxford University Press, New York

Kirtman, B., Power, S., Adedoyin, J., Boer, G., Bojariu, R., Camilloni, I., et al. (2013) Near-term climate change: projections and predictability *Chapter 11 in Climate Change 2013: The Physical Science Basis. Contribution of Working Group I to the Fifth Assessment Report of the Intergovernmental Panel on Climate Change* [Stocker, T., et al. (eds.)], Cambridge University Press, Cambridge and New York. https://www.ipcc.ch/site/assets/uploads/2018/02/WG1AR5_Chapter11_FINAL.pdf (viewed 23 January 2020)

Kretschmer, M., Coumou, D., Donges, J., & Runge, J. (2016) Using Causal Effect Networks to analyze different arctic drivers of midlatitude winter circulation *Journal of Climate,* **29:** 4069–4081 DOI: 10.1175/JCLI-D-15-0654.1

Kretschmer, M., Coumou, D., Agel, L., Barlow, M., Tziperman, E., & Cohen, J. (2017) More-persistent weak stratospheric polar vortex states linked to cold extremes *Bulletin of the American Meteorological Society,* **99** (1): 49–60 DOI: 10.1175/BAMS-D-16-0259.1

Kulkarni, A., & von Storch, H. (1995) Monte Carlo experiments on the effect of serial correlation on the Mann–Kendall test of trend *Meteorologische Zeitschrift,* **4** (2): 82–85

Liu, J., Curry, J., Wang, H., Song, M., & Horton, R. (2012) Impact of declining Arctic sea ice on winter snowfall *Proceedings of the National Academy of Science of the United States of America,* **109:** 4074–4079 DOI: 10.1073/pnas.1114910109

Mankin, J., Viviroli, D., Singh, D., Hoekstra, A., & Diffenbaugh, N. (2015) The potential for snow to supply human water demand in the present and future *Environmental Research Letters,* **10:** 114016 DOI: 10.1088/1748-9326/10/11/114016

Mann, H. (1945) Non-parametric tests against trend *Econometrica,* **13:** 245–259 DOI: 0012-9682(194507)13:3

Mann, M., Rahmstorf, S., Kornhuber, K., Steinman, B., Miller, S., Petri, S., & Coumou, D. (2018) Projected changes in persistent extreme summer weather events: The role of quasi-resonant amplification *Science Advances,* **4** (10): eaat3272 DOI: 10.1126/sciadv.aat3272

Mantua, N., Hare, S., Zhang, Y., Wallace, J., & Francis, R. (1997) A Pacific interdecadal climate oscillation with impacts on salmon production *Bulletin of the American Meteorological Society,* **78** (6): 1069–1079 DOI: 10.1175/1520-0477(1997)078<1069:APICOW>2.0.CO;2

Mao, J., Ribes, A., Yan, B., Shi, X., Thornton, P., Séférian, R., et al. (2016) Human-induced greening of the northern extratropical land surface *Nature Climate Change,* **6:** 959–963 DOI: 10.1038/nclimate3056

Marsh, P., Essery, R., Neumann, N., Pomeroy, J., & Tranter, M. (1999) Model estimates o f local advection of sensible heat over a patchy snow cover *Proceedings, IAHS Symposium on Interactions between the Cryosphere, Climate and Greenhouse Gases*, during the XXII General Assembly of the IUGG: Jul 1999, Birmingham, UK, **Red Book 256:** 103–110 IAHS Press

Matsumura, S., & Kosaka, Y. (2019) Arctic–Eurasian climate linkage induced by tropical ocean variability *Nature Communications,* **10** (3441): DOI: 10.1038/s41467-019-11359-7

McCusker, K., Fyfe, J., & Sigmond, M. (2016) Twenty-five winters of unexpected Eurasian cooling *Nature Geoscience,* **9:** 838–842 DOI: 10.1038/ngeo2820

Mekis, E., Donaldson, N., Reid, J., Zucconi, A., Hoover, J., Li, Q., et al. (2018) An Overview of Surface-Based Precipitation Observations at Environment and Climate Change Canada *Atmosphere-Ocean,* **56** (2): 71–95 DOI: 10.1080/07055900.2018.1433627

Ménard, C., Essery, R., Pomeroy, J., Marsh, P., & Clark, D. (2014) A shrub bending model to calculate the albedo of shrub-tundra *Hydrological Processes,* **28** (2): 341–351 DOI: 10.1002/hyp.9582

Mote, P. (2006) Climate-driven variability and trends in mountain snowpack in western North America *Journal of Climate,* **19:** 6209–6220 DOI: 10.1175/JCLI3971.1

Mudryk, L., Kushner, P., Derksen, C., & Thackeray, C. (2017) Snow cover response to temperature in observational and climate model ensembles *Geophysical Research Letters,* **44:** 919–926 DOI: 10.1002/2016GL071789

Nakamura, T., Yamazaki, K., Iwamoto, K., Honda, M., Miyoshi, Y., Ogawa, Y., & Ukita, J. (2015) A negative phase shift of the winter AO/NAO due to the recent Arctic sea-ice reduction in late autumn *Journal of Geophysical Research: Atmospheres,* **120:** 3209–3227 DOI: 10.1002/2014JD022848

Nakamura, N., & Huang, C. (2018) Atmospheric blocking as a traffic jam in the jet stream *Science,* **361** (6397): 42–47 DOI: 10.1126/science.aat0721

Neumann, N., Derksen, C., Smith, C., & Goodison, B. (2006) Characterizing local scale snow cover Using point measurements during the winter season *Atmosphere-Ocean,* **44** (3): 257–269 DOI: 10.3137/ao.440304

Nolin, A. (2010) Recent advances in remote sensing of seasonal snow *Journal of Glaciology,* **56** (200): 1141–1150 DOI: 10.3189/002214311796406077

NSIDC web. State of the Cryosphere – Northern Hemisphere Snow.
https://nsidc.org/cryosphere/sotc/snow_extent.html
(viewed 10 January 2020)

O'Leary, D., Bloom, T., Smith, J., Zemp, C., & Medler, M. (2016) A new method comparing snowmelt timing and annual area burnt *Fire Ecology,* **12** (1): 41–51 DOI: 10.4996/fireecology.1201041

O'Gorman, P. (2014) Contrasting responses of mean and extreme snowfall to climate change *Nature,* **512:** 416–418 DOI: 10.1038/nature13625

Olonscheck, D., Mauritsen, T., & Notz, D. (2019) Arctic sea-ice variability is primarily driven by atmospheric temperature fluctuations *Nature Geoscience,* **12:** 430–434 DOI: 10.1038/s41561-019-0363-1

Onarheim, I., & Årthun, M. (2017) Toward an ice-free Barents Sea *Geophysical Research Letters,* **44:** 8387–8395 DOI: 10.1002/2017GL074304

Overland, J., Wood, K., & Wang, M. (2011) Warm Arctic—cold continents: climate impacts of the newly open Arctic Sea *Polar Research,* **30** (1): 15787 DOI: 10.3402/polar.v30i0.15787

Overland, J. (2016) A difficult Arctic science issue: Midlatitude weather linkages *Polar Science,* **10:** 210–216 DOI: 10.1016/j.polar.2016.04.011

Pampaloni, P. (2015) Reading snow: A note on microwave remote sensing of snow cover *In: IEEE International Geoscience and Remote Sensing Symposium (IGARSS), 26-31 July 2015, Milan, Italy,* DOI: 10.1109/IGARSS.2015.7326708

Peng, S., Piao, S., Ciais, P., Friedlingstein, P., Zhou, L., & Wang, T. (2013) Change in snow phenology and its potential feedback to temperature in the Northern Hemisphere the last three decades *Environmental Research Letters,* **8:** 14008 DOI: 10.1088/1748-9326/8/1/014008

Pettitt, A. (1980) A simple cumulative sum type statistic for the change-point problem with zero-one observations *Biometrika,* **67** (1): 79–84 DOI: 10.2307/2335319

Pickell, P., Coops, N., Gergel, S., Andison, D., & Marshall, P. (2016) Evolution of Canada's Boreal Forest spatial patterns as seen from space *PLoS ONE,* **11** (7): e0157736 DOI: 10.1371/journal.pone.0157736

Pomeroy, J., Gray, D., Shook, K., Toth, B., Essery, R., Pietroniro, A., & Hedstrom, N. (1998) An evaluation of snow accumulation and ablation processes for land surface modelling *Hydrological Processes,* **12:** 2339–2367 DOI: 10.1002/(SICI)1099-1085(199812)12:15<2339::AID-HYP800>3.0.CO;2-L

Qu, X., & Hall, A. (2007) What controls the strength of Snow-Albedo Feedback? *Journal of Climate,* **20:** 3971–3981 DOI: 10.1175/JCLI4186.1

Ramsay, B. (1998) The interactive multisensor snow and ice mapping system *Hydrological Processes,* **12:** 1537–1546 DOI: 10.1002/(SICI)1099-1085(199808/09)12:10/11

Razavi, S., & Vogel, R. (2018) Prewhitening of hydroclimatic time series? Implications for inferred change and variability across time scales *Journal of Hydrology,* **557:** 109–115 DOI: 10.1016/j.jhydrol.2017.11.053

Reeves, J., Chen, J., Wang, X., Lund, R., & Lu, Q. (2007) A review and comparison of changepoint detection techniques for climate data *Journal of Applied Meteorology and Climatology,* **46** (6): 900–915 DOI: 10.1175/JAM2493.1

Rikiishi, K., Hashiya, E., & Imai, M. (2004) Linear trends of the length of snow-cover season in the Northern Hemisphere as observed by the satellites in the period 1972-2000 *Annals of Glaciology,* **38:** 229–237 DOI: 10.3189/172756404781815329

Rittger, K., Painter, T., & Dozier, J. (2013) Assessment of methods for mapping snow cover from MODIS *Advances in Water Resources,* **51:** 367–380 DOI: 10.1016/j.advwatres.2012.03.002

Robinson, D., Dewey, K., & Heim, R. (1993) Global snow cover monitoring: an update *Bulletin of the American Meteorological Society,* **74** (9): 1689–1696 DOI: 10.1175/1520-0477(1993)074<1689:GSCMAU>2.0.CO;2

Robinson, D., Estilow, T., & NOAA CDR Program, . (2012) NOAA climate data record of Northern Hemisphere snow cover extent, Version 1, Revision 1 NOAA. National Centers for Environmental Information, DOI: 10.7289/V5N014G9 National Oceanic and Atmospheric Administration, United States of America.

Romanov, P., Gutman, G., & Csiszar, I. (2000) Automated monitoring of snow cover over North America with multispectral satellite data *Journal of Applied Meteorology,* **39:** 1866–1880 DOI: 10.1175/1520-0450(2000)039

Rutgers Snow Lab. web Rutgers University Global Snow Laboratory
http://climate.rutgers.edu/snowcover
(viewed 10 January 2020)

Sato, K., Inoue, J., & Watanabe, M. (2014) Influence of the Gulf Stream on the Barents Sea ice retreat and Eurasian coldness during early winter *Environmental Research Letters,* **9:** 84009 DOI: 10.1088/1748-9326/9/8/084009

Scaife, A., Comer, R., Dunstone, N., Knight, J., Smith, D., MacLachlan, C., et al. (2017) Tropical rainfall, Rossby waves and regional winter climate predictions *Quarterly Journal of the Royal Meteorological Society,* **143:** 1–11 DOI: 10.1002/qj.2910

Schlesinger, M., & Ramankutty, N. (1994) An oscillation in the global climate system of period 65–70 years *Nature,* **367:** 723–726 DOI: 10.1038/367723a0

Schuur, E., Vogel, J., Crummer, K., Lee, H., Sickman, J., & Osterkamp, T. (2009) The effect of permafrost thaw on old carbon release and net carbon exchange from tundra *Nature,* **459:** 556–559 DOI: 10.1038/nature08031

Screen, J., & Simmonds, I. (2014) Amplified mid-latitude planetary waves favour particular regional weather extremes *Natue Climate Change,* **4:** 704–709 DOI: 10.1038/nclimate2271

Screen, J., & Simmonds, I. (2010) The central role of diminishing sea ice in recent Arctic temperature amplification *Nature,* **464:** 1334–1337 DOI: 10.1038/nature09051

Screen, J., Bracegirdle, T., & Simmonds, I. (2018) Polar Climate Change as Manifest in Atmospheric Circulation *Current Climate Change Reports,* **4:** 383–395 DOI: 10.1007/s40641-018-0111-4

Sen, P. (1968) Estimates of the regression coefficient based on Kendall's tau *Journal of the American Statistical Association,* **63:** 1379–1389 DOI: 10.2307/2285891

Serreze, M., Barrett, A., Stroeve, J., Kindig, D., & Holland, M. (2009) The emergence of surface-based Arctic amplification *Cryosphere,* **3:** 11–19 DOI: 10.5194/tc-3-11-2009

Serreze, M., & Barry, R. (2011) Processes and impacts of Arctic amplification: A research synthesis *Global and Planetary Change,* **77** (1–2): 85–96 DOI: 10.1016/j.gloplacha.2011.03.004

Serreze, M., & Stroeve, J. (2015) Arctic sea ice trends, variability and implications for seasonal ice forecasting *Philosophical Transactions of the Royal Society A,* **373** (2045): 20140159 DOI: 10.1098/rsta.2014.0159

Sharma, A., & Déry, S. (2016) Elevational dependence of air temperature variability and trends in British Columbia's Cariboo Mountains, 1950–2010 *Atmosphere-Ocean,* **54** (2): 153–170 DOI: 10.1080/07055900.2016.1146571

Shepherd, T. (2016) Effects of a warming Arctic *Science,* **353** (6303): 989–990 DOI: 10.1126/science.aag2349

Smirnov, D., Kabanets, A., Milakovsky, B., Lepeshkin, E., & Sychikov, D. (2013) Illegal logging in the Russian Far East: global demand and taiga destruction WWF, Moscow., https://www.worldwildlife.org/publications/illegal-logging-in-the-russian-far-east-global-demand-and-taiga-destruction
(viewed 23 January 2020)

Stieglitz, M., Déry, S., Romanovsky, V., & Osterkamp, T. (2003) The role of snow cover in the warming of Arctic permafrost *Geophysical Research Letters,* **30:** 1721 DOI: 10.1029/2003GL017337

Stroeve, J., & Notz, D. (2017) Changing state of Arctic sea ice across all seasons *Environmental Research Letters,* **13:** 103001 DOI: 10.1088/1748-9326/aade56

Sturm, M., & Benson, C. (2004) Scales of spatial heterogeneity for perennial and seasonal snow layers *Annals of Glaciology,* **38:** 253–260 DOI: 10.3189/172756404781815112

Sun, L., Perlwitz, J., & Hoerling, M. (2016) What caused the recent 'Warm Arctic, Cold Continents' trend pattern in winter temperatures? *Geophysical Research Letters,* **43** (10): 5345–5352 DOI: 10.1002/2016GL069024

Thackeray, C., & Fletcher, C. (2016) Snow albedo feedback: current knowledge, importance, outstanding issues and future directions *Progress in Physical Geography,* **40:** 392–408 DOI: 10.1177/0309133315620999

Thackeray, C., Derksen, C., Fletcher, C., & Hall, A. (2019) Snow and Climate: Feedbacks, Drivers, and Indices of Change *Current Climate Change Reports,* **5:** 322–333 DOI: 10.1007/s40641-019-00143-w

Theil, H. (1950) A rank-invariant method of linear and polynomial regression analysis I, II, III *Proceedings of the Koninklijke Nederlandse Akademie Wetenschappen, Series A,* **53:** 386–392;521–525;1397–1412

Thompson, D., & Wallace, J. (2001) Regional climate impacts of the Northern Hemisphere Annular Mode *Science,* **293** (5527): 85–89 DOI: 10.1126/science.1058958

Turner, A., & Slingo, J. (2011) Using idealized snow forcing to test teleconnections with the Indian summer monsoon in the Hadley Centre GCM *Climate Dynamics,* **36:** 1717–1735 DOI: 10.1007/s00382-010-0805-3

Tyrlis, E., & Hoskins, B. (2008) Aspects of a Northern Hemisphere atmospheric blocking climatology *Journal of the Atmospheric Sciences,* **65** (5): 1638–1652 DOI: 10.1175/2007JAS2337.1

Tyrrell, N., Karpechko, A., & Räisänen, P. (2018) The Influence of Eurasian Snow Extent on the Northern Extratropical Stratosphere in a QBO Resolving Model *Journal of Geophysical Research: Atmospheres,* **123:** 315–328 DOI: 10.1002/2017JD027378

Vaughan, D., Comiso, J., Allison, I., Carrasco, J., Kaser, G., Kwok, R., et al. (2013) Observations: Cryosphere *Chapter 4 in: Climate Change 2013: The Physical Science Basis. Contribution of Working Group I to the Fifth Assessment Report of the Intergovernmental Panel on Climate Change* [Stocker, T., et al. (eds.)], Cambridge University Press, Cambridge and New York.

https://www.ipcc.ch/site/assets/uploads/2018/02/WG1AR5_Chapter04_FINAL.pdf
(viewed 23 January 2020)

Vavrus, S. (2007) The role of terrestrial snow cover in the climate system *Climate Dynamics,* **29:** 73–88 DOI: 10.1007/s00382-007-0226-0

Vavrus, S., Wang, F., Martin, J., Francis, J., Peings, Y., & Cattiaux, J. (2017) Changes in North American Atmospheric Circulation and Extreme Weather: Influence of Arctic Amplification and Northern Hemisphere Snow Cover *Journal of Climate,* **30:** 4317–4333 DOI: 10.1175/JCLI-D-16-0762.1

Viviroli, D., Dürr, H., Messerli, B., Meybeck, M., & Weingartner, R. (2007) Mountains of the world, water towers for humanity: typology, mapping, and global significance *Water Resources Research,* **43:** W07447 DOI: 10.1029/2006WR005653

Wang, L., Sharpa, M., Brown, R., Derksen, C., & Rivard, B. (2005) Evaluation of spring snow covered area depletion in the Canadian Arctic from NOAA snow charts *Remote Sensing of the Environment,* **95** (4): 453–463 DOI: 10.1016/j.rse.2005.01.006

Wang, Q., Fan, X., & Wang, M. (2015) Evidence of high-elevation amplification versus Arctic amplification *Nature Scientific Reports,* **6:** 19219 DOI: 10.1038/srep19219

Wegmann, M., Orsolini, Y., Vázquez, M., Gimeno, L., Nieto, R., Bulygina, O., & Jaiser, R. (2015) Arctic moisture source for Eurasian snow cover variations in autumn *Environmental Research Letters,* **10:** 54015 DOI: 10.1088/1748-9326/10/5/054015

Westerling, A. (2016) Increasing western US forest wildfire activity: sensitivity to changes in the timing of spring *Philosophical transactions of the Royal Society of London. Series B, Biological sciences,* **371** (1696): 20150178 DOI: 10.1098/rstb.2015.0178

WMO web Snow Watch – Snow Reporting Activity
http://globalcryospherewatch.org/projects/snowreporting.html
(viewed 10 January 2020)

Wu, T.-W., & Qian, Z.-A. (2003) The relation between the Tibetan winter snow and the Asian summer monsoon and rainfall: an observational investigation *Journal of Climate,* **16:** 2038–2051 DOI: 10.1175/1520-0442(2003)016<2038:TRBTTW>2.0.CO;2

Yeo, S.-R., Kim, W., & Kim, K.-Y. (2017) Eurasian snow cover variability in relation to warming trend and Arctic Oscillation *Climate Dynamics,* **48:** 499–511 DOI: 10.1007/s00382-016-3089-4

Yue, S., Pilon, P., Phinney, B., & Cavadias, G. (2002) The influence of autocorrelation on the ability to detect trend in hydrological series *Hydrological Processes,* **16:** 1807–1829 DOI: 10.1002/hyp.1095

Zhang, T. (2005) Influence of the seasonal snow cover on the ground thermal regime: An overview *Reviews of Geophysics,* **43:** RG4002 DOI: 8755-1209/05/2004RG000157

Zhao, L., Zhu, Y., Liu, H., Liu, Z., Liu, Y., Li, X., & Chen, Z. (2016) A stable snow-atmosphere coupled mode *Climate Dynamics,* **47:** 2085–2104 DOI: 10.1007/s00382-015-2952-z

Zhong, X., Zhang, T., Zheng, L., Hu, Y., Wang, H., & Kang, S. (2018) Spatiotemporal variability of snow depth across the Eurasian continent from 1966 to 2012 *Cryosphere,* **12** (1): 227–245 DOI: 10.5194/tc-12-227-2018

Appendix 1

This appendix contains information associated with Chapter 2, published as a supplement to –

Allchin, M.I., and Déry, S.J. (2017). A spatio-temporal analysis of trends in Northern Hemisphere snow-dominated area and duration, 1971-2014 *Annals of Glaciology,* **58**(75): 21–35 DOI: 10.1017/aog.2017.47

A1.1: Variation with latitude and elevation of NRSD terrestrial area represented within 5° cells

A1.2: Rationale for method adopted to estimate trend magnitudes

A1.3: Maps of trends in snow-dominated area as km^2 $decade^{-1}$

A1.4: Variation of significant SDA trends with latitude, longitude and elevation.

A1.5: Implications of alternative assumptions of fractional snow-cover associated with 'snow-covered' and 'snow-free' states

A1.1: Variation with latitude and elevation of NRSD terrestrial area within 5° cells

The area associated with each snow grid-point (DGP) in the NOAA – Rutgers Snow Dataset (NRSD) varies primarily with latitude, from ~10.7 × 10^3 km^2 at the lowest latitudes to ~41.8 × 10^3 km^2 near the geographic North Pole (Estilow, 2013). However, the surface footprint of the cells within the 5° grid adopted as the spatial framework for this analysis decreases with increasing latitude. Additionally, individual cells may include considerable oceanic fractions and / or DGPs excluded from the analysis (by masks for perennial cryospheric cover, previously-established unreliable snow-cover values). Therefore, the terrestrial area of each 5° cell which is represented within the NRSD varies considerably (Figure A1.1).

Together, these influences result in a highly significant negative correlation ($p < 0.001$, $R \sim -0.42$) between the terrestrial area represented within the NRSD in the 5° cells considered in the analysis and their (central) latitudes (Figure A1.2).

However, there is also a highly significant, but loose, negative correlation ($p < 0.001$, $R \sim -0.16$) between mean DGP elevation within the 5° cells and their latitudes. This is driven primarily by the major mountain ranges in the mid-latitudes, including the Western Cordillera of North America, European Alps, Himalayas and other south-central Asian ranges (Figure A1.3).

It therefore follows that a positive linear relationship ($p < 0.001$, $R \sim 0.45$) exists between mean DGP elevation within the 5° cells and their terrestrial area represented within the NRSD (Figure A1.4).

These variations in the total NRSD-represented terrestrial area within the 5° cells with latitude and elevation thus influence their maximum possible snow-covered areas, and in turn the maximum magnitudes of any trends identified.

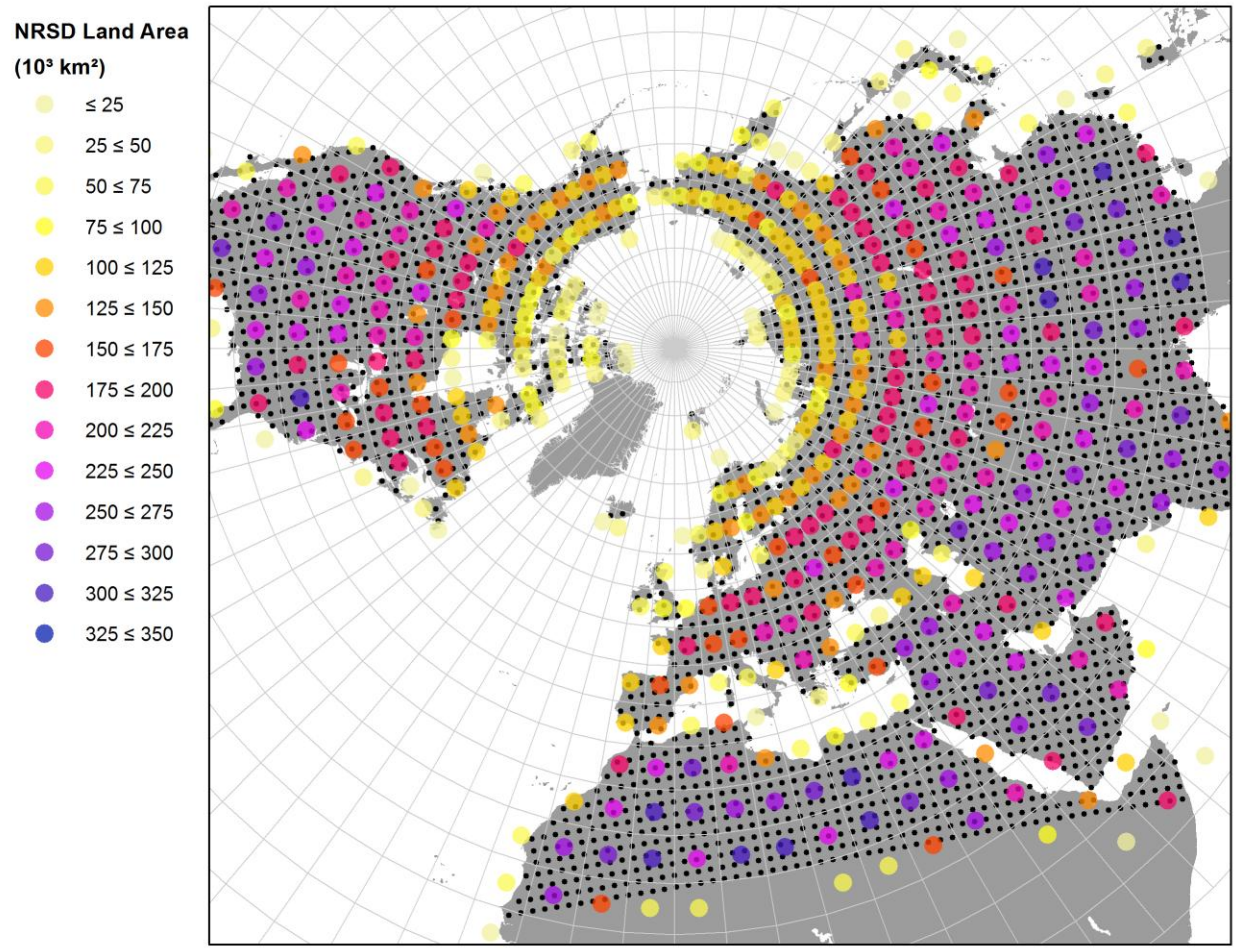

Figure A1.1: Variation of NRSD terrestrial area represented within 5° cells. The smaller dots are the NRSD snow grid-points (DGPs) considered in the analysis.

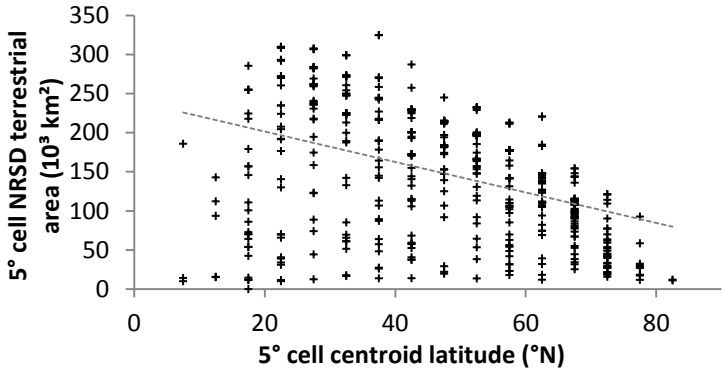

Figure A1.2: Relationship between 5° cell centroid latitude and NRSD-represented terrestrial area.

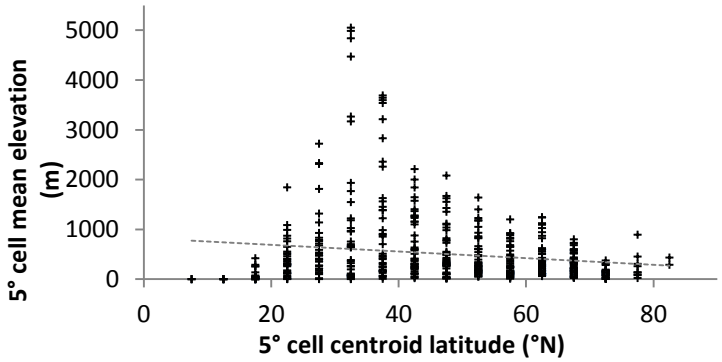

Figure A1.3: Relationship between 5° cell centroid latitude and mean elevation of constituent DGPs.

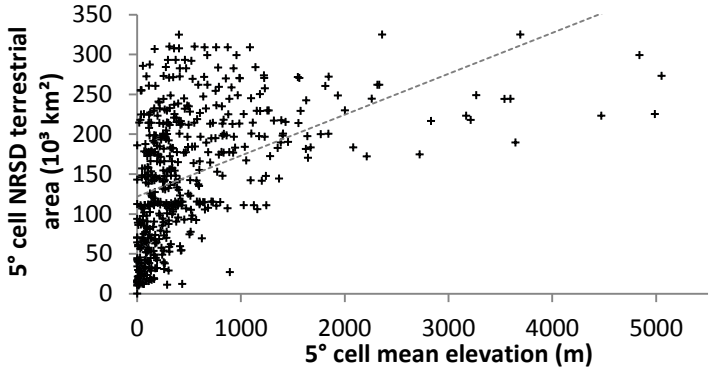

Figure A1.4: Relationship between mean elevation of constituent DGPs in 5° cells and and NRSD-represented terrestrial area.

A1.2: Rationale for method adopted to estimate trend magnitudes

Trend magnitudes were estimated in this study by least-squares regression (LSR). This was adopted instead of the Theil-Sen (TS) method (Theil, 1950; Sen, 1968) because a substantial portion of 5° cells in each month is associated with a series of snow-dominated area (SDA) values comprising more than 50% tied values (either 0% or 100%). Because TS estimates the trend magnitude from the median of all possible pairwise slopes between data-points in a series, in these cases it yields a value of zero. Given that magnitudes were only estimated for those series in which Mann-Kendall Trend Analysis (MKTA) (Mann, 1945; Kendall, 1975) has already identified the existence of a trend with a high level of confidence, LSR provided the more useful result.

Figure A1.5 illustrates variation in the total trend magnitude through the year when computed by each method, summed for 5° cells for which significant ($p < 0.05$) trends were identified by MKTA. Figure A1.6 depicts the count of cells for which significant trends were identified by MKTA and for which non-zero magnitudes were generated in each month.

To ensure that there was no systematic bias in the LSR results compared to those generated by TS, correlations were computed between the two sets of magnitudes for all cells / months in which both methods generated a non-zero estimate, and are presented here. The plots in Figure A1.7 depict correspondences between trend magnitudes calculated by the two methods, for those cells in which both methods generate non-zero values. All correlations are significant with $p < 0.001$. Differences between the two sets of estimates are greatest in July and August (driven by negative trends) and November (driven primarily by positive trends). However, the high values of Pearson's R, slopes close to unity and small intercepts relative to the trend magnitudes

together indicate that the two methods generate similar estimates. By extension, it is inferred that no substantial additional error is introduced by using LSR as the principal method for this study, and retaining values for those points / months at which TS generates zero magnitudes.

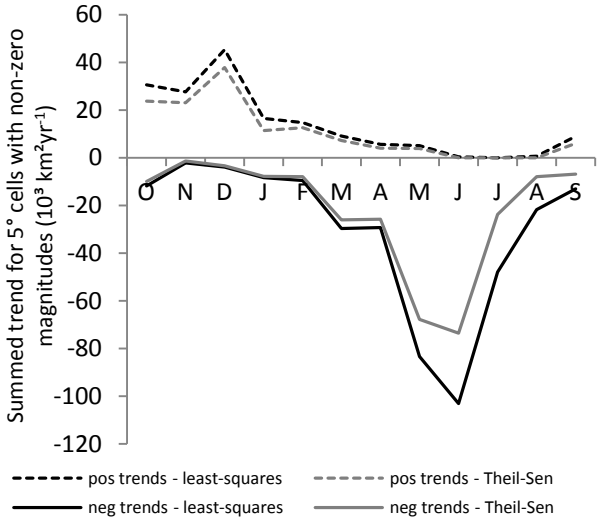

Figure A1.5: Comparison of total monthly trend magnitudes (significant with $p < 0.05$) estimated by LSR and TS

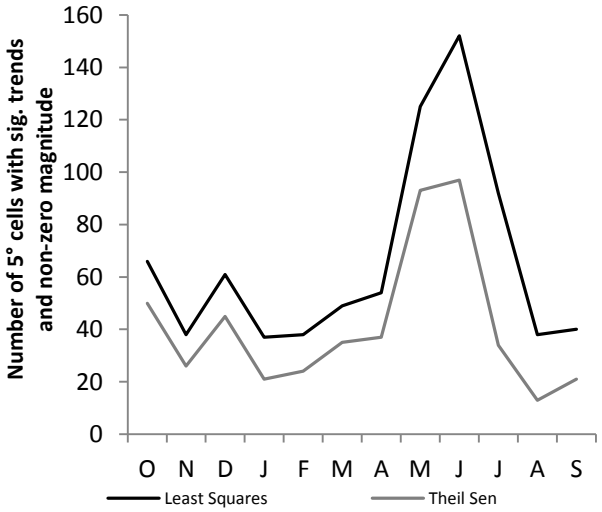

Figure A1.6: Comparison of number of 5° cells in each month for which significant ($p < 0.05$) trends are identified and which have non-zero magnitudes, as estimated by LSR and TS

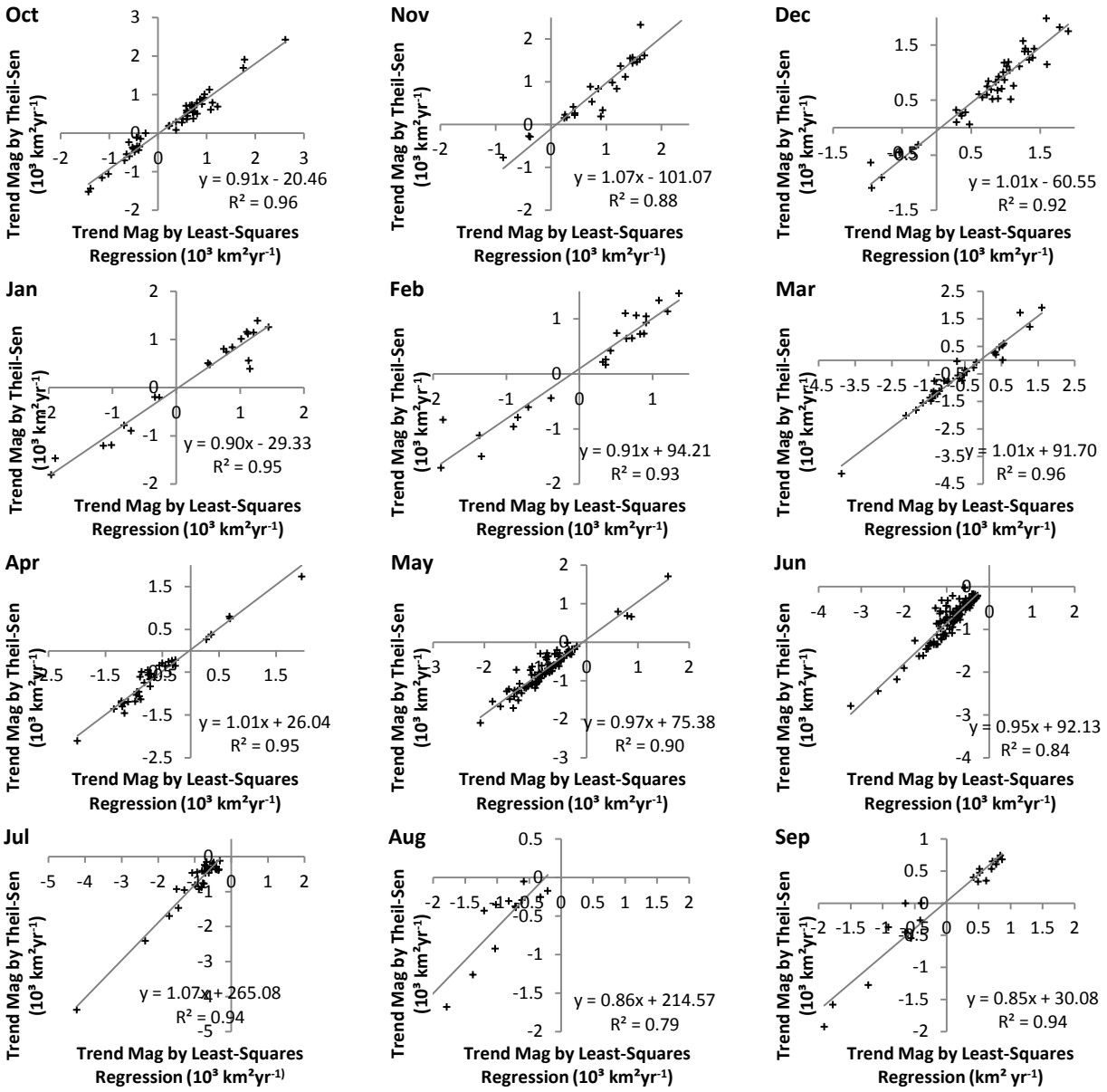

Figure A1.7: Linear correlations between non-zero magnitudes estimated for significant ($p < 0.05$) SA trends by LSR and TS in each month. All correlations are significant with $p < 0.001$.

A1.3: Maps of trends in snow-dominated area as km² decade^{-1}

The maps provided in Chapter 2 of the main text show SDA trend magnitudes in terms of changes in the fraction of snow-dominated terrestrial area in each 5° cell, represented in the NRSD, and included in the analysis. For completeness, these maps depict the magnitudes as km² decade^{-1}. The topographic shading is the same as that in Figure 6 of the main text.

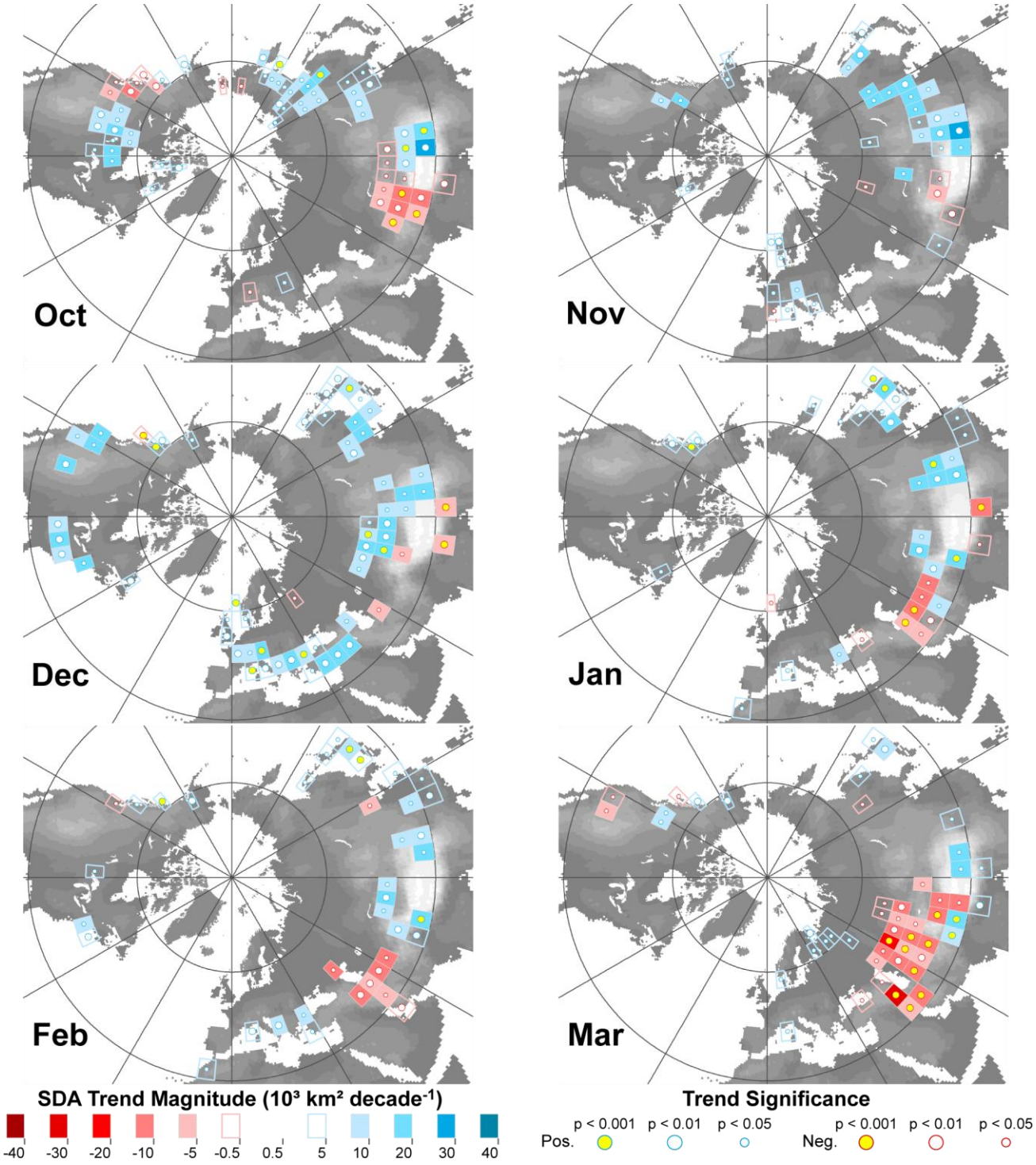

Figure A1.8a: Monthly distributions of NH SDA trends (1971 – 2014) as km² decade^{-1} (Oct. – Mar.).

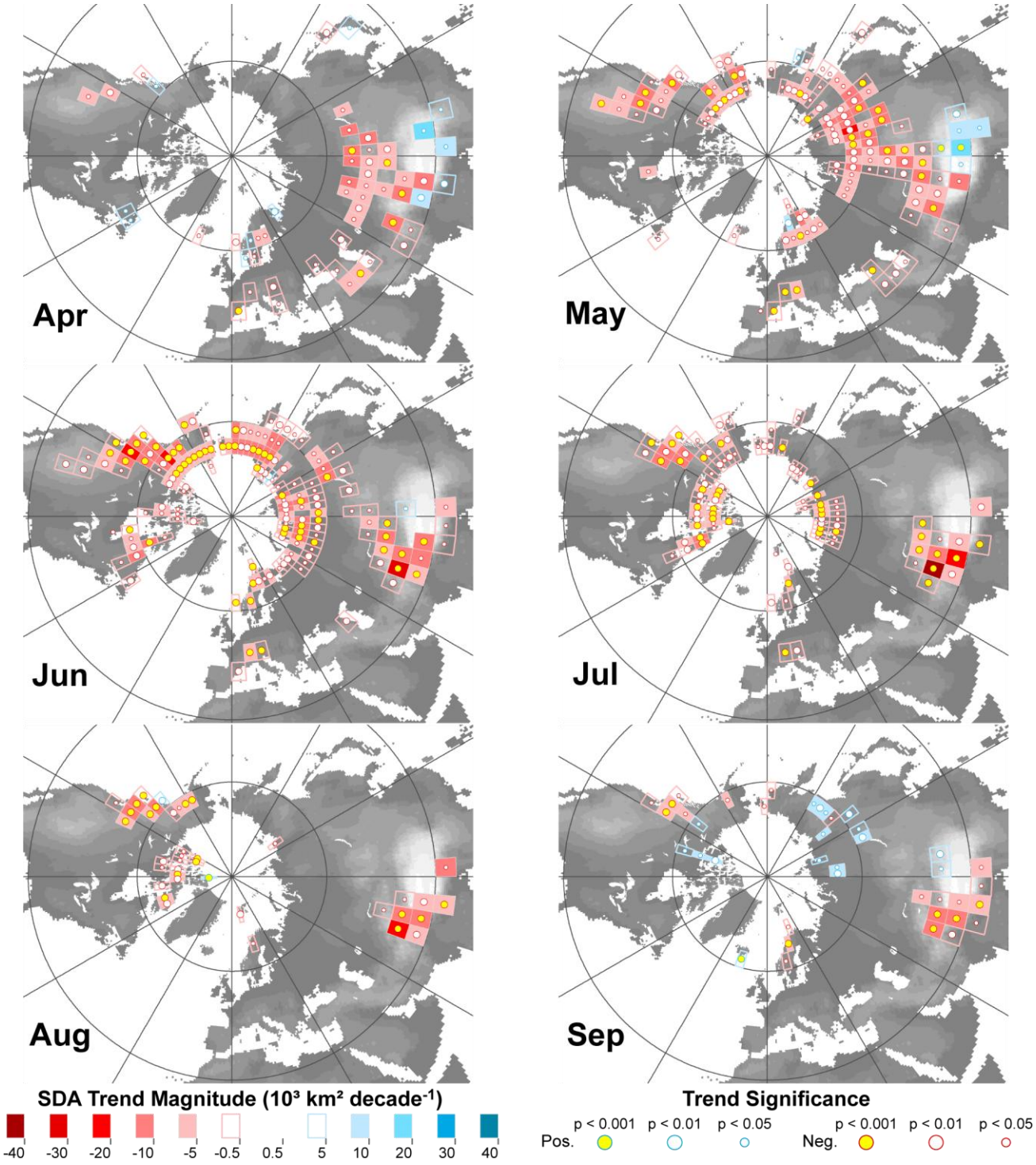

Figure A1.8b: Monthly distributions of NH SDA trends (1971–2014) as km² decade^{-1} (Apr. – Sep.).

A1.4: Variation of significant SDA trends with latitude, longitude and elevation.

These figures illustrate distributions of monthly SDA trend magnitudes with elevation, latitude and longitude in greater detail. The full definition of the units is (% of 5° cell terrestrial area represented in NRSD) decade^{-1}.

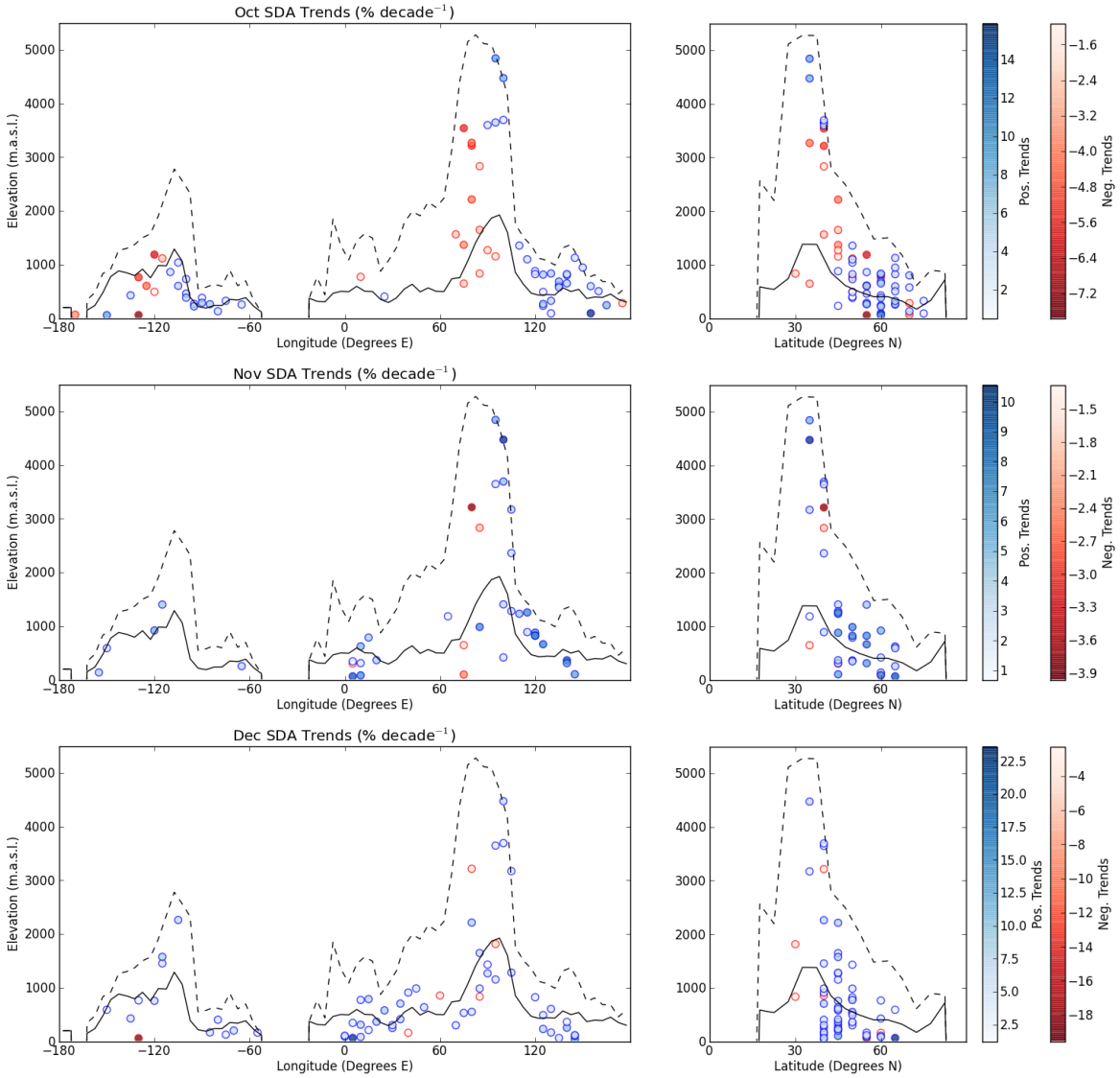

Figure A1.9a: Variations of NH SDA trends (1971 – 2014) with elevation, latitude and longitude from October to December. Solid lines represent meridional / zonal mean elevation of NRSD DGPs, dashed lines represent meridional / zonal maximum elevation of NRSD DGPs.

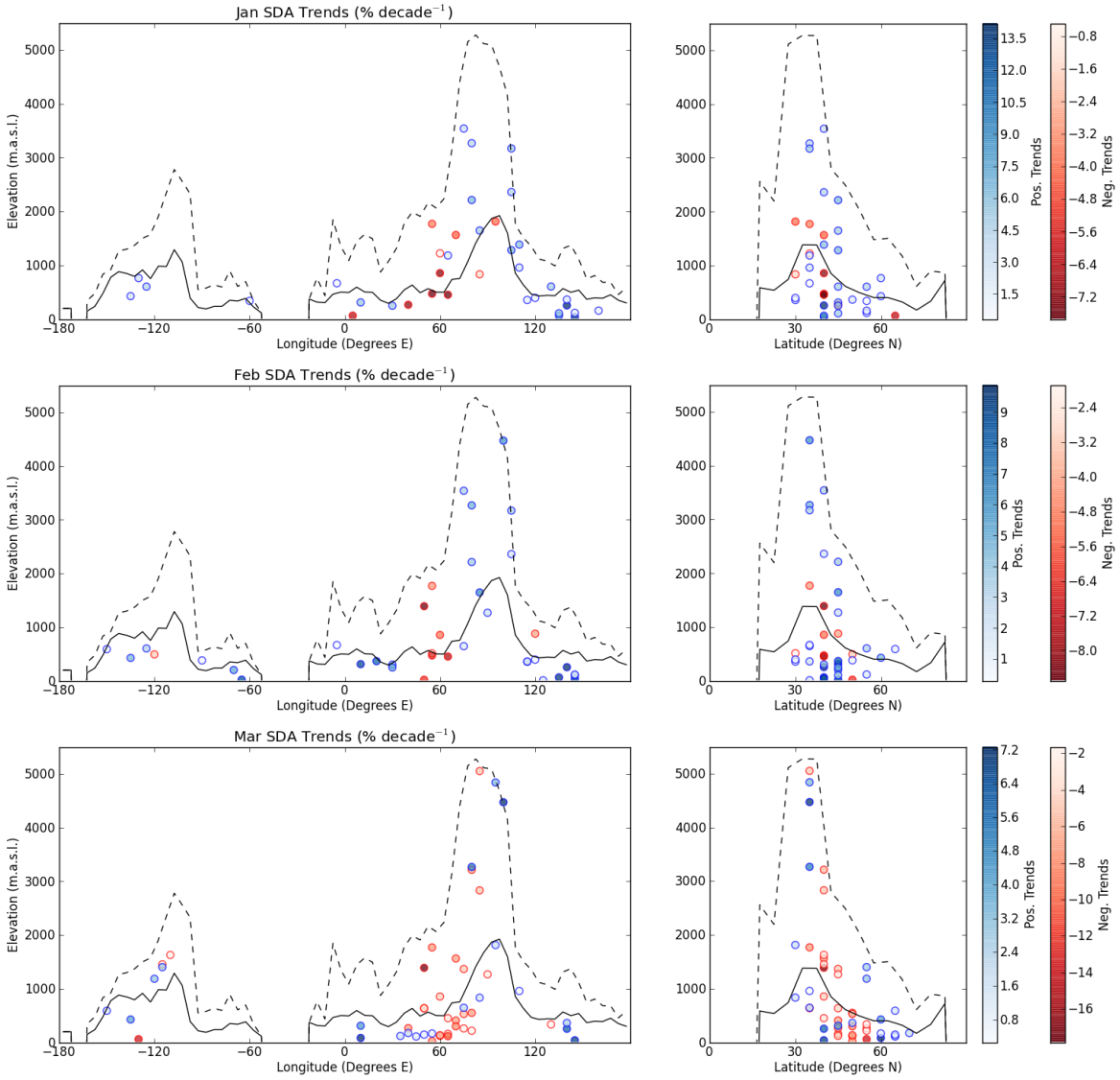

Figure A1.9b: Variations of NH SDA trends (1971 – 2014) with elevation, latitude and longitude from January to March. Solid lines represent meridional / zonal mean elevation of NRSD DGPs, dashed lines represent meridional / zonal maximum elevation of NRSD DGPs.

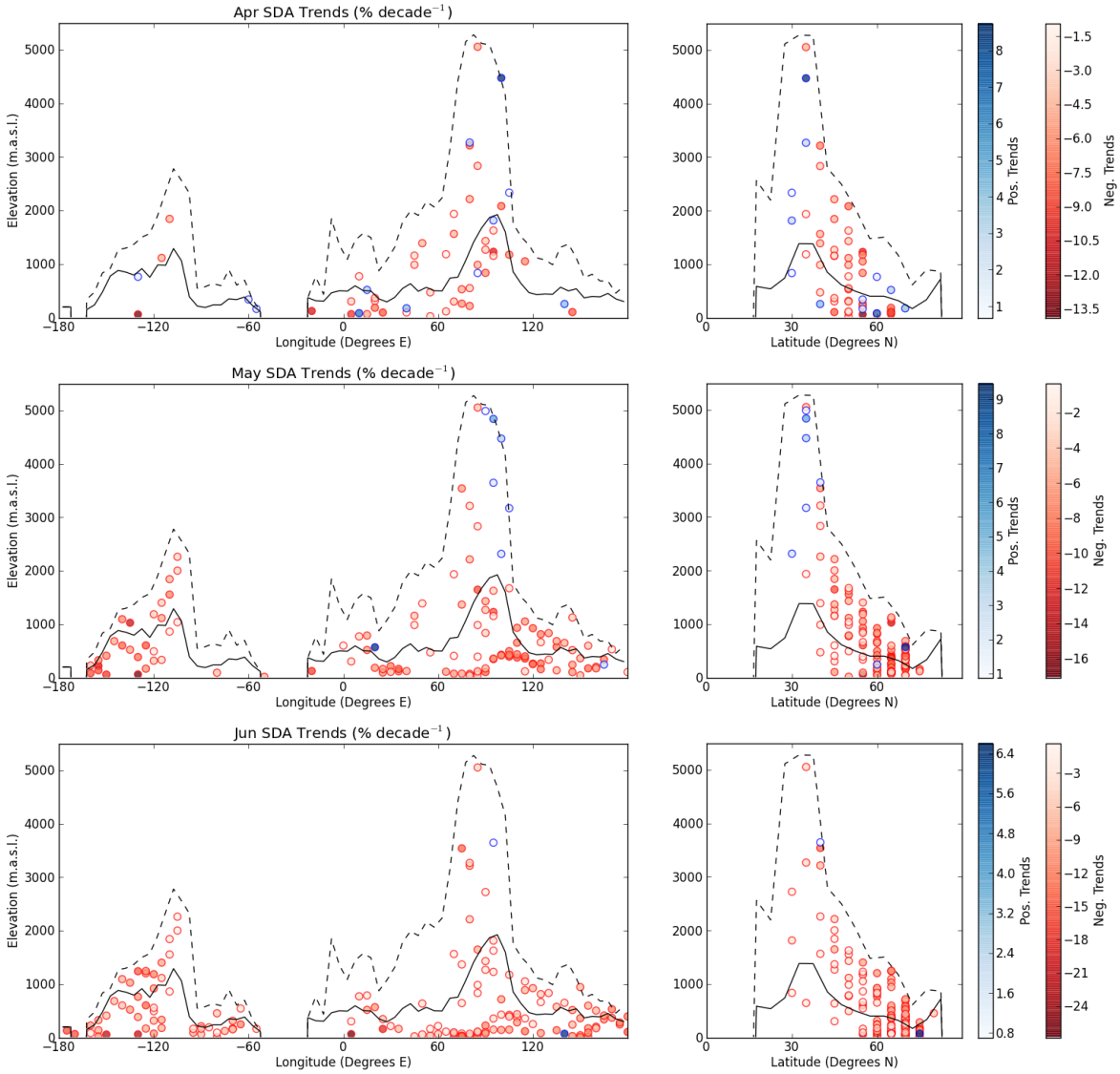

Figure A1.9c: Variations of NH SDA trends (1971 – 2014) with elevation, latitude and longitude from April to June. Solid lines represent meridional / zonal mean elevation of NRSD DGPs, dashed lines represent meridional / zonal maximum elevation of NRSD DGPs.

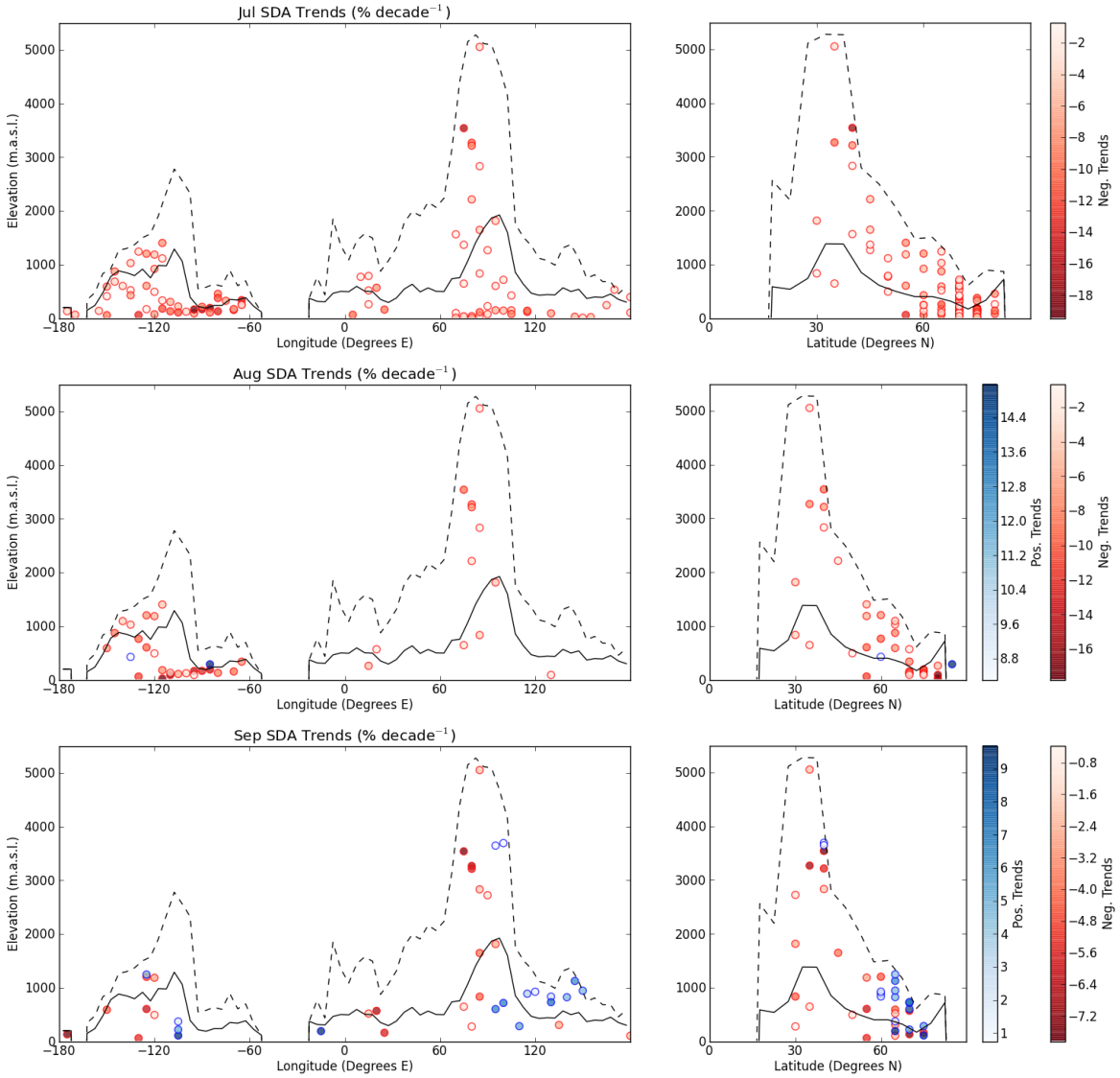

Figure A1.9d: Variations of NH SDA trends (1971 – 2014) with elevation, latitude and longitude from July to September. Solid lines represent meridional / zonal mean elevation of NRSD DGPs, dashed lines represent meridional / zonal maximum elevation of NRSD DGPs.

A1.5: Implications of alternative assumptions of fractional snow-cover associated with 'snow-covered' and 'snow-free' states

The NOAA-Rutgers Snow Archive (NRSA) classifies a dataset grid-point (DGP) as 'snow-covered' when at least 50% of the associated terrestrial footprint is interpreted as being covered by snow. The conventional assumption adopted for studies of snow-cover trends is that 'snow-covered' ('snow-free') cells have fractional snow-cover of 100% (0%). However, they may have actual fractional snow-cover of anywhere between 50% and 100% (0% and 49%). It is therefore informative to consider how applying various different values of fractional snow-cover to spatial units classified as 'snow-covered' and 'snow-free' affects estimates of trend magnitudes.

To explore this, all (non-masked) NRSD DGPs were classified as Alpine (DGP nominal elevation > 1500 m), Arctic (DGP latitude > 60°N), or Mid-Latitude (all others). Time-series of monthly snow-covered area in each of these spatial units, and for the Northern Hemisphere (NH) as a whole, were then generated for the 1971 – 2014 period of record using a range of different fixed percentage snow-cover values for 'snow-covered' and 'snow-free' states (Table A1.1).

For example, in the scenario represented by the bottom row of Table A1.1, if a given DGP is classified as 'snow-covered', then it will be assumed to have actual snow-cover of 55% of its associated terrestrial footprint, and 45% when 'snow-free'. This might approximate inter-annual variation in conditions during the snow-onset / -offset seasons.

Table A1.1: Scenario values of fractional snow-cover
used to generate alternative time-series of snow-covered area

% snow-cover assumed when 'snow-covered'	% snow-cover assumed when 'snow-free'	contrast (%)
100	0	100
90	15	75
100	45	55
55	0	55
60	35	25
55	45	10

Significant trends in snow-covered area were sought in these monthly time-series using Mann-Kendall Trend Analysis. The resultant trend magnitudes (computed by least-squares regression) are seen to be linearly proportional to the contrast in the assumed fractional snow-cover between the two classification states (Figure A1.10). The slope of this relationship varies with month and spatial unit – i.e., trend magnitudes are more or less sensitive to the assumed contrast in fractional snow-cover in the two states at different times of year and in different settings.

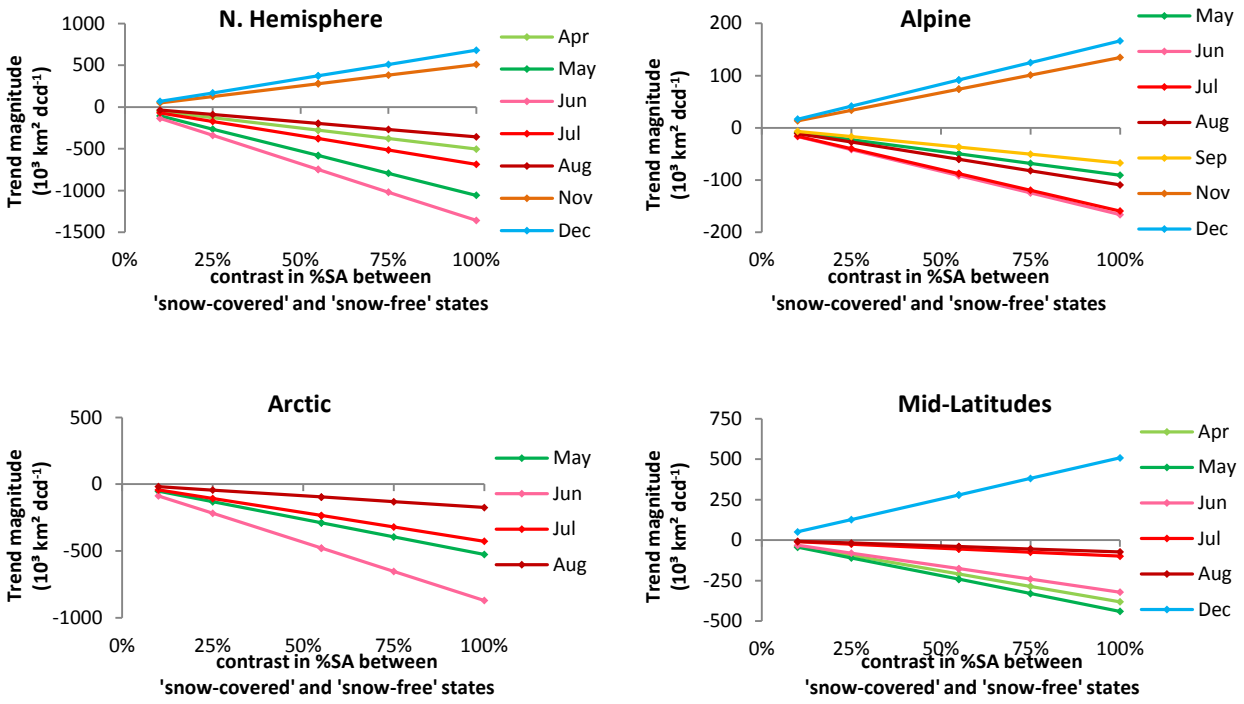

Figure A1.10: Monthly relationships between snow-covered area trend magnitudes and the contrast assumed in fractional snow-cover of 'snow-covered' and 'snow-free' DGPs

Alternative plots illustrate how the different assumed fractional snow-cover scenarios influence trend magnitudes in each spatial unit through the year (Figure A1.11).

Plotting the slopes of the linear relationships shown in Figure A1.10, for each month in which significant trends are identified and each spatial unit, illustrates the intra-annual variation in the sensitivity of trend magnitudes to the assumed contrast in fractional snow-cover in the two binary snow classification states (Figure A1.12, included in the main text as Figure 2.12a).

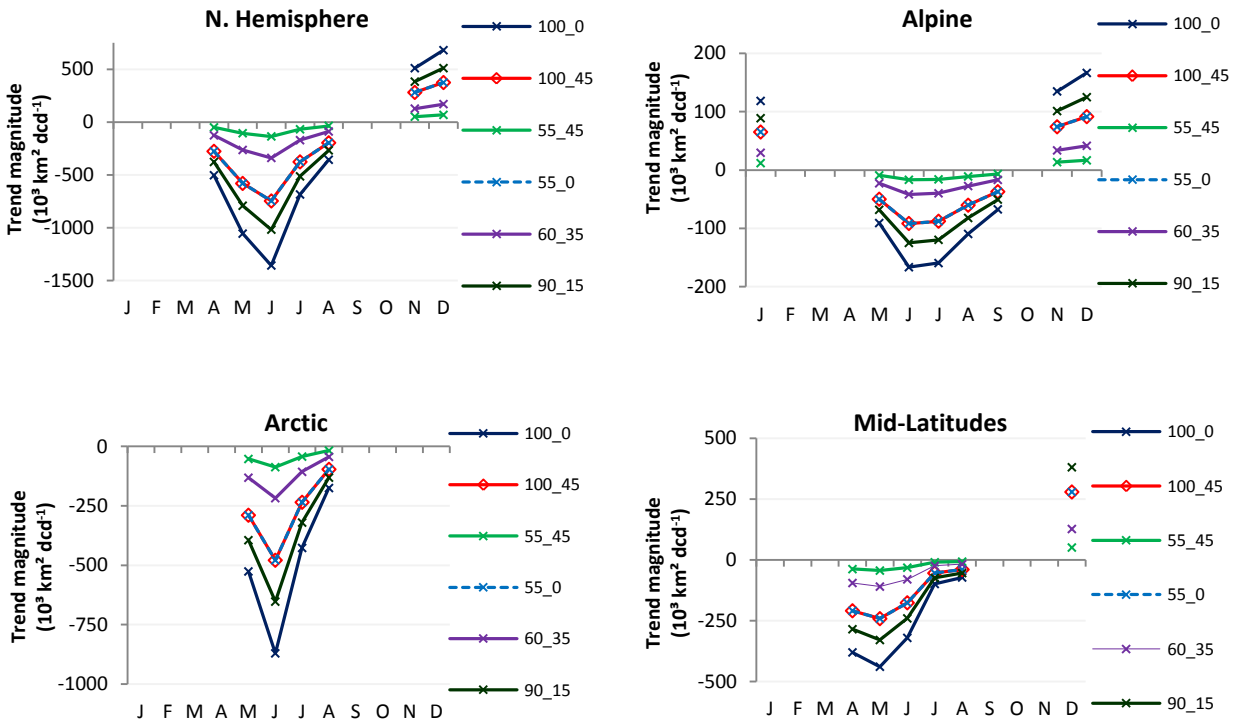

Figure A1.11: Intra-annual variation in total snow-covered area trend magnitudes, depending on the contrast assumed in fractional snow-cover of 'snow-covered' and 'snow-free' DGPs (In the legends, 'x_y' denotes snow-cover of x% is assumed for 'snow-covered' cells, and y% for 'snow-free' cells)

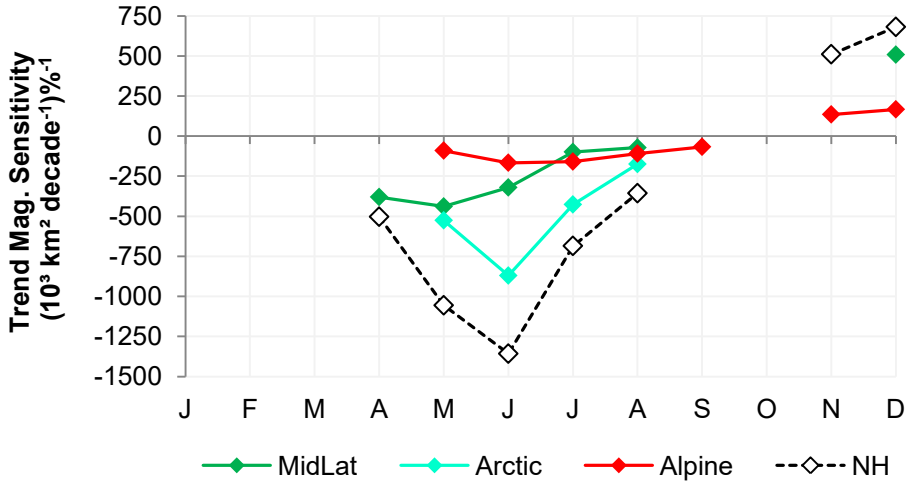

Figure A1.12: Intra-annual variation in sensitivity of snow-covered area trends to the contrast assumed in fractional snow-cover of 'snow-covered' and 'snow-free' DGPs

Appendix 2

This appendix contains information associated with Chapter 3, published as a supplement to –

Allchin, M.I., and Déry, S.J. (2019). Shifting spatial and temporal patterns in the onset of seasonally snow-dominated conditions in the Northern Hemisphere, 1972-2017 *Journal of Climate,* **32**: 4981–5001 DOI: 10.1175/JCLI-D-18-0686.1

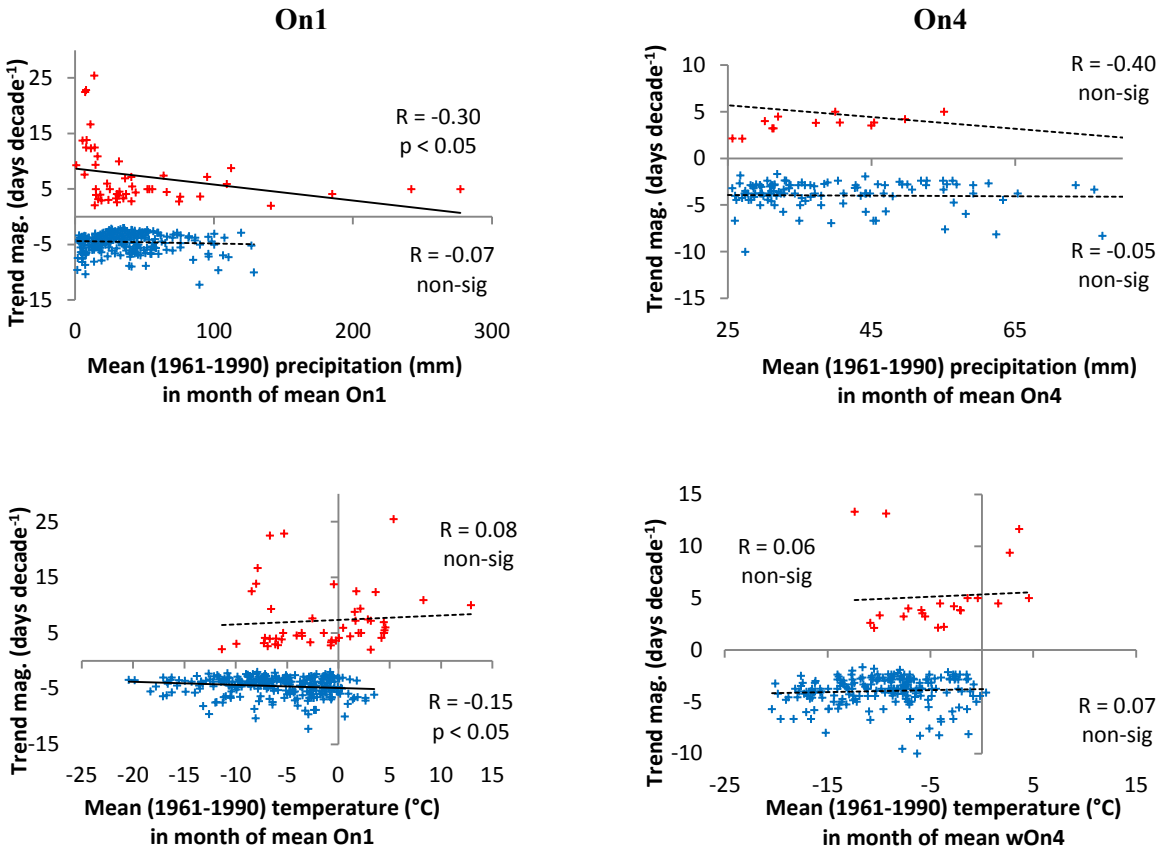

Figure A2.1: Relationships between trend magnitudes and 1961–1990 mean precipitation, temperature in month of mean onset-date.

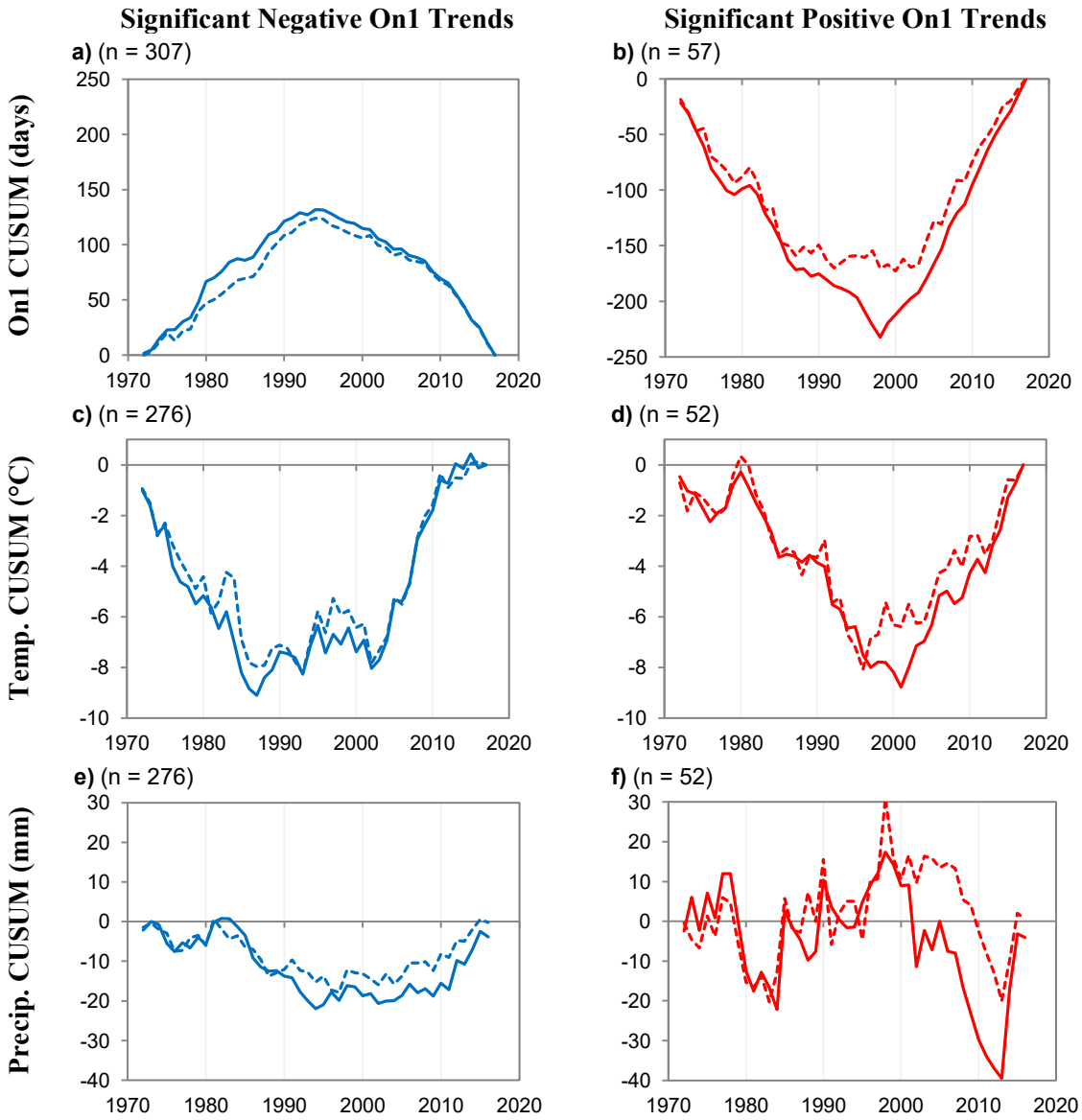

Figure A2.2: Detailed plots of variation of annual means (solid) and medians (dotted) of CUSUM series of (a, b) On1 snow onset dates, (c, d) monthly mean temperature and (e, f) monthly mean precipitation in mean onset-months, for DGPs with significant On1 trends.

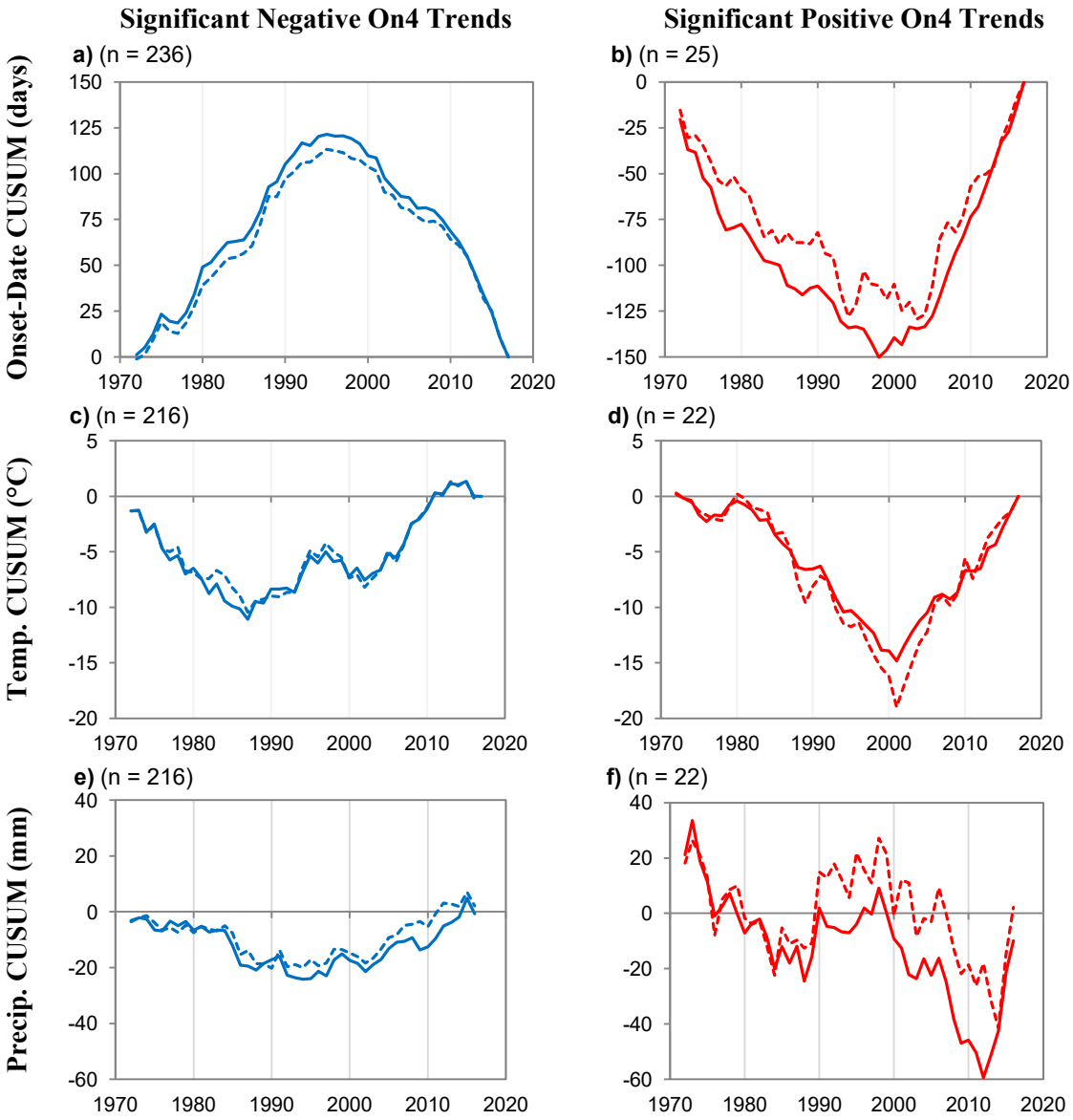

Figure A2.3: Detailed plots of variation of annual means (solid) and medians (dotted) of CUSUM series of (a, b) On4 snow onset dates, (c, d) monthly mean temperature and (e, f) monthly mean precipitation in mean onset-months, for DGPs with significant On4 trends.

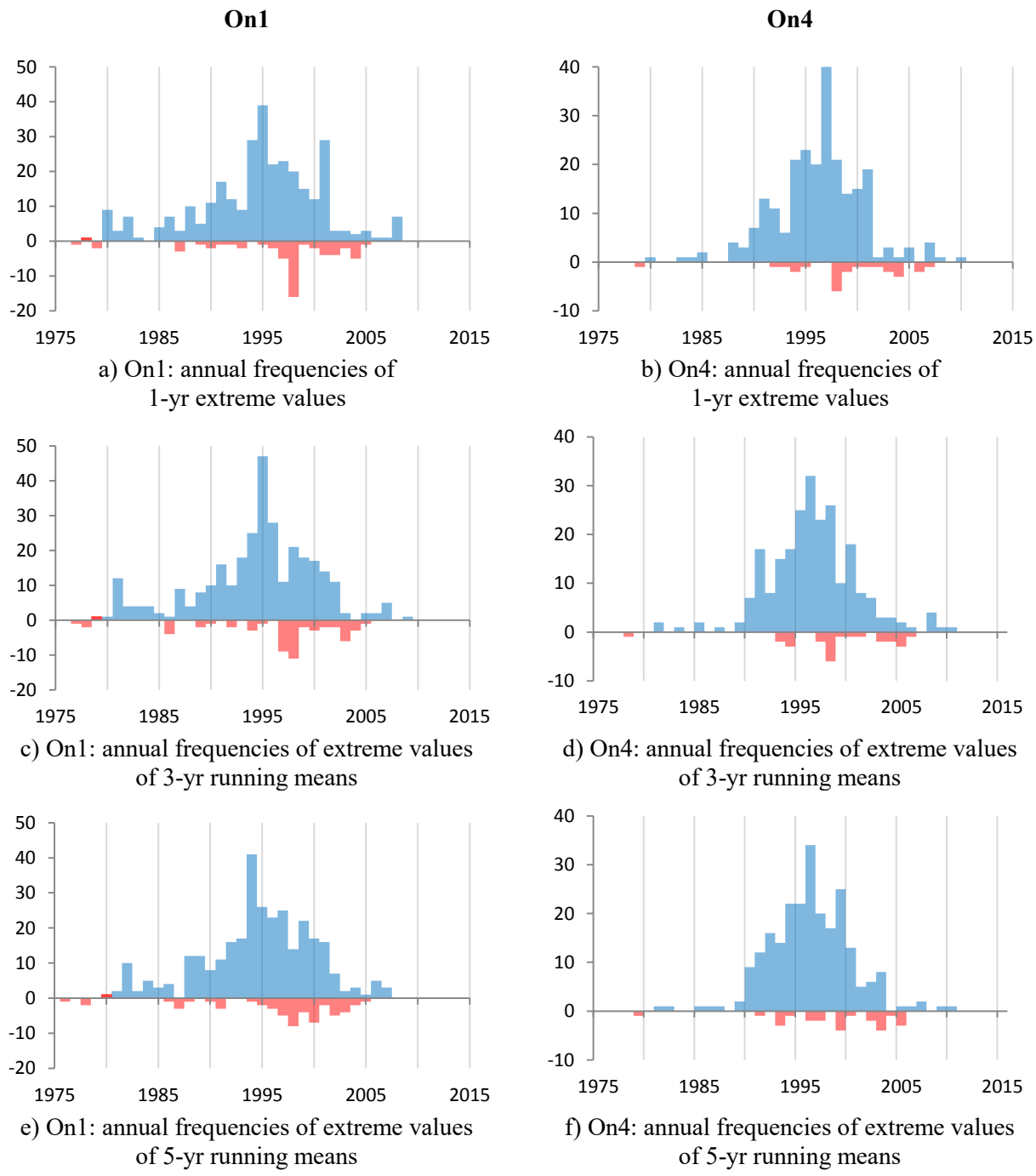

Figure A2.4: Annual frequencies of extreme values in On1 / On4 onset-date CUSUM series among DGPs with significant negative (blue) and positive (red) On1 / On4 trends, based on 1-year extreme values, extreme values of 3-year running means, and extreme values of 5-year running means.. Positive frequency values represent counts of DGPs of each trend-sign for which extreme values are maxima, negative values represent the frequencies of extreme minima (i.e., the extreme values associated with negative trends are all maxima, and (all but one of) those associated with positive trends are minima).

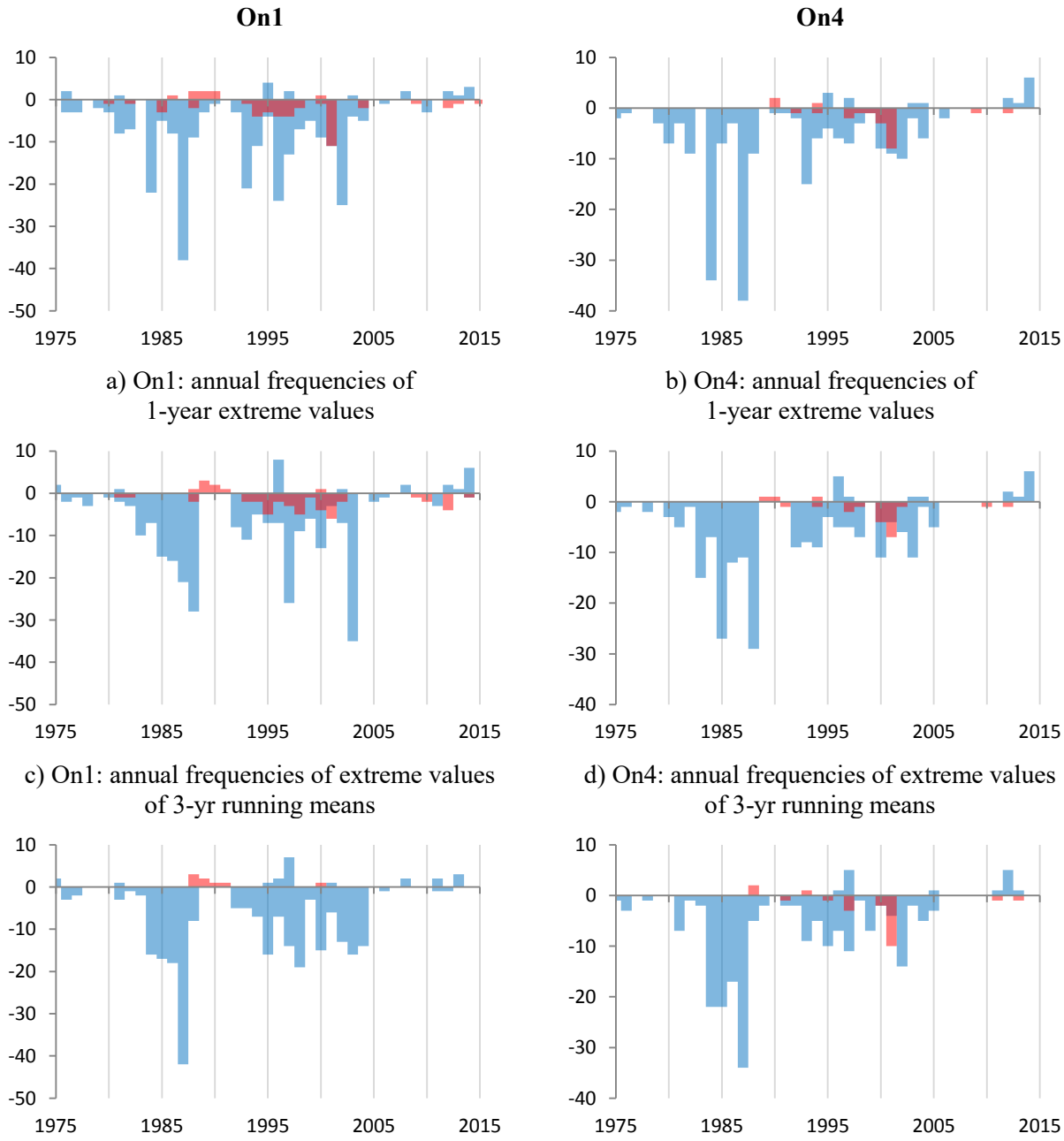

a) On1: annual frequencies of 1-year extreme values

b) On4: annual frequencies of 1-year extreme values

c) On1: annual frequencies of extreme values of 3-yr running means

d) On4: annual frequencies of extreme values of 3-yr running means

e) On1: annual frequencies of extreme values of 5-yr running means

f) On4: annual frequencies of extreme values of 5-yr running means

Figure A2.5: Annual frequencies of extreme values in mean onset-month temperature CUSUM series among DGPs with significant negative (blue) and positive (red) On1 / On4 trends, based on 1-year extreme values, extreme values of 3-year running means, and extreme values of 5-year running means. Positive frequency values represent counts of DGPs of each trend-sign for which extreme values are maxima, negative values represent the frequencies of extreme minima (i.e., the extreme values asociated with most trends of both signs are minima).

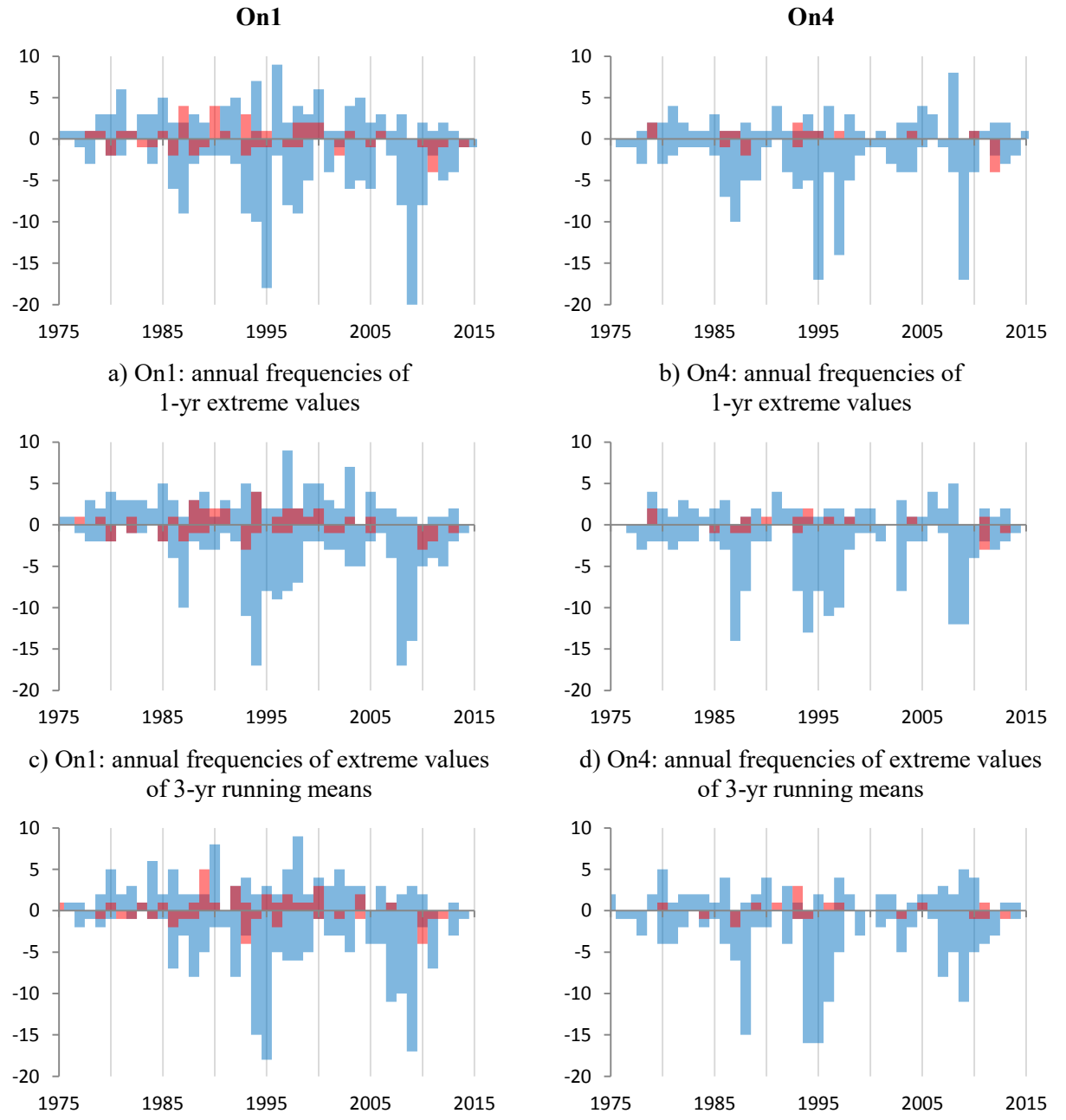

a) On1: annual frequencies of 1-yr extreme values

b) On4: annual frequencies of 1-yr extreme values

c) On1: annual frequencies of extreme values of 3-yr running means

d) On4: annual frequencies of extreme values of 3-yr running means

e) On1: annual frequencies of extreme values of 5-yr running means

f) On4: annual frequencies of extreme values of 5-yr running means

Figure A2.6: Annual frequencies of extreme values in mean onset-month precipitation CUSUM series among DGPs with significant negative (blue) and positive (red) On1 / On4 trends, based on 1-year extreme values, extreme values of 3-year running means, and extreme values of 5-year running means. Positive frequency values represent counts of DGPs of each trend-sign for which extreme values are maxima, negative values represent the frequencies of extreme minima (i.e., the extreme values asociated with most negative trends are minima).

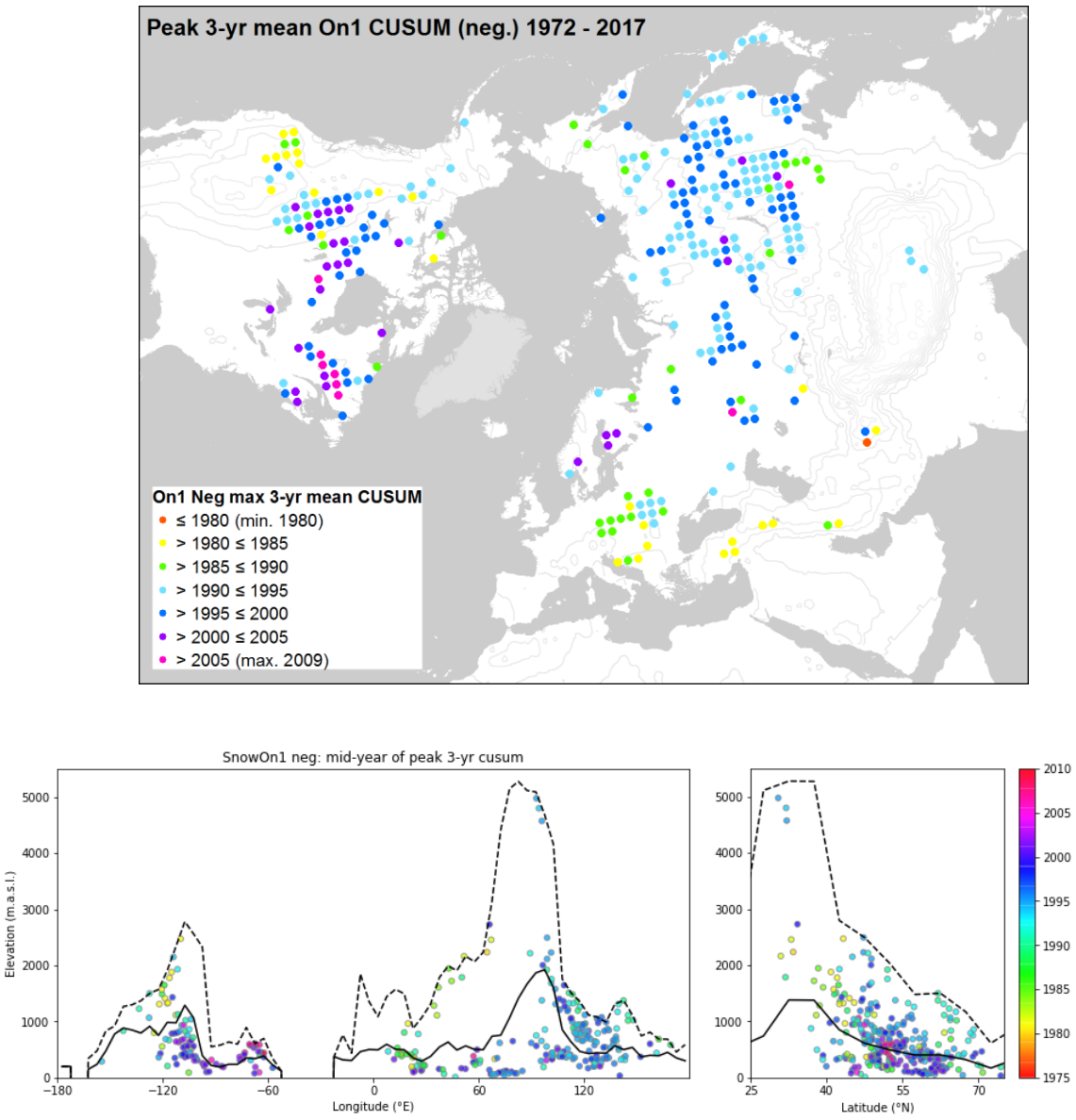

Figure A2.7: Spatial distribution of years of extreme values (maxima) of 3-year running means of CUSUM series computed from annual On1 dates for DGPs with significant negative On1 trends.

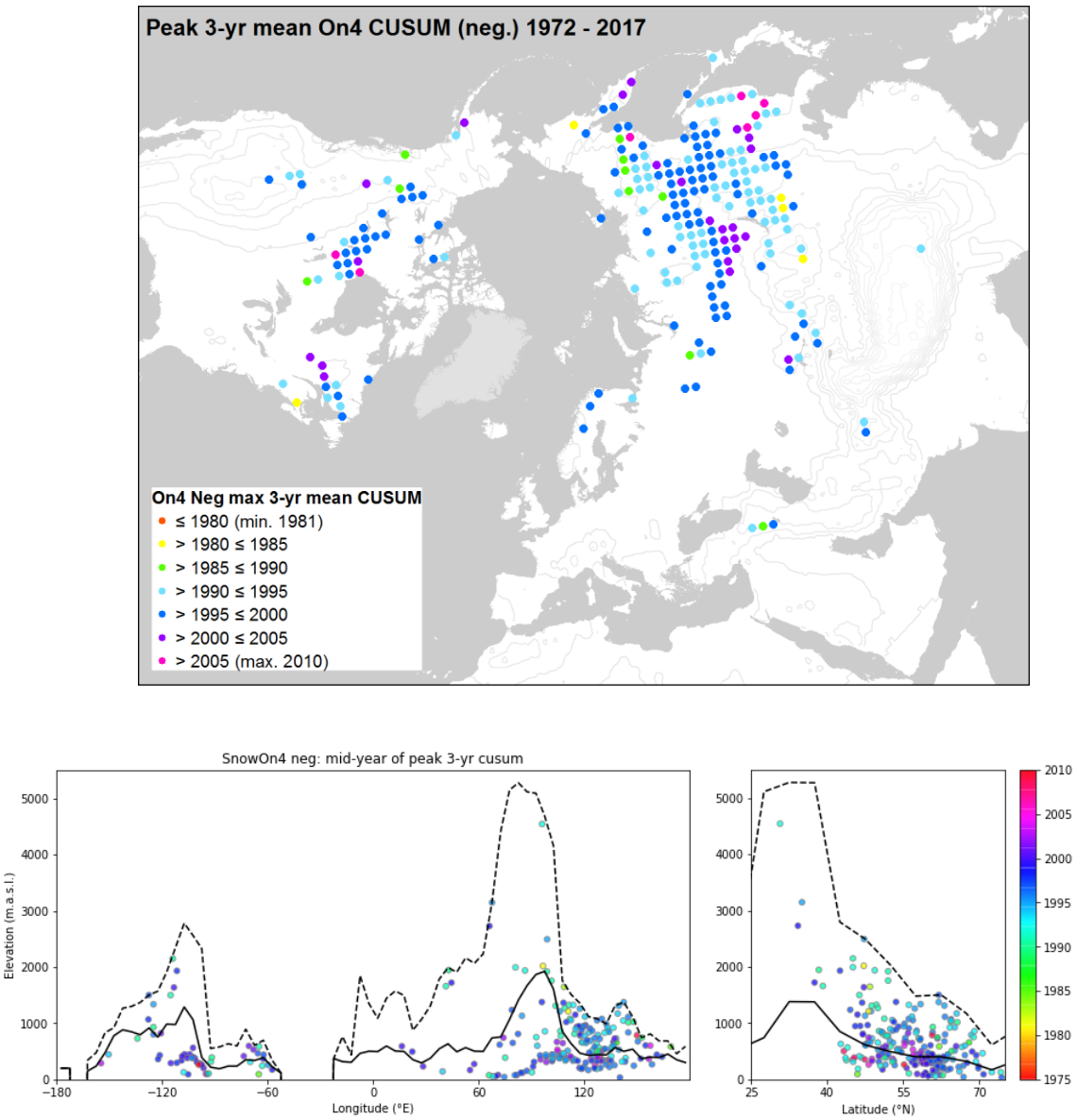

Figure A2.8: Spatial distribution of years of extreme values (maxima) of 3-year running means of CUSUM series computed from annual On4 dates for DGPs with significant negative On4 trends.

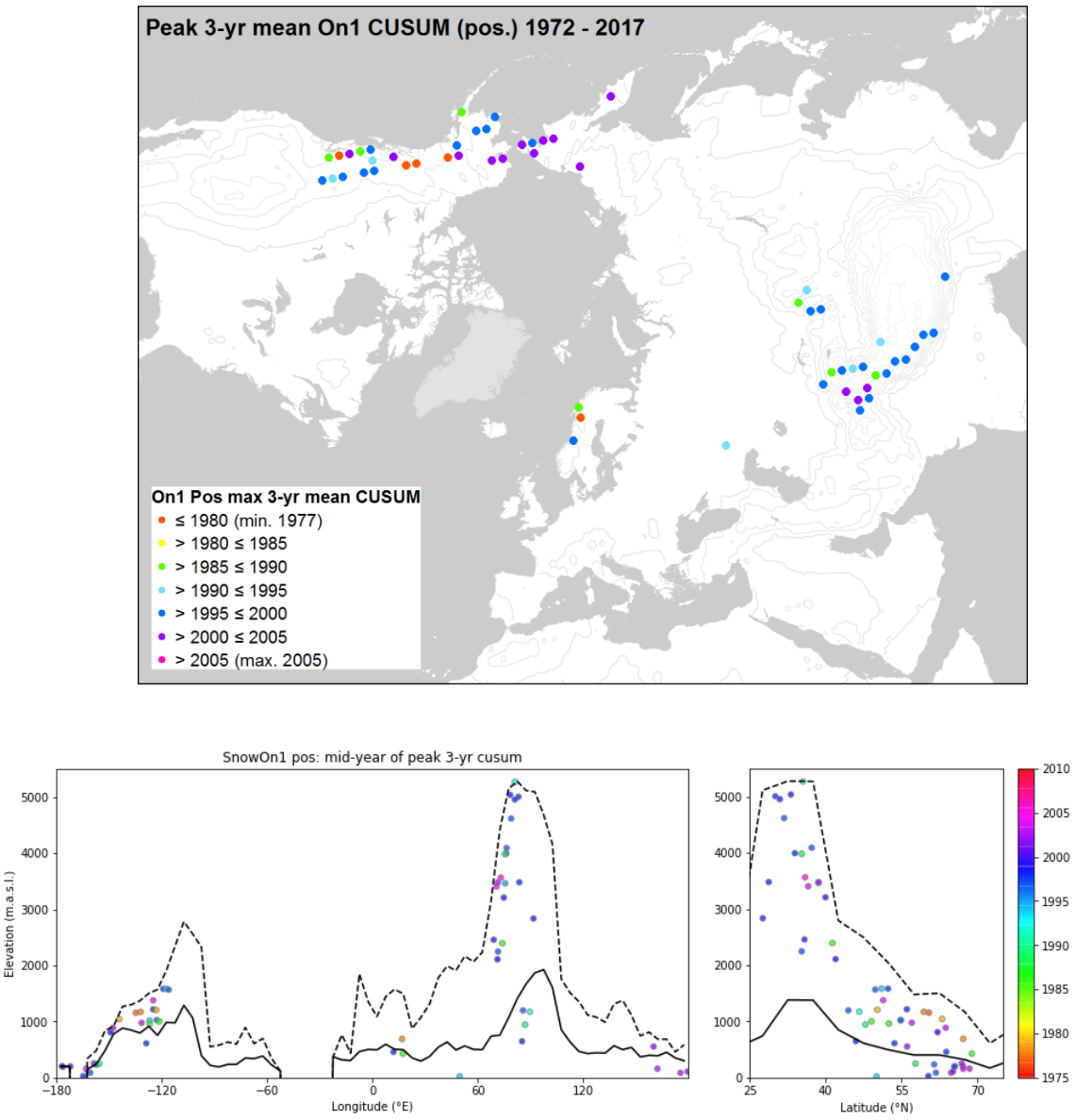

Figure A2.9: Spatial distribution of years of extreme values (minima) of 3-year running means of CUSUM series computed from annual On1 dates for DGPs with significant positive On1 trends.

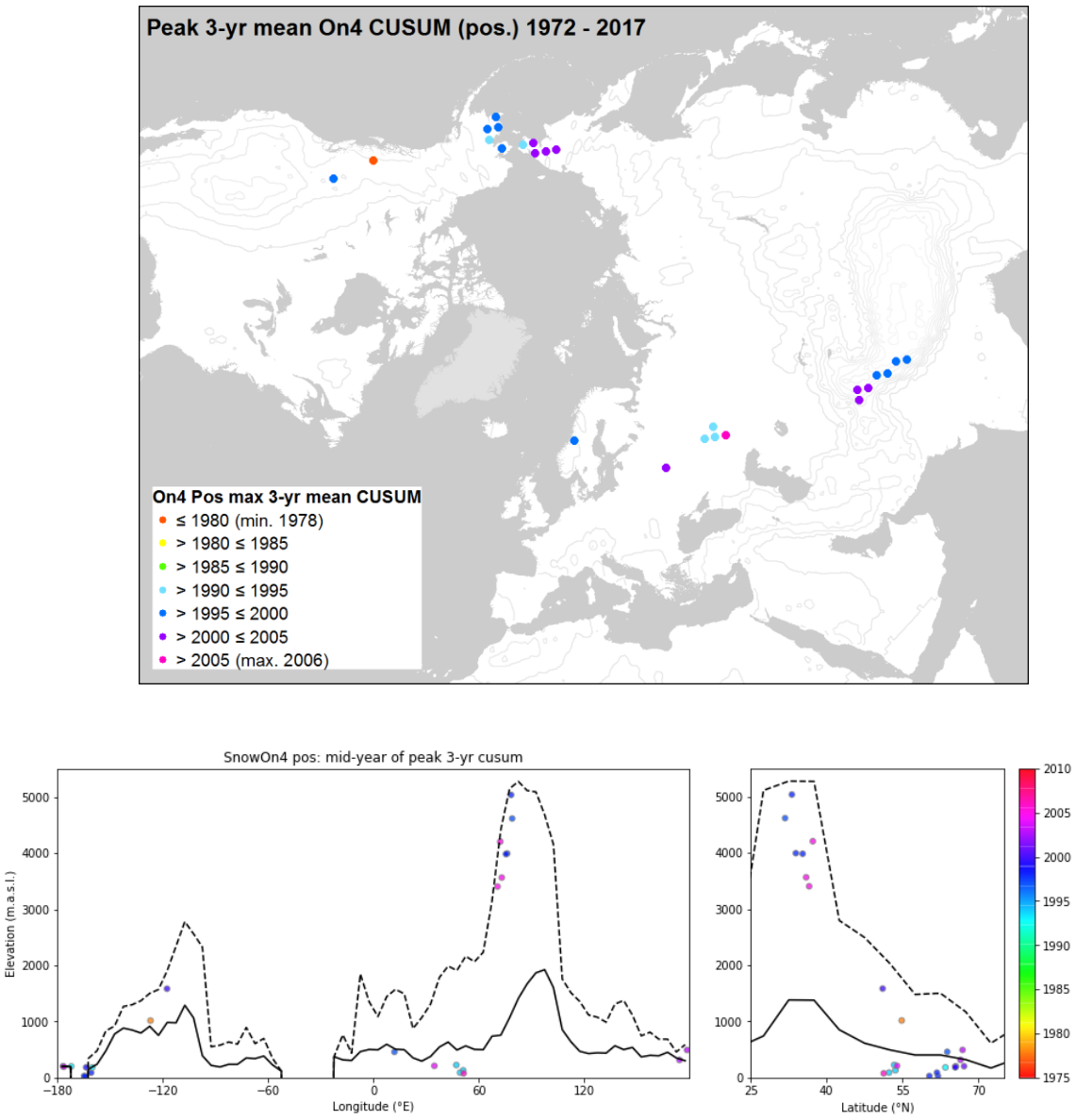

Figure A2.10: Spatial distribution of years of extreme values (minima) of 3-year running means of CUSUM series computed from annual On4 dates for DGPs with significant positive On4 trends.

Table A2.1a: Regression in 30° longitudinal bands of trend magnitudes against latitude, elevation, mean onset date - Western Hemisphere. Pale grey text denotes non-significant trends: empty boxes shown for bands with too few significant trends for regression to be possible.

longitude		180W to 150W	150W to 120W	120W to 90W	90W to 60W	60W to 30W	30W to 0
On1 negative	**n**	1	11	58	24	1	0
Mag. vs lat.	R		0.63	**0.66**	**0.58**		
slope ((days decade^{-1}) (° Lat.)$^{-1}$)			0.07	**0.12**	**0.07**		
sig			p<0.05	p<0.001	p<0.01		
Mag. vs elev.	R		-0.54	**-0.68**	0.12		
slope ((days decade^{-1}) (1000m)$^{-1}$)			-1.45	**-1.62**	0.36		
sig			-	p<0.001	-		
Mag. vs mean On1	R		-0.55	**-0.56**	**-0.55**		
slope ((days decade^{-1}) week^{-1})			-0.16	**-0.32**	**-0.11**		
sig			-	p<0.001	p<0.01		
Elev. vs lat.	R		-0.64	**-0.80**	0.46		
slope (m (° Lat.)$^{-1}$)			-27.72	**-62.93**	16.76		
sig			p<0.05	p<0.001	p<0.05		
On4 negative	**n**	2	9	27	10	2	0
Mag. vs lat.	R		0.55	**0.58**	0.39		
slope ((days decade^{-1}) (° Lat.)$^{-1}$)			0.16	**0.08**	0.08		
sig			-	p<0.01	-		
Mag. vs elev.	R		-0.26	**-0.66**	0.74		
slope ((days decade^{-1}) (1000m)$^{-1}$)			-0.79	**-1.08**	3.13		
sig			-	p<0.001	p<0.05		
Mag. vs mean On4	R		-0.50	**-0.53**	-0.59		
slope ((days decade^{-1}) week^{-1})			-0.26	**-0.20**	-0.15		
sig			-	p<0.01	-		
Elev. vs lat.	R		-0.31	**-0.75**	0.50		
slope (m (° Lat.)$^{-1}$)			-28.94	**-60.78**	23.20		
sig			-	p<0.001	-		
On1 positive	**n**	9	14	3	0	0	0
Mag. vs lat.	R	-0.03	-0.31	-0.14			
slope ((days decade^{-1}) (° Lat.)$^{-1}$)		-0.01	-0.15	-0.09			
sig		-	-	-			
Mag. vs elev.	R	0.58	-0.52	0.46			
slope ((days decade^{-1}) (1000m)$^{-1}$)		5.11	-6.46	40.70			
sig		-	-	-			
Mag. vs mean On1	R	-0.46	0.42	-0.58			
slope ((days decade^{-1}) week^{-1})		-0.16	0.60	-0.76			
sig		-	-	-			
Elev. vs lat.	R	0.21	-0.21	0.82			
slope (m (° Lat.)$^{-1}$)		4.60	-8.45	6.23			
sig		-	-	-			
On4 positive	**n**	8	1	1	0	0	0
Mag. vs lat.	R	0.07					
slope ((days decade^{-1}) (° Lat.)$^{-1}$)		0.02					
sig		-					
Mag. vs elev.	R	-0.08					
slope ((days decade^{-1}) (1000m)$^{-1}$)		-0.89					
sig		-					
Mag. vs mean On4	R	-0.35					
slope ((days decade^{-1}) week^{-1})		-0.14					
sig		-					
Elev. vs lat.	R	**0.90**					
slope (m (° Lat.)$^{-1}$)		**29.66**					
sig		p<0.01					

Table A2.1b: Regression in 30° longitudinal bands of trend magnitudes against latitude, elevation, mean onset date - Eastern Hemisphere. Pale grey text denotes non-significant trends: empty boxes shown for bands with too few significant trends for regression to be possible.

longitude		0 to 30E	30E to 60E	60E to 90E	90E to 120E	120E to 150E	150E to 180E
On1 negative	**n**	27	18	26	75	61	5
Mag. vs lat.	R	0.41	**0.64**	**0.85**	**0.67**	**0.60**	0.35
slope ((days decade^{-1}) (° Lat.)$^{-1}$)		0.11	**0.08**	**0.10**	**0.15**	**0.11**	0.16
	Sig	p<0.05	p<0.01	p<0.001	p<0.001	p<0.001	-
Mag. vs elev.	R	-0.47	-0.53	**-0.65**	**-0.69**	-0.12	0.90
slope ((days decade^{-1}) (1000m)$^{-1}$)		-3.88	-0.92	**-0.84**	**-1.43**	-0.63	11.64
	Sig	p<0.05	p<0.05	p<0.001	p<0.001	-	p<0.05
Mag. vs mean On1	R	-0.44	**-0.71**	**-0.82**	**-0.44**	**-0.65**	-0.73
slope ((days decade^{-1}) week^{-1})		-0.43	**-0.27**	**-0.31**	**-0.37**	**-0.30**	-0.69
	Sig	p<0.05	p<0.001	p<0.001	p<0.001	p<0.001	-
Elev. vs lat.	R	**-0.56**	**-0.85**	**-0.84**	**-0.74**	0.18	0.40
slope (m (° Lat.)$^{-1}$)		**-18.47**	**-56.91**	**-77.45**	**-77.13**	6.78	14.38
	Sig	p<0.01	p<0.001	p<0.001	p<0.001	-	-
On4 negative	**n**	3	6	21	71	75	10
Mag. vs lat.	R	0.95	0.89	**0.66**	**0.73**	**0.52**	0.50
slope ((days decade^{-1}) (° Lat.)$^{-1}$)		0.46	0.14	**0.14**	**0.12**	**0.10**	0.17
	Sig	-	p<0.05	p<0.01	p<0.001	p<0.001	-
Mag. vs elev.	R	-0.98	-0.90	**-0.61**	**-0.73**	-0.03	0.41
slope ((days decade^{-1}) (1000m)$^{-1}$)		-5.89	-2.14	**-1.27**	**-1.32**	-0.14	3.13
	Sig	-	p<0.05	p<0.01	p<0.001	-	-
Mag. vs mean On4	R	0.45	**-0.95**	**-0.66**	**-0.60**	**-0.54**	-0.70
slope ((days decade^{-1}) week^{-1})		1.75	**-0.58**	**-0.47**	**-0.30**	**-0.25**	-0.52
	Sig	-	p<0.01	p<0.01	p<0.001	p<0.001	p<0.05
Elev. vs lat.	R	-0.88	**-0.99**	**-0.87**	**-0.75**	0.17	0.45
slope (m (° Lat.)$^{-1}$)		-71.27	**-64.83**	**-87.02**	**-64.69**	6.94	20.70
	Sig	-	p<0.001	p<0.001	p<0.001	-	-
On1 positive	**n**	3	1	22	1	0	4
Mag. vs lat.	R	-0.53		-0.52			-0.99
slope ((days decade^{-1}) (° Lat.)$^{-1}$)		-0.37		-0.52			-0.12
	sig	-		p<0.05			p<0.05
Mag. vs elev.	R	-0.88		**0.58**			0.90
slope ((days decade^{-1}) (1000m)$^{-1}$)		-11.26		**2.20**			2.70
	sig	-		p<0.01			-
Mag. vs mean On1	R	0.99		0.08			0.84
slope ((days decade^{-1}) week^{-1})		1.52		0.19			0.68
	sig	-		-			-
Elev. vs lat.	R	0.07		**-0.84**			-0.90
slope (m (° Lat.)$^{-1}$)		3.90		**-219.11**			-37.54
	sig	-		p<0.001			-
On4 positive	**n**	1	5	7	0	0	2
Mag. vs lat.	R		-0.09	**-0.94**			
slope ((days decade^{-1}) (° Lat.)$^{-1}$)			-0.02	**-1.86**			
	sig		-	p<0.01			
Mag. vs elev.	R		0.17	0.78			
slope ((days decade^{-1}) (1000m)$^{-1}$)			0.60	5.32			
	sig		-	p<0.05			
Mag. vs mean On4	R		-0.61	0.62			
slope ((days decade^{-1}) week^{-1})			-0.19	0.82			
	sig		-	-			
Elev. vs lat.	R		0.80	-0.69			
slope (m (° Lat.)$^{-1}$)			50.81	-199.35			
	sig		-	-			

Appendix 3

This appendix contains information associated with Chapter 4, submitted as supplementary materials to the *Journal of Geophysical Research – Atmospheres*.

A3.1 Introduction

In this analysis, a synthesis of climatological influences on progressively earlier or later incidence of snow-cover was developed through consideration of the spatial and temporal variations of eight atmospheric metrics describing activity in the mid-to-lower troposphere.

The main body of these supplementary materials comprises maps, longitudinal profiles and latitudinal profiles of monthly means and trends of these metrics during the 1972-2014 period of interest, for each month from September to December. These visualizations include representations of values derived from each point in the 20th Century Reanalysis (v. 2c), and also for each point in the NOAA-Rutgers Climate Data Record at which significant onset trends were identified.

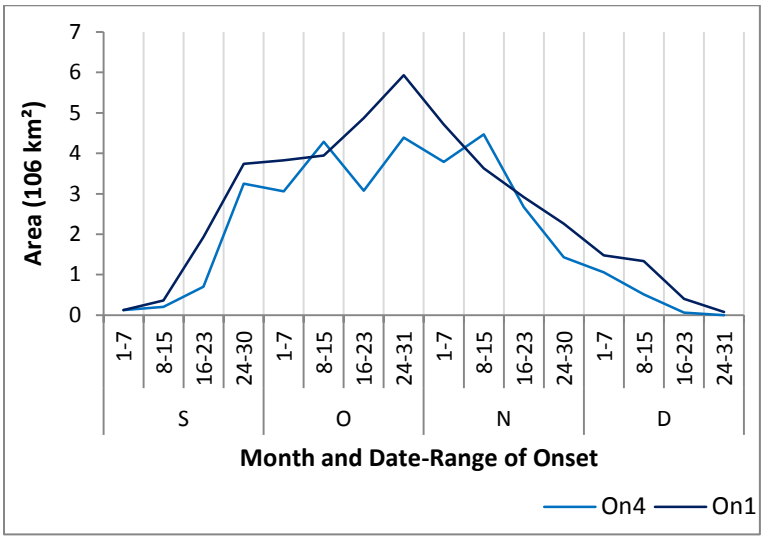

Figure A3.1: Spatial frequency distribution of 1972-2017 mean week of onset. 'On1' represents the first date of at least 50% snow-cover, regardless of subsequent duration, whereas 'On4' is the mean date of onset persisting subsequently for at least four weeks.

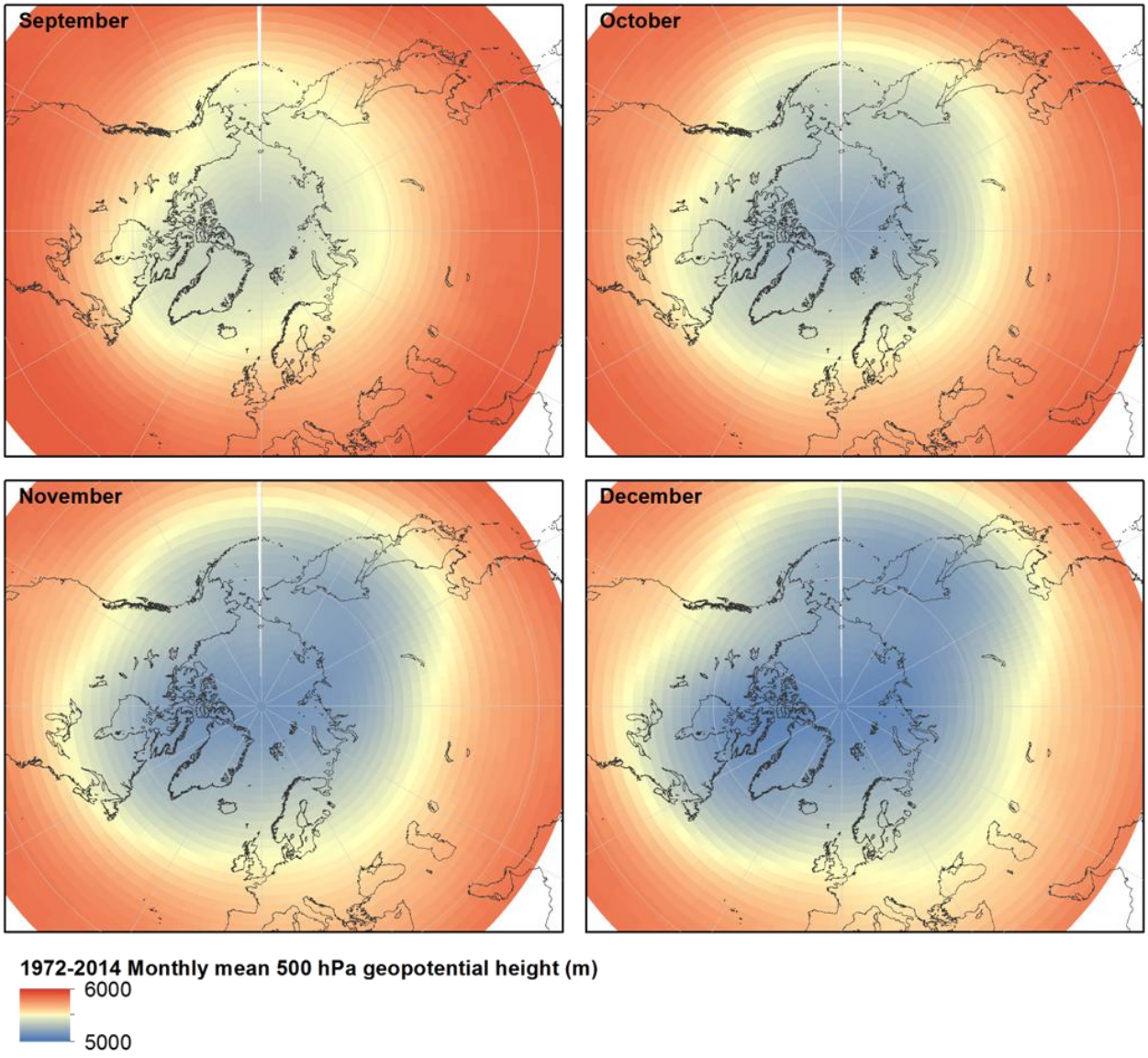

Figure A3.2a: 1972-2014 monthly mean 500 hPa geopotential height.

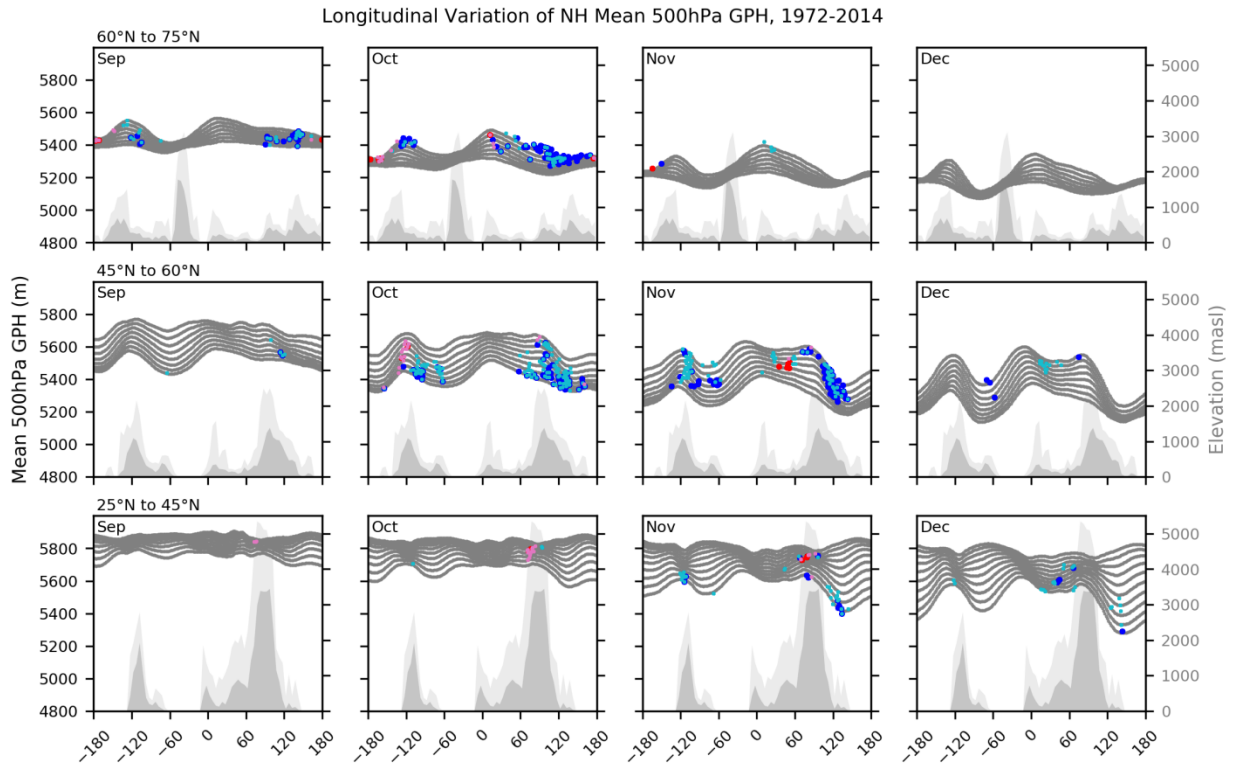

Figure A3.2b: Longitudinal distributions of 1972-2014 monthly mean 500 hPa geopotential height within three latitudinal bands. Grey points represent means at points on the reanalysis grid. Dark (light) blue (red) symbols denote values associated with points for which significant negative (positive) On4 (On1) trends were identified. Darker (lighter) shaded areas represent meridional mean (maximum) elevations at zonal intervals of 5°.

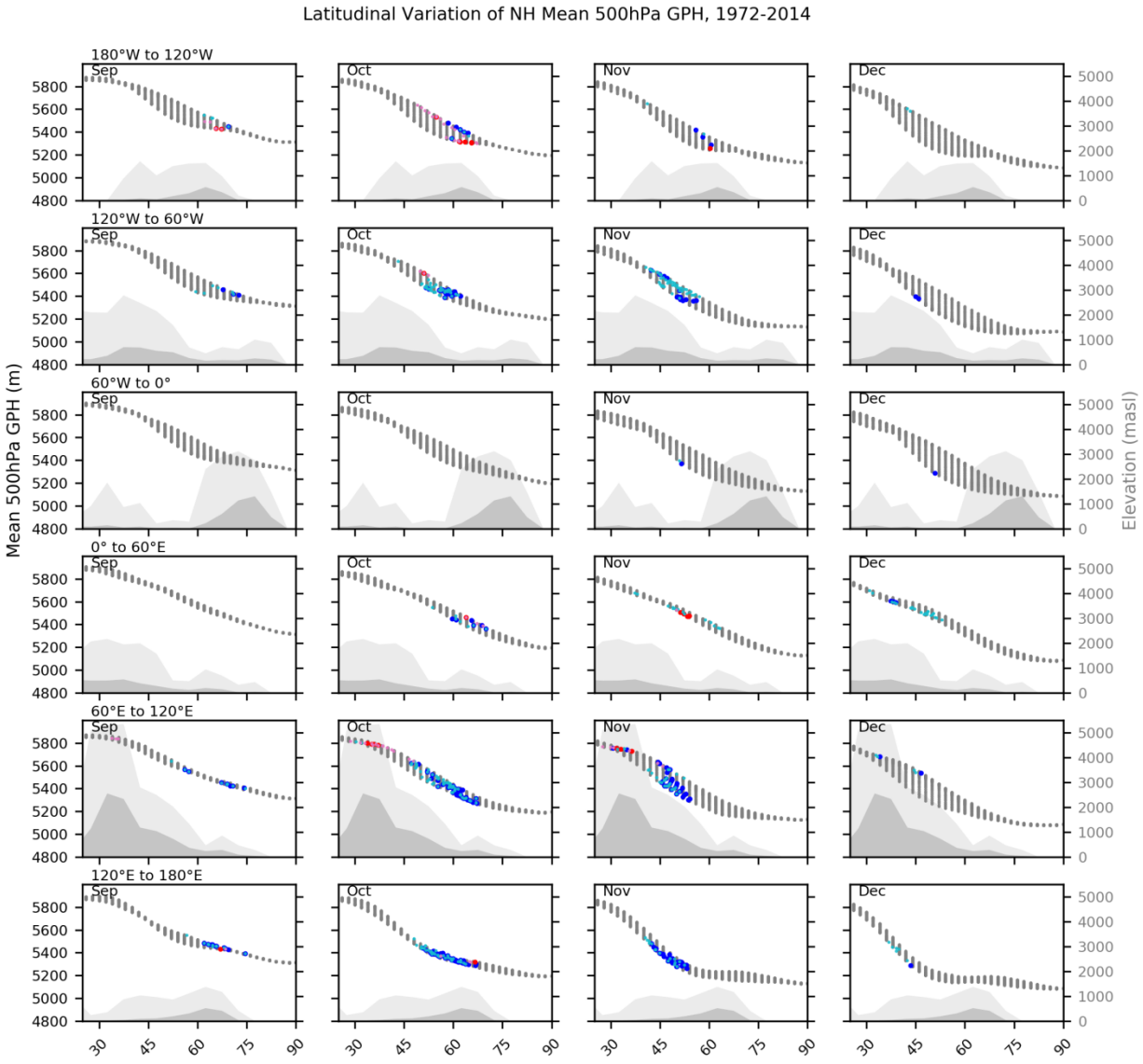

Figure A3.2c: Longitudinal distributions of 1972-2014 monthly mean 500 hPa geopotential height within six longitudinal bands. Grey points represent means at points on the reanalysis grid. Dark (light) blue (red) symbols denote values associated with points for which significant negative (positive) On4 (On1) trends were identified. Darker (lighter) shaded areas represent meridional mean (maximum) elevations at zonal intervals of 5°.

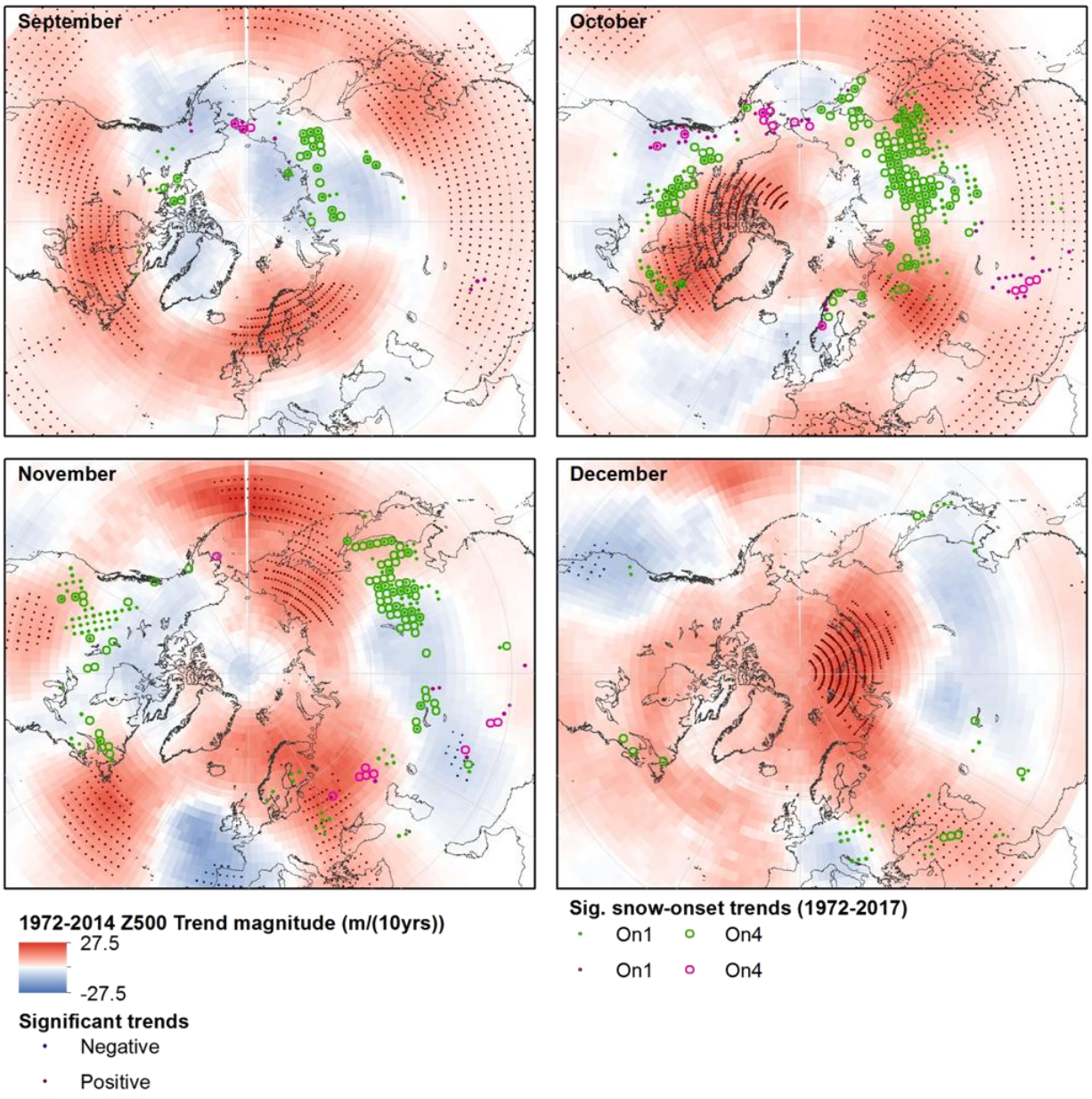

Figure A3.3a: 1972-2014 trends in monthly mean 500 hPa geopotential height.

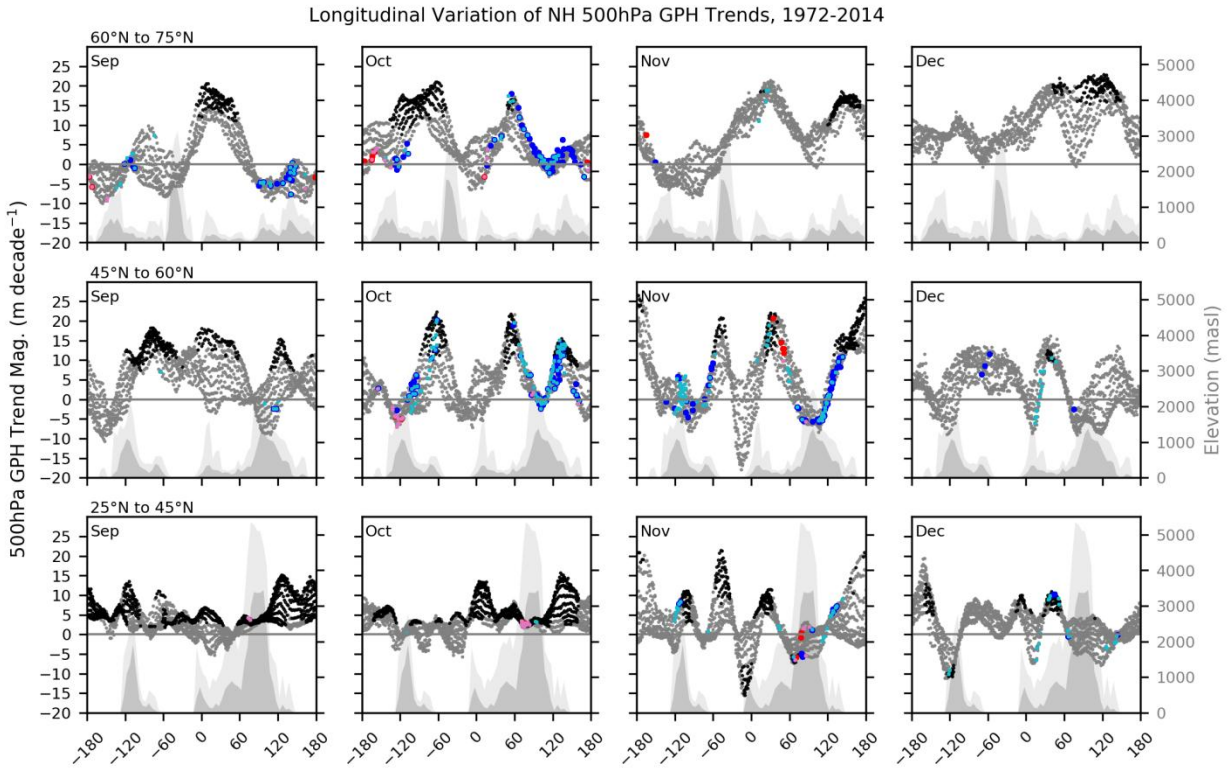

Figure A3.3b: Longitudinal distributions of 1972-2014 trends in monthly 500 hPa geopotential height within three latitudinal bands. Black (grey) points represent significant (non-significant) trend magnitudes at points on the reanalysis grid. Dark (light) blue (red) symbols denote values associated with points for which significant negative (positive) On4 (On1) trends were identified. Darker (lighter) shaded areas represent meridional mean (maximum) elevations at zonal intervals of 5°.

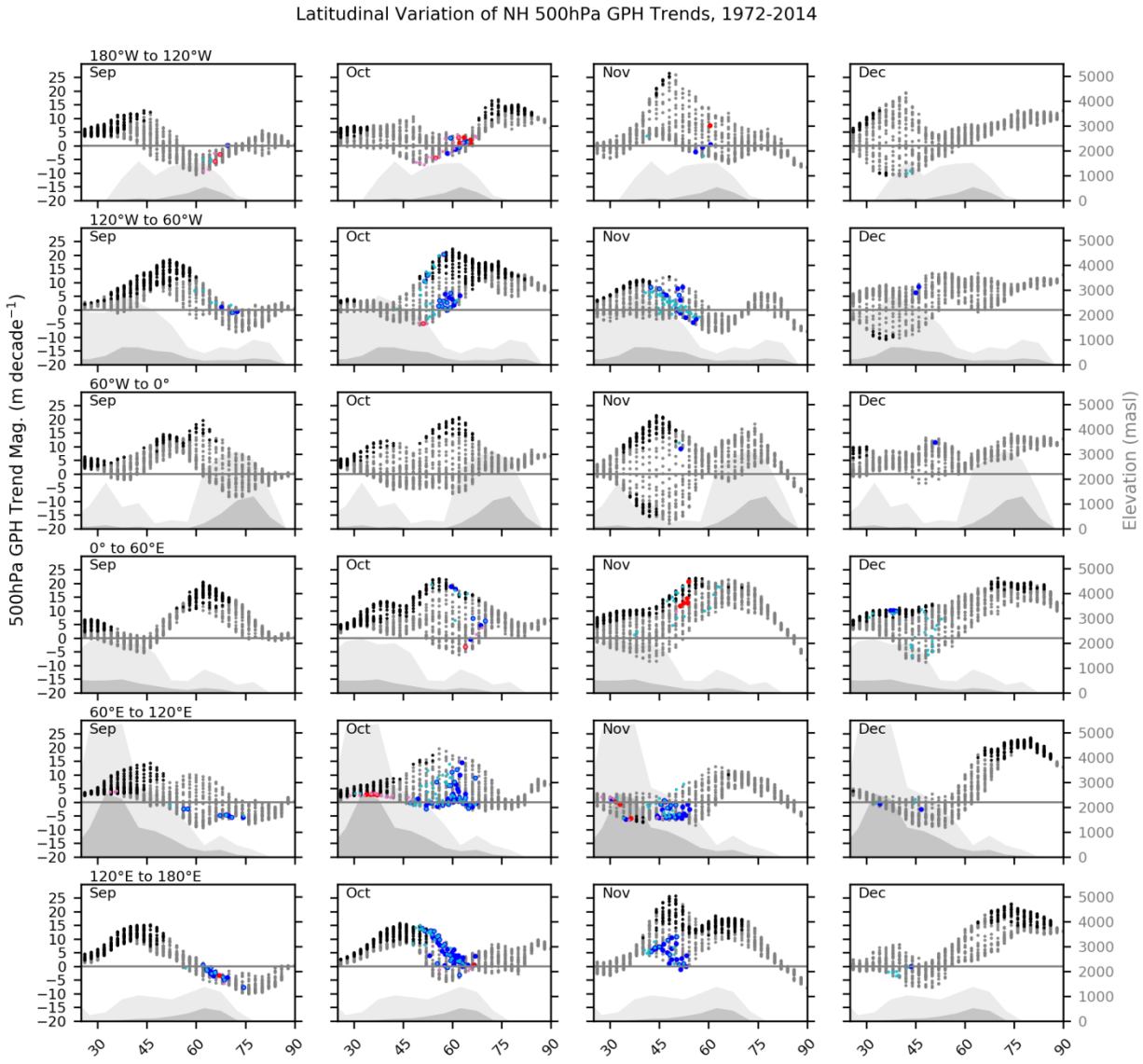

Figure A3.3c: Latitudinal distributions of 1972-2014 trends in monthly 500 hPa geopotential height within six longitudinal bands. Black (grey) points represent significant (non-significant) trend magnitudes at points on the reanalysis grid. Dark (light) blue (red) symbols denote values associated with points for which significant negative (positive) On4 (On1) trends were identified. Darker (lighter) shaded areas represent meridional mean (maximum) elevations at zonal intervals of 5°.

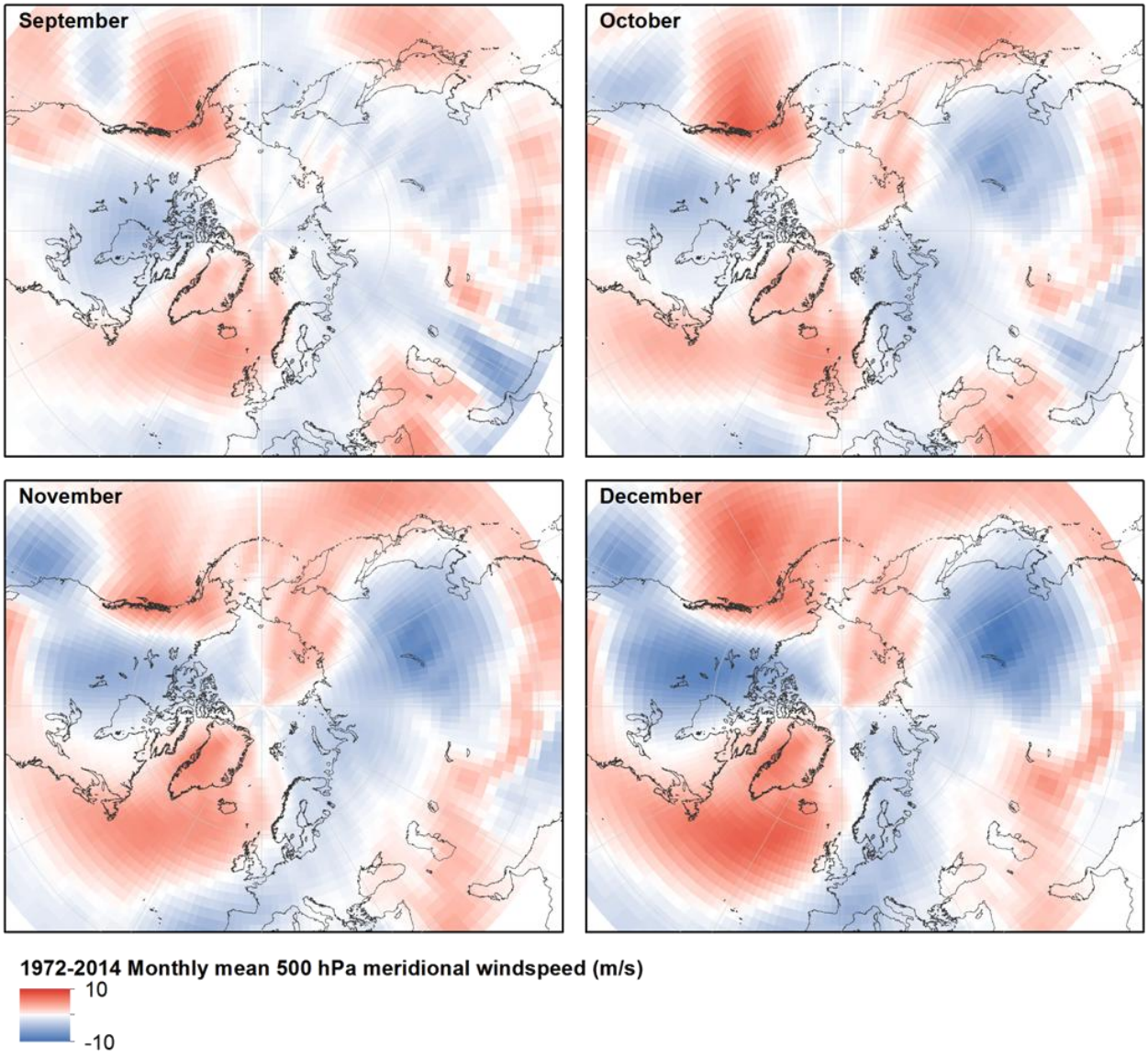

Figure A3.4a: 1972-2014 monthly mean 500 hPa meridional wind-speed.

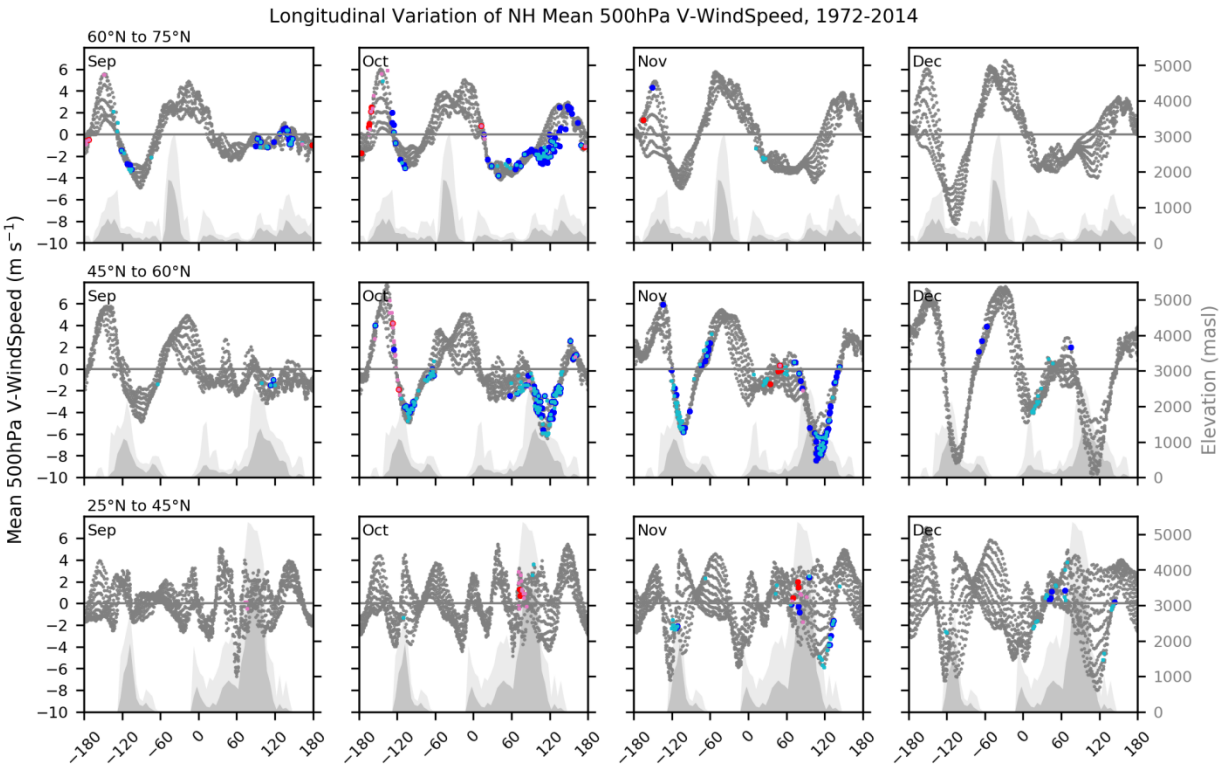

Figure A3.4b: Longitudinal distributions of 1972-2014 monthly mean 500 hPa meridional wind-speed within three latitudinal bands. Grey points represent means at points on the reanalysis grid. Dark (light) blue (red) symbols denote values associated with points for which significant negative (positive) On4 (On1) trends were identified. Darker (lighter) shaded areas represent meridional mean (maximum) elevations at zonal intervals of 5°.

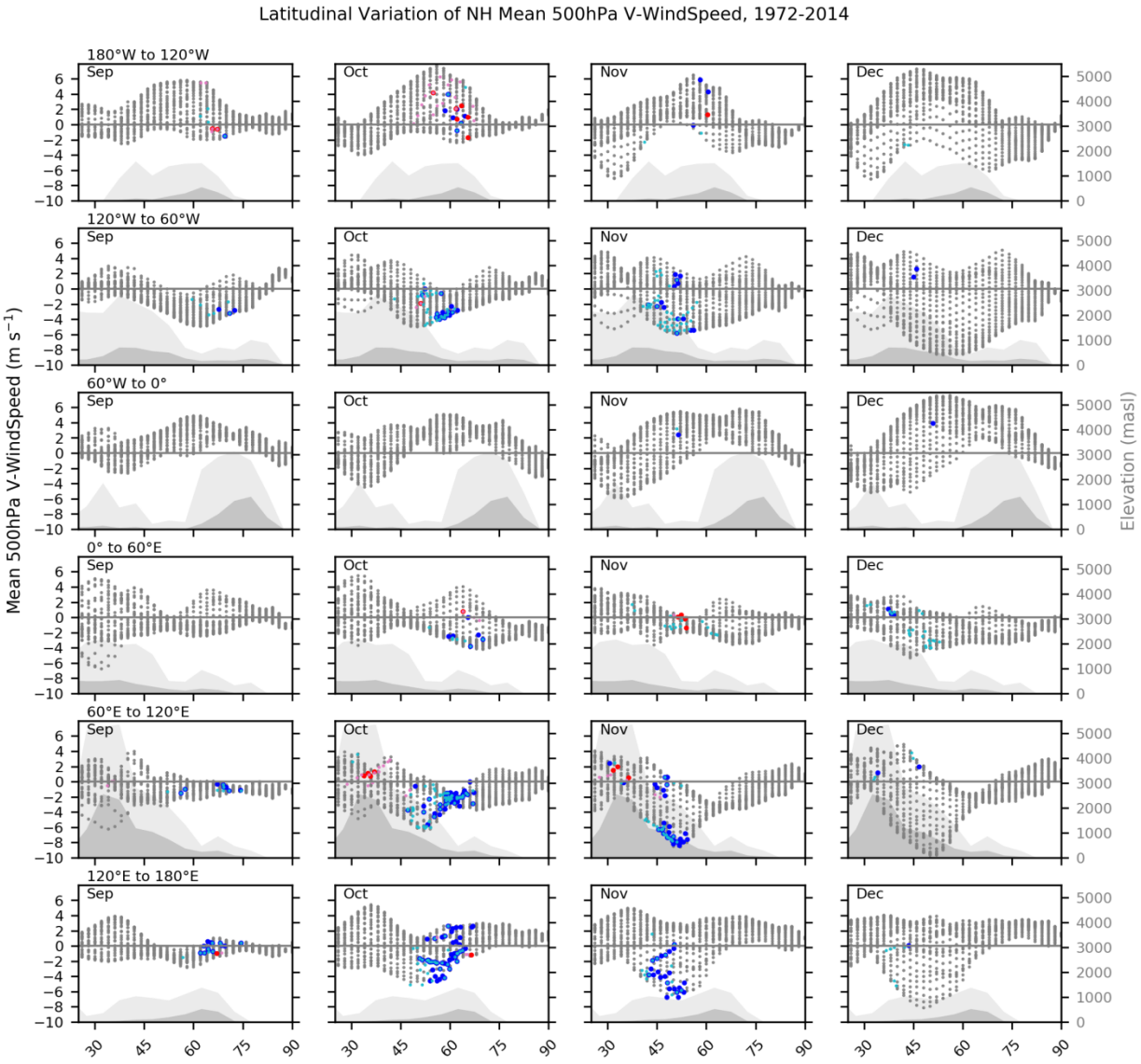

Figure A3.4c: Latitudinal distributions of 1972-2014 monthly mean 500 hPa meridional wind-speed within six longitudinal bands. Grey points represent means at points on the reanalysis grid. Dark (light) blue (red) symbols denote values associated with points for which significant negative (positive) On4 (On1) trends were identified. Darker (lighter) shaded areas represent meridional mean (maximum) elevations at zonal intervals of 5°.

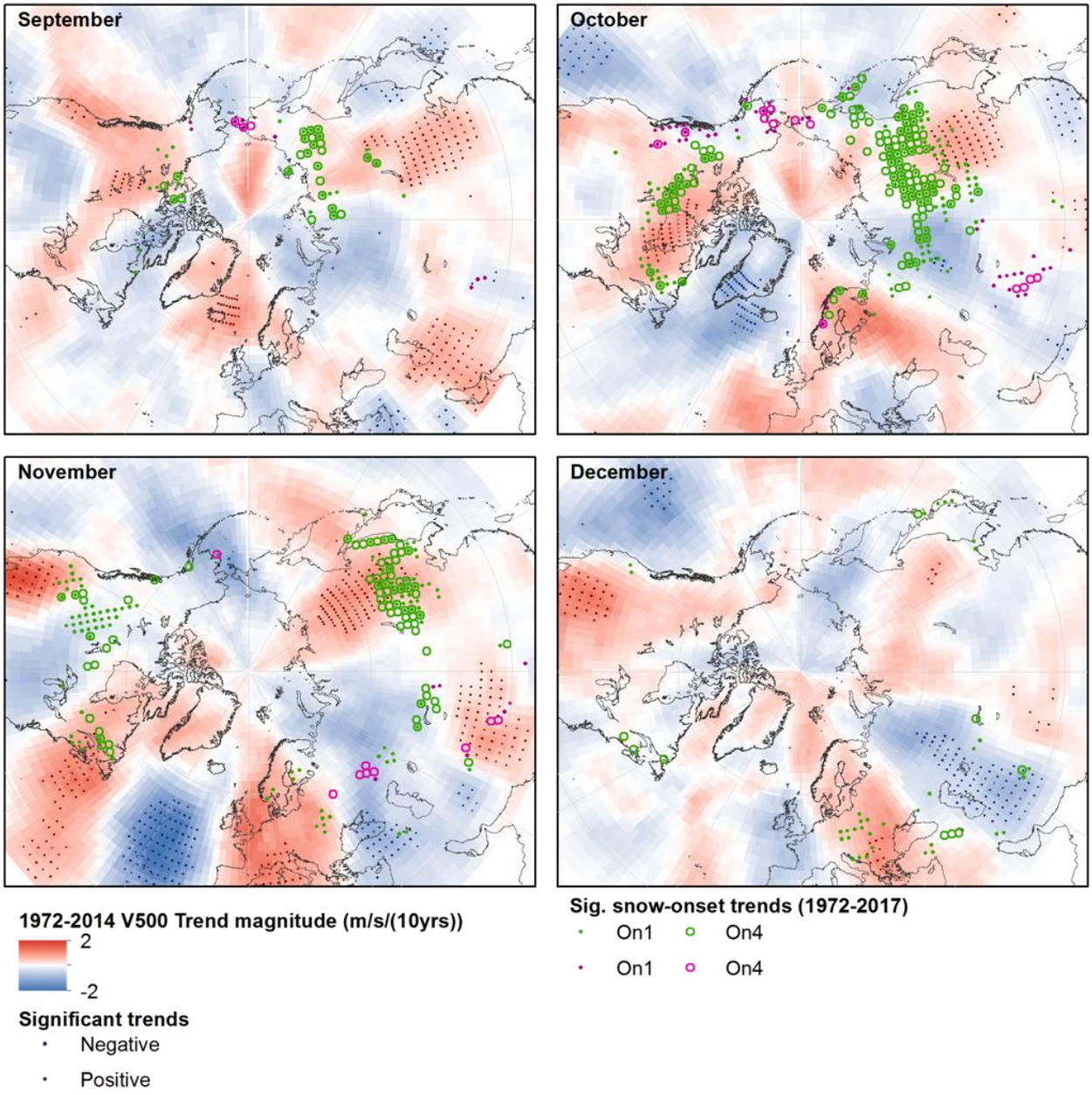

Figure A3.5a: 1972-2014 trends in monthly mean 500 hPa meridional wind-speed.

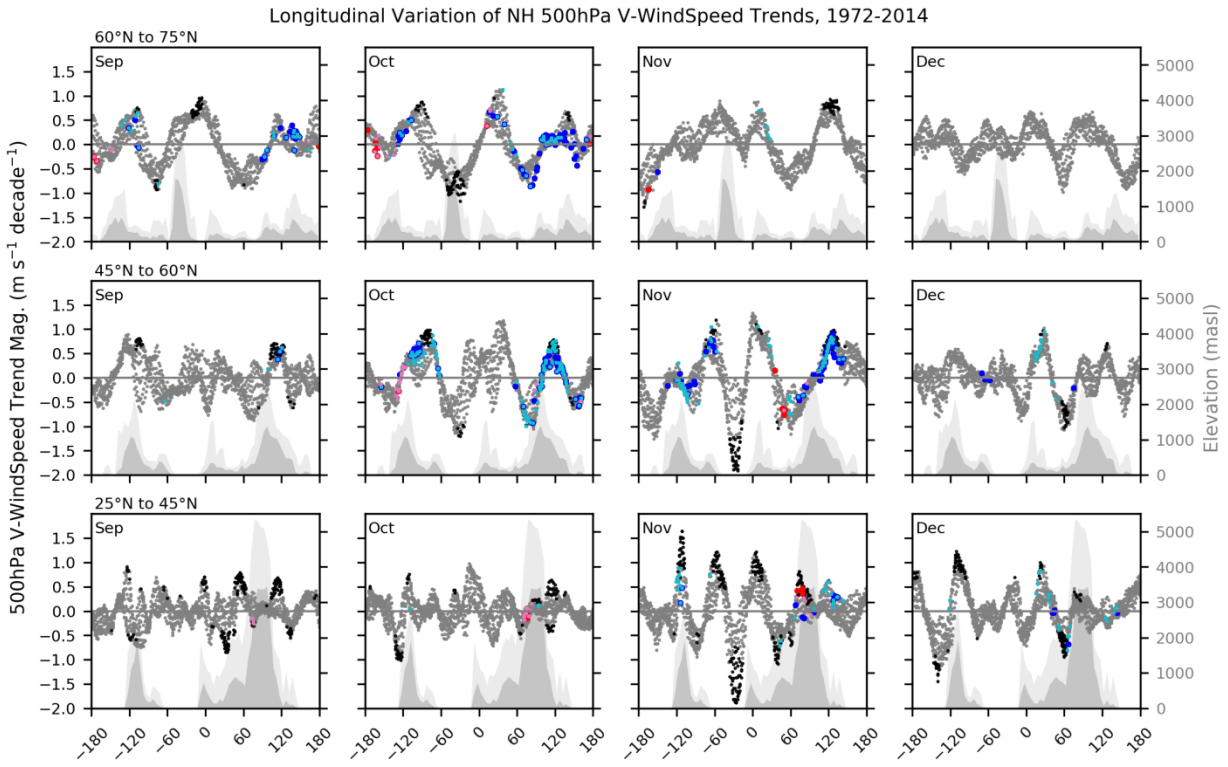

Figure A3.5b: Longitudinal distributions of 1972-2014 trends in monthly 500 hPa meridional wind-speed within three latitudinal bands. Black (grey) points represent significant (non-significant) trend magnitudes at points on the reanalysis grid. Dark (light) blue (red) symbols denote values associated with points for which significant negative (positive) On4 (On1) trends were identified. Darker (lighter) shaded areas represent meridional mean (maximum) elevations at zonal intervals of 5°.

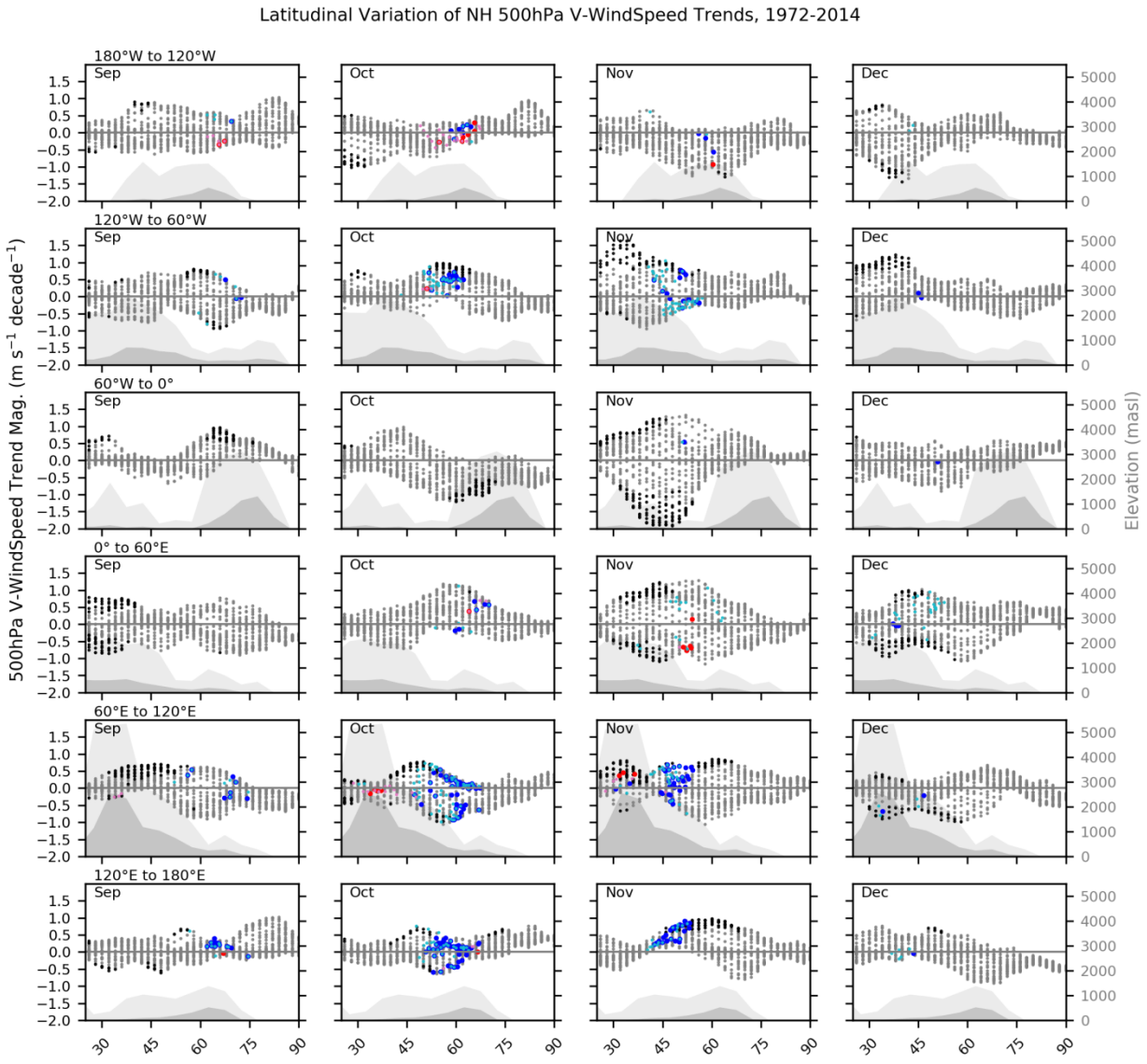

Figure A3.5c: Latitudinal distributions of 1972-2014 trends in monthly 500 hPa meridional wind-speed within six longitudinal bands. Black (grey) points represent significant (non-significant) trend magnitudes at points on the reanalysis grid. Dark (light) blue (red) symbols denote values associated with points for which significant negative (positive) On4 (On1) trends were identified. Darker (lighter) shaded areas represent meridional mean (maximum) elevations at zonal intervals of 5°.

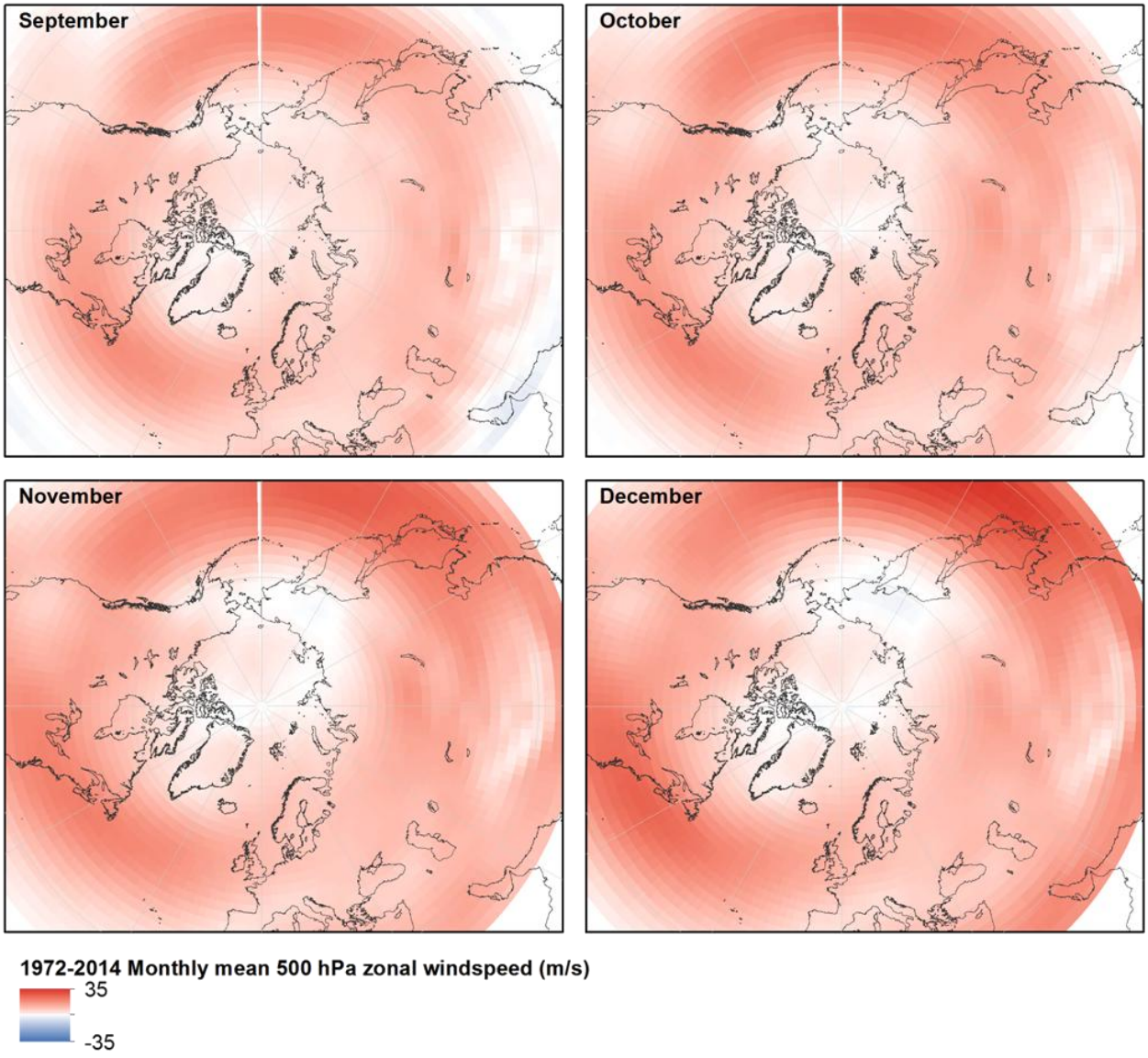

Figure A3.6a: 1972-2014 monthly mean 500 hPa zonal wind-speed.

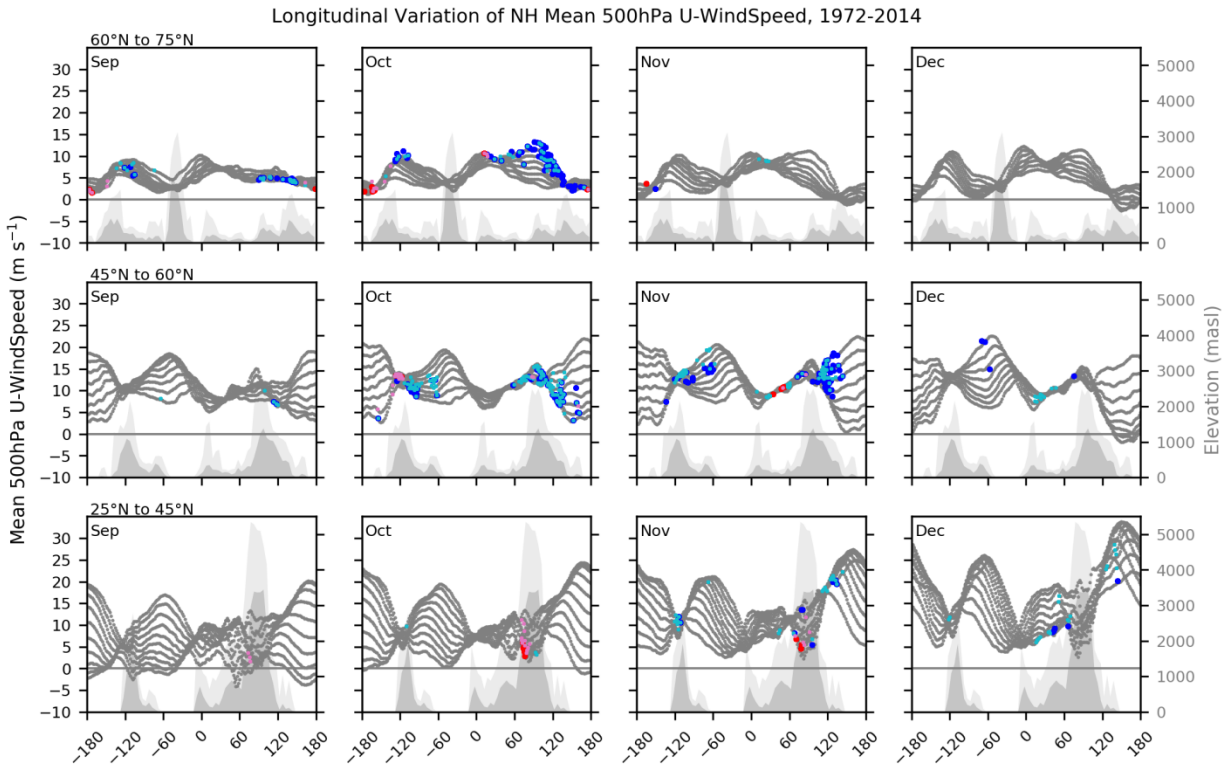

Figure A3.6b: Longitudinal distributions of 1972-2014 monthly mean 500 hPa zonal wind-speed within three latitudinal bands. Grey points represent means at points on the reanalysis grid. Dark (light) blue (red) symbols denote values associated with points for which significant negative (positive) On4 (On1) trends were identified. Darker (lighter) shaded areas represent meridional mean (maximum) elevations at zonal intervals of 5°.

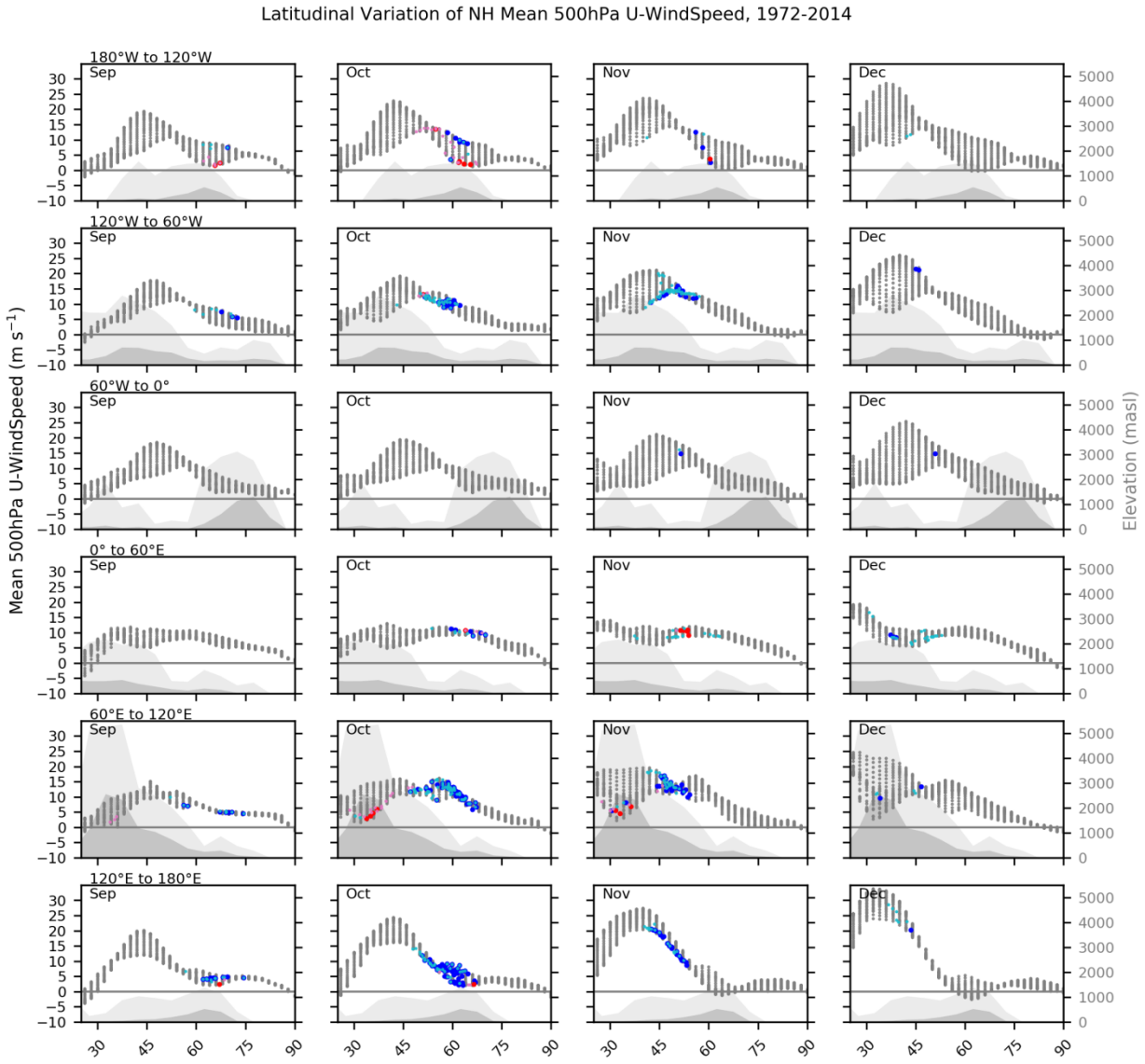

Figure A3.6c: Latitudinal distributions of 1972-2014 monthly mean 500 hPa zonal wind-speed within six longitudinal bands. Grey points represent means at points on the reanalysis grid. Dark (light) blue (red) symbols denote values associated with points for which significant negative (positive) On4 (On1) trends were identified. Darker (lighter) shaded areas represent meridional mean (maximum) elevations at zonal intervals of 5°.

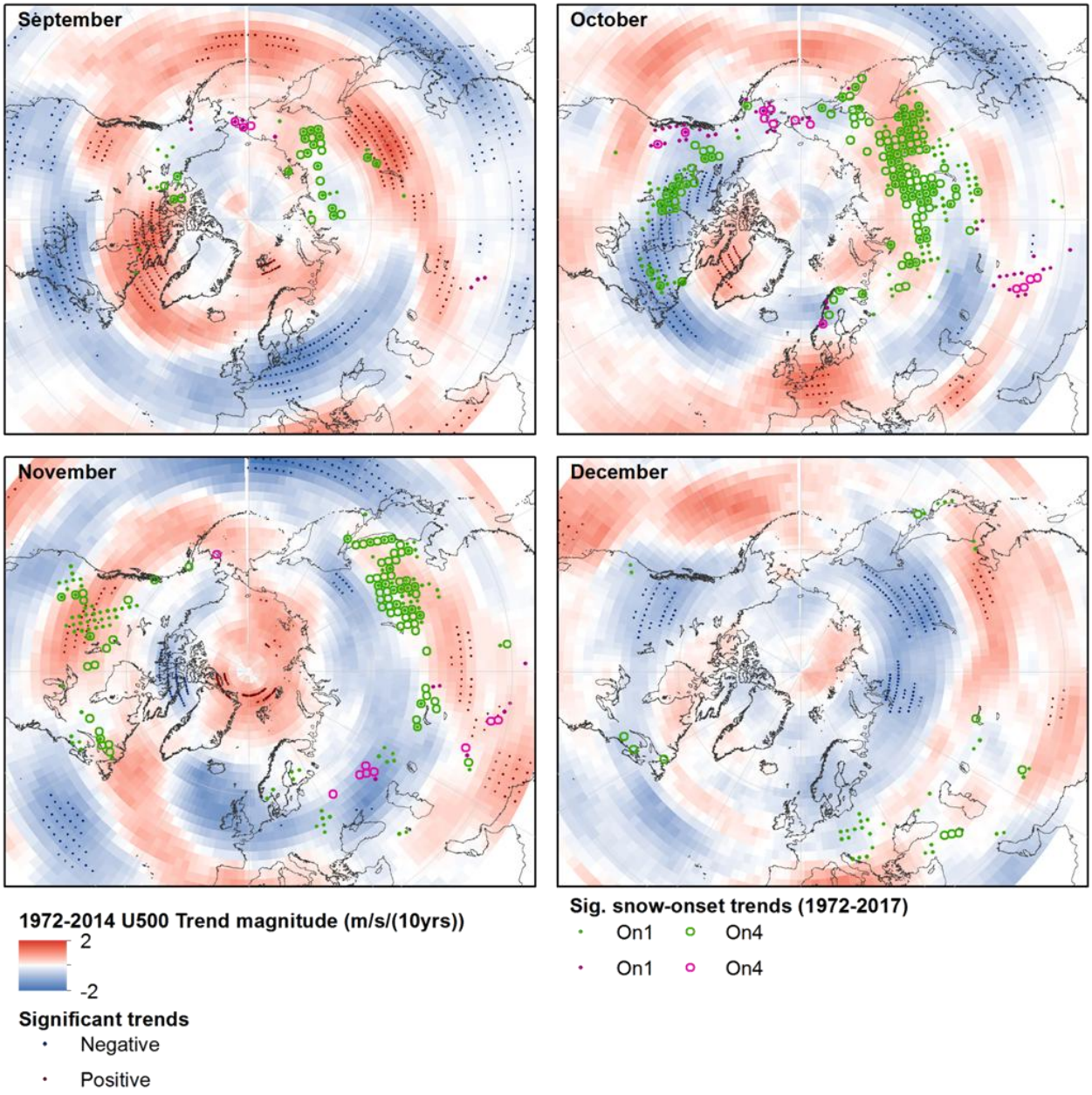

Figure A3.7a: 1972-2014 trends in monthly mean 500 hPa zonal wind-speed.

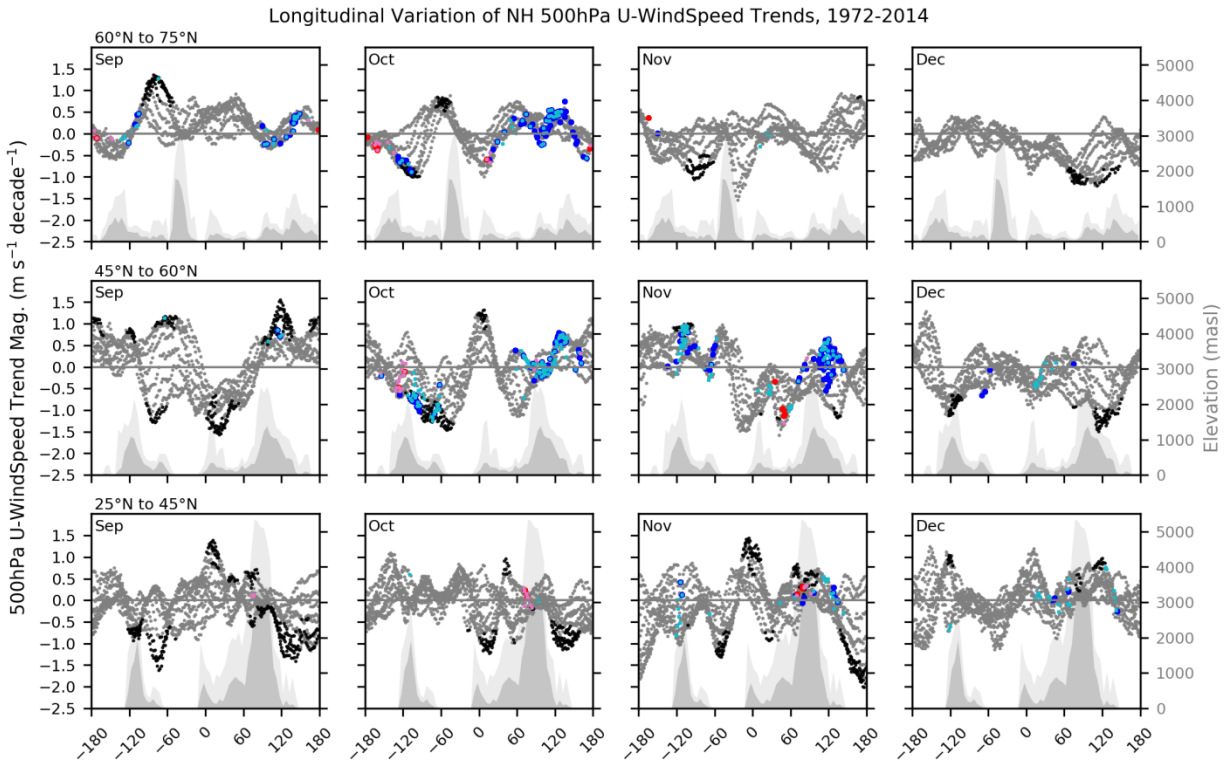

Figure A3.7b: Longitudinal distributions of 1972-2014 trends in monthly 500 hPa zonal wind-speed within three latitudinal bands. Black (grey) points represent significant (non-significant) trend magnitudes at points on the reanalysis grid. Dark (light) blue (red) symbols denote values associated with points for which significant negative (positive) On4 (On1) trends were identified. Darker (lighter) shaded areas represent meridional mean (maximum) elevations at zonal intervals of 5°.

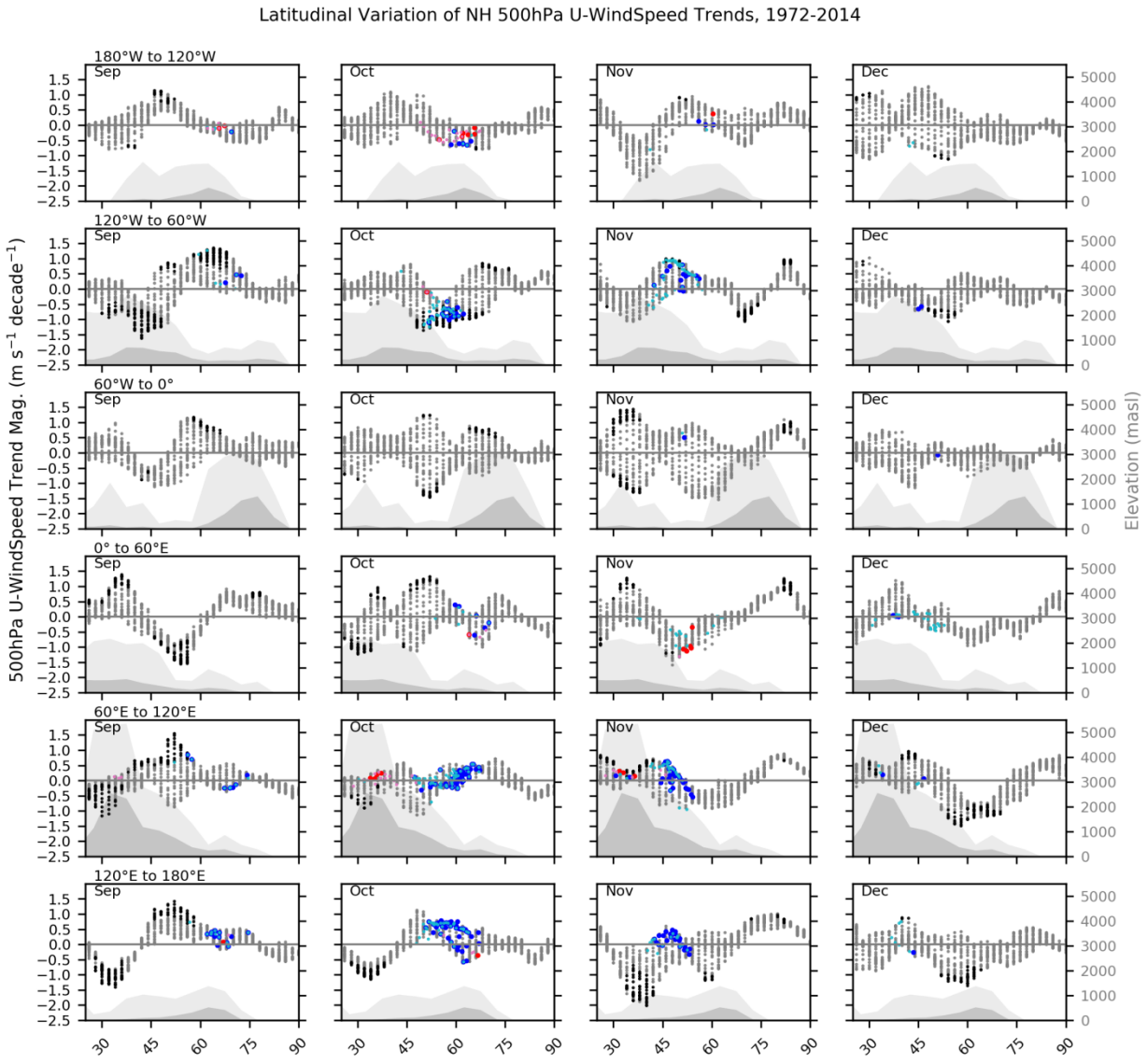

Figure A3.7c: Latitudinal distributions of 1972-2014 trends in monthly 500 hPa zonal wind-speed within six longitudinal bands. Black (grey) points represent significant (non-significant) trend magnitudes at points on the reanalysis grid. Dark (light) blue (red) symbols denote values associated with points for which significant negative (positive) On4 (On1) trends were identified. Darker (lighter) shaded areas represent meridional mean (maximum) elevations at zonal intervals of 5°.

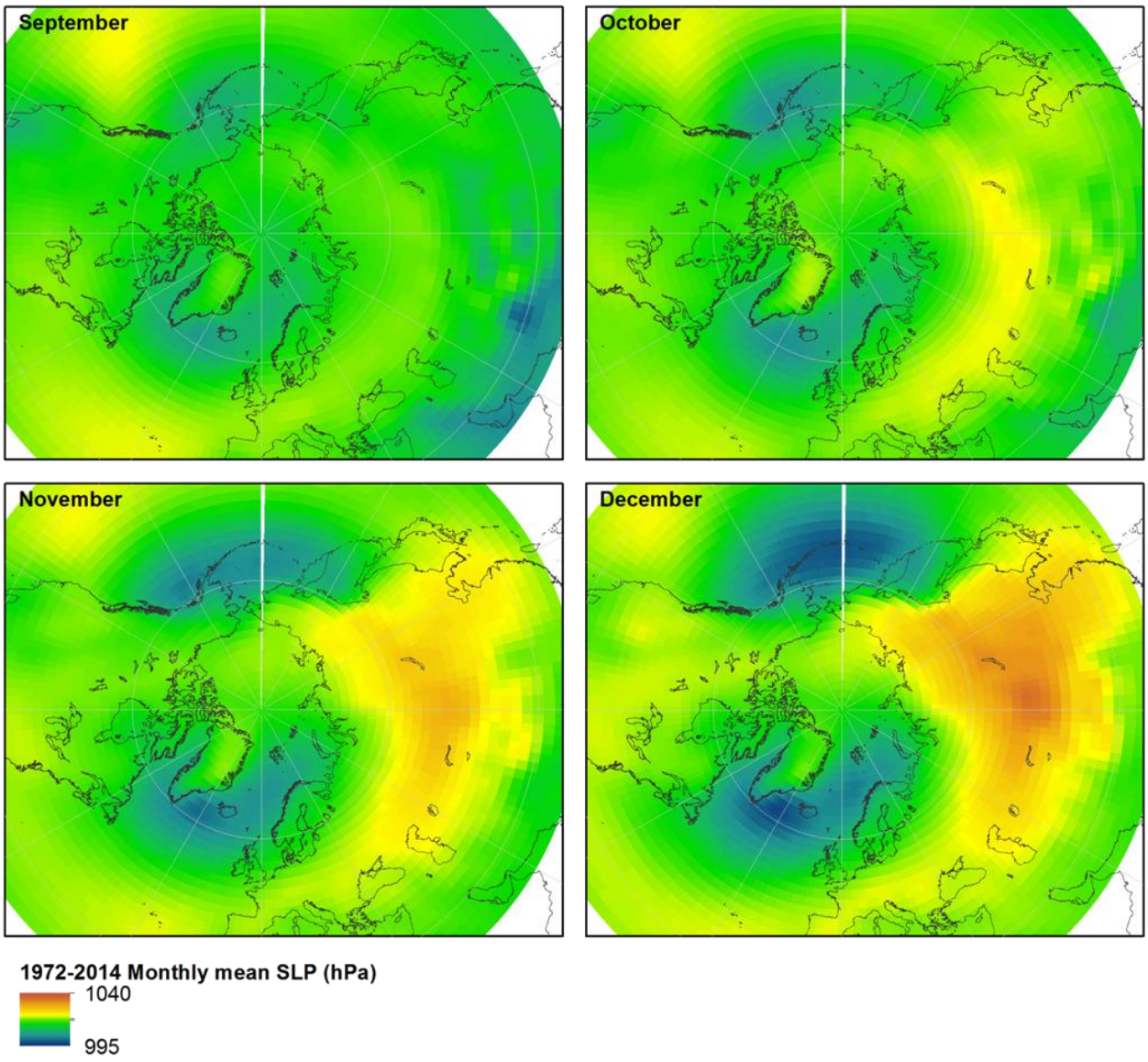

Figure A3.8a: 1972-2014 monthly mean sea-level pressure.

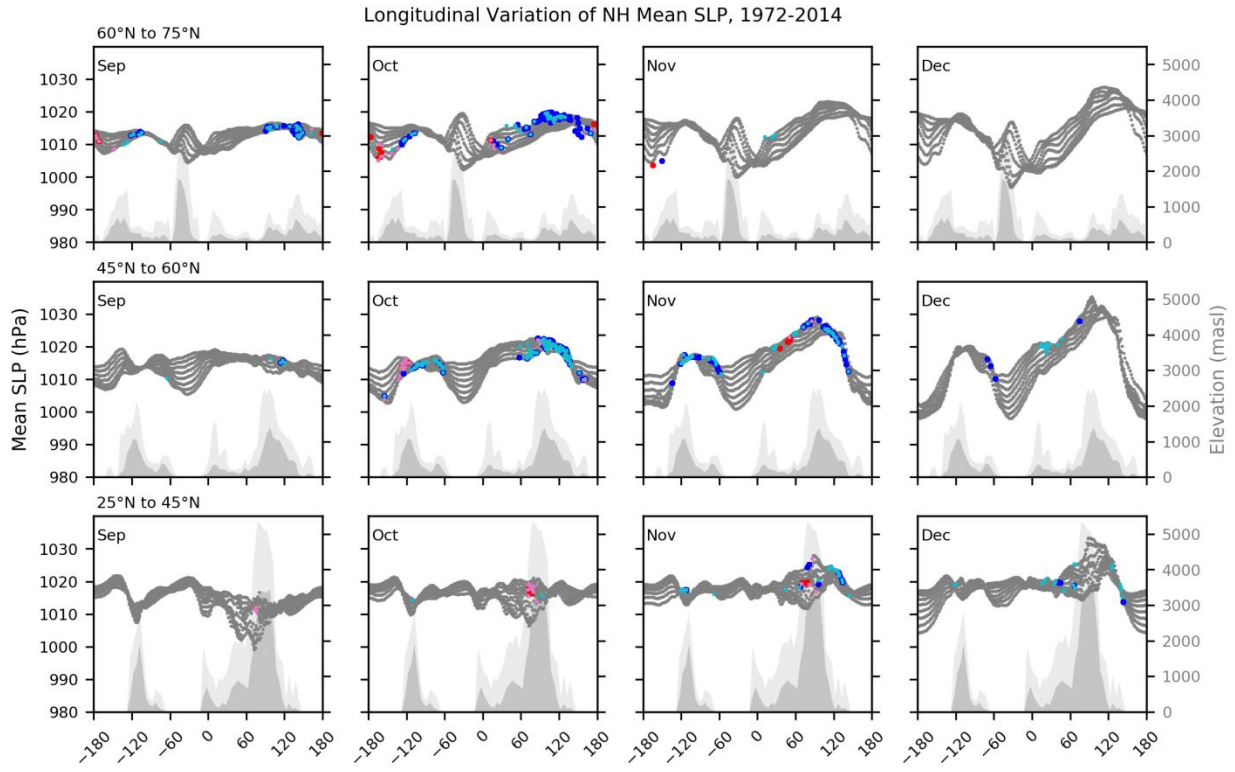

Figure A3.8b: Longitudinal distributions of 1972-2014 monthly mean mean sea-level pressure within three latitudinal bands. Grey points represent means at points on the reanalysis grid. Dark (light) blue (red) symbols denote values associated with points for which significant negative (positive) On4 (On1) trends were identified. Darker (lighter) shaded areas represent meridional mean (maximum) elevations at zonal intervals of 5°.

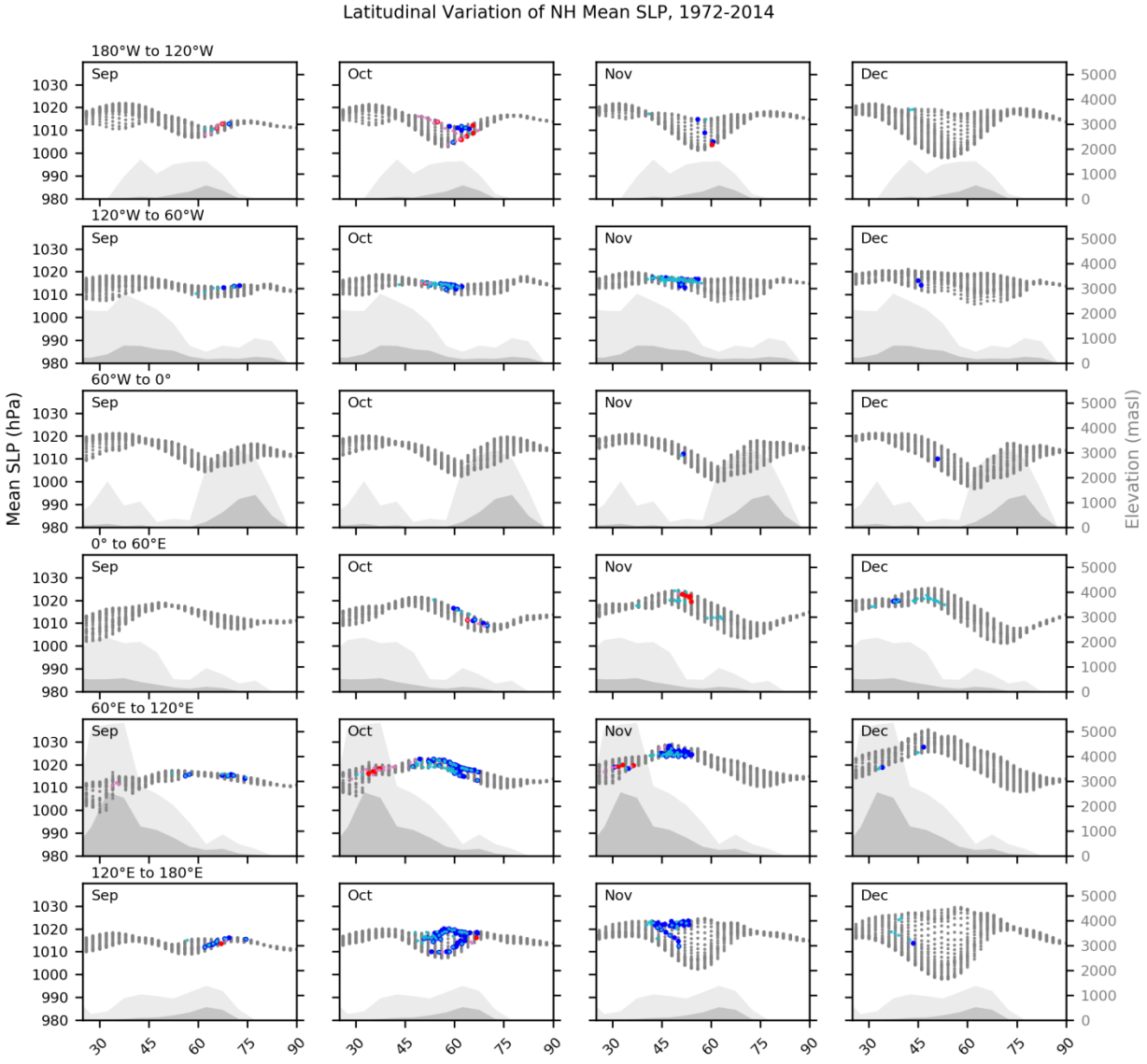

Figure A3.8c: Latitudinal distributions of 1972-2014 monthly mean mean sea-level pressure within six longitudinal bands. Grey points represent means at points on the reanalysis grid. Dark (light) blue (red) symbols denote values associated with points for which significant negative (positive) On4 (On1) trends were identified. Darker (lighter) shaded areas represent meridional mean (maximum) elevations at zonal intervals of 5°.

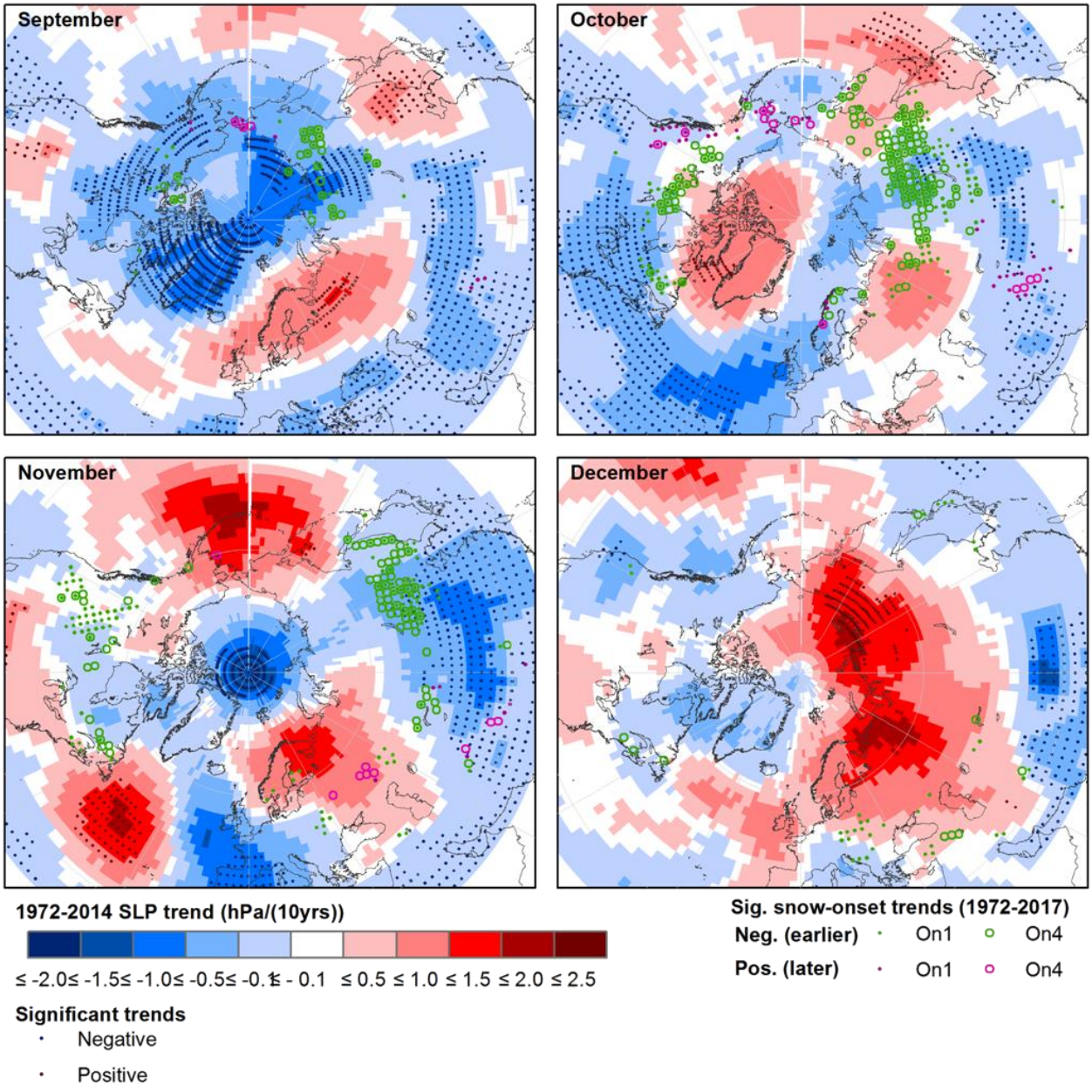

Figure A3.9a: 1972-2014 trends in monthly mean sea-level pressure.

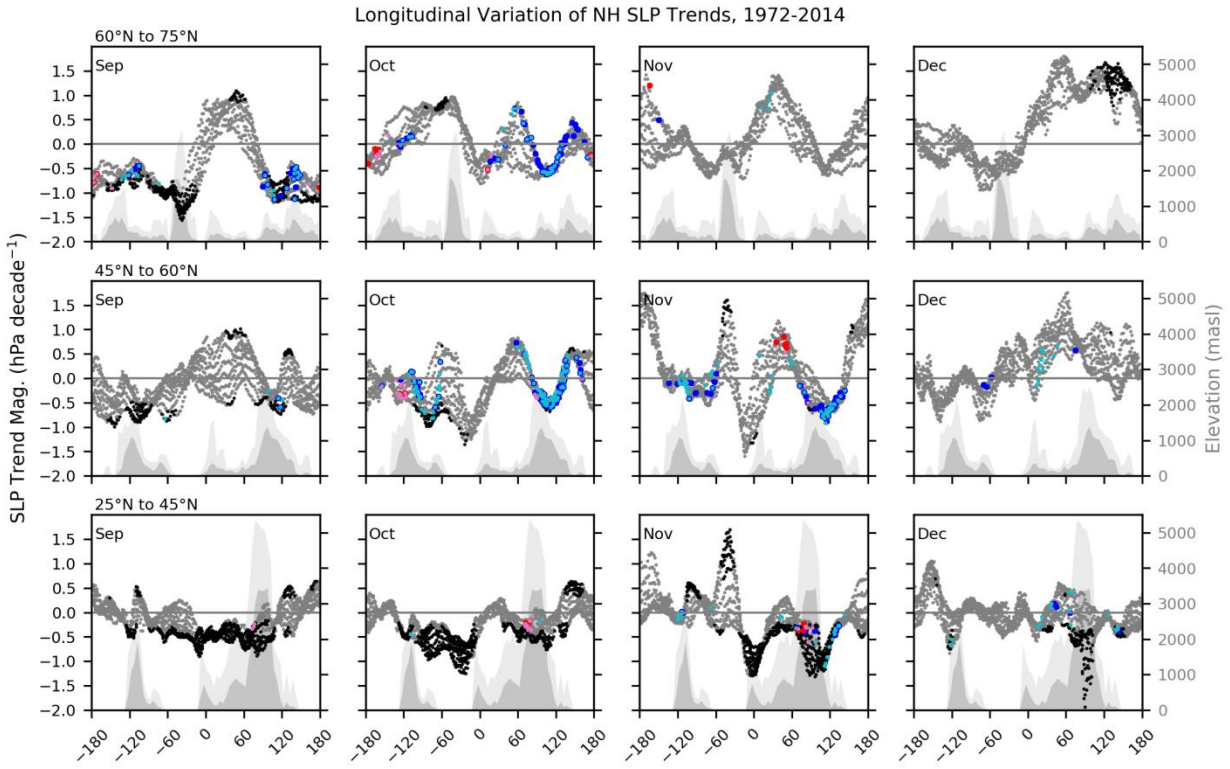

Figure A3.9b: Longitudinal distributions of 1972-2014 trends in monthly mean sea-level pressure within three latitudinal bands. Black (grey) points represent significant (non-significant) trend magnitudes at points on the reanalysis grid. Dark (light) blue (red) symbols denote values associated with points for which significant negative (positive) On4 (On1) trends were identified. Darker (lighter) shaded areas represent meridional mean (maximum) elevations at zonal intervals of 5°.

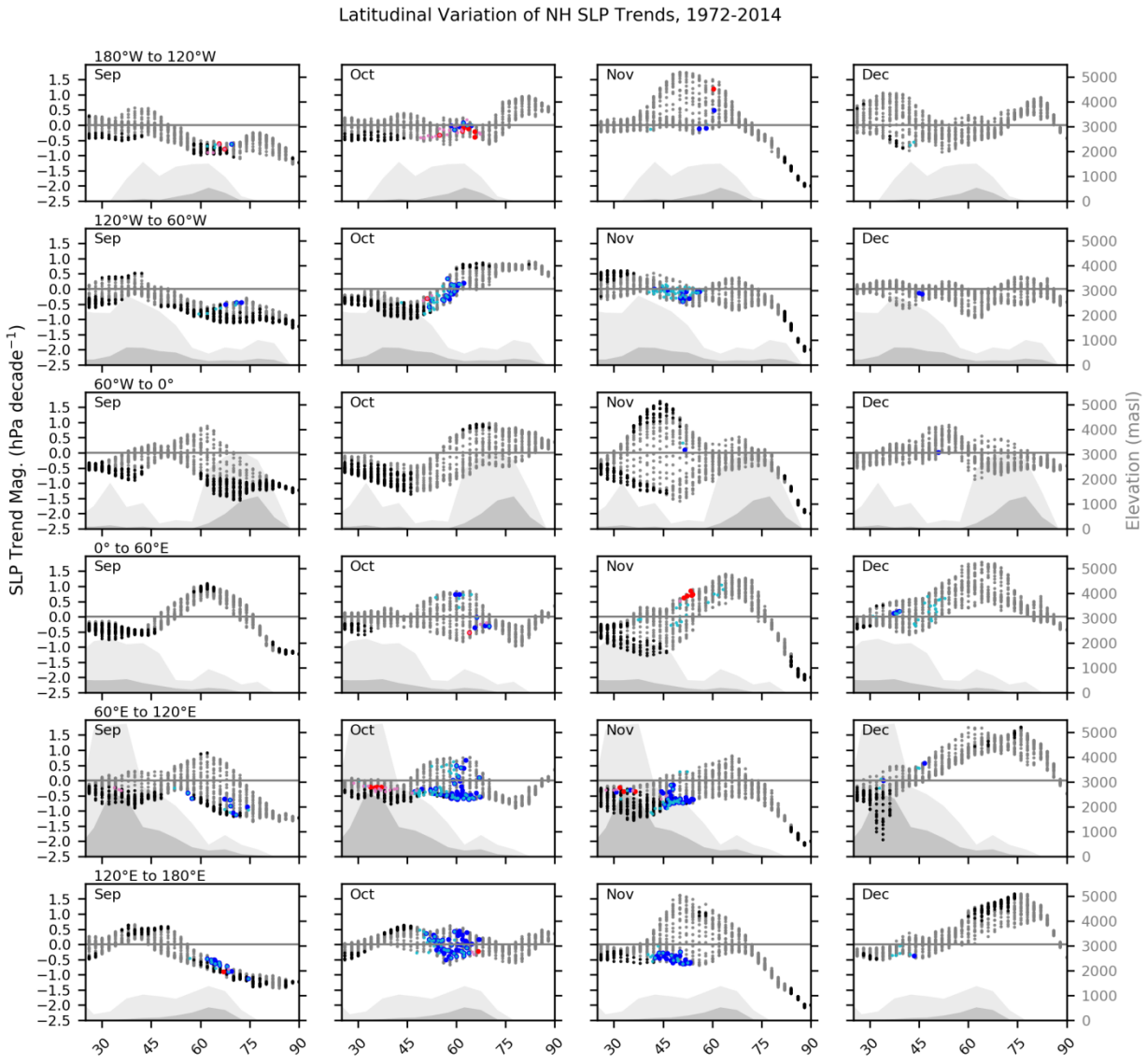

Figure A3.9c: Latitudinal distributions of 1972-2014 trends in monthly mean sea-level pressure within six longitudinal bands. Black (grey) points represent significant (non-significant) trend magnitudes at points on the reanalysis grid. Dark (light) blue (red) symbols denote values associated with points for which significant negative (positive) On4 (On1) trends were identified. Darker (lighter) shaded areas represent meridional mean (maximum) elevations at zonal intervals of 5°.

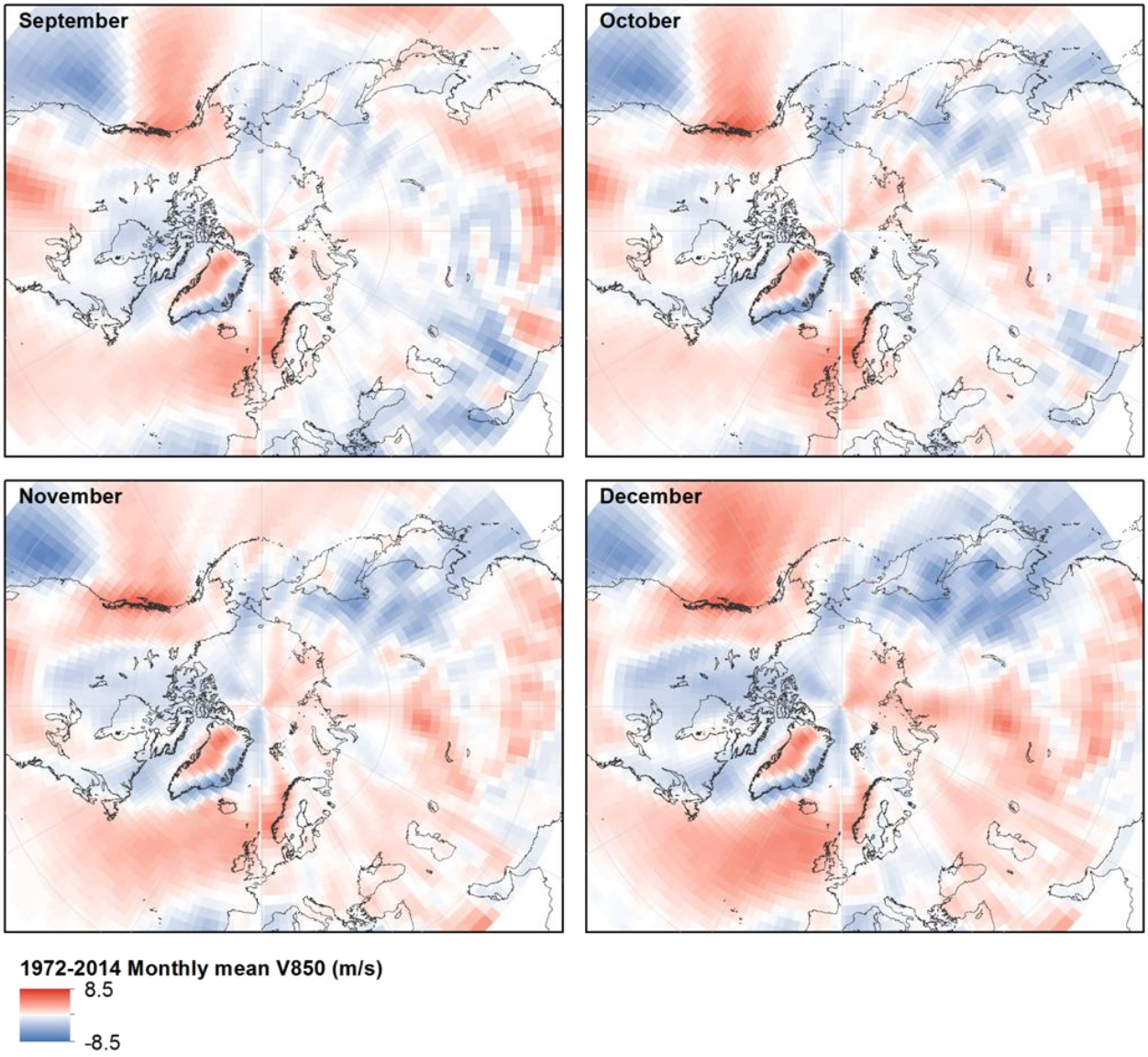

Figure A3.10a: 1972-2014 monthly mean 850 hPa meridional wind-speed.

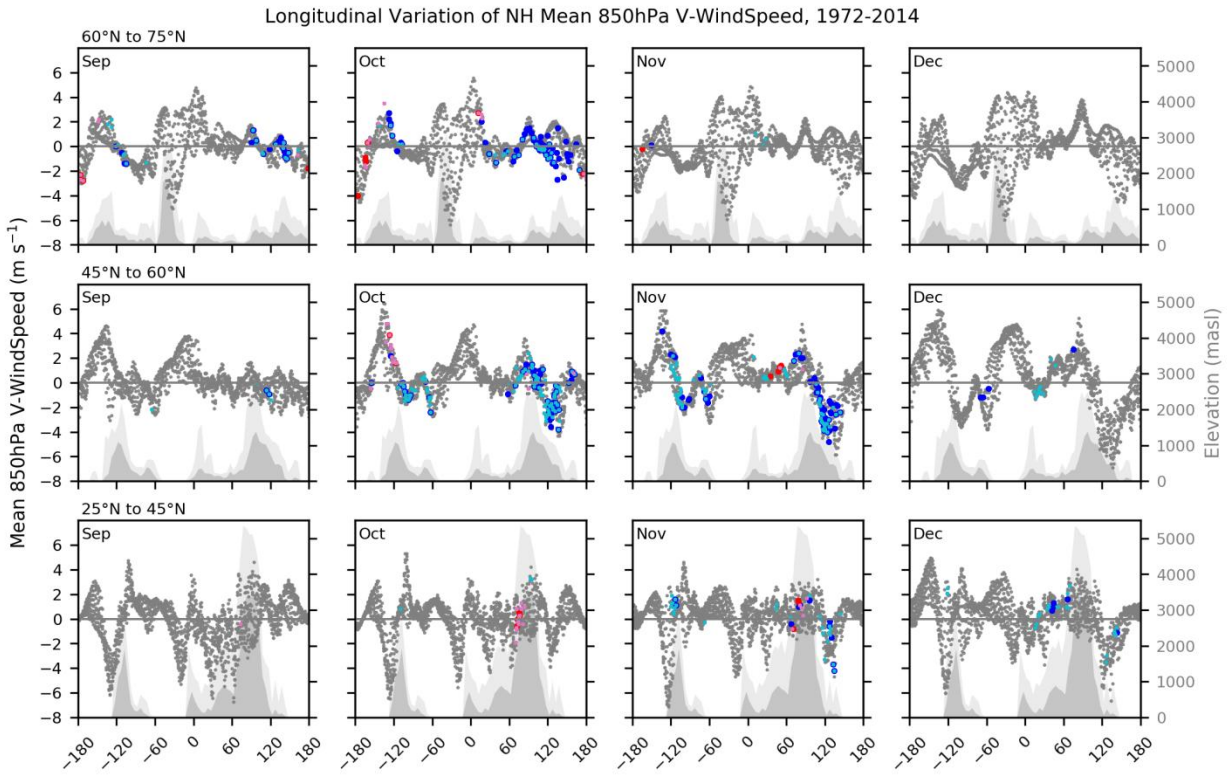

Figure A3.10b: Longitudinal distributions of 1972-2014 monthly mean mean 850 hPa meridional wind-speed within three latitudinal bands. Grey points represent means at points on the reanalysis grid. Dark (light) blue (red) symbols denote values associated with points for which significant negative (positive) On4 (On1) trends were identified. Darker (lighter) shaded areas represent meridional mean (maximum) elevations at zonal intervals of 5°.

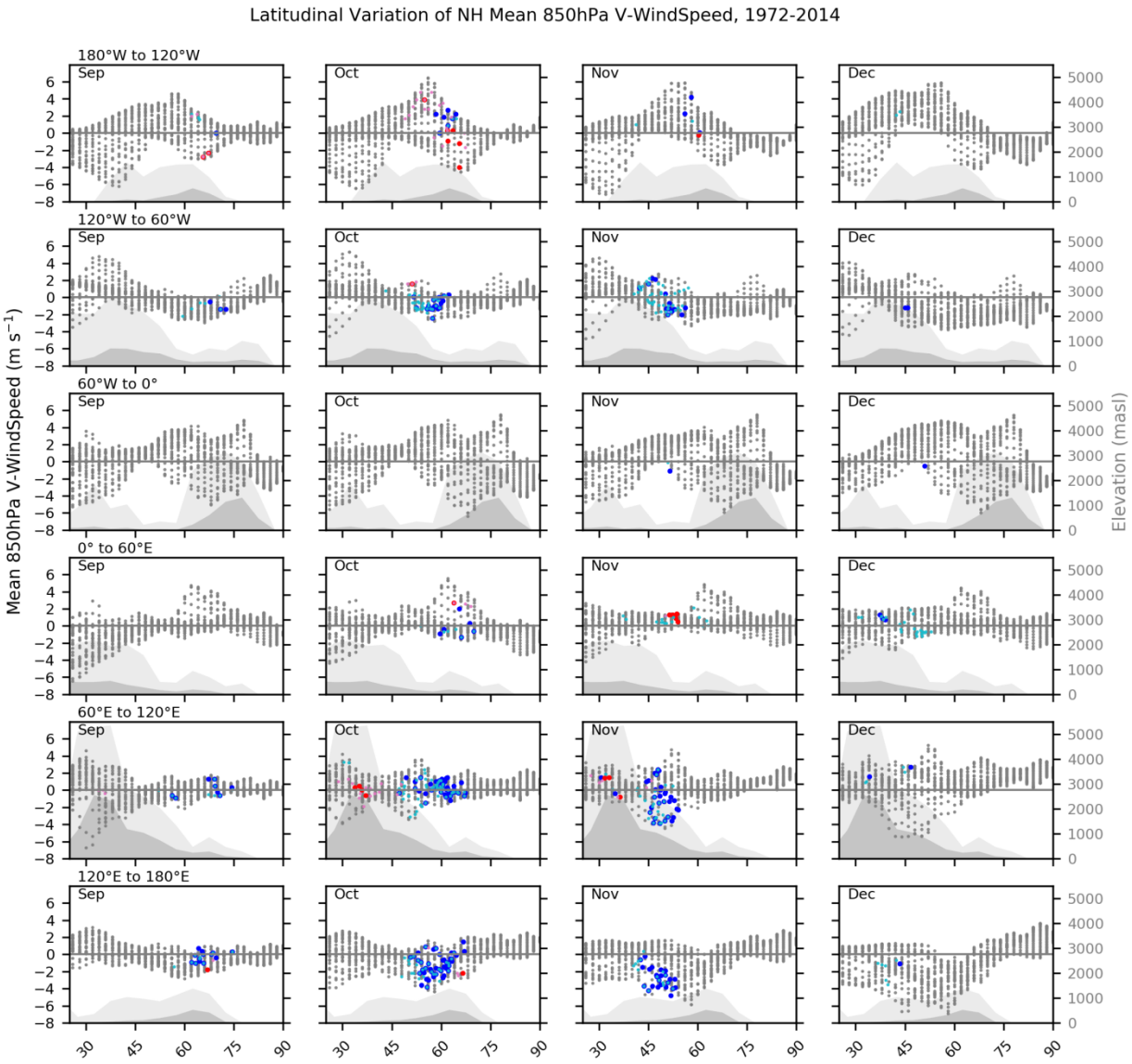

Figure A3.10c: Latitudinal distributions of 1972-2014 monthly mean mean 850 hPa meridional wind-speed within six longitudinal bands. Grey points represent means at points on the reanalysis grid. Dark (light) blue (red) symbols denote values associated with points for which significant negative (positive) On4 (On1) trends were identified. Darker (lighter) shaded areas represent meridional mean (maximum) elevations at zonal intervals of 5°.

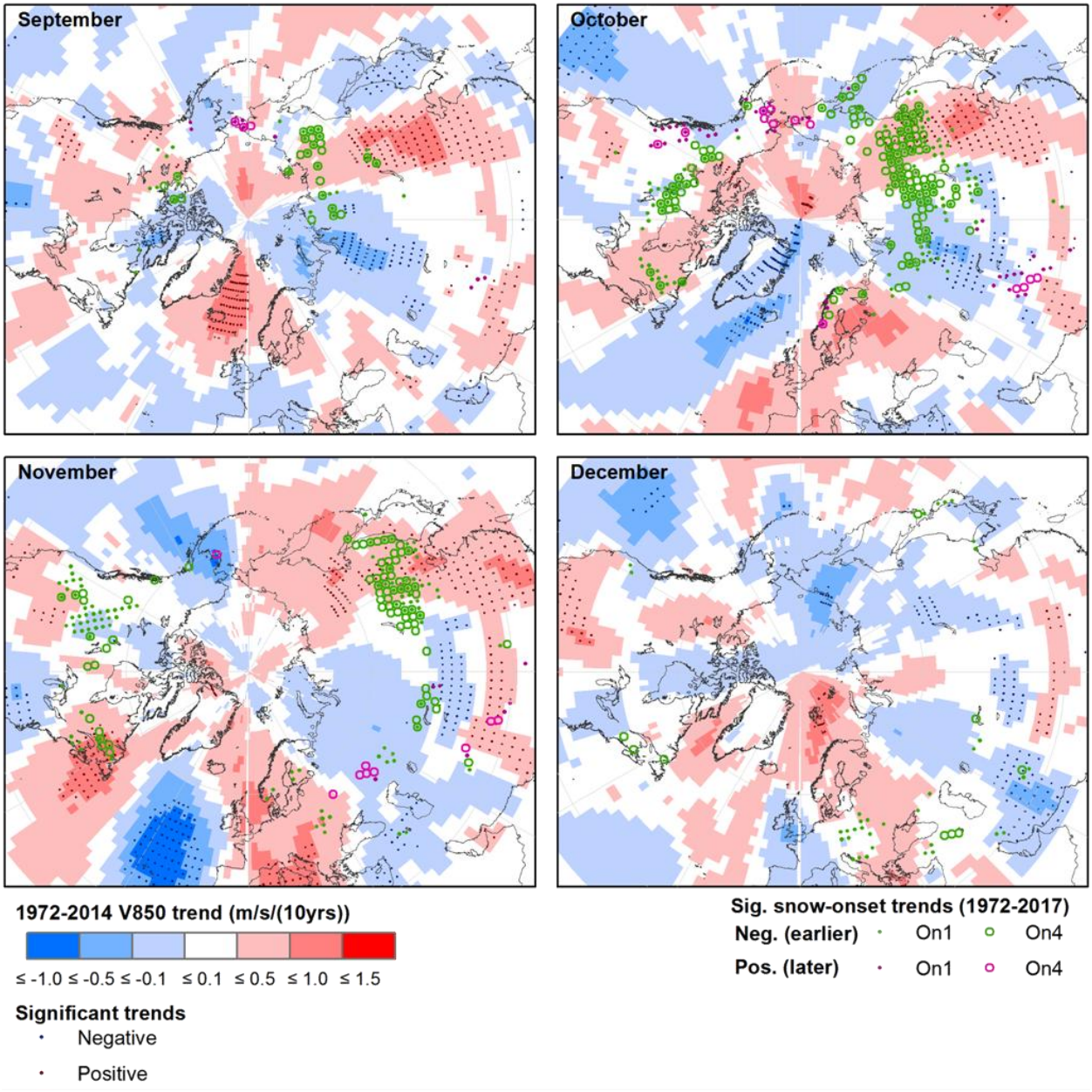

Figure A3.11a: 1972-2014 trends in monthly mean 850 hPa meridional wind-speed.

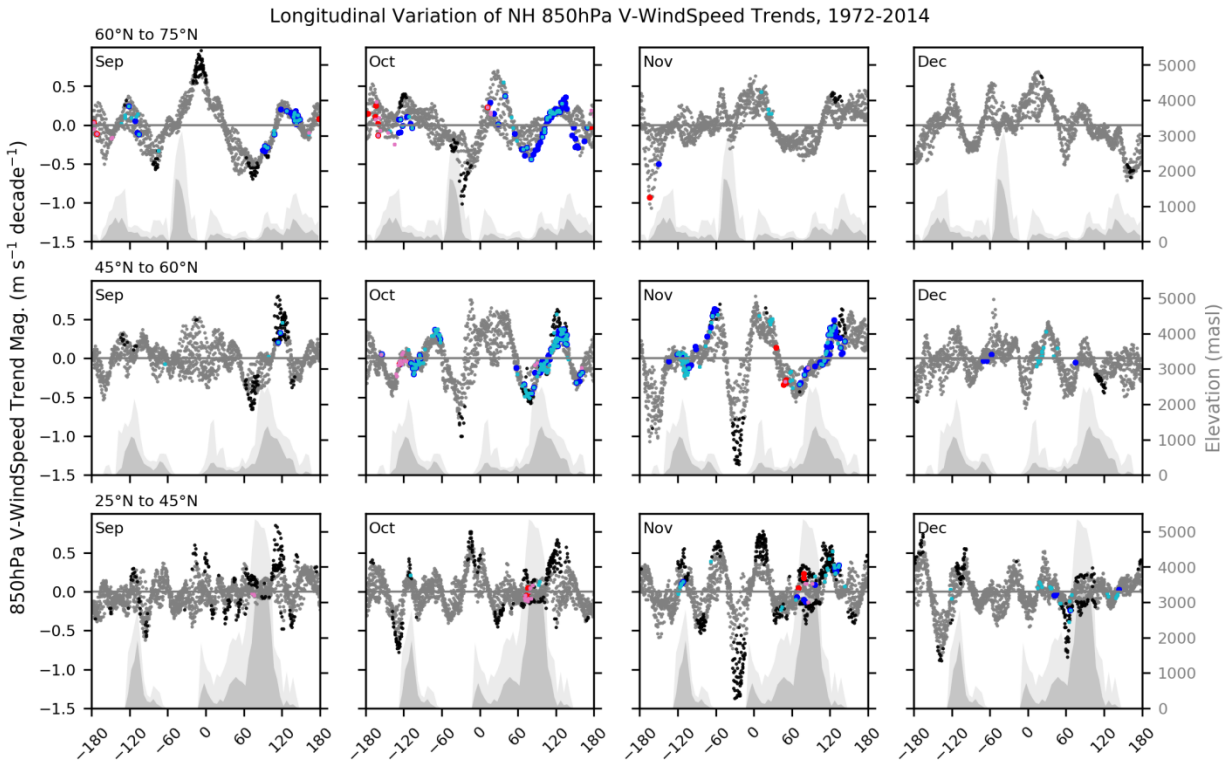

Figure A3.11b: Longitudinal distributions of 1972-2014 trends in monthly mean 850 hPa meridional wind-speed within three latitudinal bands. Black (grey) points represent significant (non-significant) trend magnitudes at points on the reanalysis grid. Dark (light) blue (red) symbols denote values associated with points for which significant negative (positive) On4 (On1) trends were identified. Darker (lighter) shaded areas represent meridional mean (maximum) elevations at zonal intervals of 5°.

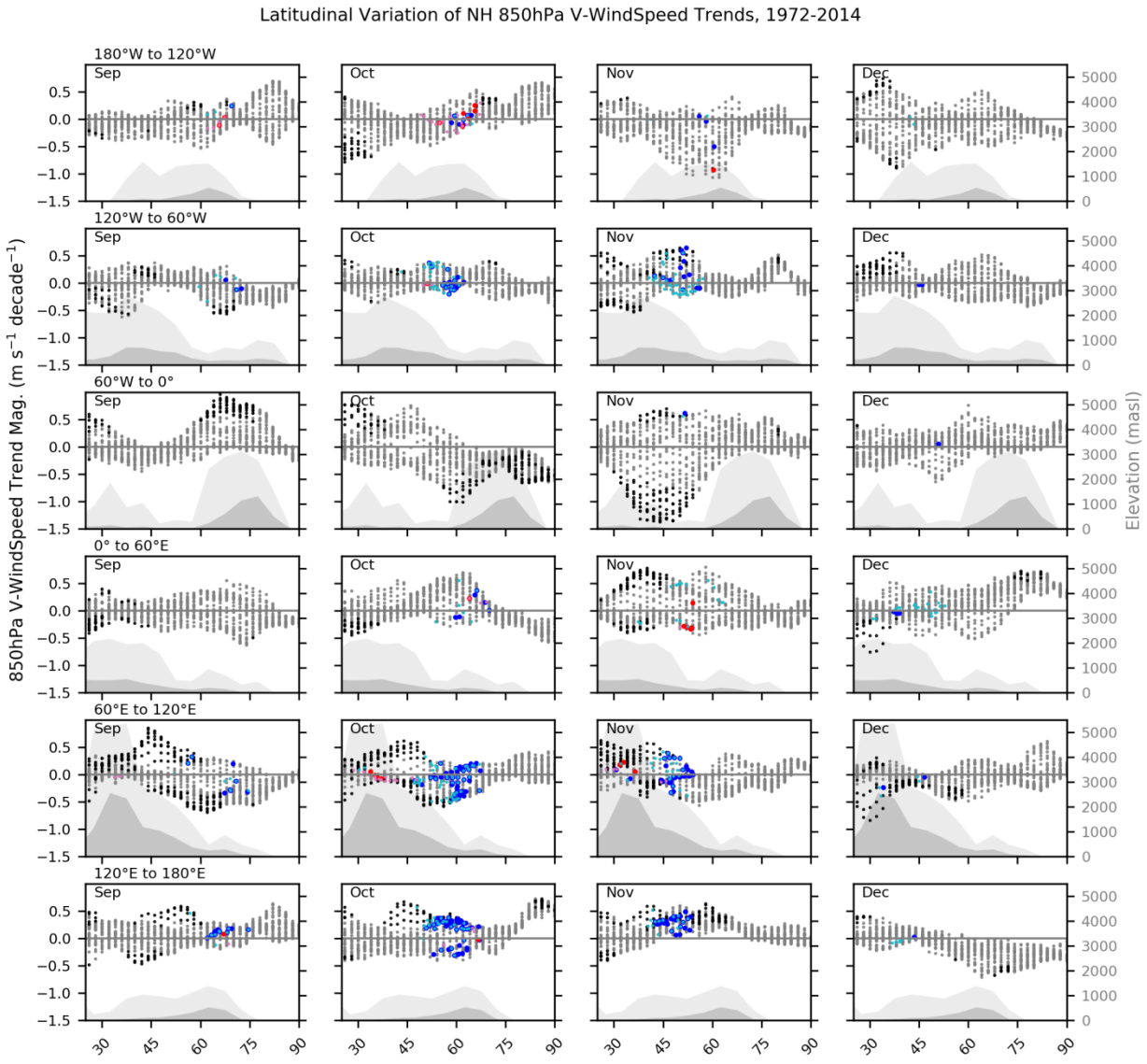

Figure A3.11c: Latitudinal distributions of 1972-2014 trends in monthly mean 850 hPa meridional wind-speed within six longitudinal bands. Black (grey) points represent significant (non-significant) trend magnitudes at points on the reanalysis grid. Dark (light) blue (red) symbols denote values associated with points for which significant negative (positive) On4 (On1) trends were identified. Darker (lighter) shaded areas represent meridional mean (maximum) elevations at zonal intervals of 5°.

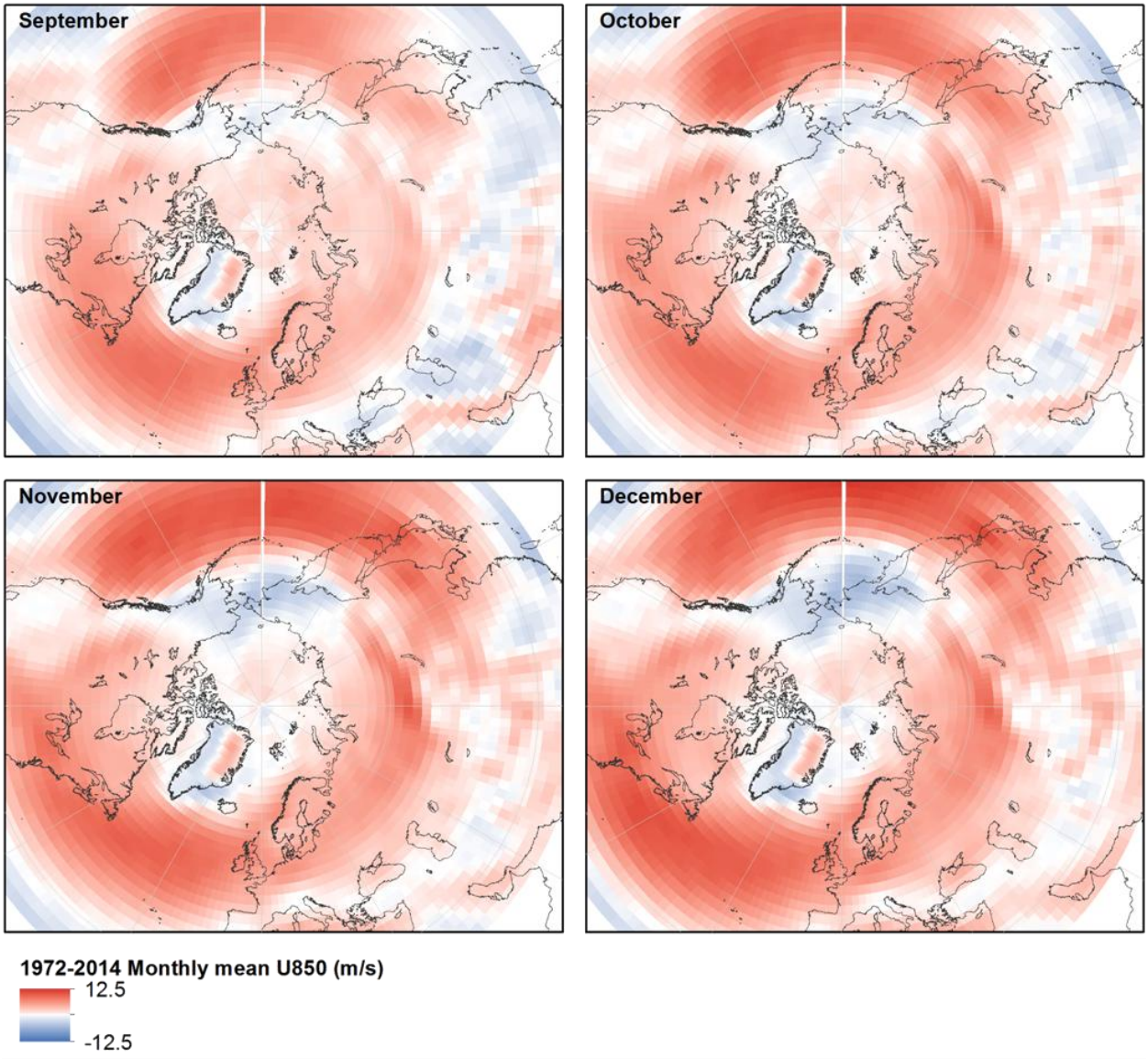

Figure A3.12a: 1972-2014 monthly mean 850 hPa zonal wind-speed.

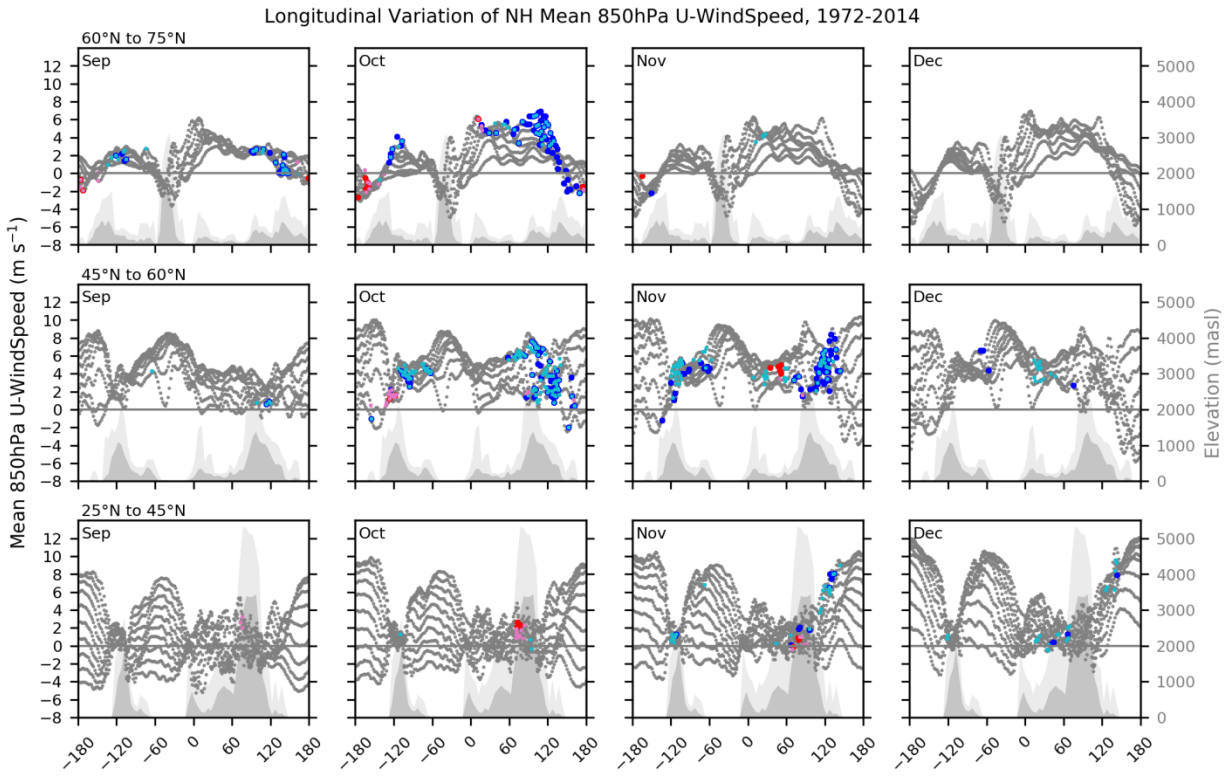

Figure A3.12b: Longitudinal distributions of 1972-2014 monthly mean mean 850 hPa zonal wind-speed within three latitudinal bands. Grey points represent means at points on the reanalysis grid. Dark (light) blue (red) symbols denote values associated with points for which significant negative (positive) On4 (On1) trends were identified. Darker (lighter) shaded areas represent meridional mean (maximum) elevations at zonal intervals of 5°.

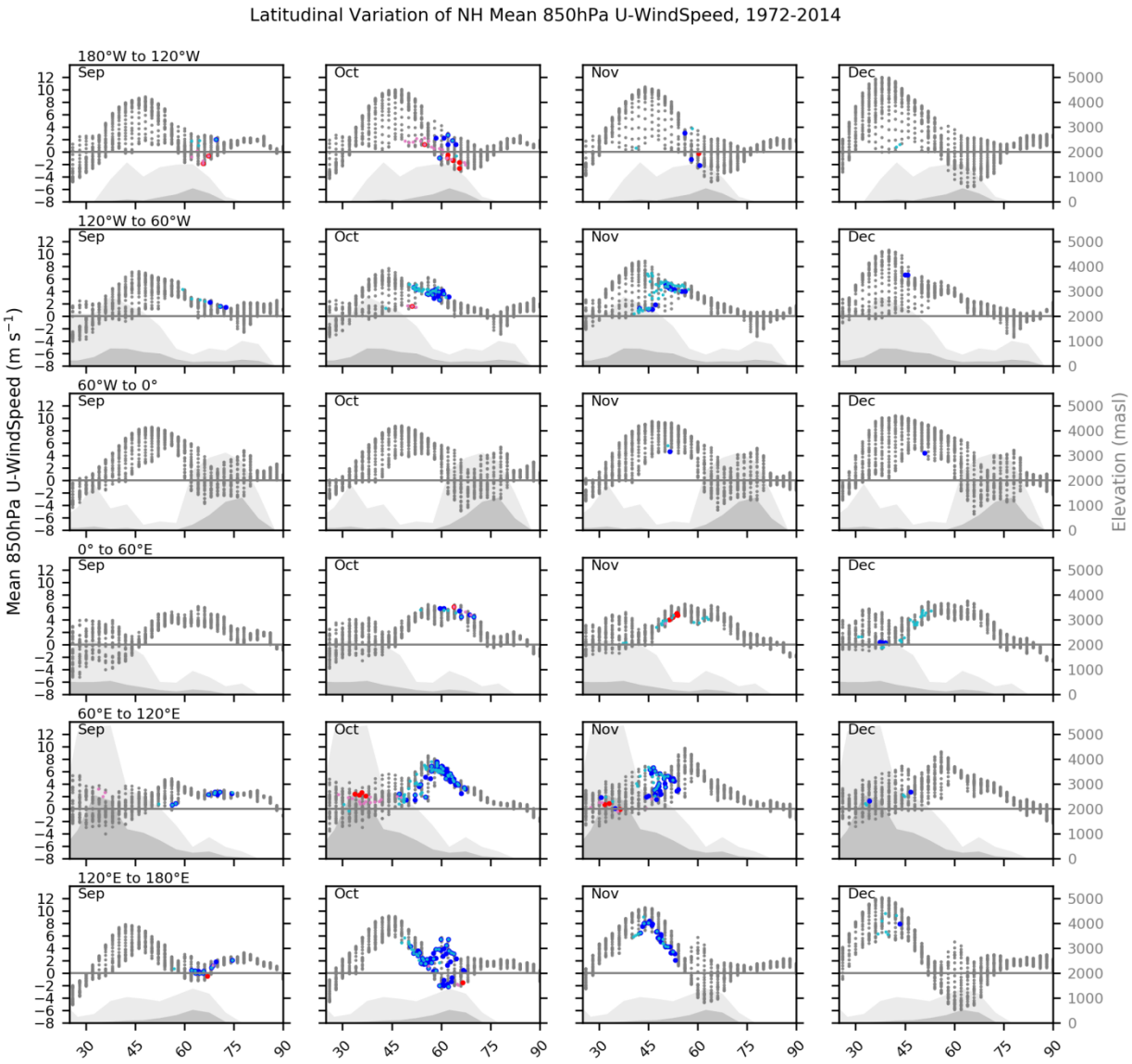

Figure A3.12c: Latitudinal distributions of 1972-2014 monthly mean mean 850 hPa zonal wind-speed within six longitudinal bands. Grey points represent means at points on the reanalysis grid. Dark (light) blue (red) symbols denote values associated with points for which significant negative (positive) On4 (On1) trends were identified. Darker (lighter) shaded areas represent meridional mean (maximum) elevations at zonal intervals of 5°.

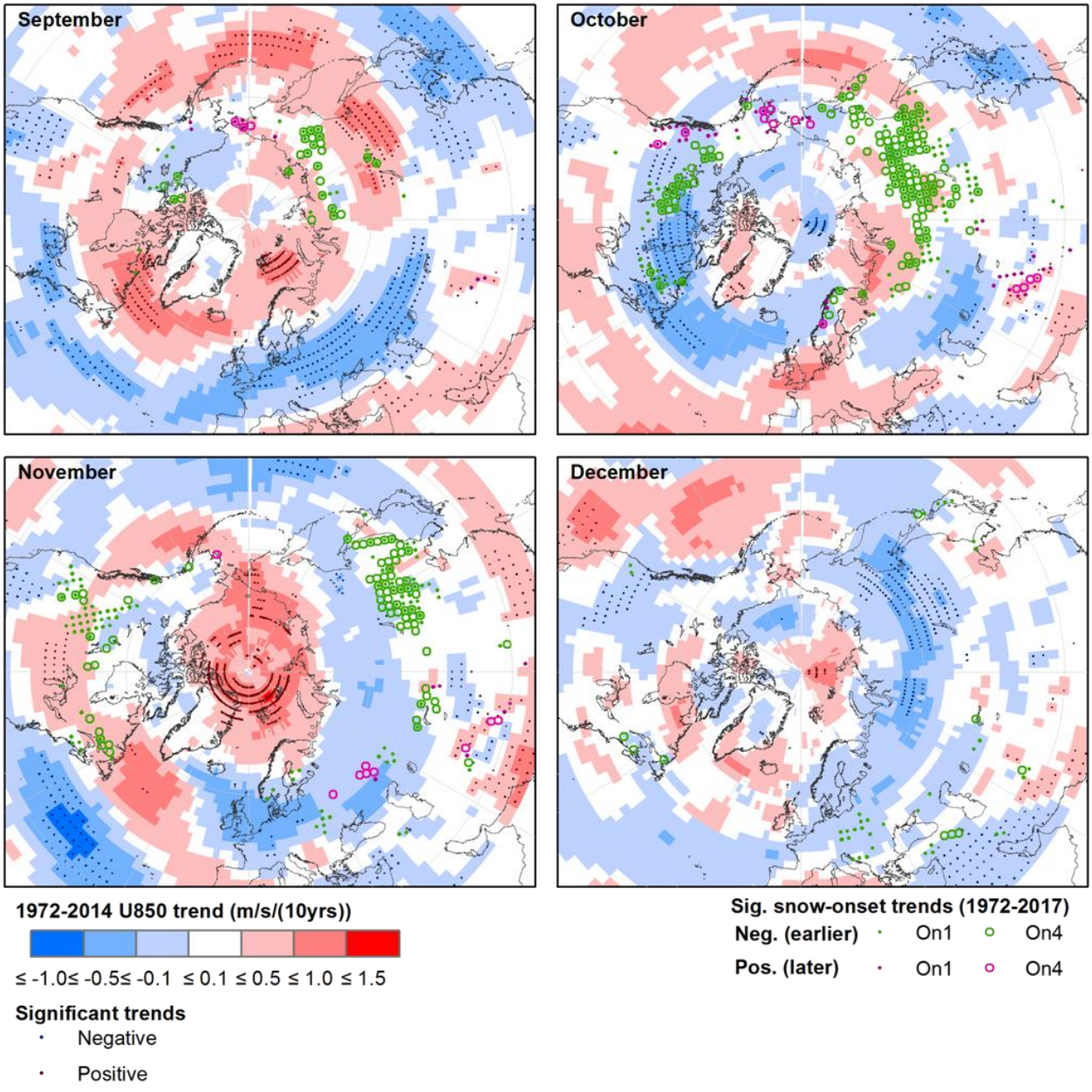

Figure A3.13a: 1972-2014 trends in monthly mean 850 hPa zonal wind-speed.

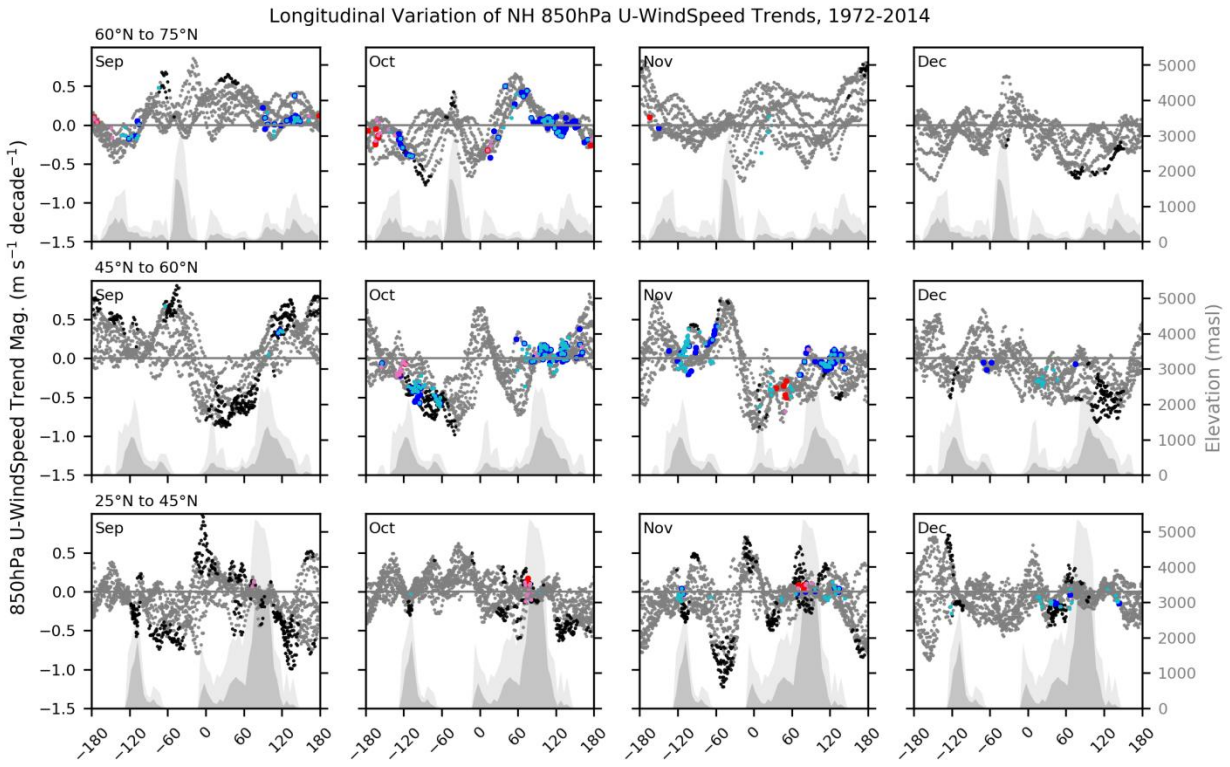

Figure A3.13b: Longitudinal distributions of 1972-2014 trends in monthly mean 850 hPa zonal wind-speed within three latitudinal bands. Black (grey) points represent significant (non-significant) trend magnitudes at points on the reanalysis grid. Dark (light) blue (red) symbols denote values associated with points for which significant negative (positive) On4 (On1) trends were identified. Darker (lighter) shaded areas represent meridional mean (maximum) elevations at zonal intervals of 5°.

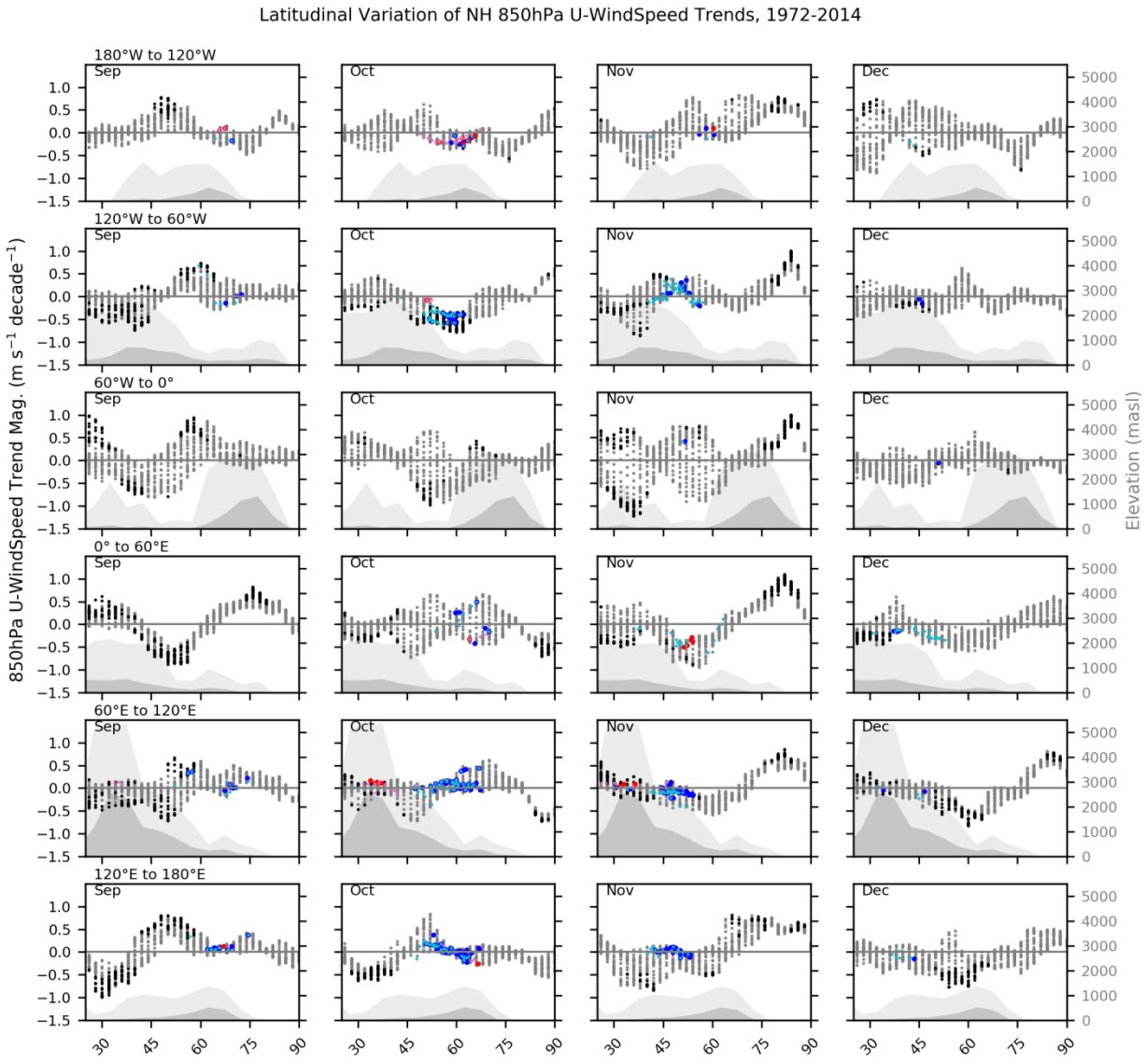

Figure A3.13c: Latitudinal distributions of 1972-2014 trends in monthly mean 850 hPa zonal wind-speed within six longitudinal bands. Black (grey) points represent significant (non-significant) trend magnitudes at points on the reanalysis grid. Dark (light) blue (red) symbols denote values associated with points for which significant negative (positive) On4 (On1) trends were identified. Darker (lighter) shaded areas represent meridional mean (maximum) elevations at zonal intervals of 5°.

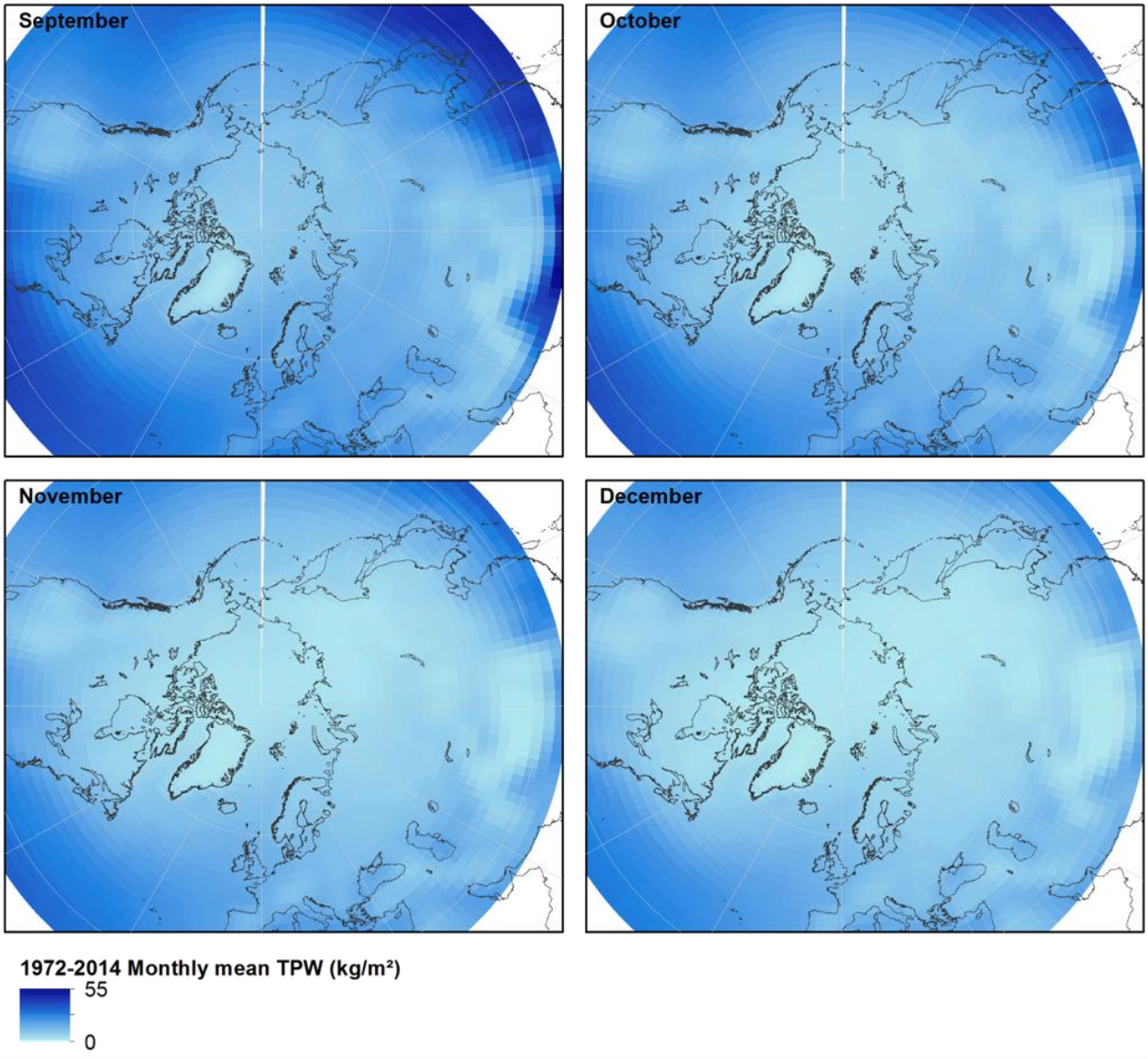

Figure A3.14a: 1972-2014 monthly mean total precipitable water.

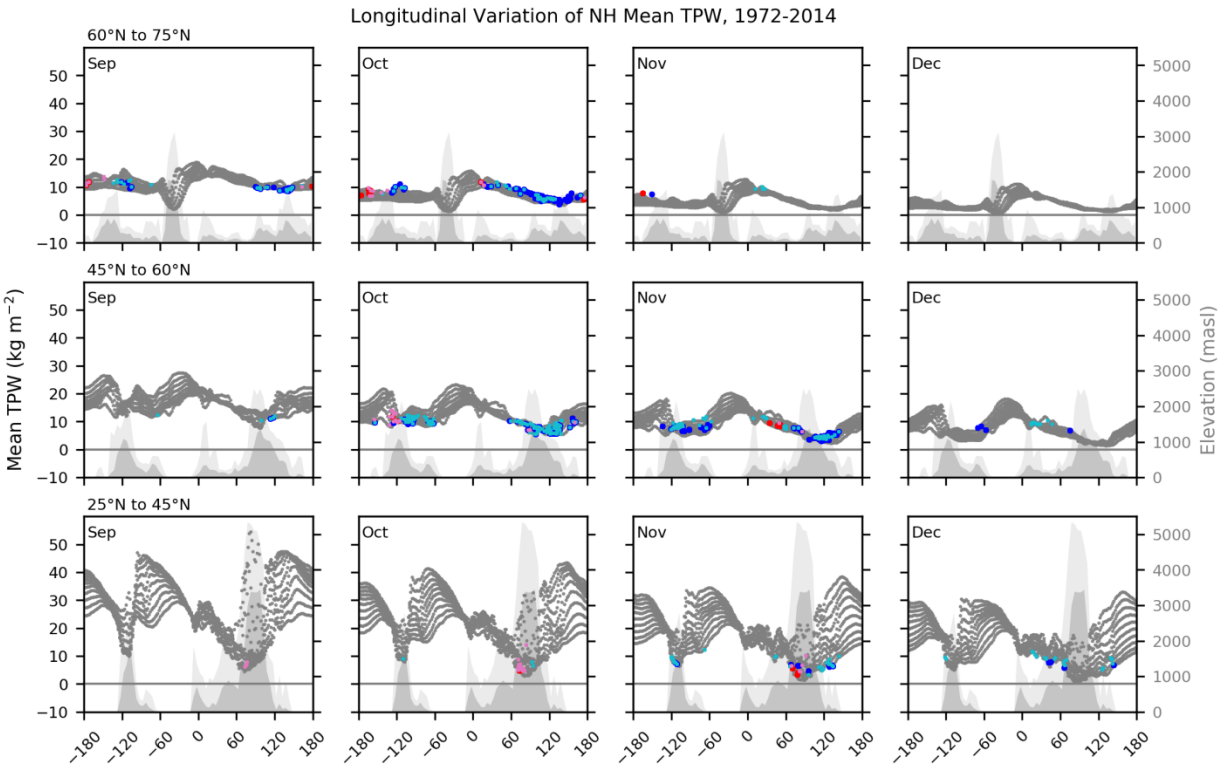

Figure A3.14b: Longitudinal distributions of 1972-2014 monthly mean mean total precipitable water within three latitudinal bands. Grey points represent means at points on the reanalysis grid. Dark (light) blue (red) symbols denote values associated with points for which significant negative (positive) On4 (On1) trends were identified. Darker (lighter) shaded areas represent meridional mean (maximum) elevations at zonal intervals of 5°.

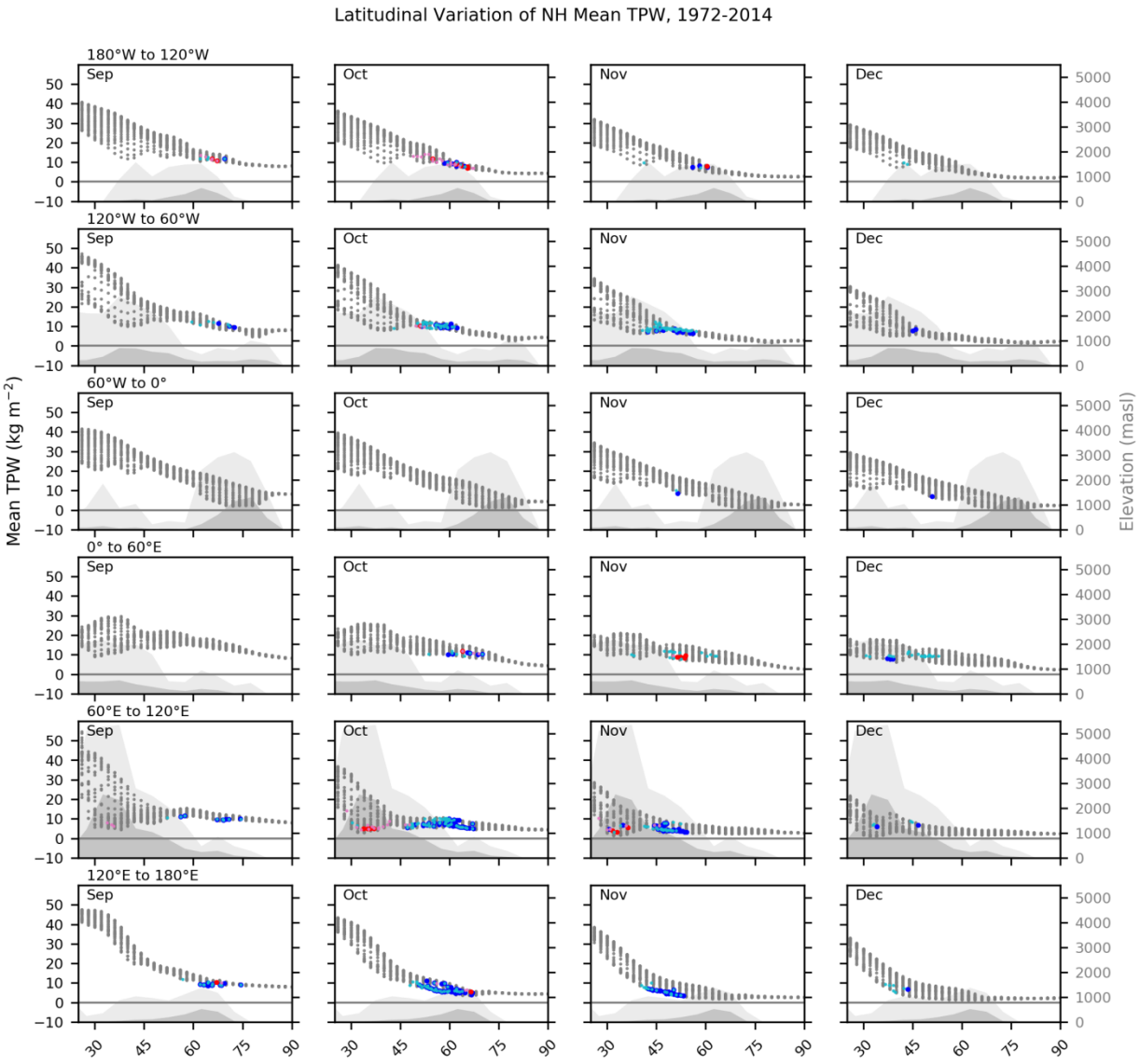

Figure A3.14c: Latitudinal distributions of 1972-2014 monthly mean mean total precipitable water within six longitudinal bands. Grey points represent means at points on the reanalysis grid. Dark (light) blue (red) symbols denote values associated with points for which significant negative (positive) On4 (On1) trends were identified. Darker (lighter) shaded areas represent meridional mean (maximum) elevations at zonal intervals of 5°.

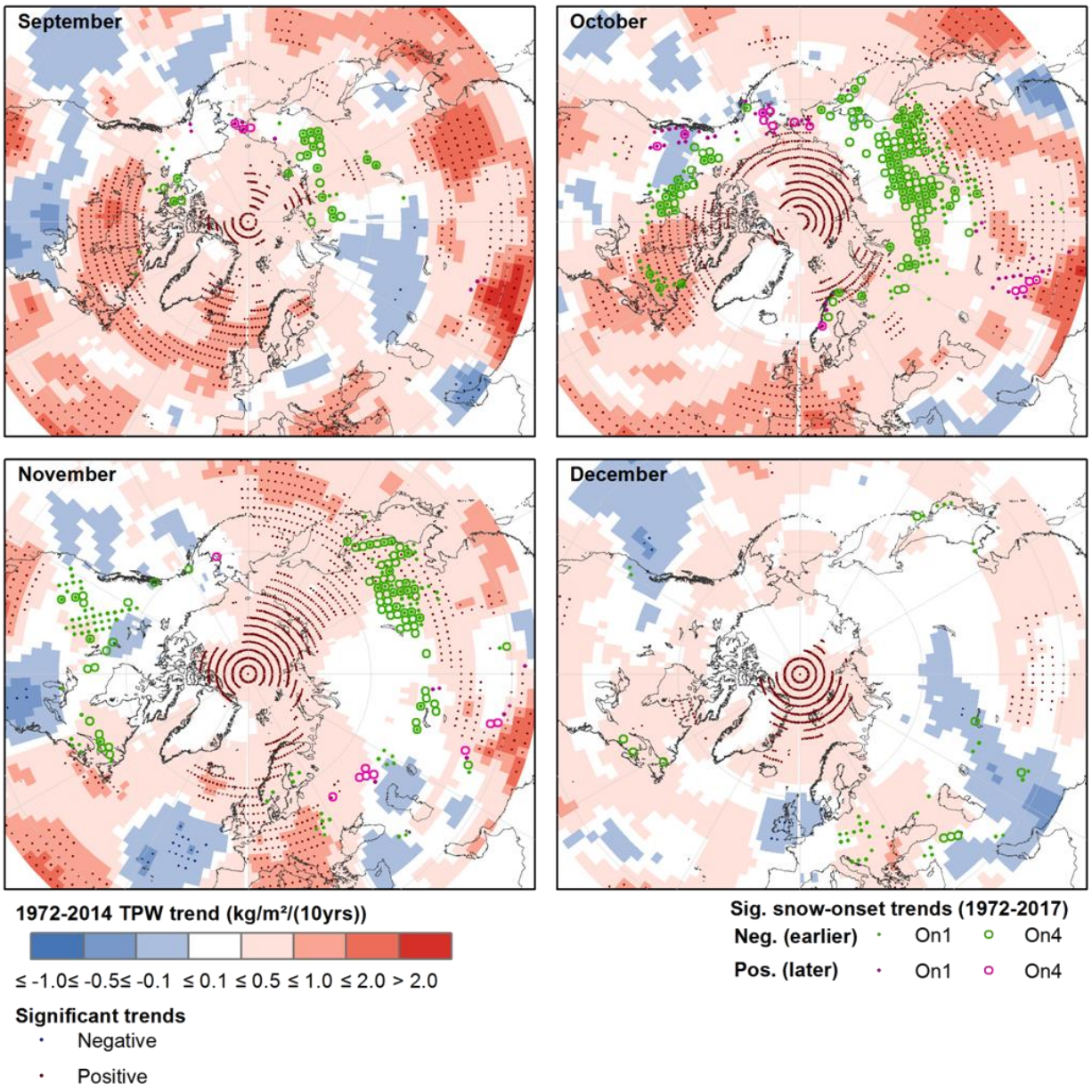

Figure A3.15a: 1972-2014 trends in monthly mean total precipitable water.

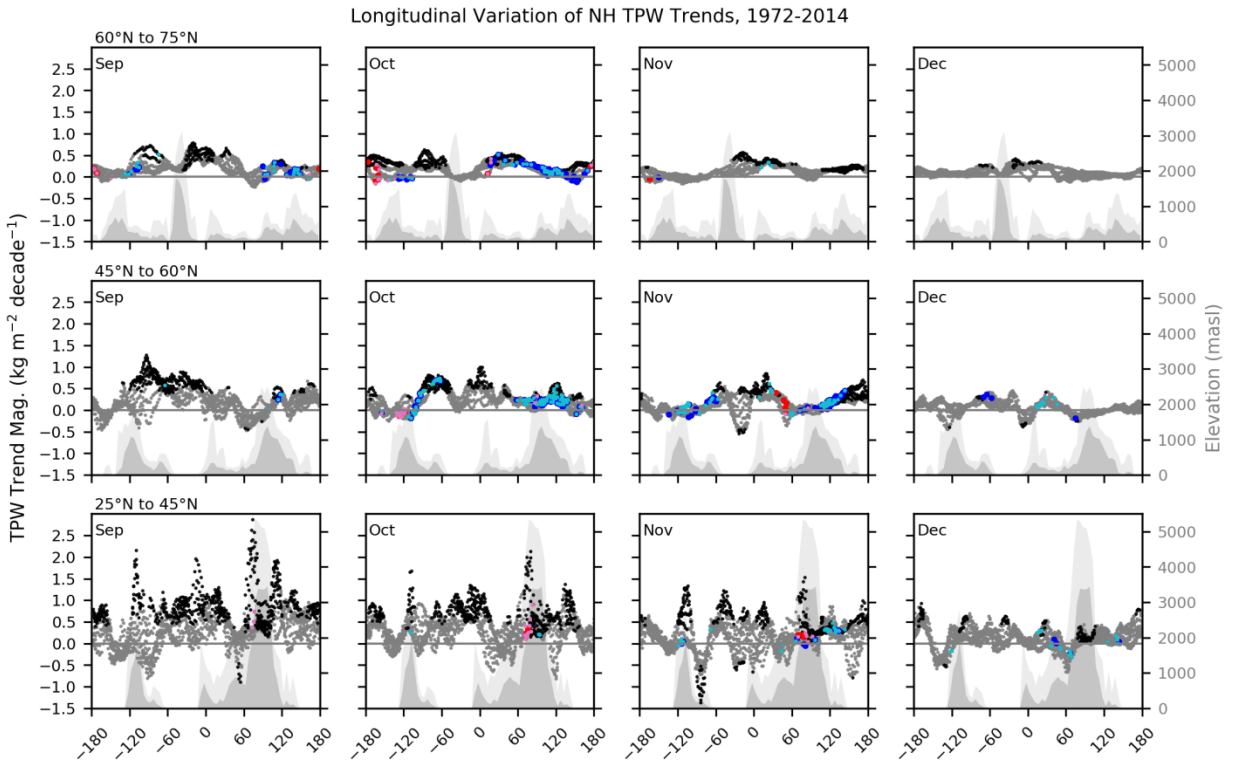

Figure A3.15b: Longitudinal distributions of 1972-2014 trends in monthly mean total precipitable water within three latitudinal bands. Black (grey) points represent significant (non-significant) trend magnitudes at points on the reanalysis grid. Dark (light) blue (red) symbols denote values associated with points for which significant negative (positive) On4 (On1) trends were identified. Darker (lighter) shaded areas represent meridional mean (maximum) elevations at zonal intervals of 5°.

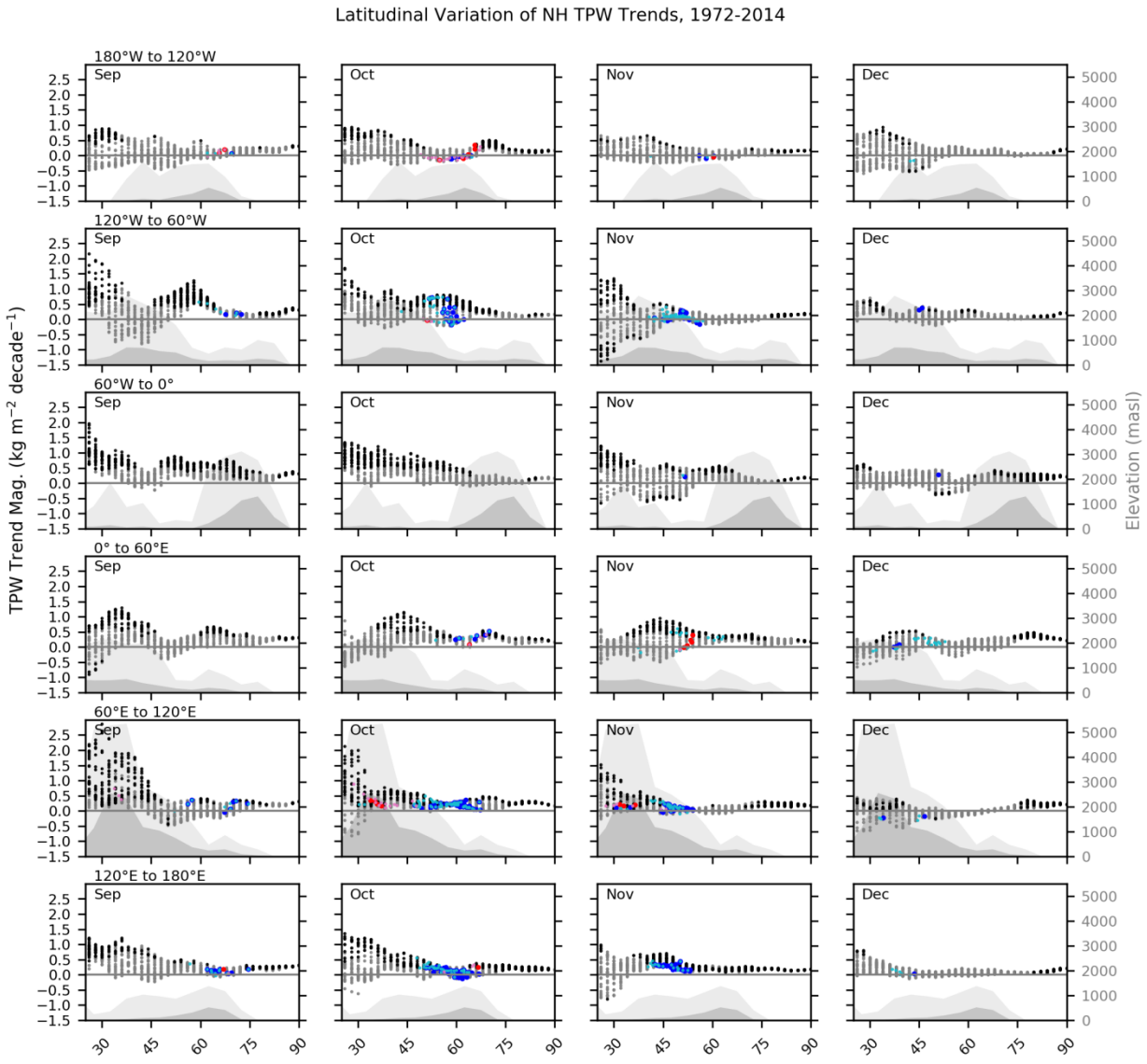

Figure A3.15c: Latitudinal distributions of 1972-2014 trends in monthly mean total precipitable water within six longitudinal bands. Black (grey) points represent significant (non-significant) trend magnitudes at points on the reanalysis grid. Dark (light) blue (red) symbols denote values associated with points for which significant negative (positive) On4 (On1) trends were identified. Darker (lighter) shaded areas represent meridional mean (maximum) elevations at zonal intervals of 5°.

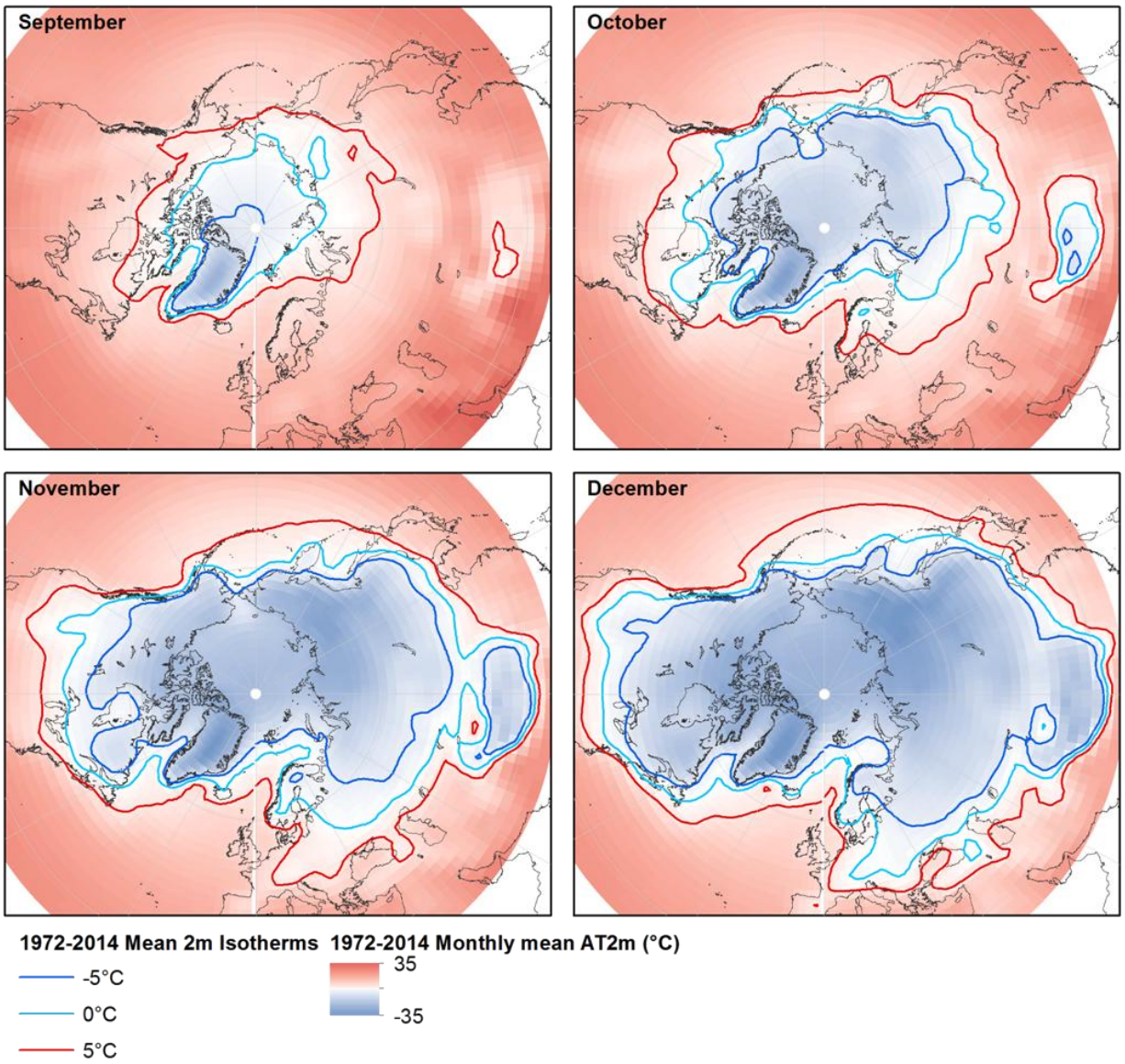

Figure A3.16a: 1972-2014 monthly mean 2m air temperature.

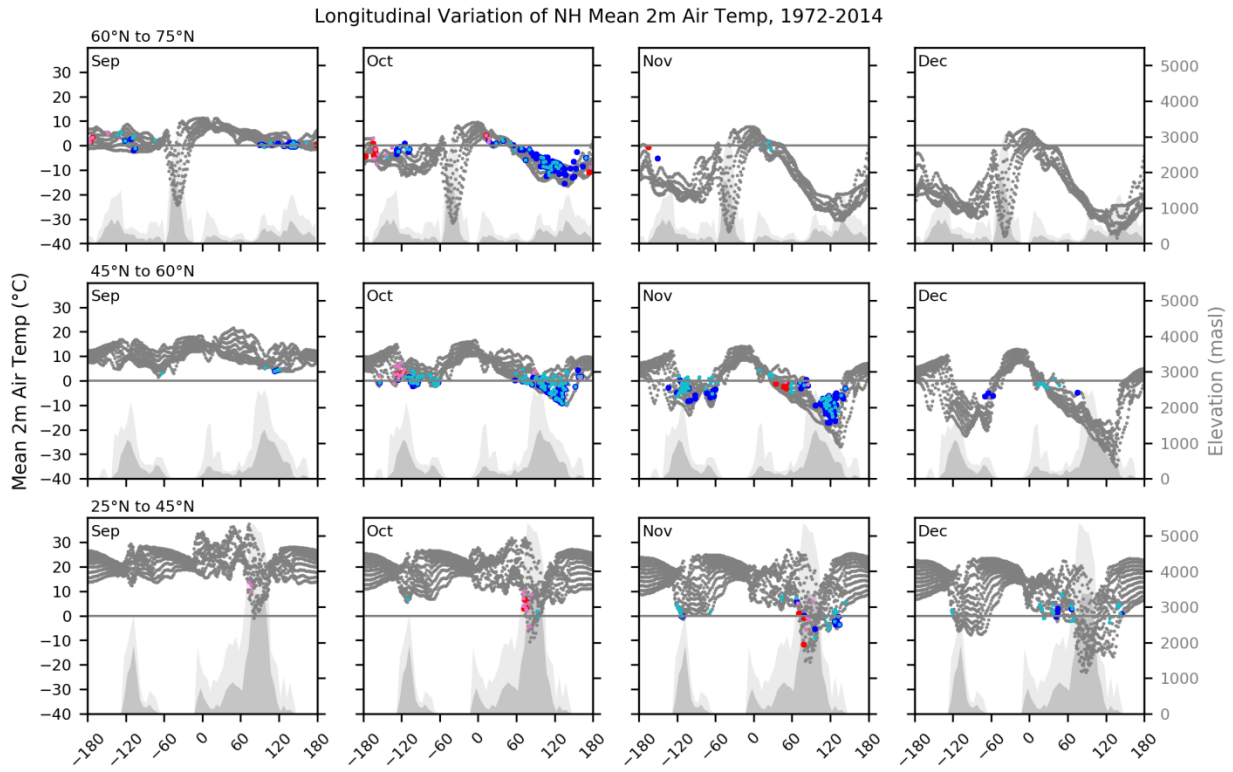

Figure A3.16b: Longitudinal distributions of 1972-2014 monthly mean mean 2m air temperature within three latitudinal bands. Grey points represent means at points on the reanalysis grid. Dark (light) blue (red) symbols denote values associated with points for which significant negative (positive) On4 (On1) trends were identified. Darker (lighter) shaded areas represent meridional mean (maximum) elevations at zonal intervals of 5°.

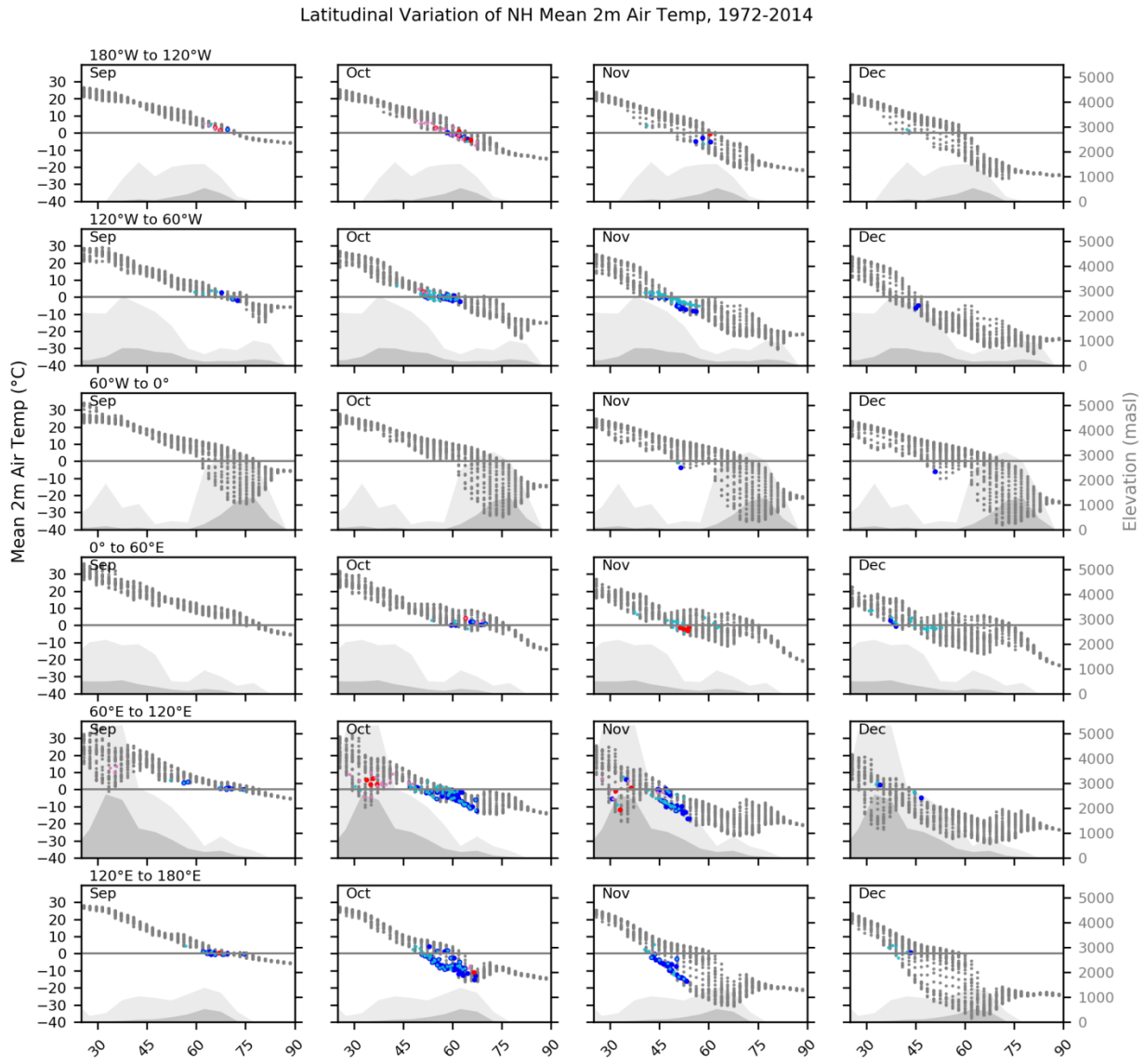

Figure A3.16c: Latitudinal distributions of 1972-2014 monthly mean mean 2m air temperature within six longitudinal bands. Grey points represent means at points on the reanalysis grid. Dark (light) blue (red) symbols denote values associated with points for which significant negative (positive) On4 (On1) trends were identified. Darker (lighter) shaded areas represent meridional mean (maximum) elevations at zonal intervals of 5°.

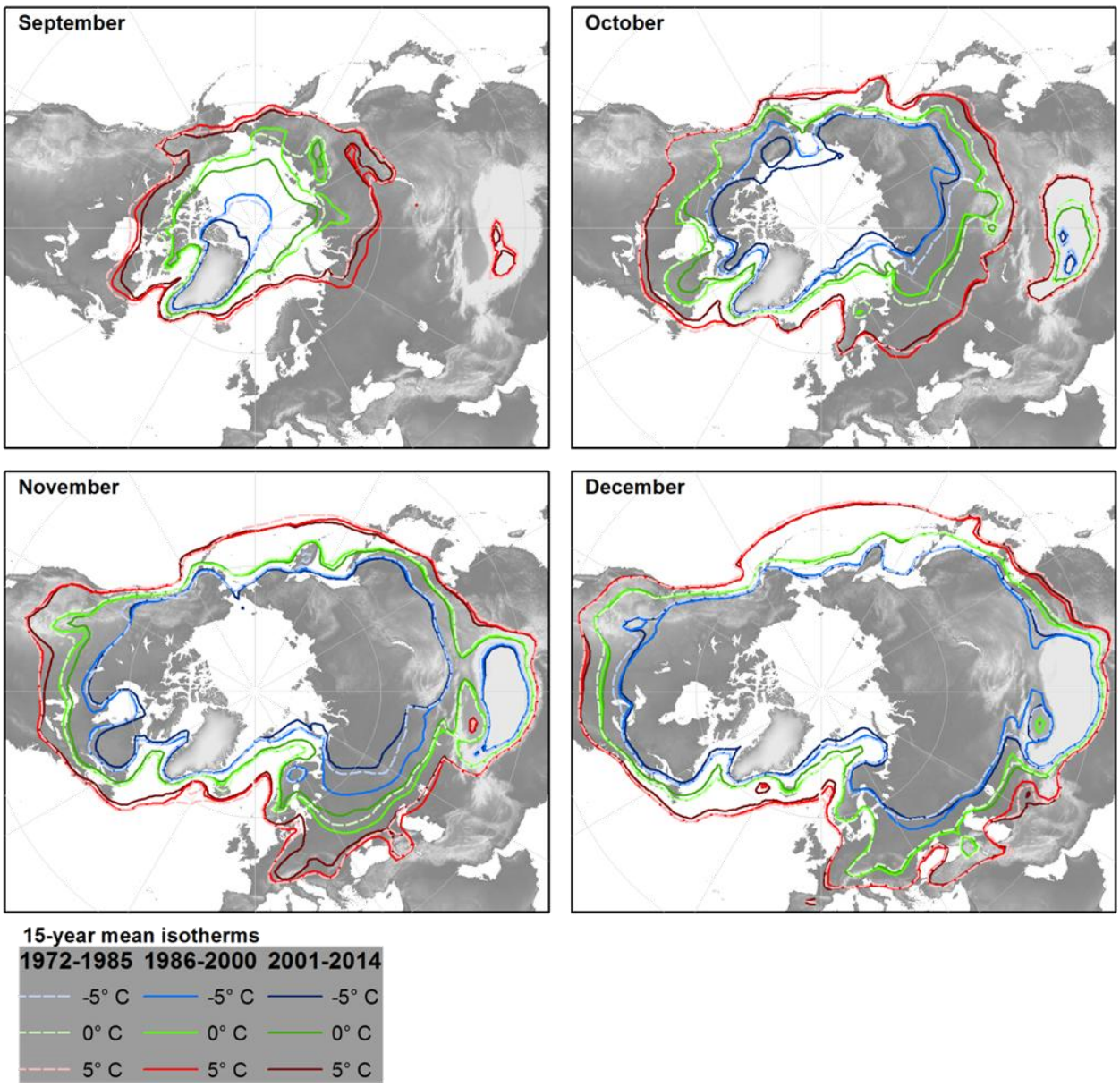

Figure A3.16d: Paths of monthly mean 5°C, 0°C, and -5°C isotherms between 1972-1985, 1986-2000 and 2001-2014.

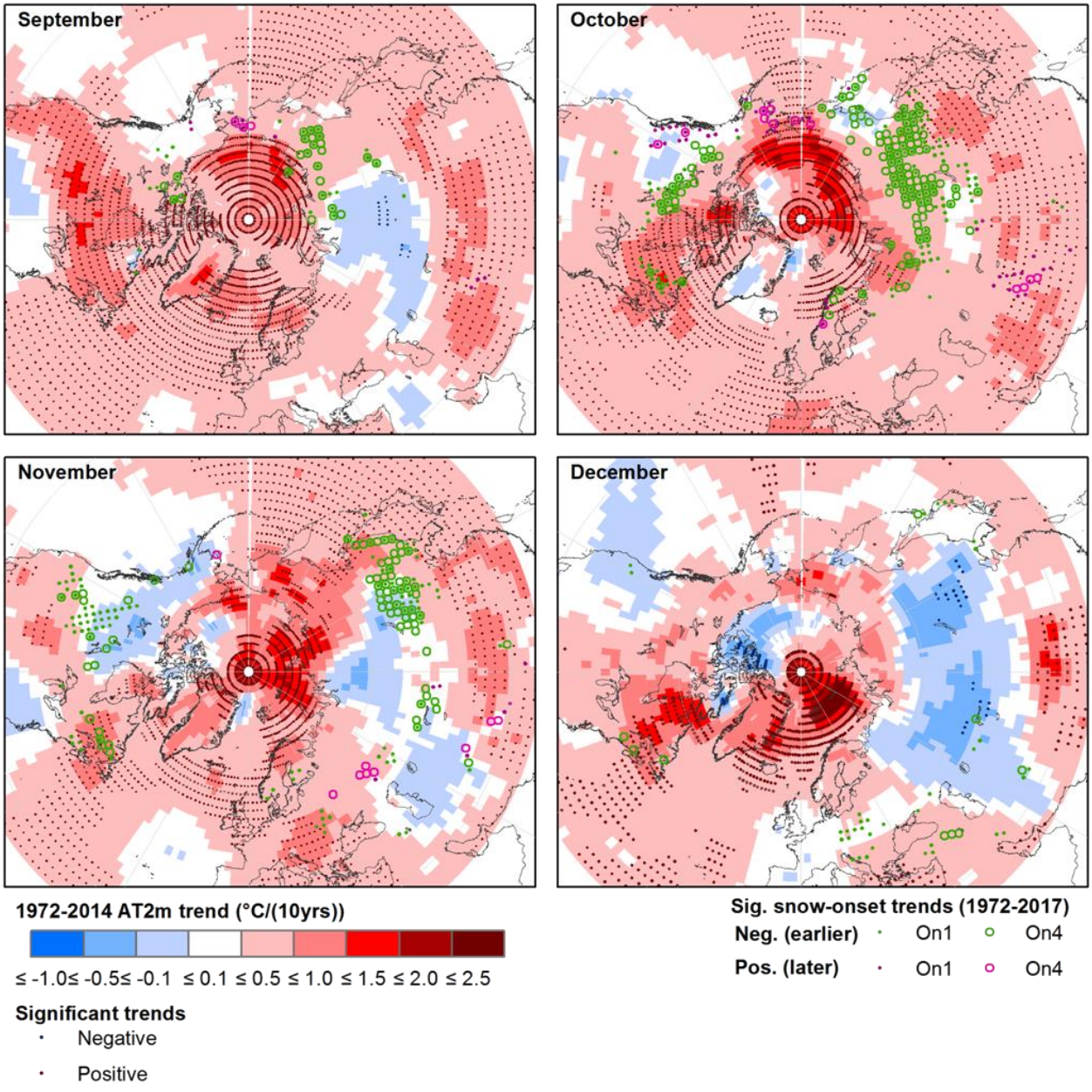

Figure A3.17a: 1972-2014 trends in monthly mean 2m air temperature.

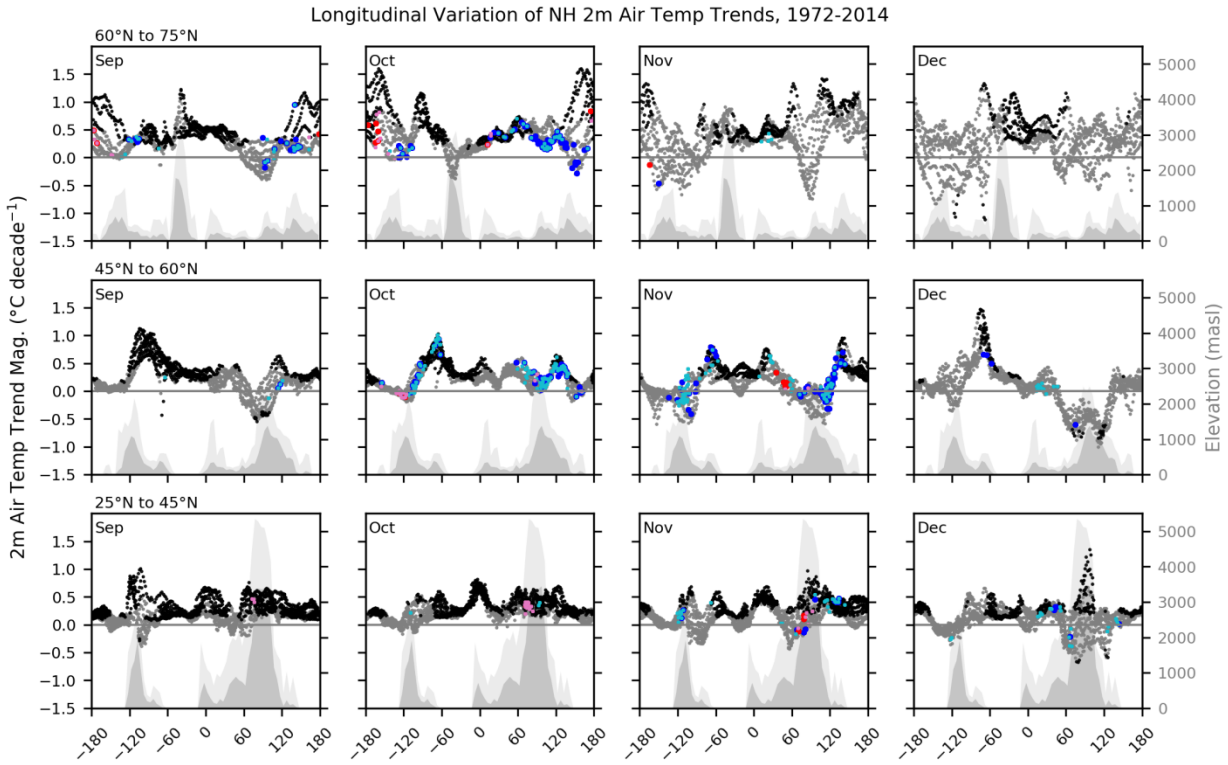

Figure A3.17b: Longitudinal distributions of 1972-2014 trends in monthly mean 2m air temperature within three latitudinal bands. Black (grey) points represent significant (non-significant) trend magnitudes at points on the reanalysis grid. Dark (light) blue (red) symbols denote values associated with points for which significant negative (positive) On4 (On1) trends were identified. Darker (lighter) shaded areas represent meridional mean (maximum) elevations at zonal intervals of 5°.

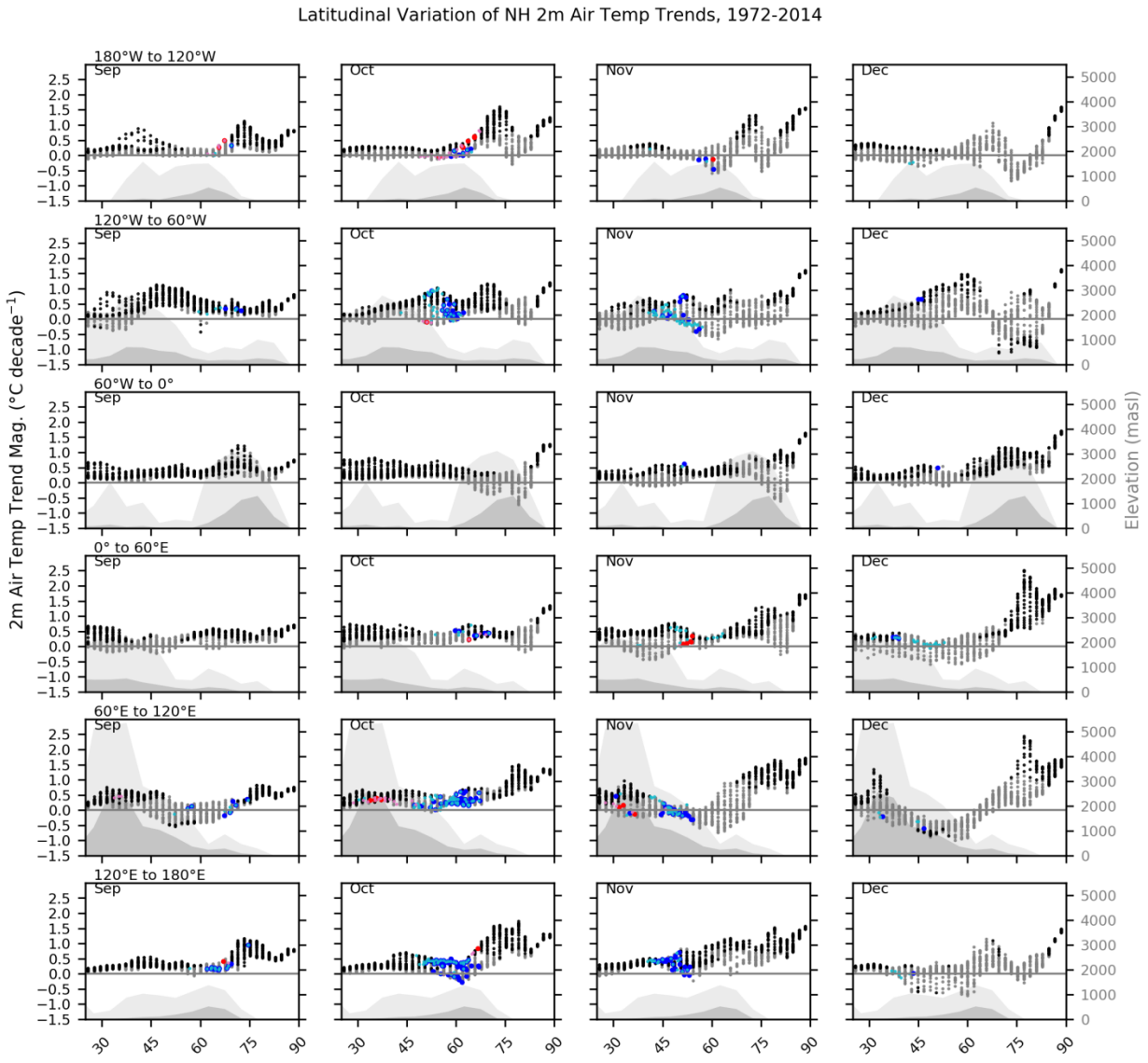

Figure A3.17c: Latitudinal distributions of 1972-2014 trends in monthly mean 2m air temperature within six longitudinal bands. Black (grey) points represent significant (non-significant) trend magnitudes at points on the reanalysis grid. Dark (light) blue (red) symbols denote values associated with points for which significant negative (positive) On4 (On1) trends were identified. Darker (lighter) shaded areas represent meridional mean (maximum) elevations at zonal intervals of 5°.

Table A3.1: Summary statistics describing distributions of significant onset trends in each month: units in all cases are days decade^{-1}.

		September		October		November		December	
		Sig. Neg.	**Sig. Pos.**	**Sig. Neg.**	**Sig. Pos.**	**Sig. Neg.**	**Sig. Pos.**	**Sig. Neg.**	**Sig. Pos.**
On1	**n**	**30**	**9**	**139**	**41**	**104**	**7**	**34**	**0**
	max.	-2.0	12.4	-2.0	22.9	-2.9	25.5	-3.3	-
	95%ile	-2.2	11.8	-2.4	13.8	-3.5	22.8	-4.2	-
	75%ile	-2.8	6.0	-2.9	8.8	-3.9	15.3	-5.2	-
	median	-3.8	4.5	-3.5	5.0	-4.7	7.6	-6.5	-
	mean	-3.7	5.9	-3.8	6.8	-5.1	11.4	-6.3	-
	25%ile	-4.6	4.1	-4.0	3.7	-5.8	6.6	-6.9	-
	5%ile	-5.6	2.8	-6.5	2.6	-8.1	4.1	-8.8	-
	min.	-6.5	2.1	-10.3	2.0	-9.6	3.3	-12.2	-
On4	**n**	**25**	**3**	**128**	**13**	**74**	**9**	**9**	**0**
	max.	-1.7	4.5	-1.8	11.7	-1.9	13.3	-4.1	-
	95%ile	-2.2	4.4	-2.4	10.3	-2.9	13.3	-4.2	-
	75%ile	-2.6	4.2	-2.8	5.0	-3.8	5.0	-4.4	-
	median	-3.8	4.0	-3.3	3.3	-4.7	3.8	-6.5	-
	mean	-3.3	3.5	-3.5	4.8	-4.8	6.1	-6.3	-
	25%ile	-4.0	3.1	-4.0	3.1	-5.7	3.8	-7.6	-
	5%ile	-4.1	2.3	-5.3	2.2	-7.3	3.6	-9.0	-
	min.	-4.2	2.1	-6.7	2.1	-10.0	3.5	-9.5	-